Universidad del País Vasco
Euskal Herriko Unibertsitatea
eman ta zabal zazu

Faculty of Engineering of Bilbao (ESI)
Department of Automatic Control and Systems Engineering (DISA)

Ph.D Thesis

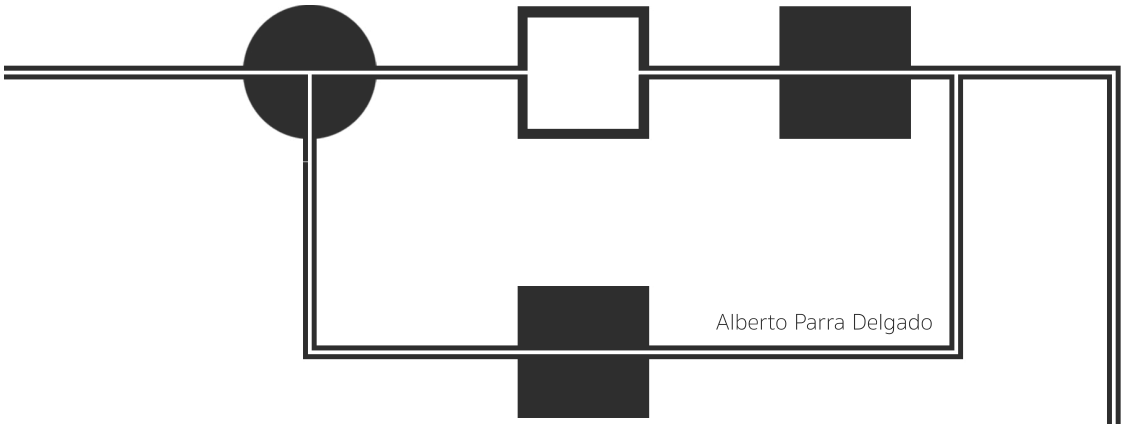

Alberto Parra Delgado

Torque Vectoring Control Strategies for Electric Vehicles

Thesis supervised by: Dr. Asier Zubizarreta Pico
Dr. Joshué Pérez Rastelli

October 2020

eman ta zabal zazu

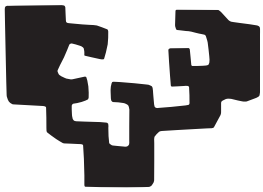

Universidad del País Vasco
Euskal Herriko Unibertsitatea

Faculty of Engineering of Bilbao
Automatic Control and System Engineering Department

TORQUE VECTORING CONTROL STRATEGIES FOR ELECTRIC VEHICLES

Alberto Parra Delgado

Thesis supervised by:
Dr. Asier Zubizarreta Pico
Dr. Joshué Pérez Rastelli


tecnalia
Inspiring
Business

Contents

List of Figures

List of Tables

List of Acronyms

4WD	Four Wheel Drive
ABS	Antilock Braking System
ADAS	Advanced Driver Assistance System
ANN	Artificial Neural Network
CAN	Controller Area Network
DiL	Driver-in-the-Loop
DOF	Degree Of Freedom
DSP	Digital Signal Processing
ECU	Electronic Control Unit
ESC	Electronic Stability Control
ESP	Electronic Stability Program
FL	Front Left
FPGA	Field Programmable Gate Array
FR	Front Right
GPS	Global Positioning System
GPU	Graphics Processing Unit
HDL	Visual Hardware Description Language
HiL	Hardware-in-the-Loop
HLS	High Levels Synthesis
HP	Horse Power
ICE	Internal Combustion Engine
IMU	Inertial Measurement Unit
ISO	International Standard Organization
LUT	Look-up-Table
MAE	Mean Average Error
MBD	Model Based Design/Development
MiL	Model-in-the-Loop
MIMO	Multiple Input Multiple Output
MISO	Multiple Input Single Output
MiW	Motor-in-Wheel
MPSoC	Multi-Processor System-on-Chip
MSE	Mean Squared Error
NN	Neural Network
RL	Rear Left
RR	Rear Right
RTOS	Real-Time Operating System

SDK	Software Development Kit
SoC	System on Chip
TCS	Traction Control System
VHDL	Visual Hardware Description Language
AFS	Active Front Steering
ATTS	Active Torque Transfer System
AYC	Active Yaw Control
ARE	Algebraic Riccati Equation
AWD	All-Wheel Drive
ABS	Anti-lock Braking System
CM	Centre of Mass
CC	Cruise Control
DOF	Degrees of Freedom
DYC	Direct Yaw Control
DARE	Discrete Algebraic Riccati Equation
EV	Electric Vehicle
EOM	Equations of Motion
EKF	Extended Kalman Filter
4WS	Four Wheel Steering
FWD	Front-Wheel Drive
HEV	Hybrid Electric Vehicle
IMU	Inertial Measurement Unit
KF	Kalman Filter
LPV	Linear Parameter Varying
LQG	Linear Quadratic Gaussian
LQR	Linear Quadratic Regulator
LTV	Linear Time Varying
MF	Magic Formula
MPC	Model Predictive Control
MIMO	Multi-Input Multi-Output
NMPC	Nonlinear Model Predictive Control
NLP	NonLinear Program
PID	Proportional-Integral-Derivative
QP	Quadratic Program
RTI	Real Time Iteration
RWD	Rear-Wheel Drive
RHE	Receding Horizon Estimation
RI	Rollover Index
SQP	Sequential Quadratic Program
SMC	Sliding Mode Control
SUV	Sport Utility Vehicle
SH-AWD	Super Handling All-Wheel Drive
TCS	Traction Control System
TV	Torque vectoring
UKF	Unscented Kalman Filter

List of symbols

α	Tyre slip angle
β	Vehicle sideslip angle at its centre of mass
δ	Steering angle at the front wheels
δ_{ratio}	Steering gear ratio
ϵ	Slack variable
μ_x, μ_y	Longitudinal and lateral tyre force coefficient
μ_{max}	Tyre/road friction coefficient
ψ	Vehicle yaw angle at its centre of mass
ω	Wheel angular rate
a_x, a_y	Vehicle longitudinal and lateral acceleration at its centre of mass
c_{drag}	Aerodynamic drag coefficient
c_F, c_R	Front and rear suspension shock absorber damping
F_x, F_y, F_z	Longitudinal, lateral and normal tyre force
g	Constant of gravitational acceleration
h	Vertical distance of centre of mass from the ground
h_{veh}	Height of the vehicle
i, j	Subscripts i = F,R (front, rear), j = L,R (left, right)
k_{aF}, k_{aR}	Front and rear anti-roll bar torsional stiffness
k_F, k_R	Front and rear suspension spring stiffness
l_F, l_R	Longitudinal distance of centre of mass from the front and the rear track
l	Length of the vehicle
m	Mass of the vehicle
m_u	Mass of the wheel
s, s_x, s_y	Total, longitudinal and lateral tyre slip
t_{wF}, t_{wR}	Lateral distance of centre of mass from the left and right wheels
t_w	Width of the vehicle
B	Pacejka's Magic Formula stiffness factor
C	Pacejka's Magic Formula shape factor
D	Pacejka's Magic Formula peak value
E	Pacejka's Magic Formula curvature shift
i_w	Wheel moment of inertia of each wheel about its axis of rotation
I_x	Vehicle moment of inertia about its horizontal axis
I_y	Vehicle moment of inertia about its lateral axis
I_z	Vehicle moment of inertia about its vertical axis
H	Horizon
H_p	Np Prediction horizon

H_u	Nu Control horizon
R	R Vehicle path radius
R_w	Wheel radius
τ	Torque
T_s	Sampling time
T_{sim}	Simulation time
V	Vehicle velocity at its centre of mass

Introduction

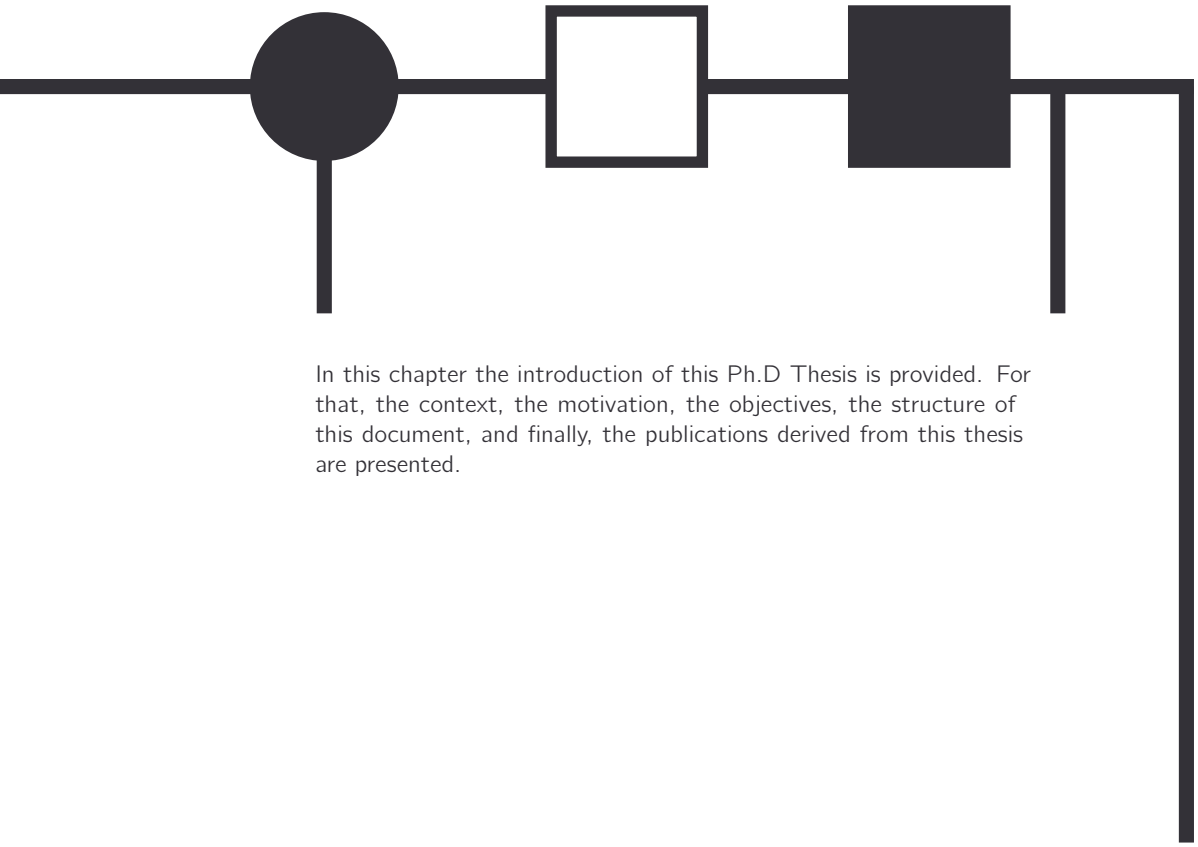

In this chapter the introduction of this Ph.D Thesis is provided. For that, the context, the motivation, the objectives, the structure of this document, and finally, the publications derived from this thesis are presented.

1- Introduction

1.1 Context

The need for reducing global warming, air pollution and oil dependency has motivated not only the use of renewable energies, but also some paradigm changes in other areas, such as transportation systems, where the development of electric vehicles (EV) has become a key strategy.

The interest in vehicles with electrified powertrains (fully electric as well as hybrid) has increased in the last years, becoming one of the main research areas for the automotive industry. The integration of electric motors in propulsion systems provides not only better energy efficiency and lower pollution, but also increased controllability, as electric motors offer better response time. These features are fuelling a notable interest in the development of Advanced Driver-Assistance Systems (ADAS) and vehicle dynamics control (VDC) systems that enhance not only the dynamic behaviour of the vehicle, but also its efficiency and energy consumption.

One of the most complete ADAS for enhancing the dynamic behaviour and stability of an electric vehicle with per-wheel motors is Torque Vectoring (TV), which focuses on the optimal driving torque distribution. Additionally, TV approaches have demonstrated their ability to also reduce the energy consumption through an optimal torque distribution, which is one of the most important obstacles for EVs adoption.

Therefore, this Ph.D. thesis focuses on this area, making contributions on TV approaches considering energy efficiency for EVs by applying advanced control approaches such as intelligent control techniques and nonlinear model predictive control.

The research work resulting in this thesis has been carried out in the Automotive Business area of Tecnalia Research & Innovation (Industry and Transport Unit), in collaboration with the Automatic Control and System Engineering department of University of the Basque Country (UPV/EHU).

Tecnalia's Automotive Business area focuses its activity in the research and development of innovative automotive oriented systems, including the following topics:

- Research, design, and development of advanced control strategies for automotive electric machines applied to electric and hybrid propulsion systems. Current research interests include the study of control strategies for high-speed operation, sensorless control, fault-tolerant operation, and multiphase machine control.

- Research and development of optimal energy management strategies, including energy recovery during regenerative braking, damage reduction on mechanical components and vehicle life-cycle and autonomy range extension.

- Research in advanced vehicle dynamics control systems, such as: traction control system (TCS), antilock braking system (ABS) and torque vectoring (TV).

- Research in automated driving, including Advanced Driver Assistance Systems (ADAS). The main focus includes decision-making systems, which enable the design of new ADAS for control sharing between the vehicle and the driver.

- Research in new multi-material structures for weight reduction purposes.

On the other hand, the Automatic Control and System Engineering department research activities include the following topics:

- Research and development on advanced control strategies for complex dynamic systems, with experience in robotics, bioengineering, automotive applications, machine-tool applications and green energy conversion.

- Research on Model Predictive Control approaches for autonomous vehicles.

- Research on Industry 4.0

- Research on Virtual Sensors based on artificial intelligence.

Additionally, the academic scope of the research has been extended by performing an international Ph.D. researcher internship of three months at the Centre for Automotive Engineering (leader Prof. Aldo Sorniotti), which is part of the Department of Mechanical Engineering of the University of Surrey (United Kingdom).

Finally, this thesis has been partially supported by several European projects:

- 3Ccar [19] (ECSEL JU under grant agreement No. 662192): the objective of this project is to address the growing complexity in mobility systems, especially in Electrified Vehicles (EV).

- ADVICE [20] (H2020 under grant agreement No. 724095): this project aims at increasing the number of Hybrid Electric Vehicles (HEVs) and Plugin-HEVs to up to 10% of all vehicles registered in the mid-term range.

- ACHILES [21] (H2020 under grant agreement No. 824311): The objective of ACHILES is to develop advanced architectures chassis/traction concept for future electric vehicles and enhance new parts and functionalities in a new E/E system architecture.

- STEVE [22] (H2020 under grant agreement No. 769944): STEVE brings together cities, industrial companies, small and medium enterprises, and academic institutions from seven European countries, for the demonstration of the integration of EL-Vs (Electrified L-category Vehicles) in the urban transport system.

1.2 Motivation

The study of chassis control systems (or vehicle dynamics control systems) has been a major research area for both the automotive industry and academia for the last decades. Chassis control can be defined as the control of the longitudinal, lateral and vertical vehicle motion to improve handling and traction/braking performance along with active safety [23]. This research topic has quickly grown into one of the most intensive subjects with a large volume of published literature [24]. This growth has a direct connection with the safety concerns caused by an increasing number of vehicles on the road, combined with the higher performance of current vehicles. At the same time, the development of embedded platforms has offered faster and cheaper devices for the deployment of chassis control solutions.

The first proposals in chassis control systems were focused on controlling each wheel, with approaches such as the Anti-lock Braking System (ABS) (1978) and Traction Control System (TCS) (1983) (Figure 1.1). Their success opened the way to more complex approaches that considered the dynamics of the vehicle as a whole [25]. This way, in the mid-1980s, the 4 Wheel Steering (4WS) and semi-active/active suspension systems were introduced. Later, in the 1990s, with the increase of computing power, the Electronic Stability Program (ESP, or ESC) was proposed [26]. These systems offered greater control over the dynamics of the vehicle, differentiating themselves from the first approaches.

One of the most interesting vehicle dynamics control approach is Torque Vectoring (TV), which was proposed first in 2005 [27]. TV approaches control both the direction and magnitude of the wheel torque to influence the dynamics of the vehicle positively [28]. Torque vectoring on a conventional driveline can be applied between axles or between wheels of the same axle, or even in a front-to-rear and left-to-right operation combining axle and centre differentials or couplings.

Although this approach was proposed more than 15 years ago, it has recently gained attention due to the possibilities that electric vehicles (EV) offer. Thanks to the wide range of powertrain topologies (from a single electric motor with a mechanical differential, to individual motors per wheel), torque vectoring may allow to enhance not only vehicle dynamics, but also the overall efficiency.

One of the main issues regarding EVs is their limited driving range, which is certainly harming their widespread adoption. The issue is being addressed through the enhancement of battery technologies [29], as well as the introduction of superfast charging stations on the road network [30]. In parallel, the efforts to increase driving range are supported by the improvement of energy efficiency of electric powertrain components, and new vehicle systems such as predictive energy management and optimal speed profiling [31].

In this sense, torque vectoring systems can also contribute to reduce the overall energy consumption through an energy efficient torque distribution. The main power losses sources of a EV come from the powertrain (inverter, electric motor and drivetrain) and the tyres. When considering the powertrain, on the one hand, several authors have tried to minimized losses by optimizing the internal control of electric motors [32], through controlling the flux [32] or suppressing certain harmonics [33].

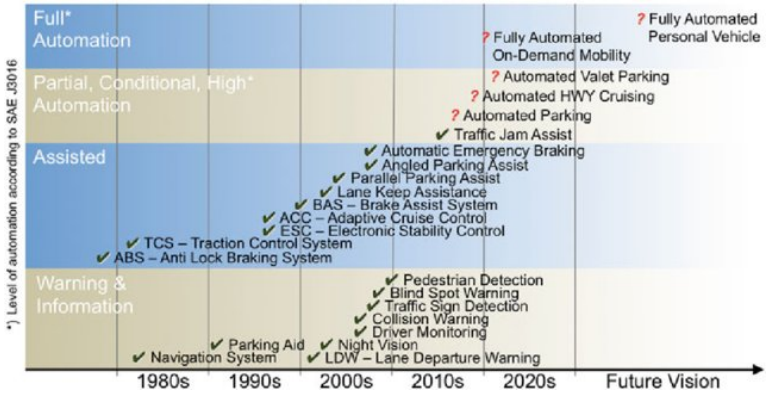

Figure 1.1: ADAS Timeline [1]

And, on the other hand, torque vectoring systems can provide torque commands that make the electric motor work in the most efficient operating point for each traction/braking and cornering condition. Regarding tyre losses, power losses arise when the tyre is slipping, both longitudinally and laterally. To avoid tyre slipping, proper measurement of tyre forces is crucial. Particularly, vertical tyre forces are very relevant in vehicle dynamics. Note that the tyres with more load present more grip, this is, they can transmit more force to the road, which is an important factor when performing the torque distribution in a TV algorithm. However, measuring these forces is a challenging (or impossible) task due to the expensive sensors that are needed, and their estimation is one of the most complex issues in vehicle dynamics, as the tyre/road contact dynamics depends on many different variables.

However, the inclusion of more and more functionalities in torque vectoring systems, such as the aforementioned dynamics enhancement and efficiency considerations, increases the complexity of the needed algorithms, in particular, for EVs. This is one of the main concerns of the automotive industry as the complexity and derived issues of the control systems required for these vehicles are reaching hardly sustainable levels, with over 100 million lines of source code distributed on board among over 100 ECUs (electronic control units) [34, 35]. In addition, the technical challenge is further increased by several industry-related constraints. Firstly, some well-known aspects inherent to the big-scale vehicle industry need to be considered, such as strong cost sensitivity and diverse requirements pushing towards modularity, combined with accelerated product cycles. Secondly, a major constraint is being added to this already challenging context: increasing impact from safety standards and regulations addressing safety-critical systems.

One of the technological enablers in this context is the new generation of high-performance embedded platforms. A diversity of heterogeneous platforms offering vast computational power is appearing on the market, including multiple cores, FPGA logic, and GPU units. These platforms are rapidly approaching towards industry suitable levels of cost and robustness, meaning that they could eventually be exploited

to cover the aforementioned issues.

Finally, testing is also a key issue when considering Torque Vectoring approaches. In this area, simulation frameworks have arisen as very useful tools for developing and testing vehicle dynamics control systems, including TV. Their effectiveness to reduce the cost and development times, while keeping flexible development capabilities and fulfilling demanding regulation standards for safety-critical systems have also aroused the interest of the industry. This way, nowadays, they are a crucial tool in the developing and testing process of control systems for automotive applications.

In summary, torque vectoring solutions are gaining more and more relevance in the vehicle dynamics control systems area as they have the potential to not only enhance the handling and safety, but also the overall efficiency, being the latter a critical issue for EVs. For this purpose, considering the powertrain efficiency map and tyre forces is crucial. And finally, considering implementability of the proposed approaches is mandatory to ensure a proper transfer to the demanding EV market.

1.3 Objectives

The main objective of this thesis is to develop a real-time capable torque vectoring control approach that is able to improve the handling and overall efficiency of All Wheel Driven (AWD) electric vehicles. This goal will help to solve some of the most important problems in EVs and, therefore, contribute to improve their widespread adoption.

In this context, the following specific objectives have been defined in order to achieve the main objective of this thesis:

(a) Define and validate a simulation framework for ADAS and vehicle dynamics control systems development, that reduces the development and validation time of TV approaches and enables a Hardware-in-the-loop approach.

(b) Analyze the proposed approaches on vehicle dynamics control systems, in particular TV systems, identifying the current limitations and technological challenges.

(c) Develop new real-time capable tyre force estimators based on intelligent approaches.

(d) Analyse the advantages of advanced model-based controllers, such as MPC, and intelligent control approaches, such as fuzzy logic, to TV.

(e) Determine the implementability of the proposed approaches.

1.4 Structure of the document

In order to develop the aforementioned objectives, this thesis is structured in six chapters. In addition to the introduction to the thesis, the document is organized as follows:

- **Chapter 2, Torque Vectoring Algorithms: State of the Art:** this chapter presents a review of the torque vectoring systems focused on EVs. The study covers the proposed approaches from an historical point of view, from the origin of TV to current EV implementations. The open challenges and main issues of the proposed approaches are identified.

- **Chapter 3, Vehicle Dynamics Simulation Framework:** this chapter presents the simulation framework used for the evaluation of the approaches presented in this Ph.D. Thesis. First, the necessity and advantages of having a reliable simulation framework in automotive industry in order to develop and validate different vehicle control systems is introduced. Then, the simulation environment proposed for this work, which is composed by a LTV MPC virtual driver model and a multibody vehicle dynamics model, is deeply explained. Finally, the validation of the proposed framework using real vehicle data is carried out. This framework will be used in the next chapters to validate the proposed TV approaches.

- **Chapter 4, Intelligent Torque Vectoring:** in this chapter the first contribution of this Ph.D. thesis is presented, which is the Intelligent Torque Vectoring system. This novel approach is based on intelligent control techniques and includes a vertical tyre forces estimator, which allows to enhance vehicle dynamics, and indirectly, efficiency. The design process and implementation of the proposed approach is deeply addressed and explained. Finally, the TV approach is evaluated by comparing its performance with other approaches proposed in the literature.

- **Chapter 5, Energy-efficient NMPC TV:** in this chapter the second contribution of this Ph.D. thesis is presented. As previously stated and analysed in Chapter 2, the limited driving range derived by the energy consumption is one of the biggest issues for EVs widespread adoption. Therefore, in this chapter an energy-efficient NMPC TV system, which includes a fuzzy logic based cost function weight adaptation mechanism, is proposed. This novel approach targets both the vehicle dynamics performance and the energy efficiency explicitly, considering the powertrain and tyre slip power losses. The proposed TV approach is compared with the one presented in the aforementioned Chapter, and the effect of the different terms of the MPC are analysed deeply.

- **Chapter 6, Conclusions and future work**. This chapter summarizes the conclusions obtained from this work, as well as its main contributions and future research lines.

1.5 Publications derived from this thesis

The journal and conference publications derived from this Ph.D. thesis are presented in this section. Table 1.1 shows the correspondence between the publications and the Chapters associated.

Chapter	Title	Publication
2	Vehicle Dynamics Simulation Framework	J4, C4
3	Torque vectoring systems state of the art	C5, C9
4	Intelligent Torque Vectoring	J1, J2, C1, C2, C3, C6, C7, C8
5	Energy-efficient NMPC TV	J3

Table 1.1: Publications derived from this thesis and their correspondence with document chapters.

Next, the publication list is detailed.

1.5.1 Publications in scientific journals

J1) **Alberto Parra**, Asier Zubizarreta, Joshué Pérez, and Martín Dendaluce, "*Intelligent Torque Vectoring Approach for Electric Vehicles with Per-Wheel Motors*", in Complexity, vol. 2018.

J2) **Alberto Parra**, Asier Zubizarreta, Joshué Pérez "*Intelligent Torque Vectoring approach based on Fuzzy Logic Controller and Neural Network tire forces estimator*", in Neural Computing & Applications **(Under review)**.

J3) **Alberto Parra**, Davide Tavernini, Patrick Gruber, Aldo Sorniotti, Asier Zubizarreta and Joshué Pérez, "*On nonlinear model predictive control for energy-efficient torque-vectoring*", in IEEE Transactions on Vehicular Technology.

J4) **Alberto Parra**, Antonio J. Rodríguez, Asier Zubizarreta, Joshué Pérez "*Validation of an efficient multibody vehicle dynamics formulation for Automotive Testing Frameworks based on Simulation*", in IEEE Access **(Under review)**.

1.5.2 Conference publications

C1 **A. Parra**, A. Zubizarreta and J. Pérez, "*An Intelligent Torque Vectoring performance evaluation comparison for electric vehicles,*" 2018 15th International Conference on Control, Automation, Robotics and Vision (ICARCV), Singapore, 2018, pp. 343-348.

C2 **A. Parra**, A. Zubizarreta and J. Pérez, "*A comparative study of the effect of Intelligent Control based Torque Vectoring Systems on EVs with different powertrain architectures,*" 2019 IEEE Intelligent Transportation Systems Conference (ITSC), Auckland, New Zealand, 2019, pp. 480-485.

C3 **A. Parra**, A. Zubizarreta and J. Pérez, "*A novel Torque Vectoring Algorithm with Regenerative Braking Capabilities,*" IECON 2019 - 45th Annual Conference of the IEEE Industrial Electronics Society, Lisbon, Portugal, 2019, pp. 2592-2597.

C4 **A. Parra**, D. Cagigas, A. Zubizarreta, A. J. Rodríguez and P. Prieto, "*Modelling and Validation of Full Vehicle Model based on a Novel Multibody Formulation,*" IECON 2019 - 45th Annual Conference of the IEEE Industrial Electronics Society, Lisbon, Portugal, 2019, pp. 675-680.

C5 **A. Parra**, A. Zubizarreta , M. Diez , J. Corral , C. Pinto, "*Fuzzy Traction Control System for Electric Vehicles,*" 15th EAEC European Automotive Congress 2017.

C6 **A. Parra**, M.Dendaluce, A. Zubizarreta and J. Pérez, "*Novel Fuzzy Torque Vectoring Controller for Electric Vehicles with per-wheel Motors,*" JJAA2017 - Jornadas de Automática, Gijón, Spain, 2017.

C7 **A. Parra**, A. Zubizarreta and J. Pérez, "*Torque Vectoring System based on Intelligent Control Techniches for Electric Vehicles with per-wheel motors,*" JJAA2018 - Jornadas de Automática, Badajoz, Spain, 2018.

C8 **A. Parra**, A. Zubizarreta and J. Pérez, "*Novel Fuzzy Torque Vectoring Controller for Electric Vehicles with per-wheel Motors,*" JJAA2019 - Jornadas de Automática, Ferrol, Spain, 2019.

C9 **A. Parra**, A. Zubizarreta and J. Pérez, "*Estrategias de Torque Vectoring en Vehículos Eléctricos: Una revisión del Estado del Arte,*" SAAEI 2019 - Seminario Anual de Automática y Electrónica Industrial, Córdoba, Spain, 2019.

Torque Vectoring Algorithms: State of the Art

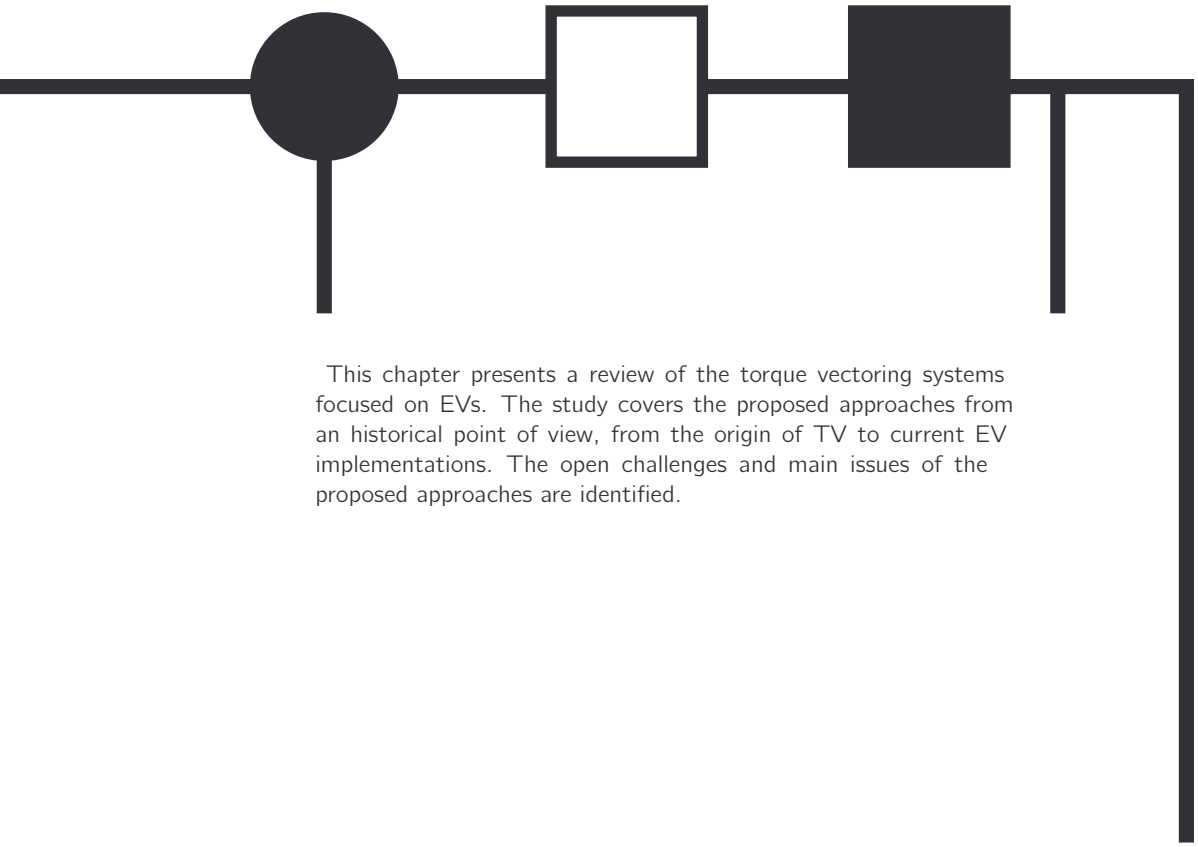

This chapter presents a review of the torque vectoring systems focused on EVs. The study covers the proposed approaches from an historical point of view, from the origin of TV to current EV implementations. The open challenges and main issues of the proposed approaches are identified.

2- Torque Vectoring Algorithms: State of the Art

2.1 Introduction

Torque Vectoring was first introduced in the 1990s to enhance the dynamics of vehicles. However, the introduction of EVs, the possibility of multi-motor topologies and the need for increasing the range of current EVs have increased the interest in this approach in the last years.

In this section, the most important TV approaches proposed in industry and academia are analysed in detail. First, a brief introduction to the fundamentals of vehicle dynamics is presented, which introduces the most important concepts and terminologies used on the rest of this Ph.D. Thesis. Then, a brief historical review on the vehicle dynamics control systems used in the literature is presented. Moreover, TV approaches proposed for EVs are analysed, detailing those considering efficiency in their formulations. Due to its relevance in TV systems, a brief review of tyre forces estimation is included in the latter subsection. Finally, the most important ideas are summarized, and the key open issues regarding TV approaches highlighted.

2.2 Vehicle Dynamics Fundamentals

The main objective of this section is to provide a brief introduction to vehicle dynamics and torque vectoring fundamentals. In addition, the concepts and terminology used in the next sections and chapters are presented.

2.2.1 Vehicle Coordinates System (ISO 8855)

In this thesis, the vehicle coordinates system defined in the ISO 8855 standard [36] is used. The axis associated with this coordinate system are shown in Figure 2.1.

This reference system has its origin in the centre of gravity (CoG) of the vehicle. The longitudinal dynamics are reflected in the x-axis, while lateral and vertical dynamics are reflected in the y and z-axis, respectively.

The orientation of the vehicle is defined by three angles defined in the Roll-Pitch-Yaw convention: the roll angle ϕ is associated to the x-axis angle; the pitch angle θ is associated to the y-axis; and the yaw angle ψ, is associated to the z-axis. For example, yaw moment (M_z) is the torque along the vertical axis, while the yaw rate ($\dot{\psi}$) is the vertical axis angular speed. This angle convention is maintained through all the thesis.

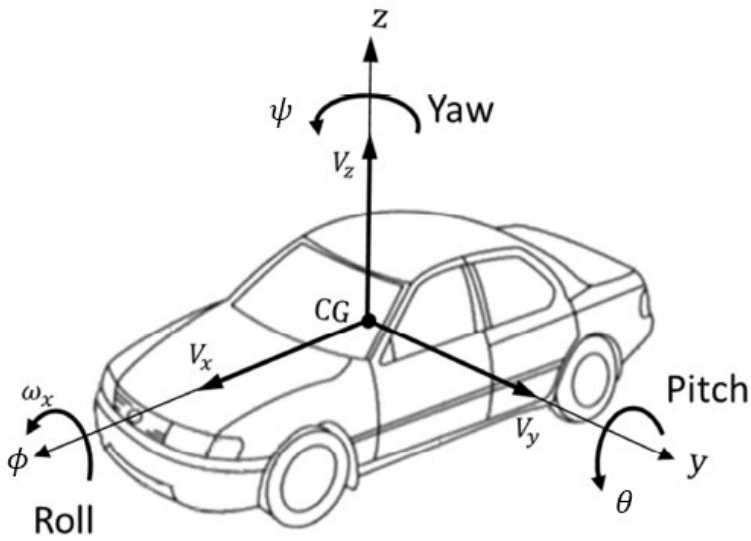

Figure 2.1: ISO 8855 [2]

2.2.2 Tyre Forces and Moments

Tyre forces are generated in the tyre contact patch due to the vehicle motion. The resultant force will determine how the vehicle is moving and can be split into three components (see Figure 2.2): the longitudinal force F_x (generated by traction and braking forces and rolling resistance), the lateral force F_y (generated when the vehicle is turning) and the vertical force F_z (generated by vehicle mass and roll and pitch dynamics). In the same way, M_y and M_z represent the moments along tyre's y-axis and z-axis. On the other hand, V represents the total speed, V_x the longitudinal speed, α the slip angle (see Section 2.2.3), ω the angular speed and r_f, r_e and r the free unloaded radius, the effective radius and the loaded radius, respectively.

2.2.3 Tyre Slip and its effect on cornering

Tyre slip in vehicle dynamics is the relative motion between a tyre and the road surface, where it is moving on. This slip can be generated either by the tyre's rotational speed being greater or less than the free-rolling speed (usually described as longitudinal slip) or by the tyre's plane of rotation, being at an angle to its direction of motion (referred to as lateral slip).

This way, the following concepts are defined:

- Longitudinal slip: also known as slip ratio,

$$\kappa = -\frac{V_x - r_e\Omega}{V_x} \tag{2.1}$$

- Lateral slip: also known as slip angle

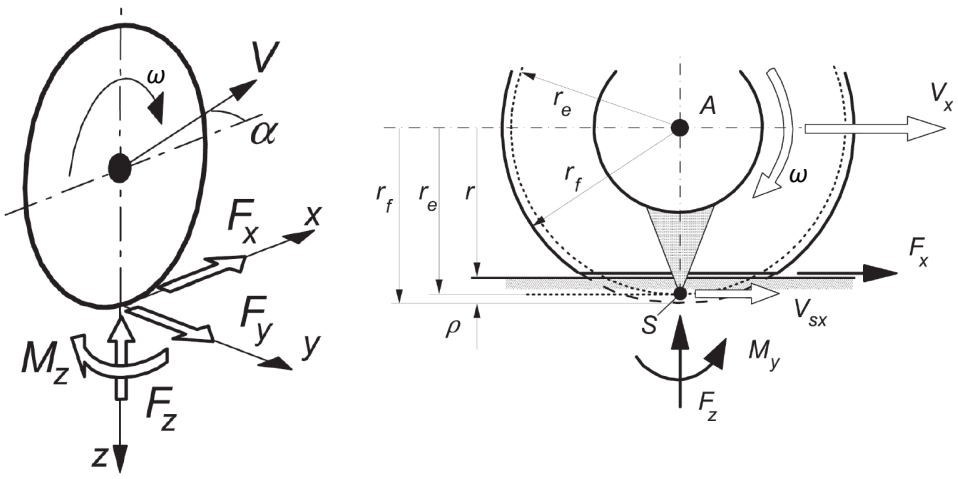

Figure 2.2: Slip angle and force and moment positive directions [3]

$$\alpha = -\arctan\left(\frac{V_y}{V_x}\right) \tag{2.2}$$

Tyre forces and the slip phenomenon have a direct effect on vehicle cornering. In this sense, a relevant variable is the so-called sideslip angle (β). This is the angle between the direction in which the chassis is pointing and the direction in which it is travelling (see Figure 2.3).

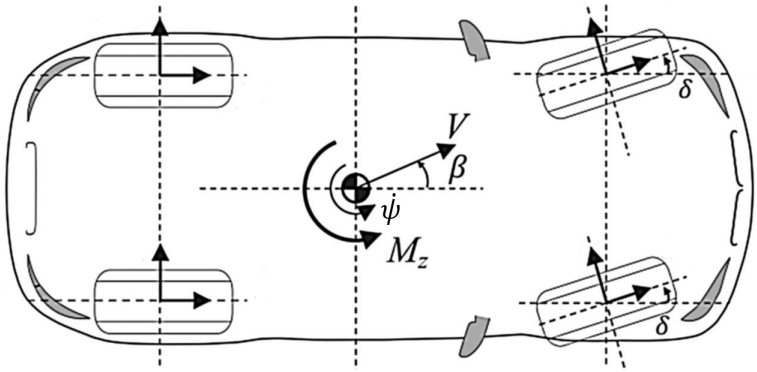

Figure 2.3: Vehicle diagram

This angle is traditionally used to define two cornering behaviours in vehicle dynamics: understeering and oversteering (Figure 2.4). Understeering is understood as

a condition where, while cornering, the front tyres begin to slip first. Since the front tyres are slipping and the rear tyres have grip, the vehicle will turn less than if all tyres had grip.

Oversteer is the opposite behaviour. This is, when the rear tyres lose more grip than front tyres, causing the rear part of the vehicle to slide towards the outside of the corner, thereby creating a feeling that the car is trying to spin.

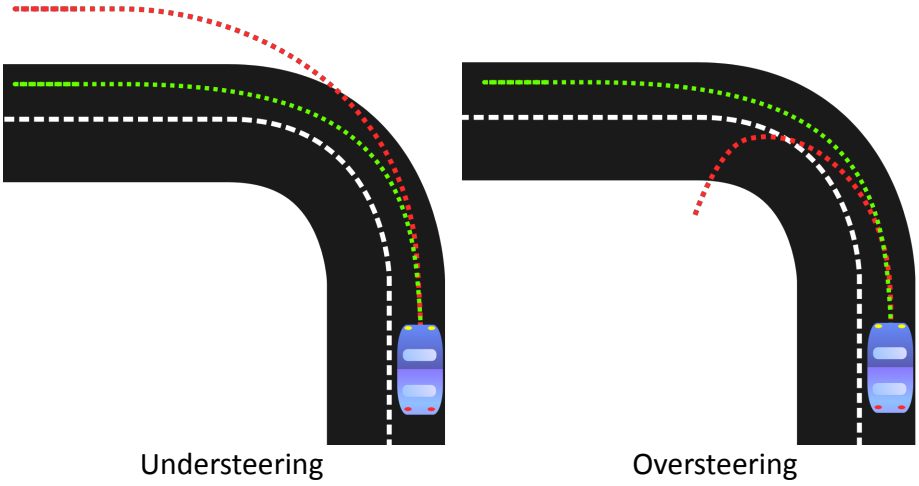

Figure 2.4: Understeering and oversteering [4]

Another important term in vehicle dynamics is the so-called understeering gradient (K). The understeering gradient is defined as the derivative of the front tyres average steer angle for the lateral acceleration imposed to the vehicle at its centre of gravity,

$$K = \frac{\partial \delta}{\partial a_y} \tag{2.3}$$

This parameter evaluates the tendency of the vehicle, in steady-state cornering, to understeer (vehicle demands higher steering angles to keep the same curve radius at higher speeds) or oversteer (vehicle demands lower steering angles to keep the same curve radius at higher speeds). Figure 2.5 shows the understeering gradient, where the neutral steer depends only on the curve radius and not on the vehicle speed.

2.2.4 Increasing Cornering Performance using proper tyre forces distribution

Once that the aforementioned terms have been explained, a brief introduction on the cornering performance enhancement through tyre forces distribution is detailed in this subsection.

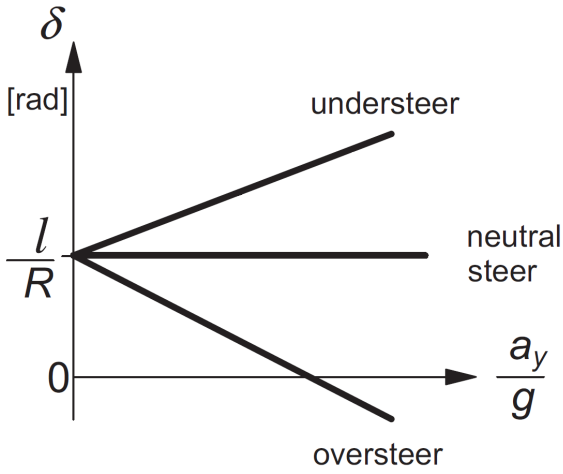

Figure 2.5: Understeering Gradient [3]

From the aforementioned definitions it can be understood that tyre forces directly affect the cornering performance of a vehicle thanks to the lateral force and yaw moment generated through the force distribution. The evaluation of the vehicle cornering performance (see Figure 2.6) is usually carried out through the analysis of the trend of the steering angle, δ, as a function of the vehicle lateral acceleration, a_y (this is, the understeering gradient K, explained in subsection 2.2.3).

In particular, the vehicle's response for a steering input is linear within a certain lateral acceleration threshold, which is usually about 0.5 g at constant vehicle speed [5]. Beyond this threshold value, the response becomes and remains nonlinear until the maximum lateral acceleration of the vehicle, i.e. its steady-state cornering limit, is reached (see the black solid curve in Figure 2.6).

The two dashed curves in Figure 2.6 represent possible targets that can be achieved through the implementation of tyre forces distribution algorithms. For instance, the linear region can be extended above the lateral acceleration limit of 0.5 g (see the green dashed curve in Figure 2.6). Also, the understeer gradient can be reduced in order to enhance vehicle responsiveness (see the blue dashed curve in Figure 2.6). Finally, the maximum level of lateral acceleration can be increased as is shown for both controlled vehicles of Figure 2.6.

In conclusion, an optimal tyre forces distribution can effectively improve the cornering performance of vehicles in several ways. This optimal distribution can be achieved controlling wheel torques, which is achieved by the use of lateral dynamics control systems. Additionally, not only understeering can be reduced, but also oversteering in stability loss situations. In the next section a deep review of vehicle dynamics control systems from a historical point of view is provided.

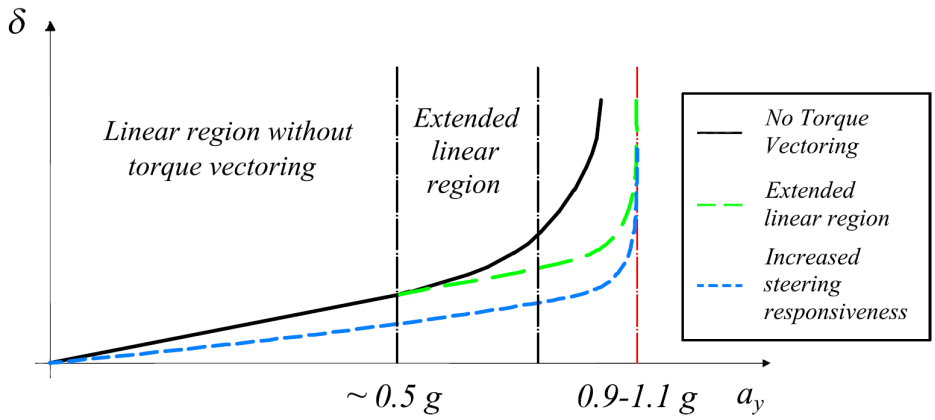

Figure 2.6: Understeering behaviour improvement thanks to TV strategy [5]

2.3 An overview on Vehicle Dynamics Control

2.3.1 Origins

The first approaches in vehicle dynamics control systems were proposed in the 80s and were focused on controlling each wheel, more specifically their slip, both in braking (ABS) and traction conditions (TCS) [37]. Their success opened the way to more complex approaches that considered the dynamics of the vehicle as a whole.

Later, in the mid-1980s, the 4 Wheel Steering (4WS) and semi-active/active suspension systems were introduced [25]. However, due to their high maintenance and production costs, they were difficult to justify for mass production, and their implementation was limited to a few vehicle models.

The increase of computational power during the 1990s, allowed for more studies in the lateral vehicle dynamics control systems field, focusing mainly on left-to-right tyre force distributions, since at that time most vehicles had either rear or front tractive wheels. Amongst these proposals, the Direct Yaw Control system (DYC) [38] was one of the most promising ones, as its objective was to control the vehicle yaw motion through the aforementioned tyre forces distribution.

This work provided several important results regarding the importance of the sideslip angle β for the stability in cornering conditions, especially in combined cornering and acceleration/braking conditions. This way its was demonstrated that the available yaw moment M_z for a specific steering angle decreases when high sideslip angle values β exist (Figure 2.7). Moreover, this study indicated that the yaw moment M_z under steady-state cornering could be expressed as a function of the longitudinal and lateral accelerations. Thus, through the use of an external yaw moment, the influence of acceleration and deceleration on the vehicle's manoeuvrability could be minimized.

The DYC approach was applied on an All-Wheel Driven (AWD) vehicle where this yaw moment was expressed as a distribution of the traction and braking forces on the

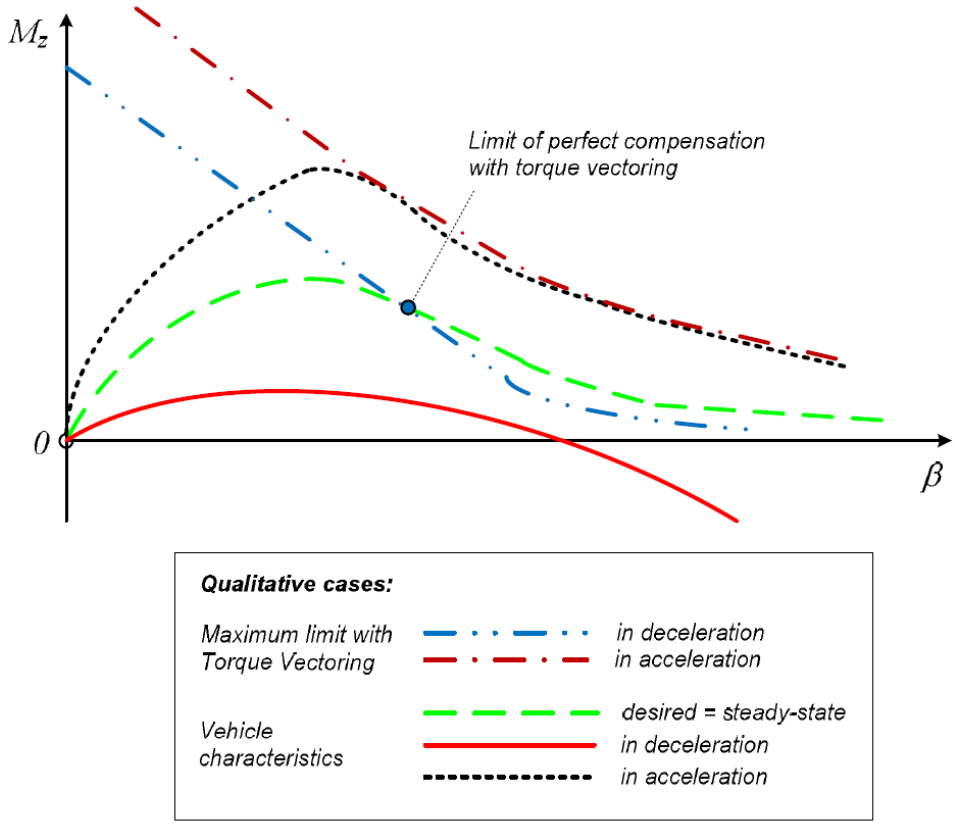

Figure 2.7: Stabilizing yaw moment as a function of vehicle sideslip angle in conditions of constant velocity and vehicle acceleration / deceleration (torque vectoring on the rear axle) [5]

rear wheels, while the front-to-rear distribution was kept constant. The simulation and experimental results showed the validity of the method, paving the way for the domination of braking-based stability systems by the end of the 90s and setting the foundations for what today is known as Torque Vectoring.

From a historical point of view, three main DYC strategies have been developed (Figure 2.8), being the Torque Vectoring the most recent of them [6]:

- Braking Based Stability Systems: These approaches started in the late 1980s and consisted in modifying the resulting yaw moment of the vehicle by creating a difference in the braking forces of the left and right side of the vehicle. This strategy could easily be implemented on vehicles that featured ABS or TCS [37].

- Lateral Torque Distribution Systems: The implementation of active differentials

allowed splitting the engine torque between the left and right wheels, resulting in a difference in the driving torque between them.

- Torque Vectoring: These approaches can transfer torque from the left to the right wheel and vice versa, as to create a braking torque on one wheel while transferring the same amount as a driving torque to the opposite wheel.

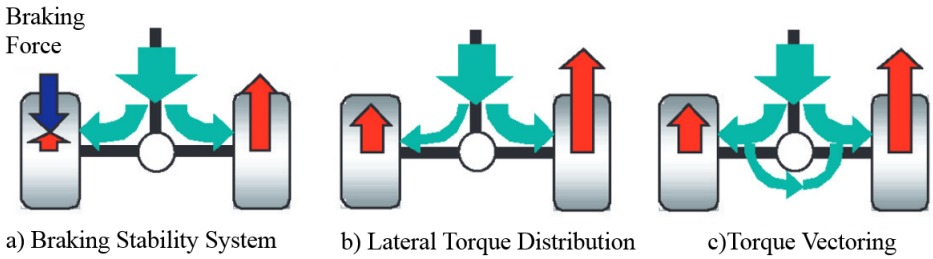

Figure 2.8: Various types of direct yaw moment control [6]

The aforementioned approaches will be analysed next in detail.

2.3.2 Braking Based Stability systems

As previously stated, the first approaches for vehicle stability improvement made use of vehicle's braking system, as the technology to control the braking torque at each wheel independently was already implemented in these vehicles.

Under this category the most successful vehicle dynamics control system in the history of automotive industry can be found: Bosch's Electronic Stability Program (ESP) [39]. While Shibahata et al. [38] analysed the effect of a corrective yaw moment on the dynamics of the vehicle across the full range of lateral acceleration, the engineers at Bosch focused only on the limit handling cases. The ESP concept was first introduced in [40], pointing out that since vehicle instability at its handling limit was caused by the deteriorating effect of large sideslip angles, it was necessary to control the sideslip angle along with the yaw motion of the vehicle. For that purpose, the ESP controlled the whole vehicle's yaw moment by manipulating the individual wheel slip by using the existing hardware for ABS and TCS [26].

In parallel, other researchers were focused on the integration of a differential braking strategy with an Active Front Steering (AFS) strategy [41] to extend the operation of the system to the whole range of lateral acceleration. An example is the work proposed in [42], where a H∞ controller is proposed for this purpose. The controller uses AFS and the differential braking to follow yaw rate and sideslip angle references, while the driver steering wheel angle command is modelled as a disturbance. It has to be noted that, as vehicle yaw rate can be easily measured by a gyroscope or Inertial Measurement Unit (IMU) and is directly related to the Yaw Moment M_z, usually this variable is used in this kind of systems for its proper performance. Another robust control based approach is proposed by [43], where a

Sliding Mode Controller (SMC) is designed to control both yaw rate and sideslip angle while taking into account variations in the longitudinal dynamics.

These aforementioned works have demonstrated that the use of brakes for yaw moment generation is effective across a wide range of vehicle operating conditions. In particular, lateral braking control is very effective when the vehicle is at its handling limit conditions, and it is widely used in these situations to ensure stability. However, placing the braking system in the centre of a vehicle dynamics control system has a deteriorating effect on the performance aspect of the vehicle as perceived by the driver [6] [44], as it creates a negative feeling due to deceleration of the vehicle [45].

2.3.3 Lateral torque distribution

Although ESP remains the preferred stability control solution due to its quick and reliable action, the negative feeling due to the braking of the vehicle in non-limit conditions led to the search of alternatives. In the late 1990s, systems that enabled lateral motor torque distribution were proposed. The basic idea was to freely split the engine's torque between the left and right wheels so that a yaw moment could be generated allowing for the correction of understeer or oversteer situations.

In this category, the most popular solutions are mainly based on active differentials which can regulate the direction of the torque towards the left or right wheels under both limit and sub-limit conditions. Honda's Active Torque Transfer System (ATTS) [46] is considered the most successful example, with the system showing better stability and handling during the combined conditions of cornering and acceleration/deceleration [24].

The main drawback of these proposals is their inability to generate a corrective yaw moment when the engine torque input is zero [47], which is a clear disadvantage during cruising or deceleration [6]. Moreover, they are expensive to develop and produce, which limited their implementation.

2.3.4 Torque Vectoring

To be able to perform a torque distribution in any condition, that is, regardless of the engine's output torque, Torque Vectoring (TV) based approaches were proposed in the late 1990s. Contrary to the aforementioned techniques, in TV systems the torque can be transmitted from the left wheel to the right wheel, and vice versa, to generate an amount of braking torque on one wheel while generating the same amount of driving torque on the other wheel by using active differentials which feature a clutch mechanism at either side. Therefore, it is possible to generate the yaw moment at any time regardless of the engine's torque, avoiding any conflict with the driver's acceleration and braking commands.

An example of a commercial implementation in this category is the *Mitsubishi Active Yaw Control System* (AYC) installed on the 1996 Mitsubishi Lancer Evolution IV [48], along with its subsequent variant, the Super AYC [6]. Following its basic operating principle, torque vectoring is achieved by engaging the right or left a clutch

of the differential, with the coupling of the clutches being regulated by an advanced feedback controller.

Torque Vectoring also allows considering other torque distributions when the vehicle powertrain topology allows it. In particular, in the case of All-Wheel Driven (AWD) vehicles, the possibility of performing front-to-rear tyre forces distribution through torque split between axles was first considered. With the increased popularity of the Sport Utility Vehicle (SUV) segment in the turn of the century, interest in this area aroused, with an increased number of related works.

Results demonstrate that this approach can also help to control the vehicle's yaw motion, as it can modify its understeering characteristics. Piyabongkarn [44] [49] showed that if torque is transferred from the front to the rear wheels of the vehicle, then, oversteering is induced.

However, the approach is not as effective as left-to-right torque distribution. An early analysis from Motoyama [50] shows that front-to-rear has a clear lower potential than left-to-right torque distribution in improving the cornering response of a vehicle. These results were later confirmed by more recent works, motivated by SUV popularity [28] [51] [52].

Finally, full torque distribution was analysed in [6] for AWD vehicles. In this work it is demonstrated that torque distribution to all wheels is the best solution compared to a Front Wheel Driven (FWD) or Rear Wheel Driven (RWD) approaches if the generated distribution is appropriately carried out. However, as AWD vehicles are not widely spread, and their typical applications are all-terrain vehicles, in which dynamic performance on regular roads is not the priority, the commercial application of these TV approaches are very few.

Nevertheless, the interest on TV approaches for AWD vehicles is prone to change due to the introduction of a new generation of vehicles focused on sustainability: electric vehicles (EVs). These provide exciting new possibilities in terms of powertrain topologies, as multi-motor layouts are easy to implement, and electric motor control allow further possibilities to develop novel vehicle dynamics control systems.

2.4 Torque Vectoring Algorithms for EVs

In recent years, environmental issues such as pollution and global warming have encouraged researches on highly energy-efficient systems. In this context, transport is one of the sectors with a higher contribution to greenhouse gas (GHG) emissions, with up to 27% of the global CO_2 emissions [53]. Particularly, road transport represents 75% of the total transport emissions [54–56]. For this reason, the automotive industry is actively involved in the reduction of such pollutants. The electrification of road transport is opening new opportunities and challenges to the mechanical, electronics and control engineers in the automotive industry [57–59].

Although there are clear advantages for using electric powertrains so as to achieve a reduction of pollution emissions, there are still some open issues regarding their implementation. From vehicle dynamics point of view, certain challenges arose when the powertrain is exchanged from a conventional Internal Combustion Engine (ICE) to

an electric motor. The most important ones are the increased sprung mass, packaging constraints (mainly related to the necessary inclusion of the battery) and, in case of in-wheel motors, also the increased unsprung mass and suspension packaging. Nevertheless, for this last case, in particular, the powertrain architecture is greatly simplified with less mechanical parts which offers further gains in terms of vehicle's overall packaging [60].

Several studies [61] have been carried out analysing the impact of the EV architecture on the overall vehicle dynamics in comparison with traditional ICE vehicles. The results reveal that the increase in the sprung mass due to the extra load from the batteries can impact roll stability, ride vibration and comfort while the increase in the unsprung mass in the case of in-wheel motors makes the vertical wheel motion control more challenging. The use of in-wheel motors may create even further problems, such as the re-design of the steering system and suspension kinematics. Besides, in-wheel motors powertrains may results in a lower unsprung mass natural frequency, bringing it undesirably close to the frequency range that is most sensitive for the human body in the vertical direction (4-8 Hz) [62]. Finally, regenerative braking functionality needs to be properly studied, as the overall braking performance needs to appropriately blend the regenerative braking with the existing hydraulic brake system, in order to provide the exact braking force demanded by the driver while vehicle's handling and balance are not disturbed.

When considering vehicle dynamics control solutions, the same approaches detailed in the previous section (TCS, ABS, ESP and DYC) can be applied. However, thanks to the characteristics of electrified powertrains the distinction between the different situations (traction, braking and cornering) can be eliminated, and optimal performance in every condition can be achieved using only one type of actuator, the electric motor. This is mostly possible due to the possibility of using the motor in either motor or generator mode with an almost equal efficiency. Additionally, they present other advantages over conventional drivelines, such as extremely quick and accurate response and high energy efficiency of up to 90% [63] [64].

Besides, as detailed in the aforementioned section, the use of electric motors open a wide set of possibilities regarding the powertrain topology (see Figure 2.9). Multi-motor ones can be easily implemented and can provide an improvement on the vehicle handling characteristics along the whole range of vehicle operation, combining functionalities like the ESP, ABS/TCS and TV. In this sense, a large progress in TV systems has been achieved in the last decade.

In the next sections, the typical structure of torque vectoring strategies for multi-motor EVs will be detailed, and the different torque vectoring strategies proposed in the literature analysed.

2.4.1 General Structure of a TV controller for EVs

Figure 2.10 shows the structure of a typical TV controller for EVs with multiple motors [65]. It consists of three layers:

1. A reference generator, which provides the target dynamic behaviour of the

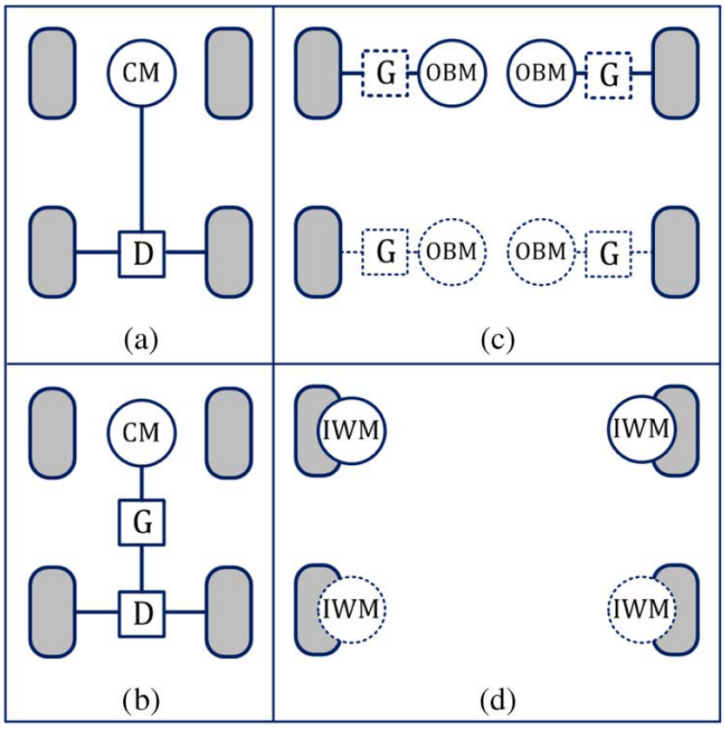

Figure 2.9: Powertrain architecture of full electric vehicles. CM—central motor, OBM—on-board motor, IWM—in-wheel motor, G—gearbox, D—differential gear. Variants: (a) Direct central; (b) central with transmission; (c) on-board; (d) in-wheel. Variant (c) can have either direct drive or gearbox transmission. Variants (c) and (d) can have two- and four-wheel-drive implementation [7]

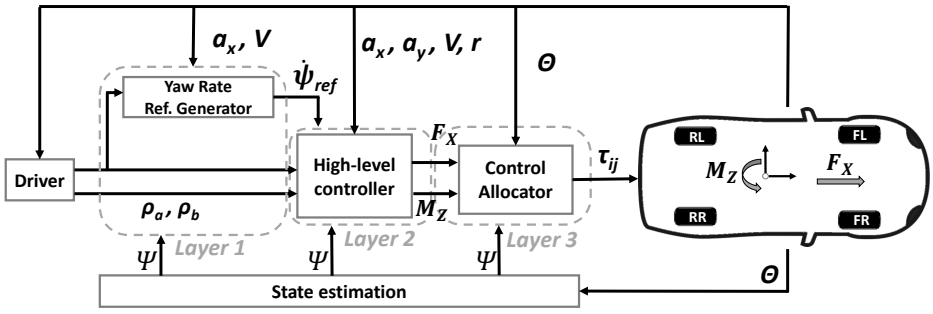

Figure 2.10: Typical TV structure for EVs

vehicle. This reference (for instance, the reference yaw rate ($\dot{\psi}_{ref}$)) is calculated by considering the driver inputs (steering wheel angle (δ)) and the vehicle states (e.g. vehicle speed (V), longitudinal acceleration (a_x)).

2. A high-level controller, which generates the overall traction/braking force demand (F_X) and yaw moment (M_z) demand, considering the reference values generated in Layer 1, the driver inputs (steering wheel angle (δ), pedals position (ρ_a and ρ_b)) and the vehicle states (e.g., vehicle speed (V), longitudinal and lateral accelerations (a_x, a_y)).

3. A low-level controller (or control allocator), which calculates the reference torques (τ_{ij}) for the individual wheels or motors considering different vehicle states and parameters (Θ) or estimated state or variables (Ψ), such as tyre forces.

Note that in addition to these three layers, a set of State Estimators could be required, which are common to all layers. This set of estimators for the variables of the vehicle are required when the target variables are difficult to measure (or even impossible). In particular, the knowledge of tyre forces is of interest in several TV approaches, which requires proper estimators, as detailed in Section 2.4.4.

The aforementioned three layers can be designed considering only the vehicle dynamics behaviour as well as other aspects such as energy efficiency or power consumption. In the following subsections, the TV solutions proposed for EVs will be detailed, classified depending on whether energy consumption is considered or not.

2.4.2 TV approaches focused on enhancing vehicle handling

In this section, the approaches that are focused on enhancing vehicle dynamics behaviour, and do not consider power consumption, are detailed.

In these approaches, the reference generator (Layer 1) usually only takes into account the desired understeering characteristics [66]. This reference is then compared with the measured yaw rate (by an Inertial Measurement Unit (IMU)), in order to calculate the desired direct yaw moment [16]. Additionally, the vehicle sideslip angle is also considered in this layer, as it provides relevant information about the vehicle dynamic state. As the measurement of this latter variable requires very expensive sensors, it is usually estimated [67] [68]. Typical approaches to estimate the sideslip angle with a good level of accuracy are the use of an Extended Kalman Filter (EKF) or a neural network (NN) [69].

Different control solutions have been proposed in the literature for the high-level controller (layer 2). The simpler ones, such as those based on Proportional Integral Derivative control (PID) [16], demonstrate good performance in steady-state conditions. More complex control techniques, such as Linear Parameter Varying Control (LPV) [70], Sliding Mode Control (SMC) [71] [72] or Nonlinear Model Predictive Control (NMPC) [73] provide better results both in steady-state and transient conditions. However, the latter approaches usually imply higher computational cost and present higher model dependency, limiting their performance if proper modelling and

identifications are not carried out. Hence, with the purpose of reducing model dependency while maintaining the performance, Intelligent Control Approaches, such as Neural Networks [74] or Fuzzy logic systems [75], have been considered. These latter approaches usually require less computational cost and are able to handle multiple objectives easily [76].

The Control allocation (layer 3) is only active in AWD vehicles, as it is possible to distribute the torque between the front and the rear axle. If energy consumption is not considered, the control allocation is usually carried out attending to variables related to the tyres, such as the slip ratio [77] or tyre forces. In particular, one of the most effective methods is to estimate (using the state estimation block in Figure 2.10) the tyre vertical forces, as the tyres with a greater load will be able to transmit more torque to the road [78, 79]. A detailed analysis of the tyre forces estimation is carried out in Section 2.4.4.

In summary, the TV approaches that only consider vehicle dynamics behaviour have reached a good level of maturity, having a good adoption in the automotive industry. For this reason, currently, most of the works related to TV Systems are focused on strategies that include other terms. In particular, as driving range is one of the main concerns in EVs and one of the most important obstacles for their widespread adoption, there is an increasing number of works that include energy efficiency terms in the TV control approach. These approaches will be detailed in the next section.

2.4.3 TV approaches focused on enhancing vehicle handling and energy efficiency

The wheel torque distribution has an important effect on the powertrain losses, which include the losses related to the inverter, electric motor and transmission (if present), as well as on the longitudinal and lateral tyre slip power losses [80] [81]. Hence, a TV strategy can have an impact not only on vehicle dynamics but also on energy efficiency.

The implementation of energy-efficient TV approaches can be carried out considering the different layers detailed in Section 2.4.1. Regarding the reference generation layer (Layer 1), recent experimental and simulation-based research works, see [80] [81] and [82], show that, during cornering, the level of vehicle understeer (typically decided by Layer 1 of the TV control structure) has at least an equivalent impact on the energy consumption as the control allocation algorithm (layer 3). These preliminary studies discuss the potential benefits of energy-efficient direct yaw moment characteristics on powertrain and tyre slip power losses and obtained through suboptimal rule-based or open-loop algorithms. For example, Kobayashi et al. [81] demonstrate that the minimization of the tyre slip power losses occurs if the tyre slip velocity vectors (which are directly related to tyre forces) are the same at the four vehicle corners. Hence, in this work is demonstrated that to minimize the tyre slip power losses the knowledge of tyre forces is crucial. In [65], De Filippis et al. obtain an analytical expression of the energy-efficient direct yaw moment in terms of powertrain power losses, implying the activation of an increasing number of powertrains with increasing torque demand. In case of redundant optimal solutions from the powertrain

power losses point of view, rules are set to select the best option in terms of tyre slip power losses. A quasi-static vehicle modelling approach is adopted in [83] to derive rules for the calculation of a feedforward energy-efficient direct yaw moment controller as a function of torque demand, with a feedback contribution intervening only in safety-critical conditions.

The previous studies show the energy-saving potential of shaping the reference cornering response and establish the path for developing energy-efficient TV systems. Nevertheless, the main disadvantage that they present is that they are not implemented through feedback control structures, and therefore, they are not capable of compensating unexpected EV behaviour caused by the variation of system parameters or transients, as they use simplified feedforward controllers or rule-based algorithms.

To solve this issue, in the last two years there has been an increasing number of works that propose feedback TV controllers, considering energy efficiency terms that are implemented on Layers 2-3 (Figure 2.10). Generally, these works use optimization-based controllers. In [84], a hybrid MPC (hMPC) TV controller (layer 2) combined with a Multi-Objective torque distribution strategy (layer 3) that minimizes the powertrain losses in a 4WD vehicle is proposed, achieving an energy consumption reduction of 26,7% in the single lane change manoeuvre (compared to ESP method) and a 9.29% in the NEDC (New European Driving Cycle). In [85], an energy-efficient NMPC TV system is proposed. This approach only considers the powertrain power losses and tries to minimize the tyre slip power losses through a soft constraint for the slip ratio in the cost function, achieving an increment of 4.50% and 0.80% compared to [86] in energy-saving under double lane change and straight acceleration manoeuvres respectively. Finally, Zhao et al. [87] propose a LQR based stability control system, which combines a TV controller with an AFS, that minimizes tyre slip power losses, showing that in a lane change manoeuvre tyre slip power losses can be reduced up to 16%.

Due to their potential, intelligent control techniques have also been applied for developing energy-efficient TV approaches. In [88], an energy-efficient TV is presented, which combines a Fuzzy Logic-based yaw moment controller (layer 2) with a control allocation system (layer 3) that minimizes the total instantaneous output power and maximizes the tyre adhesion margin. The system has been tested through the double lane change manoeuvre in low and high friction conditions and results show that the proposed system can reduce the energy consumption up to 23% and 12%, respectively.

Both approaches, optimization-based controllers and intelligent control based systems provide advantages and disadvantages. While optimization-based controllers seem to be the most natural solution when considering energy efficiency, as several variables have to be tracked and minimized, their model dependency can cause several problems in real vehicles due to parameter uncertainties. On the other hand, controllers based on intelligent control techniques can reduce the model dependency, but their tuning becomes much more complex as many variables have to be considered. Therefore, the control technique to be used is still an open point in energy-efficient TV systems.

Hence, although it has been demonstrated that energy-efficient TV systems can effectively help to reduce the overall energy consumption, reducing both powertrain losses and tyre slip power losses, this is still an open research area. In fact, from the analysis carried out, it can be concluded that four key issues should be considered when designing an energy-efficient TV approach: First, both main power losses sources, this is powertrain and tyres, should be considered to improve efficiency. Second, generating the yaw rate reference (layer 1) considering the control allocation algorithm (layer 3) is required to prevent conflicts between the different control layers involved in the power loss management. Third, the TV approach should allow operational flexibility depending on the driving situation, i.e., prioritize energy efficiency during normal driving and vehicle safety and stability in extreme manoeuvres. Finally, if tyre power losses are considered, the estimation of the forces actuating on them is a crucial issue.

2.4.4 Tyre forces estimation

The aforementioned TV approaches require, for their operation, state variables related to the vehicle (Figure 2.10), such as the measurement or estimation of the yaw rate or the slip.

However, one of the most challenging variable to be measured are the tyre forces (see Section 2.2.2 and Figure 2.2), which some TV approaches require to operate [78–81, 83]. Note that these variables are the most significant element influencing the vehicle longitudinal and lateral behaviour [89], and are also essential for safety purposes [90, 91].

Ideally, the best solution would be to measure directly the forces generated at the tyre contact patch. According to the literature reviewed, there exist three main solutions to achieve this task: Smart tyres [92] [93], Wheel Force Transducers (WFT) [94] and load-Sensing Hub Bearings (LSB) [95] [96] (see Figure 2.11). The Smart Tyre technology is still under development [97] and current results indicate that further investigations are required before this technology can be implemented in regular tyres. WFT are still too costly to be mounted in production vehicles [98] and their use is reduced to testing activities during vehicle development stages [99]. Finally, despite some companies have developed different LSB designs, these are still not commercially available.

The limitations derived from the previous solutions have contributed to increase the interest in approaches to estimate tyre forces from measurements already available in the CAN bus of modern vehicles. This way, estimators for the tyre forces usually can be classified into two groups: those which estimate planar forces (XY axis) and those which estimate vertical forces (Z-axis).

In the literature, both model [90, 98, 100, 101] and model-less [3, 90, 102–109] approaches have been proposed to estimate the x and y tyre force components. However, these estimators are typically used for motorsport applications, but not for implementing in TV systems.

On the other hand, the estimation of the tyre vertical forces F_z provides important information for optimum torque distribution, as the tyres with more vertical force have

Figure 2.11: Pirelli smart tyres, Kistler WFT and NSK LSB

greater grip and are able to transmit more force to the road. Neglecting aerodynamic effects, tyre vertical forces can be considered a sum of the following terms: static loads, chassis inertial loads, and wheel dynamic loads. These are reflected in Eq. 2.4,

$$F_z = F_{z,st} + \Delta F_{z,road} + \Delta F_{z,ai} \quad i \in x, y \tag{2.4}$$

where $F_{z,st}$ represent the static loads, chassis inertial loads $\Delta F_{z,ai}$ are caused by the lateral and longitudinal accelerations experienced by the sprung and unsprung mass, while wheel dynamic loads $\Delta F_{z,road}$ are caused by the road disturbances.

The estimation of F_z has been carried out with two main approaches in the literature: Static and dynamic estimators. The first neglect the wheel dynamic loads ($\Delta F_{z,road} = 0$), roll and pitch dynamics ($\dot{\theta}_b, \ddot{\theta}_b \approx 0, \dot{\phi}_b, \ddot{\phi}_b \approx 0$) and assume that the weight transfer occurs as a consequence of continuous quasi-static events (see Figure 2.2). However, due to these simplifications these approaches [18, 100, 104, 110] are only suitable for steady-state conditions, and the accuracy of the estimation depends on the degree of complexity introduced in the weight transfer model. Therefore, these types of estimators are not optimal for vehicle dynamics control application, such as TV systems.

Moreover, Dynamic-based estimators can improve the vertical force estimation during transient situations, as they consider the dynamic forces interacting on the wheel, and hence, they are the most suitable ones for their application in TV systems. Traditionally, their implementation has been carried out using model-based observers. These require the parametrization of the suspension and the measurement or estimation of the roll and pitch angles. The estimation of the latter is out of the scope of this thesis and a deep discussion can be found in [111] [91] [112].

Depending on the complexity of the suspension dynamics, different approaches have been proposed in the literature. The simpler ones consider only roll dynamics, as in [90] and [98], which use a Linear Kalman filter (LKF) to estimate the total lateral load transfer. This is used as a pseudo-measurement in a second observer, based on an Extended Kalman Filter (EKF), to estimate the wheel-ground normal forces using a static approach. The observer structure is tested experimentally in a slalom test, where low errors (below 3% average) are obtained. In [78], a similar

approach is used, but the roll angle is estimated using the approach described in [91] and the longitudinal weight transfer contribution is calculated using a static approach.

Both roll and pitch dynamics are considered in [113], which is an extension of [90]. In this approach, roll and pitch angles are determined from suspension deflection sensors, the roll and pitch centres are assumed to be static, and the derivative terms of the lateral and longitudinal accelerations are modelled as random-walk variables. The observer is first simulated and then validated experimentally under dynamic manoeuvres performed on banked roads. The results show that the accuracy of the estimations is improved, from 4% to 2% average, for the cases in which only roll dynamics are considered.

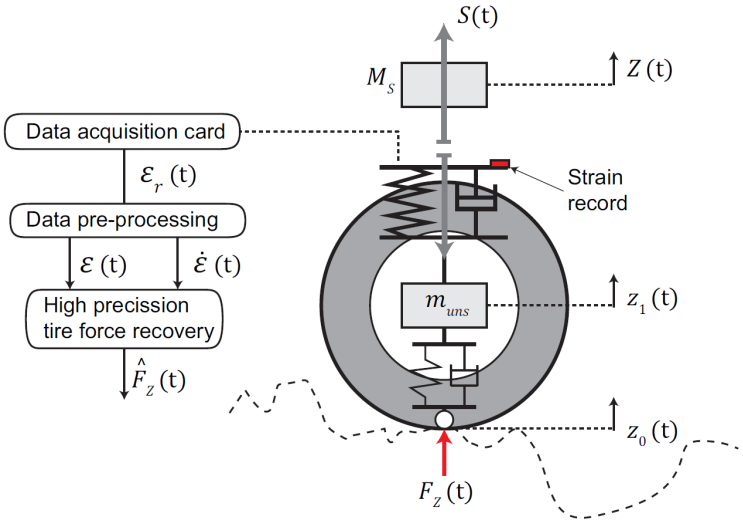

Figure 2.12: Scheme of the quarter-car model [8, 9]

The previous approaches present a common limitation as they do not consider the vertical force component due to the road disturbances. Thus, they are only suitable to estimate the tyre vertical forces when the road is smooth and severe irregularities are not present. To capture the wheel dynamic loads, it is necessary to model the relative displacement between the sprung and unsprung mass. In [9], a linear quarter-car vehicle model, is proposed to estimate the dynamic vertical loads (Figure 2.12). The suspension force $S(t)$ is assumed to be determined by measuring the elastic deformations inside or near the suspension top mounts. Then, using a linear simplified suspension dynamics model, the tyre force F_z is related to the strain measured at the suspension top mount. The observer is validated in Simulink and CarSim. Results demonstrate that the observer performs well, although some inaccuracies are seen due to the suspension system non-linearities and unmodelled longitudinal and lateral dynamics (unsprung mass and kinematic weight transfer).

In general terms, model-based observers perform better when the model complexity is increased, this is, when more dynamic effects are considered on it (roll, pitch,

weight transfer). In the particular case of TV, proper approximation during transient situations is required, as one of the most important situations where TV systems have to act are in emergency manoeuvres. However, two main issues arise when considering these approaches. First, the need to model and characterize properly the suspension dynamics of the vehicle; and second, the need to measure or estimate suspension related variables such as roll and pitch states, which is not a trivial task.

Due to these issues, in the last decade Artificial Intelligence-based estimators have been proposed, such as artificial neural networks (ANN) [108] or fuzzy logic [109]. These approaches do not require an explicit model to operate, but a proper experimental dataset to be trained and evaluated. Besides, due to recent advances in embedded platforms, the computational cost related to these approaches can be reduced significantly, being able to be implemented in real ECUs and fulfil real-time targets [114]. Currently, this is an open research area with big application potential for TV systems and other vehicle dynamics control approaches.

2.5 Conclusions

From the analysis carried out it can be concluded that vehicle dynamics control systems for EVs are a key element to not only enhance the vehicle dynamics performance, but also to reduce the energy consumption of the vehicle. In fact, energy-efficiency is a key issue for the Automotive Industry and one of the most active research topic in this area, as advances in this area will help to increase the widespread adoption of EVs.

Among the different vehicle dynamics control systems, TV systems are one of the most successful ones, as they allow to distribute optimally the acceleration or braking torque among the different wheels. However, designing and implementing a TV system is not trivial, as several aspects have to be considered.

First, the specific control technique has to be properly selected. Simple controllers, such as PID controllers, are able to provide good performance only in steady-state conditions. When more complex scenarios are considered, such as those where transient conditions are critical, more complex controllers are required. Two main approaches are of interest in this area: model based controllers, such as MPC, which presents high flexibility to include additional terms at higher model dependency and computational cost; or intelligent control approaches, which present proper performance with lower model dependency.

When considering handling enhancement, the consideration of the tyre forces (implicit or explicitly) is of great importance, as this knowledge allows to determine which tyres have the possibility of transmitting more force. However, measuring tyre forces is complex, typically requiring the use of estimators. Although model-based ones provide the best accuracy, their parameters are complex to identify, and some of the variables required to estimate the forces using these approaches are, again, difficult to measure. In this sense, the use of intelligent approaches to estimate tyre forces is a promising area of research.

On the other hand, when considering energy-efficiency, typically TV approaches

focus on optimizing the energy-efficiency of each control layer independently. This derives in conflicts between layers, which may reduce the overall efficiency increase of the TV approach. In this sense, the integration of several layers seems the best alternative to avoid this effect.

In addition, being tyres one of the most important elements for vehicle dynamics, they are also an important source for power losses due to slip. Hence, energy-efficient TV approaches should focus on minimizing not only the powertrain losses, but also the losses due to tyre slip. This can be carried out considering directly the power loss term in the controller, or indirectly by minimizing the slip of the wheels.

Moreover, TV response is very important in critical situations where stability is to be maintained. Although this is a key issue in the TV approaches proposed exclusively for enhancing vehicle dynamics behaviour, when energy-efficient considerations are included the TV performance in critical scenarios can be reduced. Hence, TV approaches for EVs should consider operational flexibility depending on the driving situation, i.e., prioritize energy efficiency during normal driving and vehicle safety and stability in extreme manoeuvres.

Finally, in order to be successful, implementability has to be considered when designing a TV approach. Some of the approaches with higher potential, such as MPC or intelligent approaches, can present high computational cost when more and more terms are included in the controller. However, new embedded platforms that combine different hardware devices, such as a microcontroller and a FPGA, have opened the door to the implementation of each subsystem of the controller in the most suitable device, reducing the execution time and enabling real-time performance. In this sense, proper hardware-in-the loop testing is mandatory to ensure the performance of the controller.

Taking into account the aforementioned key areas, in this PhD Thesis two TV approaches are proposed. First, an intelligent TV approach, based on intelligent control techniques and the use of an intelligent vertical tyre forces estimator (Chapter 4). This approach tries to reduce the power losses of the tyres implicitly, and provides a very low model dependency, which allows to be easily applied to different vehicles and conditions. Second, an energy-efficient nonlinear MPC TV approach which considers power losses explicitly in its formulation, combining several layers to obtain the optimum efficiency (Chapter 5).

In addition, as previously stated, implementation has also to be considered. Hence, in order to test the aforementioned approach, a complete Simulation Framework to test ADAS and vehicle dynamics control systems has been developed. This framework which enables a hardware-in-the-loop setup, is detailed first in the next Chapter, as it will be the basis for the validations in Chapters 4 and 5.

Vehicle Dynamics Simulation Framework

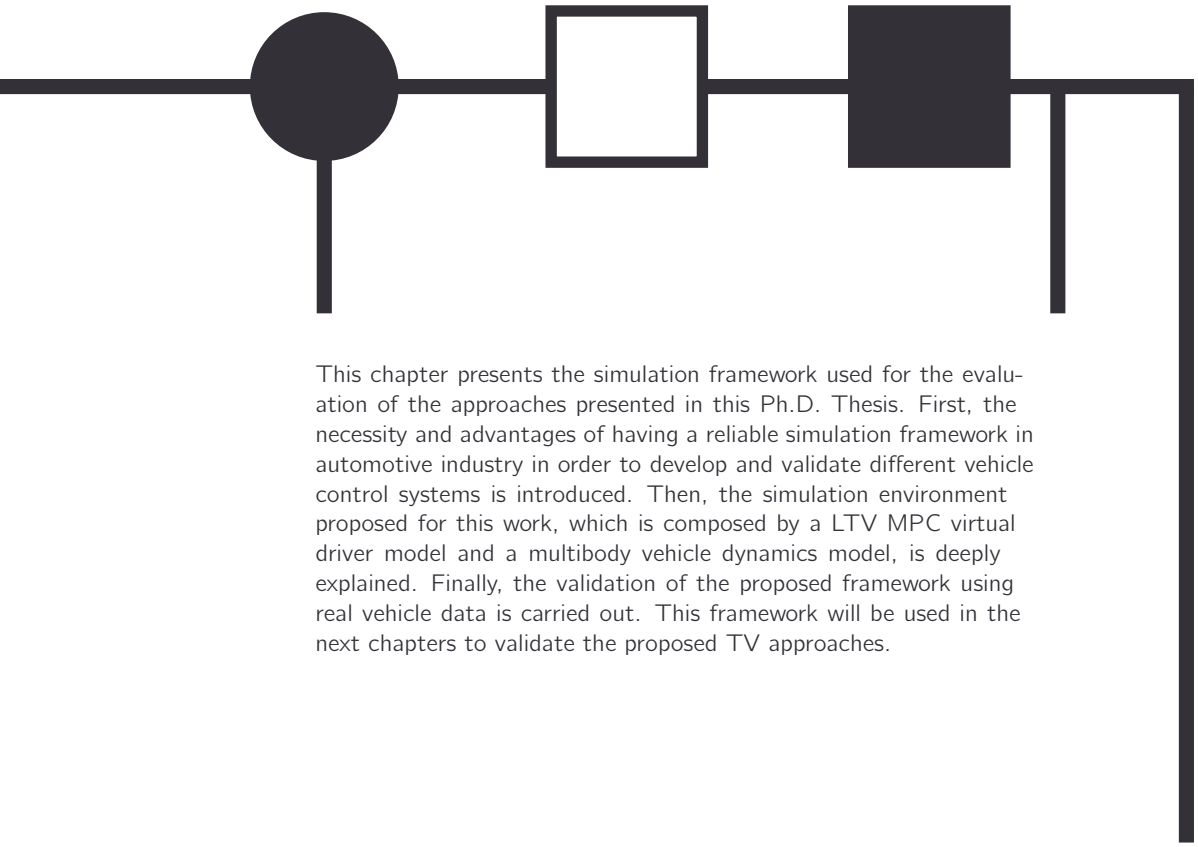

This chapter presents the simulation framework used for the evaluation of the approaches presented in this Ph.D. Thesis. First, the necessity and advantages of having a reliable simulation framework in automotive industry in order to develop and validate different vehicle control systems is introduced. Then, the simulation environment proposed for this work, which is composed by a LTV MPC virtual driver model and a multibody vehicle dynamics model, is deeply explained. Finally, the validation of the proposed framework using real vehicle data is carried out. This framework will be used in the next chapters to validate the proposed TV approaches.

3- Vehicle Dynamics Simulation Framework

3.1 Introduction

Testing and validation is a key area in the automotive industry. Each new feature and functionality, such as new TV approaches, has to be properly tested, validated and certified before their implementation in marketed vehicles, to ensure their safety and effectiveness.

However, modern vehicles are becoming more and more complex due to the increase on new functionalities such as electrified multi-motor powertrains, vehicle dynamics control systems such as TV, and automated driving (AD) features. These complex algorithms are certainly further pushing the complexity of traditional validation approaches [34, 115–117]. In fact, traditional track-based scenarios, wide-spread in the automotive industry, do not provide enough flexibility to test all possible situations that these new features can handle, and significantly increase the cost and time to market [115] [118].

Hence, the development of accurate and reliable simulation frameworks that can replicate the behaviour of real vehicles has become mandatory in the Automotive Industry. These can be used to reduce the complexity of testing and validation tasks. Besides, these frameworks can also reduce their cost and required time, by providing a more flexible development environment that can also be combined with traditional track testing.

In this context, in this Chapter, a novel vehicle dynamics simulation framework is proposed, which will be used in the following chapters to test the proposed TV algorithms. The proposed framework is based on the multibody vehicle dynamics simulator Dynacar [119] designed by Tecnalia [120]. It will consider critical situations when driving, allowing to compare in an objective way the algorithms proposed.

This Chapter is structured into two main sections. First, the proposed simulation framework for ADAS and vehicle dynamics control systems testing is presented, and its fundamental blocks detailed. Second, the framework is validated considering a real study case, a set of experimental tests and a HiL setup. This latter section will demonstrate the validity of the framework to test the TV approaches proposed in this PhD. Thesis.

3.2 Simulation Framework

The main goal of this section is to explain the structure and the subsystems that define the proposed *Vehicle Dynamics Simulation Framework*. The proposed simulation framework can be implemented in different real-time environments, such as Matlab/Simulink [121] or Veristand [122], and different hardware, such as PCs or

National Instruments PXI platforms, which allow co-simulation and hardware in the loop (HiL) testing setups. A general view of the framework is shown in Figure 3.1, in which five main blocks are identified: a Virtual Driver, a Controller block for vehicle dynamics control systems (or ADAS) implementation, a Powertrain model, the vehicle dynamics model and, finally the road/scenario block.

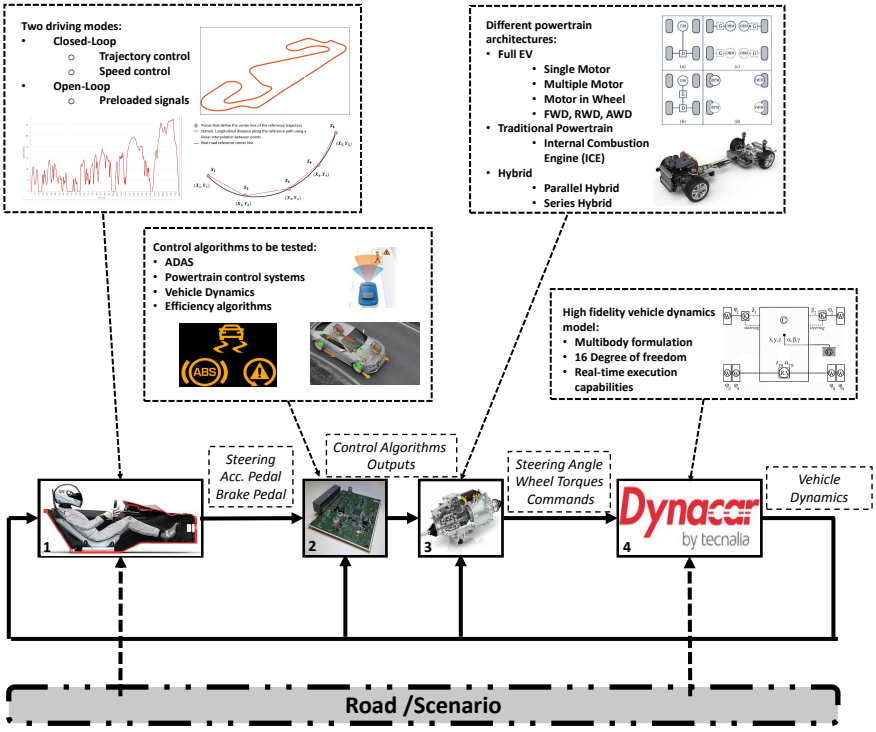

Figure 3.1: Structure of the proposed framework

The Virtual Driver block provides the steering angle and throttle/brake pedal signals. These three signals can be obtained by the use of a Virtual Driver Model, implemented using a LTV Model-based Predictive Controller (closed-loop tests), or by introducing preloaded signals (open loop tests).

An appropriate Driver Model is crucial for ensuring an objective evaluation of the simulated tests and their repeatability. It also should be able to reproduce the driver behaviour and be tuned for emulating different scenarios (sporty driving, efficient driving,...). This way, these different driving behaviours can also be tested and validated before track testing. More detailed analysis of the implementation of the Driver Model will be presented in Section 3.2.2.

The second block implements the control algorithm to be tested. In this subsystem, the desired ADAS/ADS or vehicle dynamics control system (such as TV) can be

implemented, in order to validate its performance in different scenarios before testing them in the real vehicle. The TV algorithms proposed in this PhD. Thesis (detailed in Chapters 4 and 5) have been implemented in this subsystem for testing.

The third and fourth blocks implement the vehicle to be tested. Different from other frameworks, in the proposed one the powertrain model is differentiated from the vehicle dynamics. The powertrain model will receive the control signals and generate the required torques on the tractive wheels. Note that Hybrid Vehicles and EVs permit the implementation of different powertrain architectures (internal combustion engine, hybrid powertrain, pure electric with multiple motors), hence, this structure provides flexibility when testing different powertrain configurations for the same vehicle.

The fourth block represents the vehicle dynamics model, which will define the motion of the vehicle considering the driving and braking torques calculated by the powertrain model, the steering wheel and the particular scenario loaded (the road parameters). The main goal of this block is to emulate as accurately as possible the dynamics of a real vehicle, so that the tested control approaches can be validated in a realistic scenario while ensuring real-time performance for simulation purposes. Hence, the model complexity and accuracy need to be balanced. For this purpose, a computationally efficient 14 degrees of freedom multibody dynamic model is implemented. The outputs of this block, this is, the vehicle motion and internal parameters, are used as feedback for the rest of the blocks. More detail regarding the particular multibody formulation implemented in this block is given in Section 3.2.1.

Finally, the road/scenario block, where the test to be performed and the physical environment is set. Therefore, this block provides relevant information to both the virtual driver model and the vehicle dynamics model. In particular, it provides the reference trajectory and the physical ground, respectively.

In the next sections, both the multibody vehicle dynamics model and the Virtual Driver model will be explained in more detail, as they are considered crucial elements in the developed validation framework.

3.2.1 Multibody Vehicle Dynamics Model

In the literature, several vehicle model approaches can be found. Traditionally, simple models based on analytical approaches [67, 123–125] are used when testing control approaches in real-time, as they are easy to implement. However, their accuracy is limited to certain scenarios, as they neglect lateral, longitudinal or vertical dynamics [126].

When accuracy is required in a wider set of scenarios, including those related to critical ones, the multibody formulation [89, 127] is traditionally used. A multibody model is defined as an assembly of two or more bodies imperfectly joined together, having the possibility of relative movement between them. This approach can describe more accurately vehicle dynamics, while increasing its complexity and computational cost.

To reduce the execution time, and provide a balance between computational cost and accuracy, several considerations can be implemented in the formulation, such as simplifications in the model and a proper selection of the numerical integrator [89].

In this section, the computationally efficient 14 degrees-of-freedom model presented in [127], and used for vehicle dynamics purposes in [128] is explained to describe the dynamics of the vehicle. The proposed approach is computationally efficient, allowing to be executed in real-time.

Next, the modelling approach will be detailed. For that purpose, first, the coordinates selection to describe the model will be defined. Second, the multibody formulation and the defined simplifications will be detailed. Third, the implemented tyre model will be described. Finally, the suspension and steering models will be explained.

In order to provide a more clear view of the multibody vehicle dynamics model structure, a simplified diagram is shown in Figure 3.2.

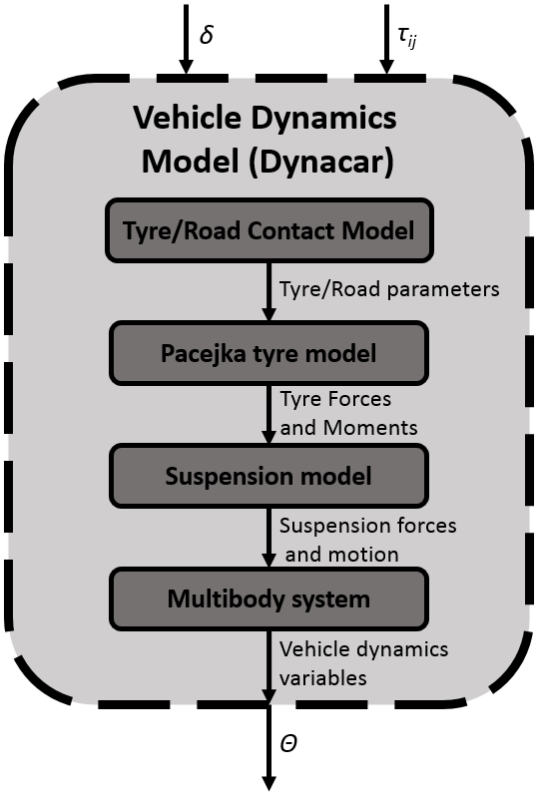

Figure 3.2: Vehicle dynamics model structure

3.2.1.1 Coordinates Selection

Since the coordinates selected have direct effects on the complexity of a multibody model, and hence, on its real-time performance, it is important to select first an appropriate set of coordinates. In this sense, two main choices have to be performed

about the type of coordinates used (independent or dependent) and the approach used to define the coordinates (global or topological approaches).

Regarding the types of coordinates, traditionally two different methods have been used in the literature: independent or dependent coordinates. Using the latter one means that the number of coordinates is equal to the number of degrees-of-freedom and is therefore minimal, leading to a more efficient simulation. However, in closed-loop systems employing independent coordinates could result in an undetermined system. On the other hand, dependent coordinates can define unequivocally the movement of a system, employing a higher number of coordinates. Nevertheless, they must be related with constraint equations, which increases the computational cost of the simulation [89].

The definition of the coordinates also impacts the complexity of the model. Global methods are used to define the system in an absolute form, being systematic to implement, but not very efficient since they lead to a high number of variables and constraint equations [10]. On the other hand, topological methods define the coordinates of each body of the system with respect to the previous one, allowing to use recursive procedures in order to obtain the motion of each body. These methods lead to a system with a minimum number of dependent coordinates [89].

The multibody approach for vehicle modelling proposed in [128], which is considered in this Ph.D. Thesis, considers an efficient topological method based on recursive techniques, which reduce the computational cost of the model [10]. Moreover, this approach models the vehicle with one coordinate for each of the 14 degrees-of-freedom considered, which avoids the need for constraint equations and optimizes the computational cost.

This way, the chassis frame presents six-degrees-of-freedom: three Cartesian coordinates of a point in the front part of the car (x, y, z), along with the three Cardan angles of the chassis for the inertial frame of reference (α β γ), are selected.

An independent suspension system is considered, with two degrees-of-freedom in each wheel: the compression of the spring $\bar{z}_i$ and the steering angle δ. Note that the suspension system can have different geometries and is typically composed of several closed loops, which makes the use of independent coordinates not advisable. To overcome this issue, the suspension mechanism is replaced by a *macro-joint* approach [128]. This method defines the kinematics of the centre of the knuckle in terms of the Cartesian coordinate for the vertical suspension displacement $\bar{z}_i$ and the steering input δ by using a table, which can be computed offline.

Finally, the last independent coordinates are the relative orientation of each wheel with respect to the knuckle, which is defined by an angle around the wheel axis, (φ_1, φ_2, φ_3, φ_4).

This makes a total of fourteen independent coordinates, which are grouped into vector $\mathbf{z}$ (See Figure 3.3). It must be noted that the steering angle δ is not included since it is an input to the model and not a coordinate itself.

$$\mathbf{z}^T = \left\{ x\ y\ z\ \alpha\ \beta\ \gamma\ \bar{z}_1\ \bar{z}_2\ \bar{z}_3\ \bar{z}_4\ \varphi_1\ \varphi_2\ \varphi_3\ \varphi_4 \right\} \tag{3.1}$$

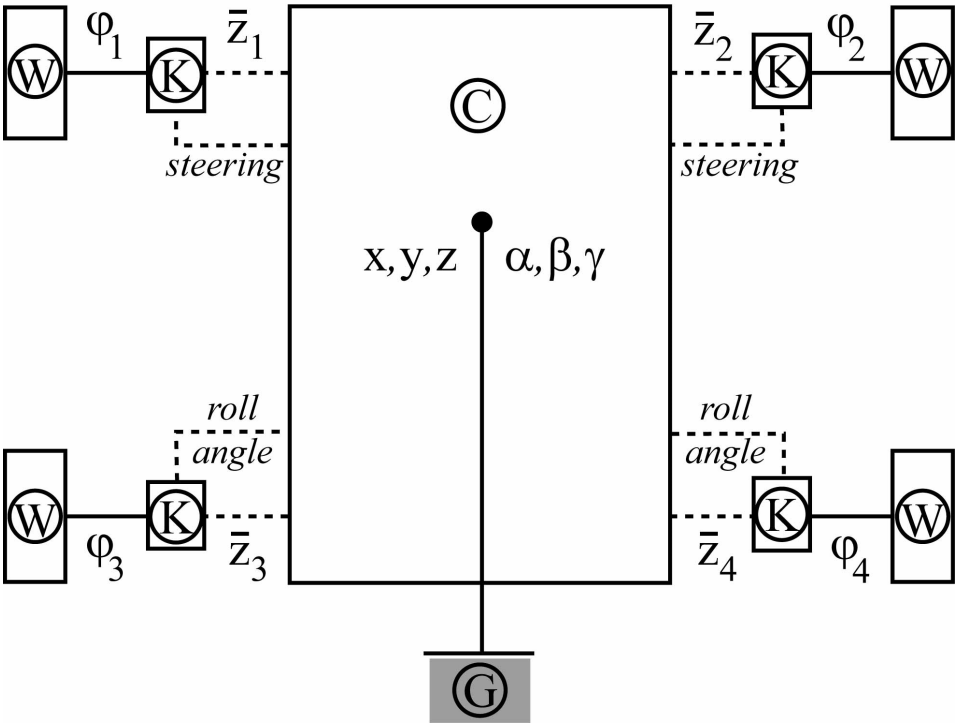

Figure 3.3: Vehicle Multibody Scheme [10]

Finally, the local reference system established for each body has been defined according to the ISO 8855 [36].

3.2.1.2 Multibody Formulation

As detailed previously, the semi-recursive dynamic formulation proposed in [10] has been used to derive the equations of motion of the vehicle model. As the **z** coordinates (Eq. 3.1) defined for the modelling are independent, no constraint equations must be considered and the equations of motion will be defined as a set of ordinary differential equations (ODEs).

However, the definition of the equations of motion in terms of the coordinates **z** (see Eq. 3.1) is not trivial. Thus, the semi-recursive formulation employs a set of the so-called body coordinates to define the equations of motion of each body. Then, the body coordinates are related with the independent coordinates **z**.

The body coordinates can be expressed for each body at velocity level in the following form,

$$\mathbf{Z} = \begin{Bmatrix} \dot{\mathbf{s}} \\ \boldsymbol{\omega} \end{Bmatrix} \tag{3.2}$$

where $\dot{\mathbf{s}}$ is the velocity of the point of the body which at that particular time is coincident with the fixed frame origin, and $\boldsymbol{\omega}$ the angular velocity of the body.

Hence, the relation between the body coordinates (and their time derivatives) of two neighbour bodies is given by,

$$\mathbf{Z}_i = \mathbf{Z}_{i-1} + \mathbf{b}_i \dot{\mathbf{z}}_i \tag{3.3}$$

$$\dot{\mathbf{Z}}_i = \dot{\mathbf{Z}}_{i-1} + \mathbf{b}_i \ddot{\mathbf{z}}_i + \mathbf{d}_i \tag{3.4}$$

where $\mathbf{b}_i$ and $\mathbf{d}_i$ are the terms that relate the body coordinates with the independent coordinates. Explicit expressions of $\mathbf{b}_i$ and $\mathbf{d}_i$ terms are available for conventional joints [10], such as the rotational joint that connect the wheels and the knuckles. Nonetheless, for the *macro-joints* that connect the chassis to each knuckle, the procedure detailed in [89] is used.

Once all the terms have been evaluated, the relation between the body coordinates $\mathbf{Z}$ that is used in the semi-recursive formulation and the set of independent coordinates $\mathbf{z}$ that define the vehicle is established. The equations of motion in body coordinates that describe the dynamics of the vehicle can be then projected into the independent relative coordinates yielding,

$$\mathbf{R}^T \bar{\mathbf{M}} \mathbf{R} \ddot{\mathbf{z}} = \mathbf{R}^T \left(\bar{\mathbf{Q}} - \bar{\mathbf{M}} \dot{\mathbf{R}} \dot{\mathbf{z}} \right) \tag{3.5}$$

where $\mathbf{R}$ is the matrix that relates the body coordinates and the independent coordinates based on the terms $\mathbf{b}_i$ and $\mathbf{d}_i$ [10]; and $\bar{\mathbf{M}}$ and $\bar{\mathbf{Q}}$ are the mass matrix and force vector of the system for body coordinates. This equation can be reduced to,

$$\mathbf{M} \ddot{\mathbf{z}} = \mathbf{Q} \tag{3.6}$$

where $\mathbf{M}$ and $\mathbf{Q}$ are obtained in a recursive form, accumulating the body mass matrices and forces from the leaves to the root of the kinematic chain (See Figure 3.3) [10]. Their full expressions are detailed in [89].

Once the equations of motion are defined (see Eq. 3.6), they need to be integrated to solve the time evolution of the vehicle when considering a specific torque input in the wheels (external force). For that purpose, an implicit single-step trapezoidal rule with a fixed time step has been adopted. Combining the integrator equations with the equations of motion, and taking the positions as primary variables, a nonlinear system of equations $\mathbf{f}(\mathbf{z}_{n+1}) = 0$ is obtained, where $\mathbf{z}_{n+1}$ is the vector of independent coordinates at the next time step, which can be solved using a Newton-Raphson iterative procedure, being the residual vector and the approximated tangent matrix,

$$\mathbf{f}(\mathbf{z}) = \frac{\Delta t^2}{4} \left(\mathbf{M} \ddot{\mathbf{z}} - \mathbf{Q} \right) \tag{3.7}$$

$$\frac{\partial \mathbf{f}(\mathbf{z})}{\partial \mathbf{z}} = \mathbf{M} + \frac{\Delta t}{2} \mathbf{C} + \frac{\Delta t^2}{4} \mathbf{K} \tag{3.8}$$

where

$$\mathbf{K} = -\partial \mathbf{Q} / \partial \mathbf{z} \tag{3.9}$$

$$\mathbf{C} = -\partial \mathbf{Q} / \partial \dot{\mathbf{z}} \tag{3.10}$$

represent the contribution of damping and elastic forces to the tangent matrix, and Δt is the time step.

3.2.1.3 Tyre Modelling

To model the tyres, Pacejka's 2006 "Magic Formula" semi-empirical approach has been implemented [3], where the tyre is characterized by a list of coefficients that have to be experimentally tuned. This model enables fast and robust tyre-road contact force and moment simulation for steady-state and transient tyre behaviour, using longitudinal slip, lateral slip, turn slip, wheel inclination angle and indentation characteristics as input quantities.

The ground (included in the road/scenario subsystem) is defined by a triangular mesh, whose element size can be modified to increase the precision in the obstacles of the terrain, such as bumps. This mesh will be employed during the simulation to determine parameters as the contact point, the normal direction of the terrain and the indentation of the tyre into the terrain. These parameters are required to reach a correct road-vehicle interaction during the simulation.

The contact point is obtained through a boundary volume around the wheel: any element of the mesh inside the boundary volume is considered to define the contact plane. This plane determines the deformation of the tyre and, therefore, its accurate calculation is critical, especially when the vehicle is over an obstacle. For this purpose, the method presented in [129] is used (see Figure 3.4). In this approach, a set of ellipses are projected from the wheel centre into the selected elements of the mesh. The intersection points between ellipses and mesh are employed to define a plane, from where a mean value of the normal direction of the contact is obtained. At a final step, the indentation of the tyre into the normal direction is calculated, which is employed in the Pacejka Magic Formula together with the normal direction of the plane to obtain the magnitude and direction of the tyre forces.

3.2.1.4 Steering and Suspension system

One of the approaches implemented to simplify the modelling while maintaining a high level of accuracy is the use of *macro-joints* to model the suspension system. These *macro-joints* are implemented through the use of tables that define the kinematic motion of the centre of the knuckle in terms of the Cartesian coordinate for the vertical suspension displacement $\bar{z}_i$ and the steering angle input δ.

The use of look-up tables allows fast online calculation of the suspension dynamics. However, it requires an offline kinematic analysis to generate it accurately. For this purpose, for each steering position δ, the vertical displacement of the spring $\bar{z}_i$ is modified from the whole range of the vertical motion of the suspension, obtaining the position of the centre of the knuckle for each pair of steer and spring compression values. Once that the positions for the entire range of movement of the suspension are

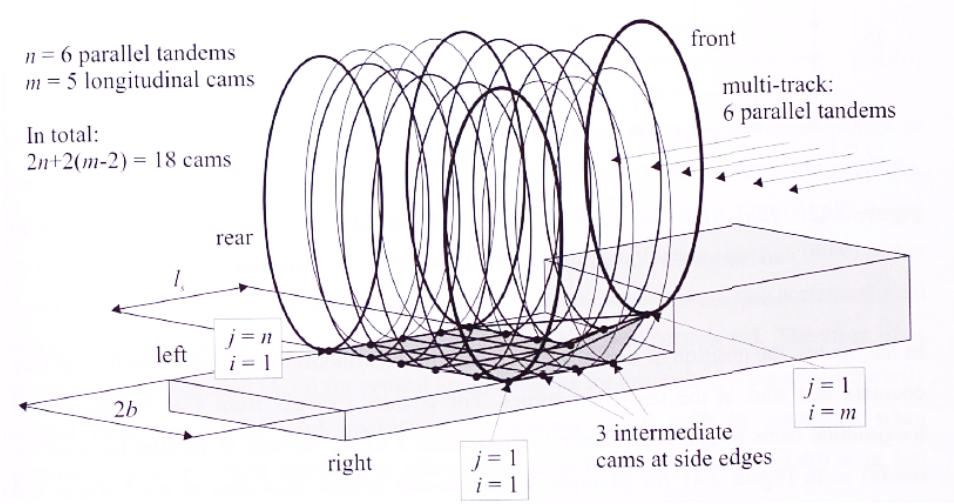

Figure 3.4: Ellipses model for tyre contact point [11]

gathered, the velocities and accelerations are derived through numerical differentiation of the positions.

Additional parameters can be tuned to adapt the behaviour of the suspension. Different deflections of the spring can be considered through the motion ratio of the suspension and its spring/damper characteristics. Also different compliance coefficient have been included, as the relation of the toe, camber and longitudinal displacement of the suspension with the longitudinal force; the effects of the steer, inclination of the suspension and lateral displacement on the lateral forces; and the steer and inclination influence on the steering torque of the wheel. For each parameter, a table can be generated following the aforementioned procedure, so that the data can be used online.

This way, during a simulation, each degree of freedom of the suspension system is integrated each time step except for the steering value, since it is an input to the model. After each integration, the values of each degree of freedom are introduced into the table obtaining the kinematic data of each wheel centre. Later, the spring and damper forces, together with the contact forces can be derived to solve the dynamics of the vehicle.

3.2.2 Driver Model (Virtual Driver)

Once the vehicle dynamics model has been detailed, the Driver Model implemented in the proposed framework will be explained. A Driver Model is an algorithm that emulates the behaviour of a human driver, allowing to parametrize this behaviour to ensure objective testing and repeatability in simulation frameworks such as the one proposed in this section.

In the literature, drivers have been traditionally modelled using approaches inspired

in automated driving algorithms based on control techniques such as: Proportional Integral Derivative (PID) [130], Fuzzy [131], Neuro-Fuzzy [132] or Model Predictive Control (MPC) [133–137], among others.

Among all the proposed approaches, two main groups can be detected: one focuses on dividing the control effort into two controllers, one for longitudinal control (i.e. speed control), and other for lateral control (i.e. path tracking); the other is based on developing a single controller that handles both longitudinal and lateral control.

In the first group, each control problem is handled separately. For the lateral, one approach consists in imitating the human behaviour by scanning the future desired path within a finite future path horizon [138]. Most of the recent works are based on the use of Model Predictive Control (MPC), which computes optimum steering inputs to minimize both lateral tracking errors and control effort in a predicted horizon, and allows to introduce constraints in the formulation. Approaches based on linear models [139], nonlinear ones [140] or on-line successive linearisation approaches [141, 142] have been proposed. In these control approaches, the complexity of the model is directly related to the computational cost, requiring a proper compromise for real-time implementation.

On the other hand, attending to longitudinal control, [143] provides a deep review of the proposed approaches, in which the use of simple PID based controllers and Fuzzy logic based algorithms are common. In general, in this work, it is stated that the use of PID based controllers provide significant tracking errors in comparison with Fuzzy logic based algorithms. However, more complex approaches also are proposed, especially when other considerations, such as comfort, are to be considered [135].

The second group of control approaches considers the whole vehicle, being its inputs the throttle/brake pedals and the steering wheel angle. In these approaches, MPC controllers are the most implemented ones, as they provide intuitive tuning, easily emulate human behaviour and allow to include constraints [144, 145].

In the proposed *Vehicle Dynamics Simulation Framework*, the use of a MPC approach which considers the whole vehicle model is considered as the best option to implement the Driver model. As previously detailed, the complexity of the model is a critical point for MPC approaches, hence, in order to balance computational cost and accuracy, and better emulate human behaviour, a vehicle dynamics model based on a nonlinear bicycle model for the lateral dynamics and a simplified point mass model for the longitudinal dynamics is considered. Note that the vehicle model used is nonlinear, hence, to reduce the computational cost required to execute the control loop, a linear MPC formulation will be used. This will require to formulate the model as a Linear Time-Varying (LTV) model that is calculated at each time step.

In the following sections, an overall view of the Driver Model, and its main functional blocks are detailed.

3.2.2.1 Overall view of the Driver Model

As previously stated, the proposed Driver Model algorithm is based on a MPC controller, which uses a model to estimate the future behaviour of a system in order to

calculate the best control action sequence to minimize an objective function. Thus, a MPC controller operates similar to a human being, as a human driver uses his or her model (vehicle knowledge) to predict the behaviour of the vehicle and determine the best course of action considering the future references (the road ahead) and constraints (traffic signals and vehicle limitations).

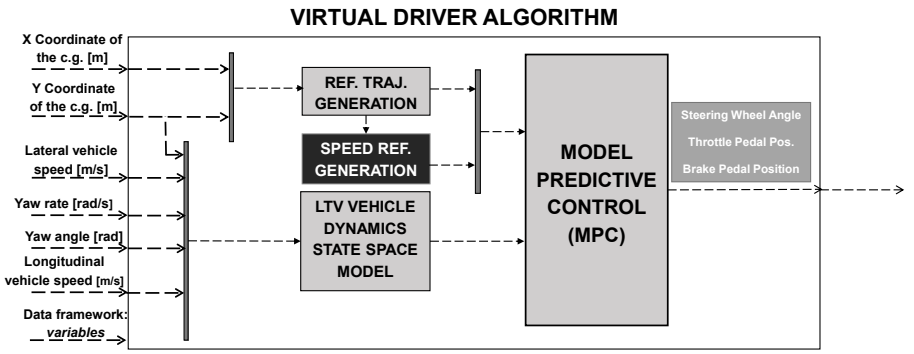

Figure 3.5: Driver Model General Structure

Figure 3.5 shows the general structure of the proposed Driver Model, which is divided into four subsystems: the reference path planning, the speed generation, the vehicle dynamics model (LTV model) and the MPC algorithm. In the next sections, each of these blocks will be detailed.

3.2.2.2 Reference trajectory generation

The MPC controller requires a future reference to operate, defined in terms of the output variables of the model used. As it has been previously detailed, a nonlinear bicycle model in combination with a point mass model is used to model the vehicle's dynamics. This model calculates the time evolution of the vehicle in terms of the local variables (x, y, ψ) related to reference system associated to the Centre of Gravity (CoG) of the vehicle (Figure 3.6).

However, the definition of reference paths can be defined more intuitively in a Global reference frame (this is, on a map), in which a series of plane coordinates (X_i, Y_i) associated to the road to be followed can be easily defined (Figure 3.7).

In addition, a new variable is defined, Station (S_i), to represent the longitudinal distance advanced along the desired path (Figure 3.7). This allows, to define any position of the trajectory uniquely, as there is only one point that defines each position in the global reference system for a value of this variable. For instance, this will allow to drive several turns in the same circuit. The current value of the Station is calculated as the sum of its previous value and the distance from the previous to the new point,

$$S_i = S_{i-1} + \sqrt{(X_i - X_{i-1})^2 + (Y_i - Y_{i-1})^2} \tag{3.11}$$

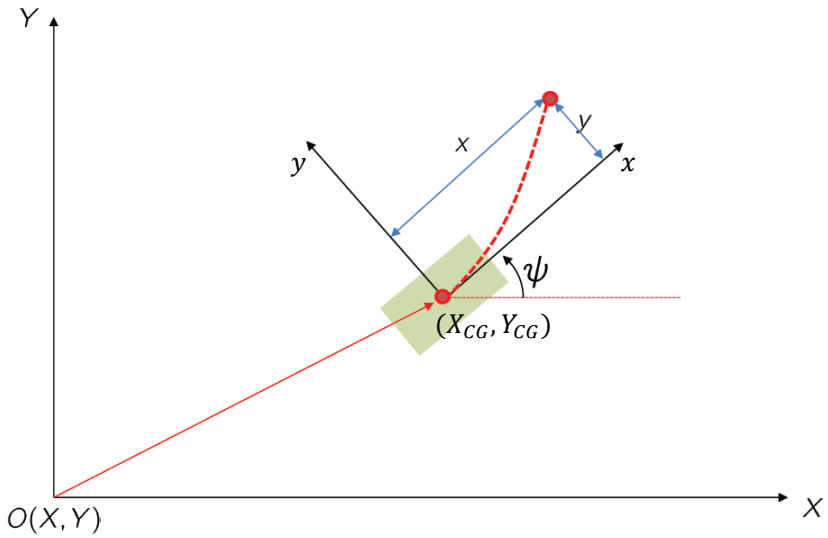

Figure 3.6: Global and Local Reference System

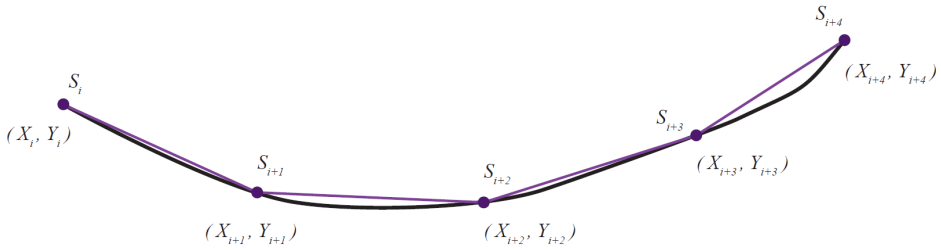

Figure 3.7: Reference Trajectory [12]

Once a dataset or *road* is defined in the Global Frame, consisting on a set of (X_i, Y_i, S_i) points, a reference has to be defined for each time step considering the current position of the vehicle, which is determined by its Center of Gravity (CoG) (X_{CG}, Y_{CG}). For that purpose, the closest point of the reference path (X_{min}, Y_{min}) to the CoG is calculated. The value for the station variable on this point will be defined as S_{min}.

Once the current location on the road is determined, the local future reference trajectory can be defined for the MPC controller. For that purpose, a constant longitudinal speed V_x is assumed over the prediction horizon H_p. Thus, considering the time step T_s of the controller the future target station values $\mathbf{S}_{\text{target}}$ are calculated,

$$\mathbf{S}_{\text{target}} = [S_{min} + T_s\dot{x}, S_{min} + 2T_s\dot{x}..., S_{min} + H_pT_sV_x] \tag{3.12}$$

Once $\mathbf{S}_{\text{target}}$ values are calculated, the corresponding set of reference points in the global frame $(\mathbf{X}_{\text{target}}, \mathbf{Y}_{\text{target}})$ are obtained,

$$\mathbf{X}_{\text{target}} = [X_{T_1}, X_{T_2}, X_{T_3}..., X_{T_{Hp}}] \tag{3.13}$$

$$\mathbf{Y}_{\text{target}} = [Y_{T_1}, Y_{T_2}, Y_{T_3}..., Y_{T_{Hp}}] \tag{3.14}$$

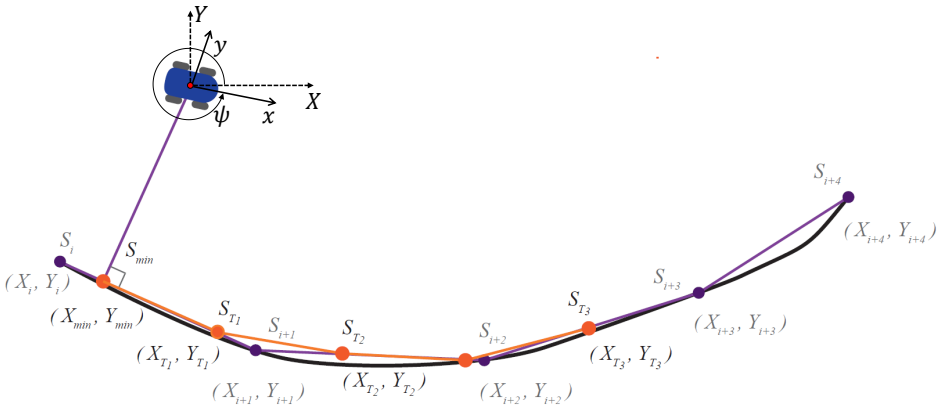

Figure 3.8: Target Points Representation [12]

The aforementioned points are defined in the global reference frame. However, as previously stated, the internal model used by the MPC is defined in the local coordinates associated with the frame attached to the chassis of the vehicle on its CoG for a given time step. This way, the reference for the lateral motion $\mathbf{w}_y$ needs to be transformed into the local frame (Figure 3.6), as the relative deviations in the local y axis need to be compensated by the controller. On the other hand, the orientation $\mathbf{w}_\psi$ reference is calculated as the slope between two consecutive target points $(m_1, m_2, ...m_{H_p})$,

$$\mathbf{w}_y = \begin{bmatrix} (X_{T_1} - X_{CG})\cos(\psi) - (Y_{T_1} - Y_{CG})\sin(\psi) \\ (X_{T_2} - X_{CG})\cos(\psi) - (Y_{T_2} - Y_{CG})\sin(\psi) \\ ... \\ (X_{T_{Hp}} - X_{CG})\cos(\psi) - (Y_{T_{Hp}} - Y_{CG})\sin(\psi) \end{bmatrix} \tag{3.15}$$

$$\mathbf{w}_\psi = \begin{bmatrix} \arctan(m_1) - \psi \\ \arctan(m_2) - \psi \\ ... \\ \arctan(m_{H_p}) - \psi \end{bmatrix} \tag{3.16}$$

3.2.2.3 Speed reference generation

The proposed driver model handles both lateral and longitudinal dynamics. For this purpose, a longitudinal speed reference is also required. The proposed speed planner considers two possibilities, based on the type of test to be performed. This way, if a driving cycle, as the WLTP (Worldwide Harmonized Light-Duty Vehicles Test

Procedures) [146] or an open-loop test, has to be carried out, the speed reference is provided by the speed profile or will be kept constant, accordingly to the test requirement . However, if the test consists to track the trajectory, i.e. circuit tests, the reference speed for each time step has to be generated following the requirements of the MPC controller.

For the latter case, a speed reference generator is designed, which calculates the maximum speed at which the vehicle can negotiate the path to be followed considering a set of parameters that will characterize the *driving style*.

For that purpose, the reference path planner introduced in the previous section is used, as it based on the current vehicle's position, it allows to define a future reference trajectory for a given prediction horizon H_p. As the reference path is known, its turning radius can be easily calculated. Additionally, the maximum lateral acceleration $a_{y,max}$, and the maximum longitudinal accelerations for traction and braking conditions ($a_{x,max}$ and $a_{x,min}$) can be defined. Note, that these variables allow configuring different driving styles, i.e. sport mode, normal mode, and ECO driving mode, among others. Based on these parameters and the turning radius, the maximum speed at which the vehicle can negotiate the desired trajectory is calculated as follows,

$$V_{max} = \sqrt{a_{y,max} R_{traj}} \tag{3.17}$$

Therefore, for acceleration conditions:

$$V_{ref} = \begin{cases} min(V_{max}, V + a_{x,max}), & \text{if } \dfrac{(V_{max} - V)}{dt} \geq 0 \\ min(V_{max}, V + a_{x,min}), & \text{otherwise} \end{cases} \tag{3.18}$$

Note that the speed reference V_{ref} is considered constant for the whole prediction horizon H_p, as this will be the basic assumption for the implementation of a LTV model in the MPC, as detailed next.

3.2.2.4 LTV Dynamic vehicle model

The vehicle model used for implementing the MPC based Driver Model combines the well-known and cost-effective bicycle model (see Figure 3.9) for the lateral dynamics [67] and a point-mass model for the longitudinal dynamics. This model is defined in the local frame associated with the CoG of the chassis (x, y, z) for a given time step.

If small angle approximations are considered, the lateral dynamics defined by the bicycle model can be defined as,

$$\begin{aligned} a_y = &-\frac{2(C_{\alpha F} + C_{\alpha R})}{mV_x} V_y - \left[\frac{2(l_F C_{\alpha F} - l_R C_{\alpha R})}{mV_x} + V_x\right] \dot{\psi} \\ &+ \frac{2C_{\alpha F}}{m} \delta \end{aligned} \tag{3.19}$$

$$\begin{aligned} \ddot{\psi} = &-\frac{2(l_F C_{\alpha F} - l_R C_{\alpha R})}{I_z V_x} V_y - \frac{2(l_F^2 C_{\alpha F} + l_R^2 C_{\alpha R})}{I_z V_x} \dot{\psi} \\ &+ \frac{2 l_F C_{\alpha F}}{I_z} \delta \end{aligned} \tag{3.20}$$

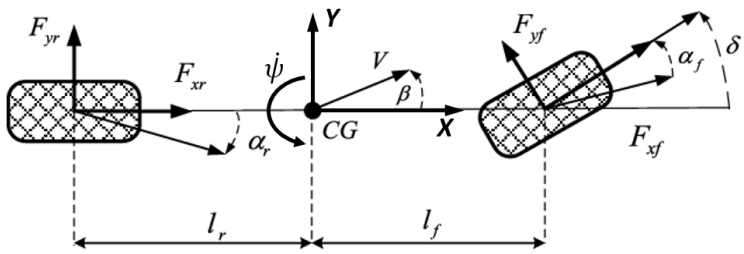

Figure 3.9: Modelling of a vehicle through the "bicycle model"

where $\ddot{\psi}$, a_y, V_y and V_x are the vehicle's local yaw acceleration,lateral acceleration, lateral speed and longitudinal speed, respectively. $C_{\alpha F}$ and $C_{\alpha R}$ are the front and rear tyre cornering stiffness coefficients. I_z is the inertia moment along the vertical axis z and δ is the steering angle of the front wheels. Finally, l_F and l_R are the fronts and lateral track widths.

The longitudinal dynamics are defined by Eq. 3.21, which represents a point mass model,

$$\sum F_x = F_{tract} + F_{aero} + F_{rollingres} + F_{slope} \tag{3.21}$$

where $\sum F_x$ is the total force along the x axis, a_x is the longitudinal acceleration, F_{trac} is the total traction force, F_{aero} is the aerodynamics resistance force, $F_{rollingres}$ is the resistance force due to the tyre rolling resistance, and finally, F_{slope} is the force due to the road inclination. These forces are detailed next,

$$F_{aero} = \frac{1}{2}\rho_{air} C_{drag} A_f V_x^2 (-sign(V_x)) \tag{3.22}$$

$$F_{rollingres} = f_r mg(-sign(V_x)) \tag{3.23}$$

$$F_{slope} = -mg\sin(\theta_{slope}) \tag{3.24}$$

$$F_{tract} = \tau / R \tag{3.25}$$

where m is the vehicle mass, ρ_{air} is the air density, C_{drag} is the drag coefficient, A_f is the vehicle front area, V_x is the longitudinal vehicle speed, f_r is the rolling resistance coefficient, g is the gravity acceleration, θ_{slope} is the road inclination angle, τ is the total wheel torque and R is the tyre radius.

Based on Equations. 3.19-3.25, a state-space model can be defined. This model is represented by the state space variable,

$$\boldsymbol{x_c(t)} = [y(t)\ V_y(t)\ \dot{\psi}(t)\ \psi(t)\ V_x(t)]^T \tag{3.26}$$

where $y(t)$ is the lateral displacement and $\psi(t)$ is the yaw angle in the local z axis.

Additionally, the control variables are defined by the steering angle $\delta(t)$ and the wheels total torque torque $\tau(t)$,

$$\boldsymbol{u_c(t)} = [\delta(t)\ \tau(t)]. \tag{3.27}$$

Hence, the model can be represented in a state-space form in continuous time as,

$$\dot{\boldsymbol{x}}_{\boldsymbol{c}}(\boldsymbol{t}) = \mathbf{A}_{\mathrm{c}}\, \boldsymbol{x}_{\boldsymbol{c}}(\boldsymbol{t}) + \mathbf{B}_{\mathrm{c}}\, \boldsymbol{u}_{\boldsymbol{c}}(\boldsymbol{t}) + \boldsymbol{v}(\boldsymbol{t}) \tag{3.28}$$

with,

$$\mathbf{A}_{\mathrm{c}} = \begin{bmatrix} 0 & 1 & 0 & v_x & 0 \\ 1 & a & 0 & b & 0 \\ 0 & c & 0 & d & 0 \\ 0 & 0 & 1 & 0 & 0 \\ 0 & 0 & 1 & 0 & e \end{bmatrix} \quad \mathbf{B}_{\mathrm{c}} = \begin{bmatrix} 0 & 0 \\ \frac{2(C_{\alpha F})}{m} & 0 \\ \frac{2(l_F C_{\alpha F})}{I_z} & 0 \\ 0 & \frac{1}{m\, R} \end{bmatrix} \quad \mathbf{v}(t) = \begin{bmatrix} 0 \\ 0 \\ 0 \\ 0 \\ \frac{F_{slope}}{m} \end{bmatrix} \tag{3.29}$$

and,

$$\begin{aligned} a &= -\frac{2(C_{\alpha F} + C_{\alpha R})}{m\, V_x} \\ b &= -\frac{2(l_F\, C_{\alpha F} - l_R\, C_{\alpha R})}{m\, V_x} - V_x \\ c &= -\frac{2(l_F\, C_{\alpha F} - l_R\, C_{\alpha R})}{I_z\, V_x} \\ d &= -\frac{2(l_F^2\, C_{\alpha F} - l_R^2\, C_{\alpha R})}{I_z\, V_x} \\ e &= -\frac{C_{drag} A_f \rho_{air}}{2m} - f_r\, g \end{aligned} \tag{3.30}$$

As it can be seen, there is a dependency of matrix $\mathbf{A}_{\mathrm{c}}$ for the longitudinal speed v_x. Hence, to achieve a linear model and reduce the computational cost, a constant longitudinal speed $\mathbf{V}_{\mathrm{x}}$ is considered for the prediction horizon H_p. This way, each time step, the model will have to be updated with the current value of the longitudinal speed, and matrix $\mathbf{A}_{\mathrm{c}}$ will have to be recalculated for that time step, defining a LTV model.

It should be noticed that the F_{slope} is not included in this state-space model, as it is considered as a measurable disturbance $v(t)$ to the MPC controller.

3.2.2.5 MPC Formulation

The proposed Driver Model is implemented using a linear MPC (a deeper explanation of this control technique is presented in Chapter 5), to reduce the computational cost. A widely known state-space based formulation [147] has been implemented using the aforementioned LTV model and reference generators.

MPC approaches are implemented on discrete-time. The model defined in Eq. 3.28 is an LTV model defined in continuous time and depends on the value of the longitudinal speed of v_x. Hence, in each time step first the current speed v_x is measured and assumed constant for the prediction horizon H_p of the MPC. Then, for the particular value of the measured V_x, matrix $\mathbf{A}_{\mathrm{c}}$ (Eq. 3.28) is calculated, and the resulting model is discretized using the Zero Order Hold method.

$$\begin{aligned}\mathbf{x}(k+1) &= \mathbf{A}_\mathrm{d}\,\mathbf{x}(k) + \mathbf{B}_\mathrm{d}\,u(k)\\ \mathbf{y}(k+1) &= \mathbf{C}_\mathrm{d}\,\mathbf{x}(k+1)\end{aligned} \tag{3.31}$$

where $\mathbf{x}(k)$ and $\mathbf{u}(k)$ are the discretized states (see Eq. 3.26) of the vehicle and its control inputs (see Eq. 3.27), and $\mathbf{y}(k)$ defines the discretized outputs whose error will be optimized by the controller, this is, the lateral displacement $y(k)$, the vehicle orientation $\psi(k)$ and the longitudinal speed $V_x(k)$,

$$\mathbf{y(k)} = [y(k)\ \psi(k)\ V_x(k)]^T \tag{3.32}$$

Once the model is discretized, a linear State-Space formulation of the MPC in incremental variables is implemented [147] to include an integrative effect. Thus, the control law of the MPC that defines the Driver Model is defined as follows,

$$\begin{aligned} V \ &= \ \min_{\Delta \mathbf{u}^+} J(\mathbf{\Delta u}^+, \mathbf{x}(t)) \\ s.t. & \\ & \mathbf{A}_\mathrm{c}\,\mathbf{\Delta u}^+ \leq \mathbf{B}_\mathrm{c} \end{aligned} \tag{3.33}$$

where $\mathbf{A}_\mathrm{c}$ and $\mathbf{B}_\mathrm{c}$ are used to model the physical constraints of the vehicle as linear constraints (minimum and maximum (min/max) steering angle δ, min/max vehicle speed V and min/max longitudinal and lateral acceleration a_x and a_y, respectively) and $\mathbf{\Delta u}^+ = \left[\Delta u(k) \ldots \Delta u(k+H_p-1)\right]^T$ is the resulting sequence of control input variations that ensures the minimum value of the Cost Function J, which is defined as,

$$J = \left(\hat{\mathbf{y}} - \boldsymbol{\omega_y}\right)^T\ \mathbf{R}\ \left(\hat{\mathbf{y}} - \boldsymbol{\omega_y}\right) + \mathbf{\Delta u}^{+T}\,\mathbf{Q}\,\mathbf{\Delta u}^+ \tag{3.34}$$

where $\mathbf{R}$ and $\mathbf{Q}$ are the cost matrices used to tune the MPC controller; $\hat{\mathbf{y}} = \mathbf{G}\,\mathbf{\Delta u}^+ + \mathbf{f}$ is the vector output prediction for the whole prediction horizon H_p, which is calculated from the LTV model Eq. 3.28 and the current state measurement $\mathbf{x}(t)$ following the procedure detailed in [147]; and $\boldsymbol{\omega_y}$ is the future reference for the output variables $\mathbf{y}$, as calculated in sections 3.2.2.2 and 3.2.2.3.

As detailed previously, the MPC is defined in incremental variables. Hence, the MPC calculates the variations of the control action to be applied for the previous iteration. Hence, the control action for a given time step $k = t$ is calculated as follows,

$$\Delta u(k) = u(k) - u(k-1) \tag{3.35}$$

3.3 Framework Validation

The aforementioned *Vehicle Dynamics Simulation Framework* will be used to validate the Torque Vectoring approaches proposed in this PhD. Thesis. To demonstrate the accuracy and validity of the framework, and thus, of the simulations and virtual tests carried out in it, first, a series of validation tests based on experimental (real) results are carried out. Then, as the TV systems proposed in Chapters 4 and 5 will be

validated in a HiL setup, the real time capabilities of the proposed framework will be analysed through a circuit test.

3.3.1 Study Case: Light duty truck

For the validation of the proposed *Vehicle Dynamics Simulation Framework*, a real IVECO light duty truck (Figure 3.10) has been selected as a test vehicle. This vehicle has been fully instrumented (IMU, GPS and a robot for steering and throttle/brake pedal commands). The main parameters of the vehicle, which have been experimentally identified, are summarised in Table 3.1.

Figure 3.10: Tested Vehicle - Real and virtual

Table 3.1: Vehicle Parameters

Mass (kerb) (kg)	2067
Mass (test condition) (kg)	3267
Wheelbase (m)	3.725
Front Axle Distance to CoG (m)	1.162
CoG height (m)	0.716
Front Axis Track (m)	1.745
Rear Axis Track (m)	1.545
Tyre Radius (m)	0.349
Frontal Area (m)	3.8
Drag Coefficient	0.7
Rolling resistance Coefficient	0.009
Tyre Cornering Stiffness [N/deg]	1791

The real vehicle has been modelled using the procedure detailed in Section 3.2.1. The characterization of the suspension has been made through the well known K&C (kinematics and compliance) tests and the dampers have been tested in a proper test-

bench. Besides, a set of tests has been carried out experimentally with professional equipment at IDIADA's [148] facilities to identify the Pacejka's Tyre Model parameters. The powertrain has been modelled considering a simplified model of the one implemented on the real vehicle (a Diesel Internal Combustion Engine (ICE) with a power of 110 kW and a gearbox of 6 different gear ratios). In particular, in addition to the effect of the gearbox, the engine brake has been modelled based on experimental data. Figure 3.10 shows the real and the virtual vehicle as modelled in the proposed framework.

In the following sections, the tests defined to validate the accuracy of the vehicle dynamics model, and the proposed framework, will be detailed and analyzed.

3.3.2 Vehicle Dynamics Model Validation

In order to determine the accuracy of the vehicle dynamics modelling procedure defined in Section 3.2.1, a series of standardized manoeuvres have been carried at IDIADA's facilities with the real vehicle: Coast Down, Step Steer, Ramp Steer and Frequency Response. The obtained experimental data have been compared with the ones obtained by introducing the real inputs in the model in order to evaluate the accuracy of the model.

3.3.2.1 Coast Down

This manoeuvre is one of the most frequent tests for motor vehicles. It consists in running the vehicle in a straight line, starting at a certain speed and letting it slow down until it stops. The main goal of this test is to evaluate the values of the resistant forces acting on the vehicle at a certain speed and road conditions, which will validate the longitudinal dynamics model.

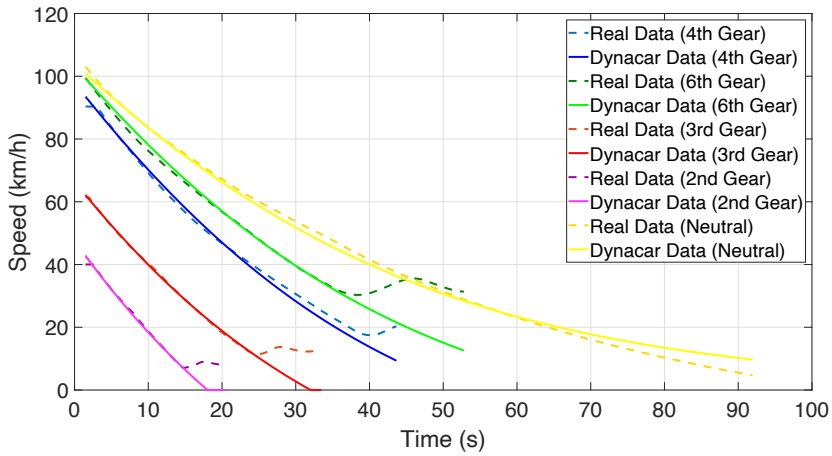

Figure 3.11: Coast Down maneuver

Figure 3.11 shows the time evolution of the speed for both real and simulated vehicles for different gears. The speed differences at the end of the tests, with the 2nd to 6th gear, are due to the idle speed controller implemented in the real vehicle. This functionality has not been considered in the simulation, as this work does not focus on the powertrain model.

The speed root mean square errors (RMSE) for different gears obtained for this manoeuvre are shown in Table 3.2, and their low values demonstrate the accuracy of the model in this manoeuvre. Note that the RMSE calculation has been made considering that the manoeuvre ends when the idle speed function previously commented is activated, except for the test in neutral, as in this case this function is not activated.

Table 3.2: RMSE - Coast Down manoeuvre

Gear	2nd	3rd	4th	6th	Neutral
RMSE (km/h)	0.51	0.32	1.7	1.01	2.0

3.3.2.2 Step Steer

The main objective of this normalized manoeuvre [149] is to describe the lateral dynamic behaviour of a vehicle. Driving in a straight line at a constant speed, the steering wheel is rotated as fast as possible to the target angle position, in which the vehicle's lateral acceleration will start to increase as it begins to turn.

This manoeuvre has been carried out for different steering wheel angles and at different speeds, to demonstrate the model's accuracy in a wide range. Results are shown in Figures 3.12 - 3.15 and summarized in Table 3.3. The lateral acceleration and the yaw rate RMSE show the accuracy of the developed model.

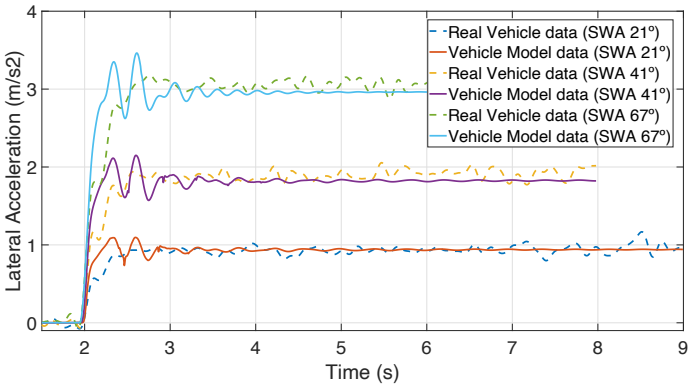

Figure 3.12: Lateral Acceleration - Step Steer (50km/h)

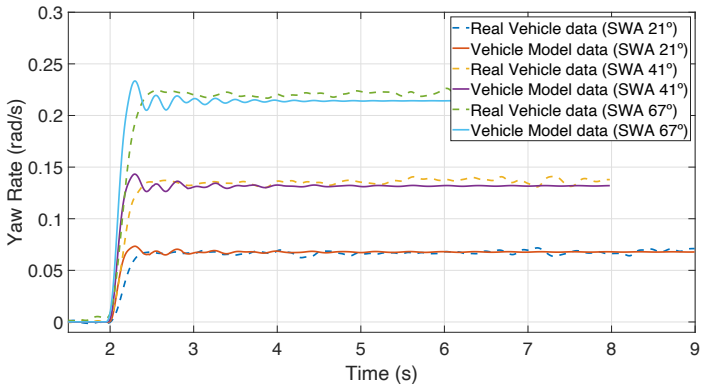

Figure 3.13: Yaw Rate - Step Steer (50km/h)

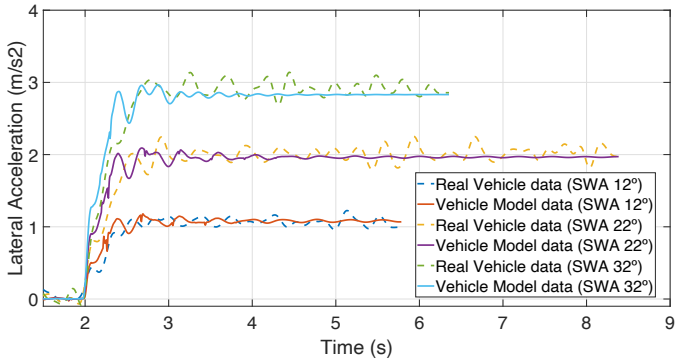

Figure 3.14: Lateral Acceleration - Step Steer (80km/h)

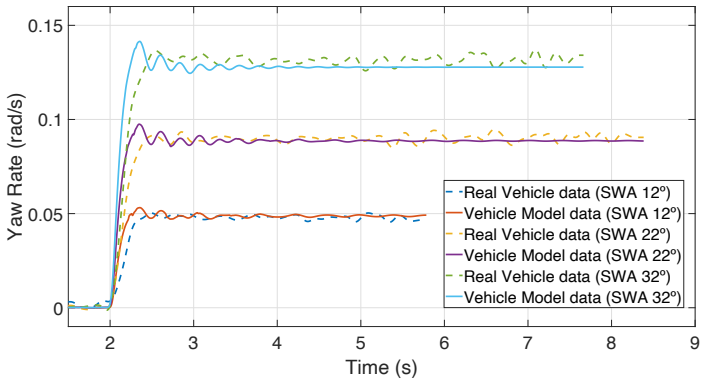

Figure 3.15: Yaw Rate - Step Steer (80km/h)

Table 3.3: RMSE - Step Steer manoeuvre

	Steering wheel angle [deg]					
	V=50 km/h			V=80 km/h		
	21	41	67	12	22	32
Lat. Acc. RMSE (m/s^2)	0.076	0.146	0.237	0.083	0.156	0.219
Yaw Rate RMSE (rad/s)	0.004	0.008	0.013	0.003	0.005	0.008

3.3.2.3 Ramp Steer

The goal of this normalized manoeuvre [150] is to determine the steady-state circular driving characteristics of the test vehicle when increasing the lateral acceleration. This test is handled at a constant speed the lateral acceleration is increased by applying a ramp input to the steering system until the limit of adherence is reached.

Figures 3.16 and 3.17 and Table 3.4 show the results obtained for the ramp steer manoeuvre, which has been carried out at two different speeds (50 km/h and 80 km/h). As this manoeuvre takes the vehicle to its limits in terms of lateral dynamics, the variables captured are the lateral acceleration (0.35 m/s^2 average error) and the yaw rate (0.0097 rad/s average error). Results show the effectiveness of the developed vehicle model in such a challenging manoeuvre.

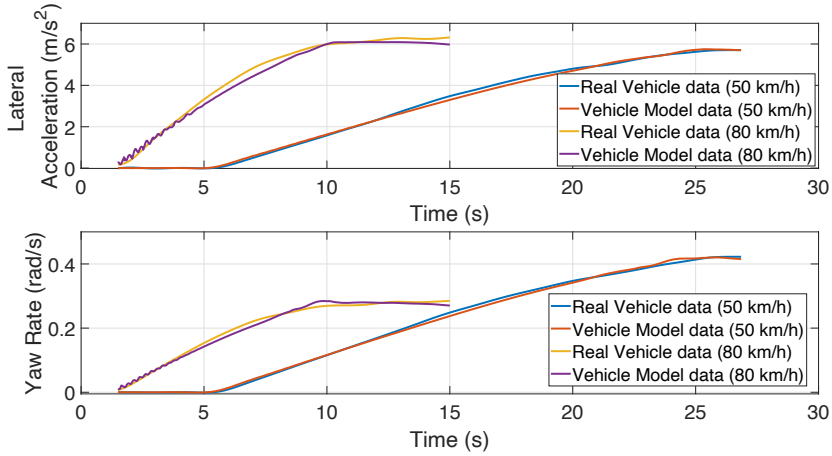

Figure 3.16: Lateral Acc. & Yaw Rate - Ramp Steer Manoeuvre

Table 3.4: RMSE - Ramp Steer Manoeuvre

	Vehicle Speed	
	50 km/h	80 km/h
Lat. Acceleration RMSE (m/s^2)	0.3078	0.4016
Yaw Rate RMSE (rad/s)	0.0104	0.009

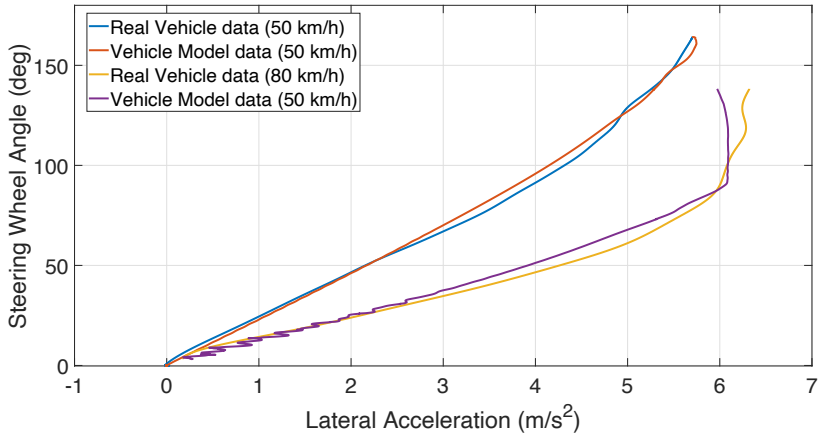

Figure 3.17: Lat. Acc. VS Steering Wheel Angle - Ramp Steer Manoeuvre

3.3.2.4 Frequency Response

This test aims to determine the lateral transient response behaviour of the test vehicle in the frequency domain. For that, the test covers a steering input frequency range between 0.1 - 4 Hz.

Figures 3.18 - 3.20 and Table 3.5 show the results obtained for the frequency response manoeuvre, which has been carried out at three different speeds (50 km/h, 80 km/h and 100 km/h). The variable selected for the validation is the yaw rate, as it represents effectively the lateral transient behaviours. RMSE errors are summarized in Table 3.5 where very low RMSE errors are shown, demonstrating the accuracy of the proposed vehicle model in such a challenging manoeuvre.

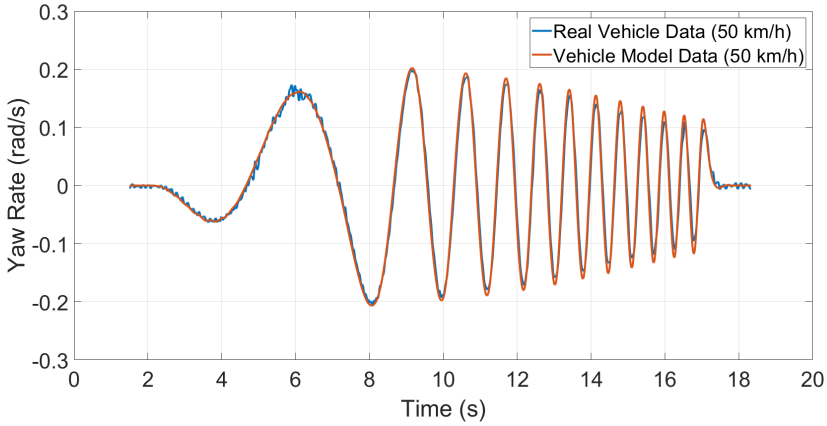

Figure 3.18: Yaw Rate - Freq. Response Manoeuvre - 50 km/h

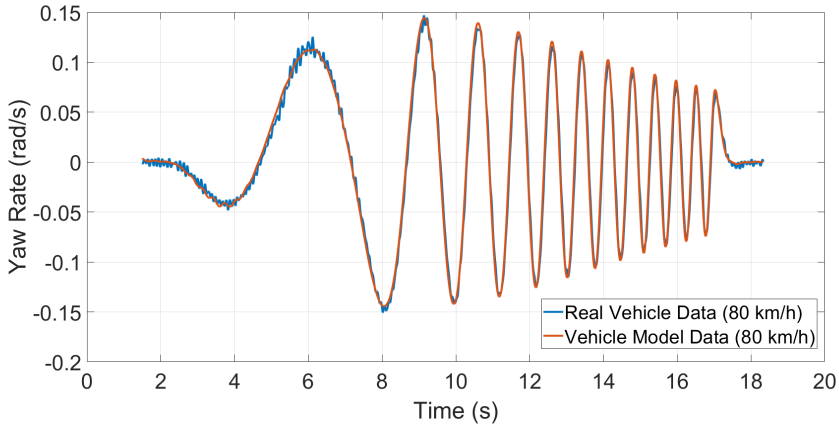

Figure 3.19: Yaw Rate - Freq. Response Manoeuvre - 80 km/h

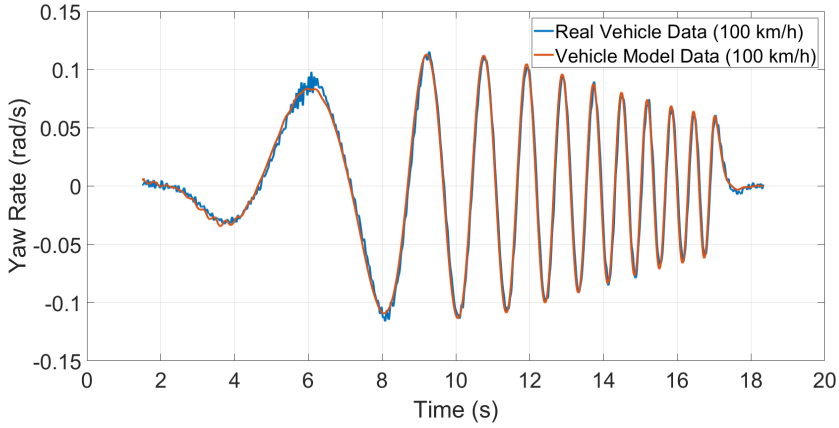

Figure 3.20: Yaw Rate - Freq. Response Manoeuvre - 100 km/h

Table 3.5: RMSE - Frequency Response Manoeuvre

	Vehicle Speed (km/h)		
	50	80	100
Yaw Rate RMSE (rad/s)	0.0101	0.0093	0.0082

3.3.3 HiL capabilities validation

Hardware in the Loop (HiL) testing is a mandatory feature for a successful simulation framework, as it allows to reduce significantly the time and cost of feature developments [151], allowing to test not only the code of the tested control system, but also its hardware and communications. However, an appropriate vehicle model

(accurate and computationally efficient) is required in order to ensure the validity of this approach, which is not always easy to obtain. Therefore, in order to demonstrate the validity and real time capabilities of the proposed framework for validating the TV systems proposed in this Ph.D. Thesis, in this section, the whole *Vehicle Dynamics Simulation Framework* will be validated in a HiL setup.

3.3.3.1 HiL Setup

Based on the model validated in Section 3.3.2 and on the Virtual Driver model presented in Section 3.2.2, the HiL setup shown in Figure 3.21 has been defined to test the proposed framework.

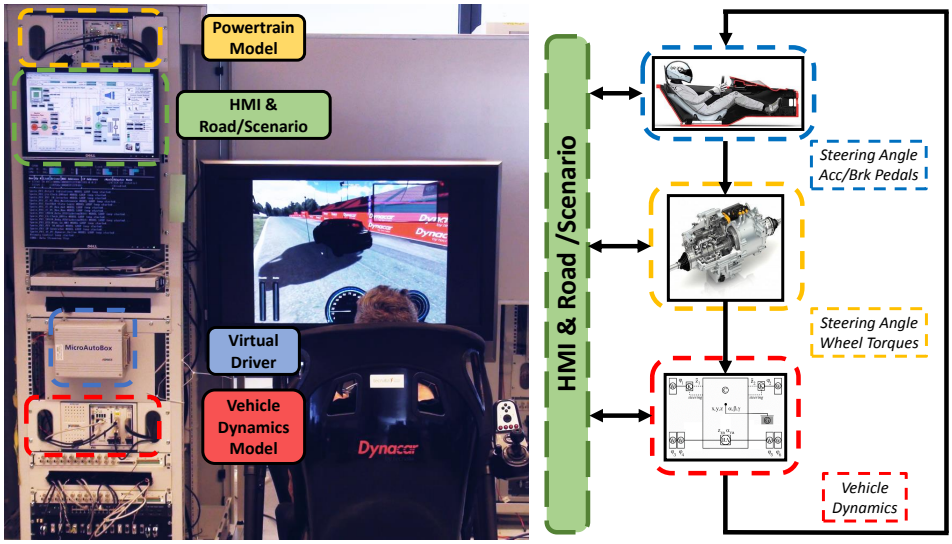

Figure 3.21: HiL Setup based on the proposed multibody vehicle dynamics model and on the proposed Virtual Driver model

Four main blocks are defined in this setup. First, the real vehicle is modelled using two blocks, a powertrain model and the proposed multibody-based model. Both are compiled as a standard C libraries, and are implemented in two National Instruments PXI Industrial PCs (2.3GHz, 8GB RAM), with an execution period of 1ms. Communications between both systems is carried out using TCP/IP protocol.

Second, the Virtual Driver Model, which provides the steering wheel angle and the pedals positions. In addition to the physical constraints of the vehicle, a maximum speed of 120 km/h and a maximum lateral acceleration of 6.0 m/s^2 have been selected as output constraints. The developed system has been implemented in a hardware platform widely used in the Automotive Industry (dSPACE MicroautoBox II [152]), running with an execution period of 10ms. Note that in order to test the corresponding control system, the MicroAutoBox II is connected to the *virtual vehicle*, implemented in the the aforementioned PXIs, using a CAN communication bus.

Finally, an Human Machine Interface and the environment model (with a simplified 3D representation) is executed in a high-end PC. This communicates using TCP/IP with the powertrain and vehicle model PXIs, so that the internal model variables and parameters can be represented, and the 3D visualization updated. In addition, this PC updates the environmental variables to the rest of the model, such as road friction coefficients and slopes depending on the position of the vehicle.

3.3.3.2 HiL Results and Computational Cost Analysis

For the validation, two Circuits have been implemented: Silverstone and Barcelona. Figures 3.22-3.25 show the results provided by the Virtual Driver model in the developed HiL setup. More specifically, Figures 3.22 and 3.24 show the lateral error between the desired trajectory and the one followed by the vehicle; while Figures 3.23 and 3.25 show the vehicle lateral acceleration. Finally, in Figures 3.26 and 3.27), the execution time of the proposed model is shown for this setup.

Results demonstrate that the proposed framework performs properly, with low tracking values in the lateral error (Figures 3.22 and 3.24 and Table 3.6) and accelerations in the constrained range (Figures 3.23 and 3.25). Moreover, the vehicle model average execution time is 0.22ms for both circuits (see Figures 3.26 and 3.27), guaranteeing proper real-time performance for the HiL setup, as it is less than 1ms.

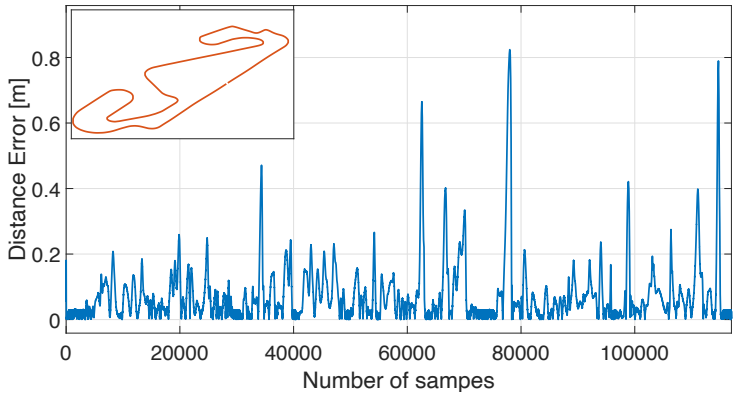

Figure 3.22: Lateral Error - Montmelo

Table 3.6: Race Track Distance RMSE

Circuit	Path tracking RMSE (m)
Montmelo	0.1252
Silverstone	0.1171

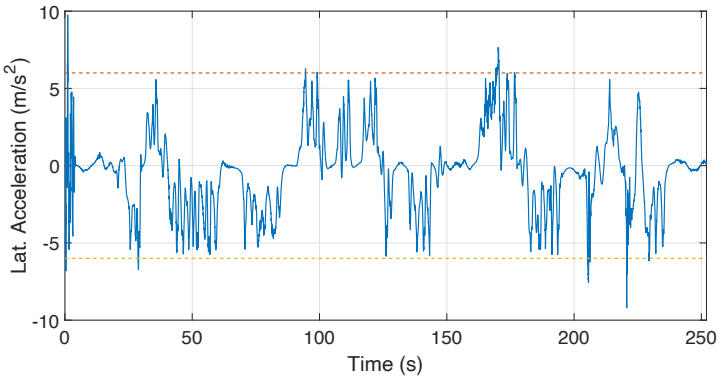

Figure 3.23: Lateral Acceleration - Montmelo

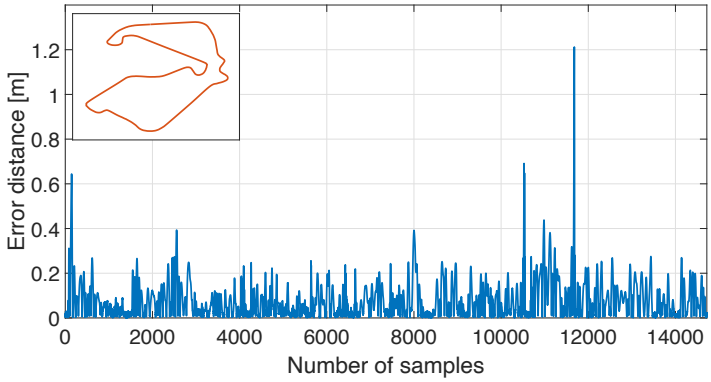

Figure 3.24: Lateral Distance Error - Silverstone

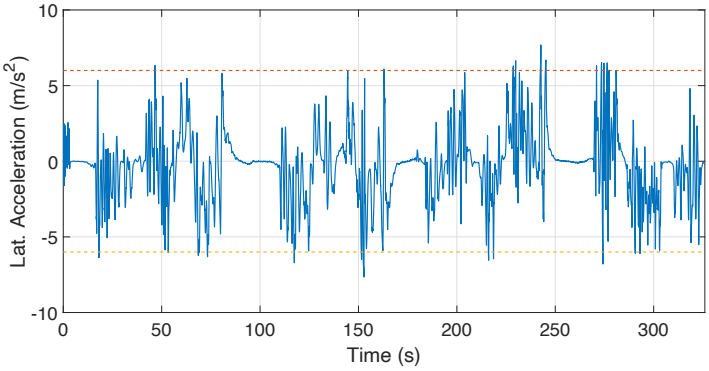

Figure 3.25: Lateral Acceleration - Silverstone

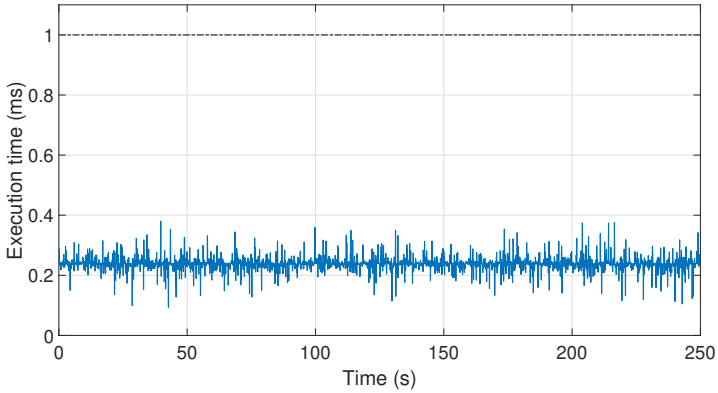

Figure 3.26: Execution Time - Montmelo Circuit

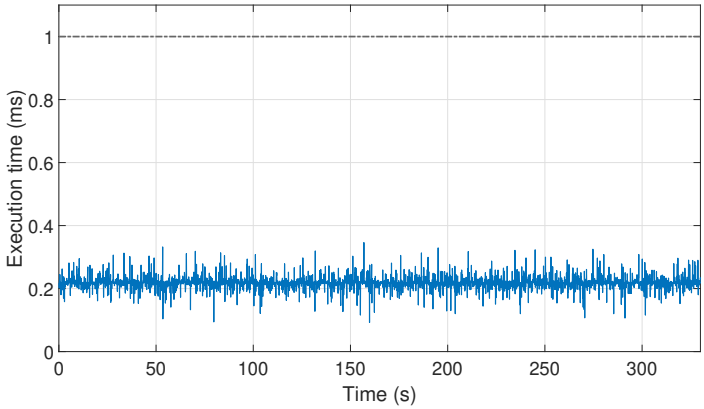

Figure 3.27: Execution Time - Silverstone Circuit

3.4 Conclusions

Simulation-based testing is mandatory for future of vehicle dynamics control systems developments. The cost and lack of flexibility of track tests limit their use when complex control systems need to be tested in vehicles. Moreover, simulation-based testing frameworks allow testing of multiple scenarios at a lower cost and minimum risk.

However, developing proper simulation-based testing frameworks is not a trivial task. Vehicle dynamics modelling is a challenging issue, as a proper balance between accuracy and computational efficiency needs to be considered, as well as flexibility and real-time capabilities. Considering the aforementioned issues, in this chapter a novel *Vehicle Dynamics Simulation Framework* is presented, which will be used to test the TV approaches proposed in this PhD Thesis.

The proposed framework uses an efficient multibody based vehicle dynamics approach, that can be executed in real-time, and a LTV MPC Driver Model, that can be used when testing control approaches in closed-loop in order to ensure repeatability. Moreover, the proposed framework is flexible, allowing to consider multiple powertrain topologies, and it allows easy implementation of cosimulation or Hardware-in-the-Loop setups thanks to its reduced computational cost (under 1ms in conventional PCs and real-time platforms).

The presented framework is validated by two different ways. First, the multibody vehicle dynamics model is validated using real data from a tested vehicle in a variety of challenging manoeuvres. Results show a great degree of accuracy, 0.4m/s^2 and 0.009rad/s of lateral acceleration and yaw rate, respectively, in a demanding maneuver, such as the ramp steer at 80 km/h, which demonstrates the validity of the proposed multibody dynamic model to reproduce the real vehicle's dynamics.

Second, and once the dynamics model have been validated, the proposed *Vehicle Dynamics Simulation Framework* has been validated as a whole in a HiL setup, focusing on the Driver Model performance and on the real-time capabilities. On the one hand, Driver Model results demonstrate its ability to ensure repeatability and emulate properly the driving style of real drivers. Results in Silverstone (0.1171m path tracking RMSE) and Montmeló Circuits (0.1252m path tracking RMSE) demonstrate that the proposed approach ensures proper tracking for these tests. Finally, the carried out execution time analysis, which has shown an 0.22ms average execution time for the proposed multibody dynamic model, demonstrates the real-time capabilities of the whole framework

The obtained results have demonstrated the accuracy of the proposed framework and its suitability for being used to validate the approaches proposed in this PhD Thesis. Hence, in the next chapters, this framework will constitute the basics for the validation of the proposed two TV approaches.

Intelligent Torque Vectoring

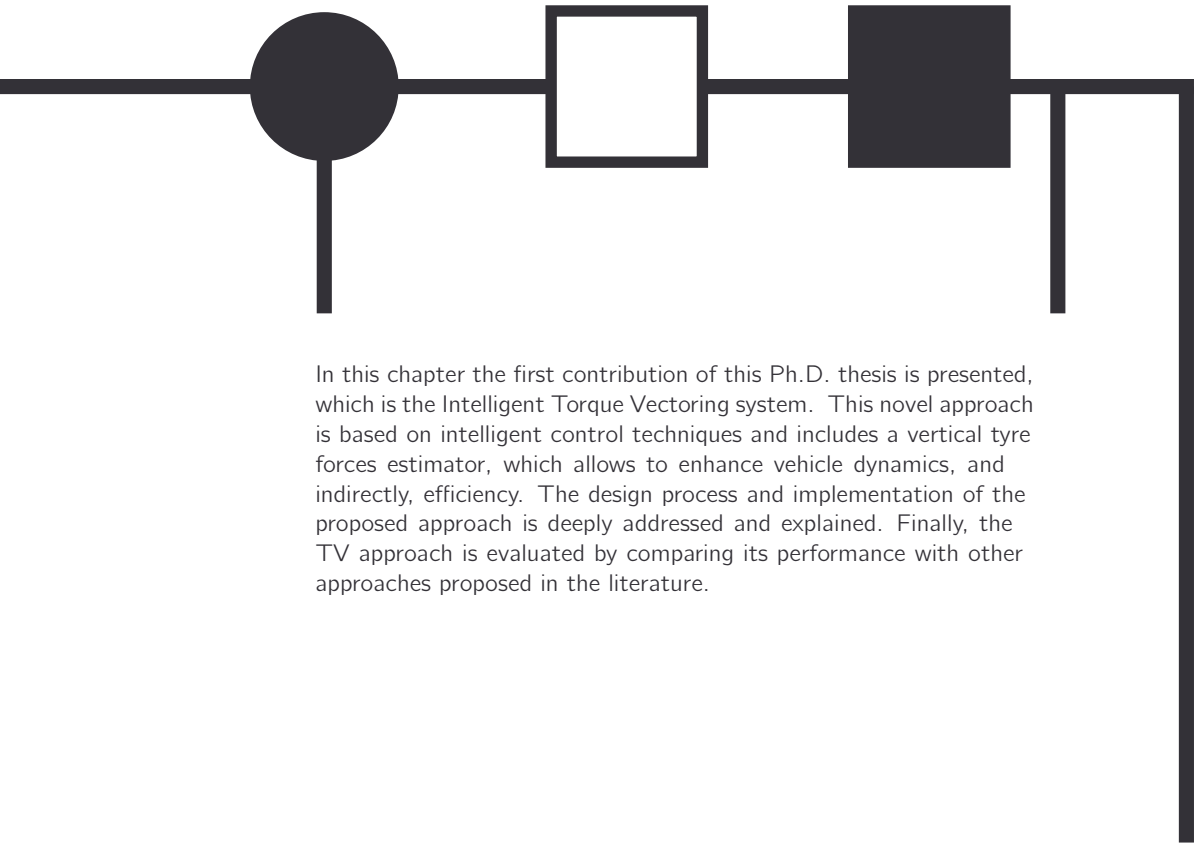

In this chapter the first contribution of this Ph.D. thesis is presented, which is the Intelligent Torque Vectoring system. This novel approach is based on intelligent control techniques and includes a vertical tyre forces estimator, which allows to enhance vehicle dynamics, and indirectly, efficiency. The design process and implementation of the proposed approach is deeply addressed and explained. Finally, the TV approach is evaluated by comparing its performance with other approaches proposed in the literature.

4- Intelligent Torque Vectoring

4.1 Introduction

As it has been analyzed in Chapter 2, current TV systems have to deal with the increased complexity of electrified powertrains and their multiple topologies. Besides to enhancing vehicle dynamics, they have to address energy efficiency to increase the driving range of these vehicles. For this purpose, tyre and powertrain losses have to be considered directly or indirectly. Moreover, implementability is also a key issue when designing a TV approach and a balance between performance and computational/economical cost has to be achieved if the proposed algorithm is to be implemented in a real vehicle.

Intelligent control approaches have demonstrated their potential to manage complex systems more easily than other control approaches while maintaining real-time capabilities. Hence, to consider all the aforementioned issues (controller design, complexity, vehicle dynamics, energy efficiency and implementability) in this chapter a novel Intelligent Torque Vectoring approach is proposed, which presents the following main contributions over the works analyzed in Chapter 2,

- A novel approach that combines a Fuzzy controller and an intelligent tyre forces estimator, focused on minimizing model dependency and energy efficiency.
- The energy efficiency is considered indirectly. Tyre losses are reduced by the knowledge of the tyre forces, which allow to reduce losses due to slip. Powertrain losses are handled by the consideration of regenerative braking in the TV approach, allowing to recover part of the braking energy.
- The tyre forces are estimated by the use of an intelligent tyre forces estimator which makes use of easily measured data, and requires no model parameter identification.
- A performance, efficiency and implementability analysis in a heterogeneous embedded platform, combining a μC and a FPGA.

This Chapter is divided as follows. Section 4.2 introduces the fundamentals of the intelligent control techniques used for the development of the proposed TV system. Section 4.3 presents the proposed Intelligent Torque Vectoring approach, explaining all the subsystems by which it is composed. In Section 4.4 the whole system validation is presented. For that, the simulation setup, implementation and the results obtained for the different carried out tests are deeply explained. Finally, Section 4.5 summarizes the main conclusions.

4.2 Fundamental Concepts

The proposed TV approach is based on the so-called Intelligent Control Techniques. To provide an appropriate context to the reader, in this section a brief introduction to the different techniques implemented in this thesis is carried out. In particular Fuzzy Logic, Artificial Neural Networks (ANN) and Adaptive Neuro-Fuzzy Inference Systems (ANFIS) will be briefly detailed.

4.2.1 Fuzzy Logic

Fuzzy logic is an extension of Boolean Logic. It was first proposed by Lot Zadeh in 1965 [153] based on the mathematical theory of fuzzy sets, which is a generalization of the classical set theory. By introducing the notion of degree in the verification of a condition, fuzzy logic provides a very valuable flexibility for reasoning, making it possible to consider inaccuracies and uncertainties. One advantage of fuzzy logic is that the rules are set in natural language.

The most common fuzzy logic system structure is shown in Figure 4.1, which is composed by four main subsystems: Fuzzification, Knowledge base, Inference Method and Defuzzification. Next, these are briefly detailed.

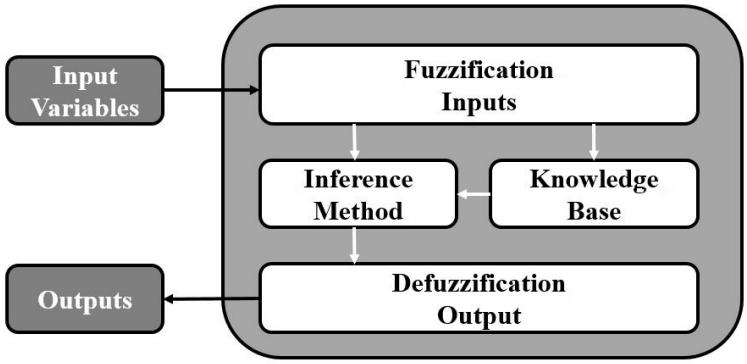

Figure 4.1: General diagram representing Fuzzy Logic approaches

4.2.1.1 Fuzzification

The fuzzification procedure transforms an input vector into the corresponding fuzzy set. This is, fuzzification is the process of determining the degree to which an input data belongs to each of the appropriate fuzzy sets via the membership functions.

4.2.1.2 Knowledge base

The knowledge of a fuzzy logic system is represented by a collection of *If-Then* rules called fuzzy implications. Every fuzzy rule establishes a local relationship between the

input and output variables, while the entire collection of fuzzy rules characterizes the behaviour of a fuzzy system.

4.2.1.3 Inference method

The inference method attempts to simulate human decisions making within the conceptual framework of the fuzzy theory. It aims to infer conclusions by employing fuzzy implications and inference rules. The conclusions can be deduced in different ways depending on the method used to represent the knowledge (rule-based unit) and the type of inference method. The most popular inference methods are the Mamdani method [153] and the Sugeno method [153]. Both methods provide different advantages and disadvantages.

Mamdani systems present more intuitive and easier to understand rule bases. Hence, they are well-suited for applications where the rules are created from human expert knowledge. On the other hand, Sugeno fuzzy inference method, also referred as Takagi-Sugeno-Kang, is more computationally efficient compared to a Mamdani system, since it uses singleton output membership functions.

4.2.1.4 Defuzzification

The output of the fuzzy inference process so far is a fuzzy set. However, in order to be used in real actuators this fuzzy set has to be transformed to a numerical output. Defuzzification is used to map fuzzy sets into numerical values. The most common methods of defuzzification are the Centre of Area (COA) and the Mean of Maxima (MOM) [154].

4.2.2 Artificial Neural Networks

Artificial Neural Networks (ANN) are nonlinear mapping systems whose structure is based on the observed human and animal nervous systems. They are mathematical approximations to the human brain function. Nevertheless, they only emulate a very simple portion of human brain functions and therefore, they are not able to simulate the highly complex relational neurological processes that occur within it. In any case, ANNs are widely used in many fields as they are also considered universal approximators [155].

Processing units are named artificial neurons, being mathematical models of biological ones (Figure 4.2). A biological neuron is a processing unit that processes electrical signals received from the rest of the neurons through the dendrites. These input signals are weighted so that they might excite or inhibit the neuron. All signals are integrated and combined in the neuron body (soma), and if a determined activation threshold is achieved, the resulting signal is transmitted through the axon to other neurons. In biological neurons, the weight values of the inputs are variable, and are influenced by the learning process.

The signal processing procedure detailed for biological neurons is emulated in the artificial neurons (Figure 4.2). Neuron inputs x_j are weighted ω_j and combined, and if a threshold value θ is surpassed, the resulting signal v is processed using an *activation*

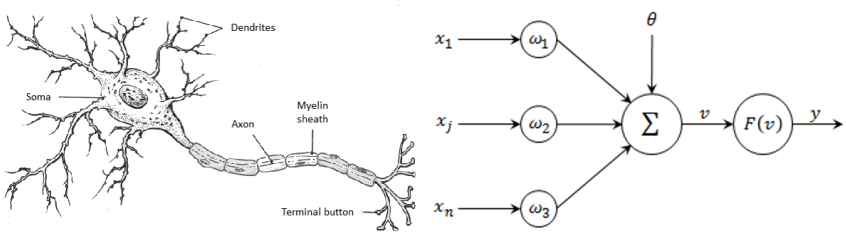

Figure 4.2: Biological neural network and ANN [13]

function. $F(v)$, which determines the output y of the neuron, which will be connected to the inputs of other neurons. A simple approximation of an artificial neuron model is,

$$y = F\left(\sum_j \omega_j x_j + \theta\right) \tag{4.1}$$

As previously stated, in biological neurons, the learning procedure modifies the weights. In the case of ANNs, these need to be *trained* to perform a particular task. This implies to generate a set of examples (input-output relations) related to the target application to *train* the ANN. The training procedure is carried out by adjusting the weights ω_j and biases θ_j of each neuron by means of a proper training algorithm, being the most popular one the *Backpropagation algorithm* [155].

4.2.3 Adaptive Neuro Fuzzy Inference System

Adaptive Neuro-Fuzzy Inference System (ANFIS) is a class of adaptive neural networks that are functionally equivalent to fuzzy inference systems. They combine the advantages of Artificial Neural Networks (learning, adaptability and nonlinear time-variant problem solving) and fuzzy set theory (approximate reasoning and treatment of information).

They are mainly used to solve complex problems that require the use of intelligent approaches, being a viable alternative to conventional model-based control schemes. Due to their hybrid structure, they allow dealing with the common issues of uncertainty and unknown variations in plant parameters and structure, hence improving robustness of the control system.

The inference method used is the Takagi-Sugeno method (see Section 4.2.1) and due to the *If-Then* rules nature, it is possible to identify two parts in the network structure: premise and consequence parts. The general architecture of an ANFIS is composed by five layers, as represented in Figure 4.3.

The first layer corresponds to the fuzzification layer and takes the input values to determine the membership functions belonging to them. The membership degree of each function are computed by using the premise parameter set. The second layer is called as "rule layer" and is the responsible of generating the rules. The role of

the third layer is to normalize the computed firing strength (w_i), by diving each value for the total firing strength. The fourth layer takes as input the normalized firing strengths $\bar{w}_i$ and the consequence parameter set. The values returned by this layer are the defuzzificated ones and those values are sent to the last layer. This layer computes the overall output as the sum of all the incoming signals.

Once the fundamental of the different intelligent control techniques have been introduced, the proposed TV approach will be explained.

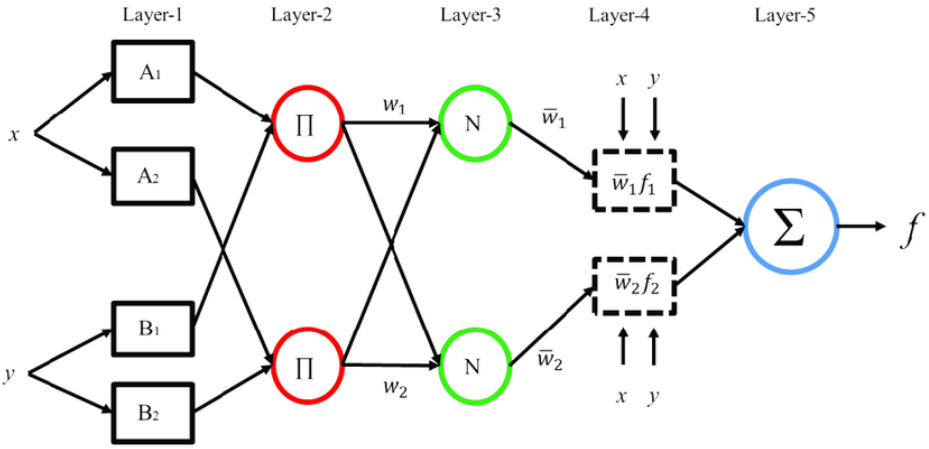

Figure 4.3: Generic ANFIS diagram [14]

4.3 Intelligent Torque Vectoring approach

The overall structure of the proposed Intelligent TV approach is shown in Figure 4.4 (which is the same as in Figure 2.10, but particularized for the approach presented in this Chapter). The approach follows the traditional structure of a TV system shown in Section 2.4.1, where three different layers are clearly differentiated,

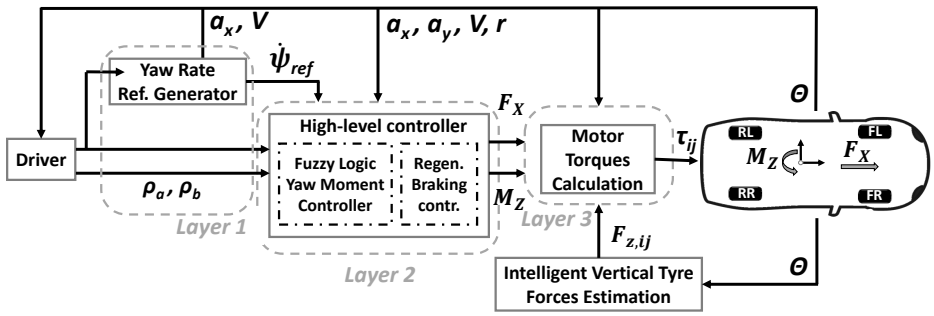

Figure 4.4: Proposed TV approach structure

1. Layer 1: It is composed of the yaw rate reference generator. This subsystem provides the reference of this variable to be tracked by the controller. In the proposed approach, this reference is generated using the well-known *bicycle model*, as it provides a good balance between accuracy and computational cost [67].

2. Layer 2: This layer includes the high-level controller. The controller is composed by a fuzzy logic-based yaw moment controller combined with a regenerative braking contribution. The first provides the lateral torque distribution by controlling both yaw rate and vehicle sideslip angle, as those are the most representative variables for vehicle dynamics. The latter is activated when a stability loss is to occur, enabling the enhancement of vehicle dynamics behaviour and overall efficiency.

3. Layer 3: This layer determines the motor torque commands and includes the longitudinal torque distribution by using the vertical tyre forces estimation data.

4. Vertical tyre forces estimator: This subsystem estimates the vertical tyre forces based on the measurable data from on-board sensors, which is one of the main contributions of the presented approach. To perform this estimation, an artificial intelligence system is proposed, with two possible implementations depending on the final target hardware of the TV ECU: an ANFIS approach, suitable for μC implementation; and a ANN approach, suitable for FPGA implementation.

In the next sections each subsystem shown in Figure 4.4 will be deeply explained.

4.3.1 Yaw Rate reference (Layer 1)

Torque Vectoring systems aim to control the yaw motion of the vehicle, selecting the yaw rate as the controlled variable for the developed control loop. Therefore, to implement the control approach, a proper reference is required. In this section, the methodology for the generation of the yaw rate reference to be tracked is detailed.

The proposed approach is based on the use of the well-known *bicycle model* (Figure 4.5). This model provides a good balance between accuracy and computational cost [67], and requires easy to measure variables, typically provided by common on-board sensors such as steering wheel angle sensor, IMU and GPS. Moreover, the model is parametrized with basic vehicle parameters: mass, trackwidth, center of gravity location and tyre cornering stiffness.

In order to increase the computational performance and generate an ideal vehicle yaw motion reference, several simplifications have been considered in the aforementioned model:

- the center of gravity is assumed to be at a height of zero.
- the variation of the vertical force of each tyre will not be taken into account.
- small slip angles assumption will be considered, so that $\beta = \frac{v_y}{v_x} \simeq \frac{v_y}{V}$, $\sin(\beta) = \beta$, and $\cos(\beta) = 1$ (linear region)

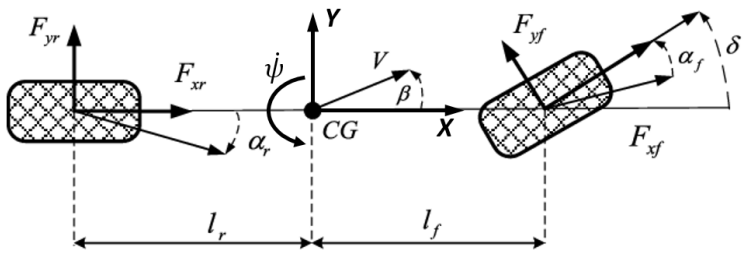

Figure 4.5: Modelling of a vehicle through the "bicycle model"

- steady-state conditions ($\dot{\beta} = 0$)
- the coefficient of lateral stiffness of the front (F) and rear (R) tyre will be considered as constant, defined by the ratio of the lateral force (F_y) to the slip angle (α), as per Eq. 4.2,

$$C_{\alpha,i} = \frac{F_{y,i}}{\alpha_i} \tag{4.2}$$

Since the lateral inertia force acting on the centre of mass of the vehicle is equal to the centrifugal force resulting from drawing a curve with a radius of (R) and an angular speed ($\dot{\psi}$) (see Figure 4.5), the following relation between the lateral acceleration (a_y), the speed (V), the yaw rate ($\dot{\psi}$), and the derivative of the vehicle sideslip angle ($\dot{\beta}$), which is assumed to be zero, can be obtained

$$F_y = ma_y = m\frac{V^2}{R} = mV(\dot{\psi} - \dot{\beta}) = mV\dot{\psi} \tag{4.3}$$

where m is the total mass of the vehicle located in the center of gravity and the remaining magnitudes represent the absolute value of their own vector.

At the same time, the front and rear tyre slip angles can be defined as follows:

$$\alpha_F = \delta - \frac{v_y + l_f\dot{\psi}}{V} = \delta - \beta - l_f\frac{\dot{\psi}}{V} \tag{4.4}$$

$$\alpha_R = -\frac{v_y - l_r\dot{\psi}}{V} = -\beta + l_r\frac{\dot{\psi}}{V} \tag{4.5}$$

where l_f and l_r are the distance to the centre of gravity of the front and rear axle respectively, and δ is the steering angle of the front wheels.

Considering the sum of moments in both axles of the vehicle (front and rear), the following equations are deduced,

$$F_{y,F}L = ma_y l_f \tag{4.6}$$

$$F_{y,R}L = ma_y l_r \tag{4.7}$$

where $F_{y,F}$ and $F_{y,R}$ are the lateral forces of the front axle and rear axle respectively, and L is the distance between axles or *wheelbase*. Combining the Eqs. 4.4-4.5 and 4.6-4.7 it is possible to obtain the following expressions,

$$C_{\alpha F}\left(\delta - \beta - l_f\frac{\dot{\psi}}{V}\right) = ma_y\frac{l_r}{L} \tag{4.8}$$

$$C_{\alpha R}\left(\beta + l_r\frac{\dot{\psi}}{V}\right) = ma_y\frac{l_f}{L} \tag{4.9}$$

where $C_{\alpha F}$ and $C_{\alpha R}$ are the lateral stiffness coefficients of the front and rear wheels, respectively. Operating,

$$\delta = \frac{L}{R} + \frac{m}{L}\left(\frac{l_r}{C_{\alpha F}} - \frac{l_f}{C_{\alpha R}}\right)a_y \tag{4.10}$$

Finally, combining Eqs. 4.3 and 4.10 the yaw rate reference expression can be expressed as follows,

$$\dot{\psi}_{ref} = \frac{V}{L + \frac{m}{L}\left(\frac{l_r}{C_{\alpha F}} - \frac{l_f}{C_{\alpha R}}\right)V^2}\delta \tag{4.11}$$

However, for safety reasons it is necessary to limit the value of the yaw rate reference generated. In this case, the limit has been set as follows [16].

$$\left|\dot{\psi}_{ref,max}\right| = \left|\frac{a_{y,max}}{V}\right| \tag{4.12}$$

where $a_{y,max}$ is the vehicle maximum lateral acceleration. Please note that this yaw rate reference does not consider the energy efficiency and that this aspect will be addressed by the next two layers.

4.3.2 High-level Controller (Layer 2)

The proposed high-level controller combines a Fuzzy Logic controller to define the lateral torque distribution and implements a correction for the moment generated by the regenerative braking. Each of these subsystems will be detailed next.

4.3.2.1 Fuzzy Logic Controller

The main controller is based on Fuzzy Logic (see Section 4.2.1) and tries to track the yaw rate reference generated in the previous section while minimizing the vehicle sideslip angle β. To achieve this, the controller uses the yaw rate and vehicle sideslip angles, and generates the lateral torque distribution (τ_{lat}) for the vehicle.

The structure of the Fuzzy controller is shown in Figure 4.6. In order to calculate the torque percentage to be applied to each side of the vehicle, τ_{lat}, the controller requires three inputs: the yaw rate error $e(\dot{\psi})$, its derivative $\dot{e}(\dot{\psi})$ and the sideslip angle error $e(\beta)$. Note that the output lateral distribution is codified in the $[0, 1]$

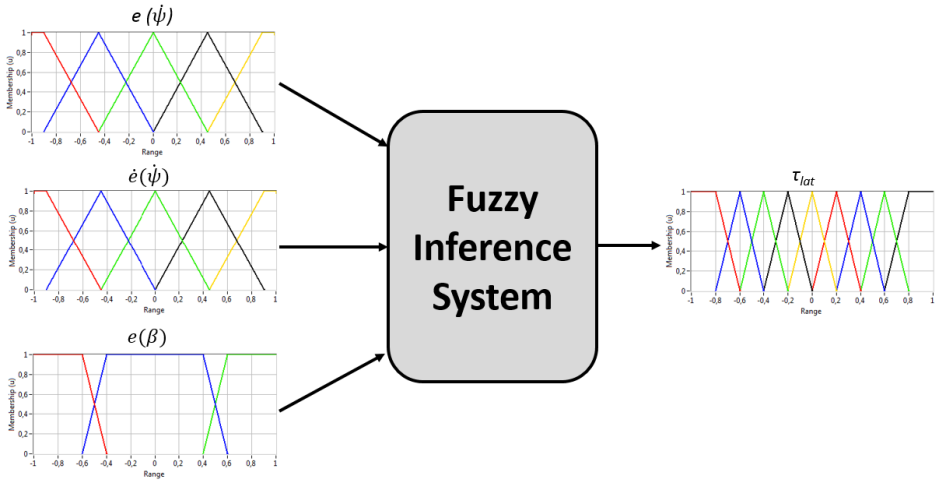

Figure 4.6: Fuzzy Logic Controller proposed

range. This is, if $\tau_{lat} = 0$ all the torque will be applied to the wheels of the right side, and if $\tau_{lat} = 1$ all the torque is applied to the wheels of the left side.

The yaw rate error $e(\dot{\psi})$ and its derivative $\dot{e}(\dot{\psi})$ are calculated considering the reference detailed in Section 4.3.1. The sideslip angle error $e(\beta)$ is calculated considering that the reference sideslip angle of the vehicle will be zero, in order to reduce the real value of the slip and achieve a neutral handling. The actual vehicle sideslip angle value is calculated using Eq. 4.13 defined in [156].

$$\beta = -\arctan\left(\frac{V_y}{V_x}\right) \tag{4.13}$$

where, V_y and V_x are the vehicle speed in the longitudinal (x) and lateral (y) local axes, which can be measured or estimated using on-board sensors.

The Fuzzy Logic controller designed is based on Mamdani fuzzy model, as it provides a more intuitive tuning [157]. For its design, the following membership functions (shown in Figure 4.7) have been defined:

- **Yaw Rate error and its derivative:** A distribution of five membership functions has been chosen for the yaw rate error $e(\dot{\psi})$ and for its derivative $\dot{e}(\dot{\psi})$. Considering the typical sideslip angle and yaw rate values achieved by a passenger car it has been considered that five membership functions cover the whole range for the first two variables with a good level of accuracy. Trapezoidal membership functions have been selected for the boundaries, while triangular ones have been selected for the rest, as they provide computationally efficient calculations [158] maintaining acceptable smoothness on the response, and are suitable to be implemented in a conventional automotive Electronic Control Unit (ECU).

- **Lateral Slip Angle error:** Three membership functions for the input of lateral slip angle, $e(\beta)$ have been defined. Moreover, the sign of the sideslip angle determines if the vehicle has a neutral, understeering or oversteering behaviour. Therefore, it has been considered that only 3 membership functions are needed for this last variable, being all trapezoidal, since the proposed controller tries to minimize this variable (and not to track it) and, therefore, accuracy in this variable is not the highest priority.
- **Lateral Torque Distribution:** For the torque percentage to be applied to each side of the vehicle, τ_{lat}, a more complex distribution of membership functions has been chosen, nine in this case. As for the yawrate error and its derivative inputs, the accuracy and smoothness are crucial in this signal, and therefore, trapezoidal functions have been selected for the boundaries, while triangular ones have been selected for the rest.

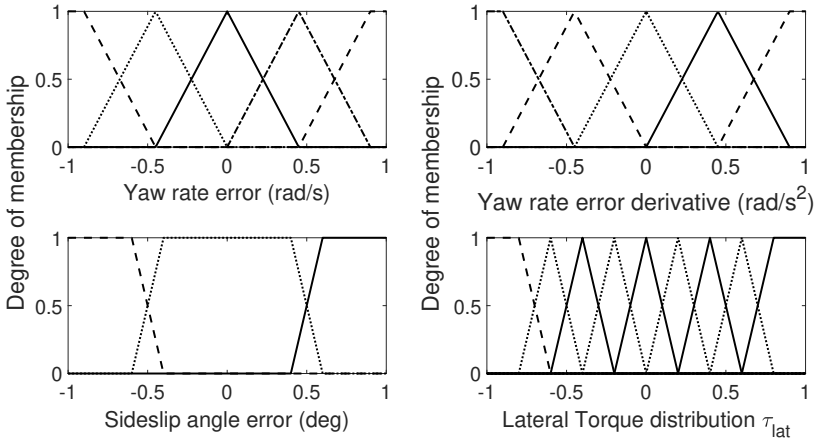

Figure 4.7: Fuzzy Logic Controller Membership Functions

The corresponding rules for the proper performance of the Fuzzy Logic controller have been implemented based on the expert knowledge of the system and human driving datasets. Table 4.1 shows the names and description of the membership functions, while Tables 4.2 to 4.4 show the implemented rules. A representation of the membership functions is also provided in Figure 4.6.

4.3.2.2 Regenerative Braking moment contribution

In electric vehicles, regenerative braking is an essential technology to improve energy efficiency. When considering a TV approach, regenerative braking can not only enhance the overall efficiency of the vehicle, but also enhance its dynamic behaviour, providing an extra yaw moment which contributes to the improvement of cornering performance, specially in emergency manoeuvres.

Table 4.1: Membership Functions Names.

Names	Description
NVL	NEGATIVE VERY LARGE
NL	NEGATIVE LARGE
NM	NEGATIVE MEDIUM
NS	NEGATIVE SMALL
ZE	ZERO
PS	POSITIVE SMALL
PM	POSITIVE MEDIUM
PL	POSITIVE LARGE
PVL	POSITIVE VERY LARGE

Table 4.2: Rules for negative yaw rate error derivative

$\dot{e}(\dot{\psi}) < 0$	$e(\dot{\psi})$					
e(β)		**NL**	**NS**	**ZE**	**PS**	**PL**
	NL	ZE	NS	NM	NL	NVL
	NS	ZE	ZE	NS	NM	NL
	ZE	ZE	ZE	ZE	NS	NL
	PS	PM	PS	ZE	ZE	NS
	PL	PL	PM	PS	ZE	ZE

Table 4.3: Rules for zero yaw rate error derivative

$\dot{e}(\dot{\psi}) = 0$	$e(\dot{\psi})$					
e(β)		**NL**	**NS**	**ZE**	**PS**	**PL**
	NL	ZE	NS	NM	NL	NVL
	NS	PS	ZE	NS	NM	NL
	ZE	PM	PS	ZE	NS	NM
	PS	PL	PM	PS	ZE	NS
	PL	PVL	PL	PM	ZE	ZE

Table 4.4: Rules for positive yaw rate error derivative

$\dot{e}(\dot{\psi}) > 0$	$e(\dot{\psi})$					
e(β)		**NL**	**NS**	**ZE**	**PS**	**PL**
	NL	ZE	ZE	NS	NS	NM
	NS	PS	ZE	ZE	NS	NS
	ZE	PM	PS	ZE	ZE	ZE
	PS	PL	PM	PS	ZE	ZE
	PL	PVL	PL	PM	PS	ZE

This way, in the proposed TV system, a regenerative braking component is implemented, which is only activated when the sideslip angle β is above 10°, as this is an indicator of undesirable behaviour (understeering or oversteering). Hence, if the lateral torque distribution generated by the Fuzzy Logic controller τ_{lat} and the moment generated by regenerative braking in critical conditions is considered, the motor torques considering the lateral distribution ζ_{ij} can be calculated as follows,

$$\begin{aligned}
\zeta_{FL} &= \begin{cases} -max(min(\tau_{lat}, (1-\tau_{lat})), \gamma_{Front}), & \text{if } \beta \geq 10 \\ \tau_{lat}, & \text{otherwise} \end{cases} \\
\zeta_{FR} &= \begin{cases} -max(min(\tau_{lat}, (1-\tau_{lat})), \gamma_{Front}), & \text{if } \beta \geq 10 \\ 1-\tau_{lat}, & \text{otherwise} \end{cases} \\
\zeta_{RL} &= \begin{cases} -max(min(\tau_{lat}, (1-\tau_{lat})), \gamma_{Rear}), & \text{if } \beta \geq 10 \\ \tau_{lat}, & \text{otherwise} \end{cases} \\
\zeta_{RR} &= \begin{cases} -max(min(\tau_{lat}, (1-\tau_{lat})), \gamma_{Rear}), & \text{if } \beta \geq 10 \\ 1-\tau_{lat}, & \text{otherwise} \end{cases}
\end{aligned} \tag{4.14}$$

As represented in Eq. 4.14, the braking torque will be applied in the inner or outer wheels, depending on the lateral torque distribution provided by the fuzzy yaw moment controller τ_{lat}. This is, this negative torque will be applied in the inner wheel when the vehicle is suffering understeering, in order to help it to increase its cornering capabilities, and in case of suffering oversteering the braking torque will be applied in the outer wheel in order to avoid the possible stability loss.

Note, however, that this extra yaw moment generated by the regenerative braking has to be strictly controlled by limiting the regenerative torque, as possible stability losses can arise if other case. Additionally, these limits have to be tuned for each axle (γ_{Front} and γ_{Rear}), as both axles (front and rear) do not brake equally.

4.3.3 Motors Torque Calculation (Layer 3)

The last subsystem calculates the exact motor torque command to be applied to each wheel τ_{ij}, based on the torque requested by the driver τ using the throttle position, the lateral torque distribution provided by the Level 2 controller ζ_{ij} (Section 4.3.2) and the vertical tyre forces information provided by the estimator that will be detailed in Section 4.3.4.

This block is used exclusively in 4WD vehicles, in which is possible to distribute the torque not only laterally but also longitudinally (between the front and rear axles). The latter is carried out by considering the information provided by the vertical tyre forces estimator, whose goal is to provide greater torque commands to the motors whose tyres have more grip. For that purpose, a simple but effective torque distribution algorithm is proposed, based on the maximum normal force that can be applied in an axle f_{max} and the estimation of the vertical forces generated by the wheels at each axle f_{wheels},

$$\tau_{long} = \frac{f_{wheels}}{f_{max}} \tag{4.15}$$

where f_{wheels} is the combination of the vertical forces of each wheel of an axle (left and right) and f_{max} is the maximum normal force that can be applied in the front axle (this is, considering that the whole mass is actuating only in one axle).

Once the longitudinal torque distribution is calculated, it is possible to calculate the exact torque command for each of the motors by combining Eqs 4.14 and 4.15.

$$\begin{aligned} \tau_{fl} &= \tau\, \tau_{long}\, \zeta_{FL} \\ \tau_{fr} &= \tau\, \tau_{long}\, \zeta_{FR} \\ \tau_{rl} &= \tau\, (1 - \tau_{long})\, \zeta_{RL} \\ \tau_{rr} &= \tau\, (1 - \tau_{long})\, \zeta_{RR} \end{aligned} \tag{4.16}$$

4.3.4 Intelligent Vertical tyre forces estimation

The dynamic behaviour of the vehicle is highly dependent on tyre forces, as these are the elements in contact with the road. However, direct measurement of these forces is not a solution, as these forces are very difficult to measure and the sensors needed are very expensive. Hence, these forces need to be estimated, which is not a trivial task, as the tyre/road contact dynamics not only has a nonlinear behaviour but also depends on a number of different variables.

As analysed in Section 2.4.4, in the literature several analytical approximations of different complexity level can be found. However, they usually present different problems related with their implementability, such as the utilization of variables difficult to measure or a high computational cost due to an elevated complexity. In this sense, in this work, the proposed vertical tyre forces estimator tries to address these two issues through the utilization of Intelligent Control techniques, as they have demonstrated to be universal approximators [155].

With the aim of avoiding to rely on variables difficult to measure in commercial cars, the proposed estimator uses variables measured by typical on-board sensors. Besides, in order to guarantee that the used data are representative enough and simplify the training procedure, data obtained experimentally with the validated vehicle dynamics model in Chapter 3 will be used.

The input data is composed by 16 variables: the steering angle (δ), the x, y and z linear acceleration (a_x, a_y, a_z), the vehicle total speed, the 3 angular speeds associated to the local axes (roll rate, pitch rate and yaw rate) and the four wheel torques ($\tau_{FL}, \tau_{FR}, \tau_{RL}, \tau_{RR}$) and wheel angular speeds ($\omega_{FL}, \omega_{FR}, \omega_{RL}, \omega_{RR}$).

All of them can be easily measured using commercially available sensors such as steering wheel angle sensor, Inertial Measurement Units (IMU), Global Positioning Systems (GPS), and motor current and angular speed sensor (both needed by the motor controller). The output data are the four vertical tyre forces estimations ($F_{z,FL}, F_{z,FR}, F_{z,RL}, F_{z,RR}$).

In this chapter, two intelligent control techniques based solutions are proposed. The first one uses an ANFIS, while the second one uses an ANN, for the vertical tyre forces estimation. As both techniques use the same input data and have been

trained with the same datasets, a comparison not only in terms of accuracy, but also in terms of implementability can show which technique is more appropriate for this particular application.

Regarding the specific structure of each solution. The ANN based estimator is composed by three layers (an input layer, a hidden layer and an output layer), while the ANFIS based estimator is composed by 5 layers (see Figure 4.3). In the first one, 7 membership functions for each input have been developed. These membership functions are of Gaussian type, as they provide better precision than triangular ones [159] [158]. In the second one, the rules established by the learning process appear. In the third and fourth layer the ratio calculation and normalisation is carried out to finally, in the fifth layer, add all the signals and generate the output.

Once, the structure of each estimator has been chosen they must be trained. In this case, the training data is proposed to be obtained through simulation experiments using the framework validated in Chapter 3. This way, despite not having a real car to obtain real data, it is possible to not only get representative data, but also, this data can represent conditions that are very difficult to obtain in real tests. Finally, once the estimators have been trained and their accuracy is high enough, they will be validated (see Section 4.4.2).

4.4 Validation

In this section, the aforementioned Intelligent Torque Vectoring approach will be validated with the framework detailed in Chapter 3. For that purpose, this section is divided as follows. First, the whole validation setup is introduced. Second, the validation of the proposed vertical tyre forces estimators is presented. Finally, the validation and performance evaluation of the proposed Intelligent TV system is deeply explained.

4.4.1 Simulation setup

The overall structure of the implemented setup is detailed in Figure 4.8, where a Hardware-in-the-Loop (HiL) validation approach has been implemented.

This way, the TV algorithm has been deployed in a real hardware, the Xilinx Zynq XC7Z020 SoC [15]. This is composed by two different hardware devices: a programmable logic part, this is a FPGA; and an ARM microcontroller (μC) of two cores and 800 MHz clock rate. This chip is present in the Xilinx ZC702 Evaluation Board (see Figure 4.9) which includes several I/O peripherals, that include communication buses, such as CAN, which are used to communicate with the rest of the simulated vehicle.

The simulated vehicle runs on a laptop (2.8GHz and 16 GB RAM) which was connected to the Xilinx Evaluation board through CAN Bus. A C-Class vehicle with All Wheel Driven (AWD) electric powertrain topology has been selected for the validations carried out in this section. The main parameters of the vehicle are detailed in Table 4.5.

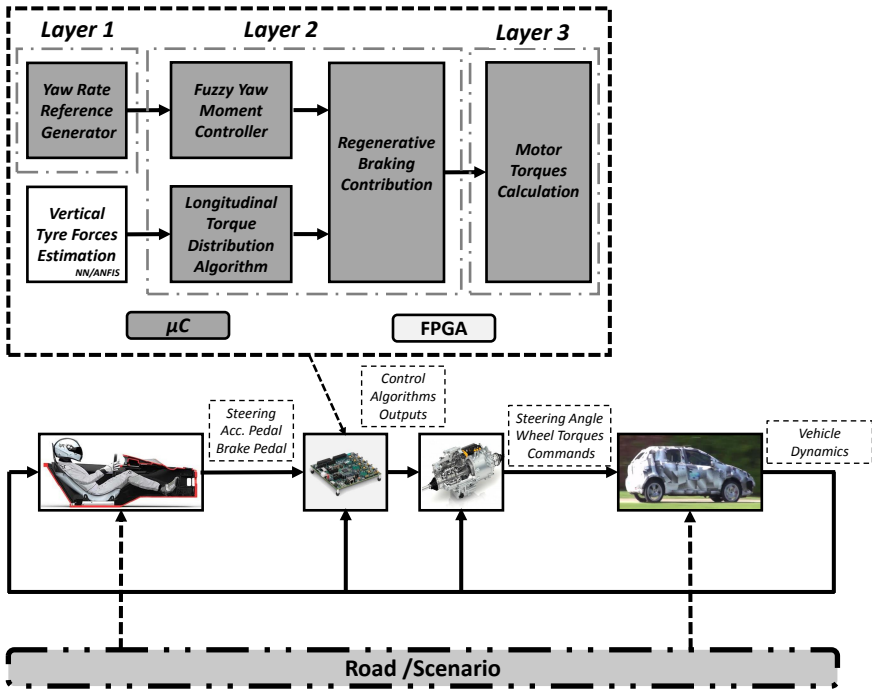

Figure 4.8: Structure of the HiL setup

Note that as the selected Xilinx Zynq XC7Z020 SoC integrates an FPGA and a microcontroller, both can used to deploy the code related to the proposed Intelligent Torque Vectoring approach.

4.4.2 Validation of the Intelligent Tyre Forces Estimators

A fundamental part of the proposed Intelligent Torque Vectoring approach is the designed Intelligent Tyre Forces estimators, which defines the longitudinal torque distribution in 4WD vehicles.

In this section, the proposed approach will be validated considering the particularities of the two possible implementations discussed in Section 4.3.4: ANN and ANFIS. As both alternatives are based on machine learning, first, their training procedure will be detailed. In the second subsection, the implementation procedures and considerations will be analyzed. Finally, both will be validated by considering an analytical benchmark tyre forces estimator proposed in the literature.

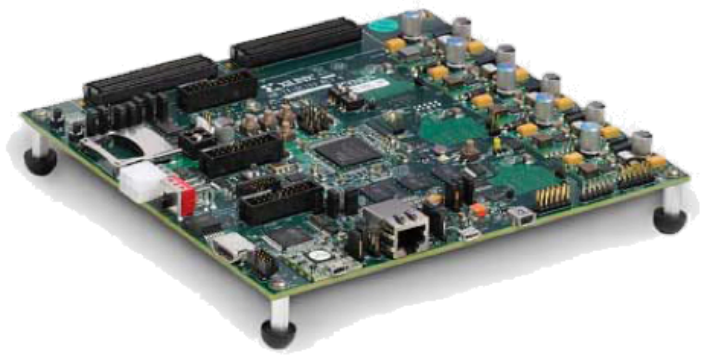

Figure 4.9: Xilinx ZC702 Evaluation Board [15]

Table 4.5: Vehicle Main Characteristics.

Mass (kg)	1623
Ix (kg m^2)	700
Iy (kg m^2)	2300
Iz (kg m^2)	2830
Wheelbase (m)	2.82
Front Axis Track (m)	1.6
Rear Axis Track (m)	1.6
Tyre Radius (m)	0.328
Center of gravity to rear axle distance (m)	1.5
Center of gravity to front axle distance (m)	1.32
Height of center of gravity (m)	0.53
Frontal Area (m)	2.2

4.4.2.1 Training Procedure

The proposed Intelligent Tyre Forces Estimators require a training procedure to *learn* the tyre dynamics. In order to train both approaches, as detailed in Section 4.3.4, a supervised training approach has been selected, which requires to create a dataset that includes both the set of inputs and their corresponding mapped outputs that the ANN or ANFIS is supposed to learn. For the considered study-case, the datasets are generated by simulating a whole lap in three different circuits. These circuits are the

following ones Nurburgring, Silverstone and Montmelo, and the data were captured by using the framework detailed in Chapter 3.

This way, as the samples were captured at 20 Hz, the dataset is composed by a total of 21792 input/output samples, representing a wide variety of the possible input ranges for the estimator. To avoid overfitting, the aforementioned dataset is divided in two sets: a training set (75% of the samples) and a validation set (25% of the samples). The selection of the samples was carried out randomly.

Once the training and validation datasets were defined, the training procedure was carried out. In the case of ANN, it has been trained for 1000 epochs, considering a single hidden layer and hyperbolic tangent activation function and using a combination of the *backpropagation* and *gradient descent* algorithms with a learning rate value of 0.1. In order to determine the optimum number of neurons in the hidden layer, a training batch has been executed from 10 to 60 neurons.

Table 4.6 summarizes the accuracy and relative improvement to the previous option provided by different ANNs, depending on the number of neurons selected.

Table 4.6: Neural Network training and results

	Number of Neurons					
	10	20	30	40	50	60
MAE [N]	4756	2181	621	159	97	95
NMAE [%]	63.96	29.33	8.35	2.13	1.30	1.27
% Improvement	N/A	54.14	71.52	74.39	38.99	2.06

The Normalized Mean Absolute Error (NMAE) for the validation data is relative low (less than 2.5%) from 40 neurons, which is considered an optimal accuracy for this application. Additionally, it can be seen that the improvement in the accuracy percentage is significantly reduced from 50 neurons. Therefore, it can be concluded that the optimal number of neurons is between the interval [40,50].

Note that as this ANN will be implemented in a FPGA, several modifications have to be carried out with the aim of achieving better computational cost and resources utilization. Hence, the exact number of neurons will be selected after the effect of all these modifications are evaluated.

Finally, as detailed in Section 4.3.4, the selected ANFIS architecture was divided in five layers. In this case, the method selected for the generation of the Fuzzy inference system is Subclustering, due to the high number of inputs. Considering the aforementioned architecture and the defined datasets an hybrid training method (see Table 4.7) during 1000 epochs has been carried out, consisting of backpropagation for the parameters associated with the input membership functions, and least squares estimation for the parameters associated with the output membership functions.

4.4.2.2 Implementation

The implementation of the aforementioned estimators in the Xilinx Zynq XC7Z020 SoC is discussed in this section. This hardware platform implements both a FPGA

Table 4.7: Parameters of the Hybrid Method Training

Range of Influence	0.5
Squash Factor	1.25
Accept Ratio	0.5
Reject Ratio	0.15

(Xilinx Artix 7 model) and a microcontroller. The use of FPGA increases computational efficiency by liberating resources from the microcontroller [114]. In addition, unlike microcontrollers, where the algorithm deployed is run as software, in FPGAs, the deployed algorithm is run as hardware. However, complex code does not fit in FPGAs, and proper code optimization is required to achieve this goal.

This way, only the ANN based vertical tyre forces estimator has been implemented in the FPGA, while the ANFIS based one has been implemented in the microcontroller by using the MATLAB Embedded Coder [121] tool. This choice is motivated by the following reasons. First, the FPGA has limited hardware resources and therefore all the subsystems cannot be implemented in this device. Second, the intrinsic mathematical formulation of neural networks make them very suitable for their implementation in FPGAs. Finally, although the ANFIS based vertical tyre forces estimator also includes an ANN, the fuzzy part increases the hardware resources requirements, making it not suitable for the device selected in this work.

However, the implementation of ANNs in FPGA has the hardware resources limited. For that reason, several modifications have to be carried out so that the ANN can fulfill the device resources restrictions without compromising its performance. These will be detailed next:

- As it is stated in [114], pipelining has to be disabled with the aim of decreasing the resource utilization.

- Due to the high amount of hardware resources that floating point mathematical operations need, the data type of the variables has to be adapted from floating point to fixed point data type. Using the Matlab Fixed-Point Toolbox [121], the optimal data type has been established experimentally as fixed point data of 24 bits, where the length of the decimal part depends on the working range of each variable.

- In addition, some mathematical operations are very inefficient to be solved in a FPGA. In particular, the activation function of the neurons is a hyperbolic tangent function, whose implementation requires a lot of resources. To optimize its execution for a fixed point implementation, this operation has been replaced by a look-up table (LUT). The maximum relative tolerance between the original output value and the output value of the approximation has been established as 2%. Additionally, the breakpoint specification has been carried out using the "EvenPow2Spacing" method, which means a power-of-two spacing, providing a

Table 4.8: NN FPGA Implementation Resources and Performance

Size	Resource Utilization								NMAE
	BRAM		DSP		Registers		LUTs		
	Total	%	Total	%	Total	%	Total	%	
40	47	33.5	216	98.18	24448	22.9	37356	70.2	2.93
50	50	35.7	270	122.7	30187	28.3	39254	73.7	1.88

fastest execution speed. The rest of the operations are additions/substractions or multiplications that can be implemented easily on a FPGA.

These modifications to the ANN estimator have to be evaluated, as they will have an impact on the accuracy of the final ANN Estimator and the resource utilization of the FPGA. Table 4.8 shows the NMAE and the percentage of FPGA resources utilization for the two ANN architectures selected in Section 4.4.2.1. In this case, the most critical resources are the DSP (220 available in the selected device). In spite of that the explained modifications have contributed to reduce the number of needed DSP in exchange of using more BRAM, registers and LUTs, the only ANN that fulfills the hardware resources requirements is the one composed by 40 neurons. As it can be seen, the 40 hidden neurons ANN Estimator is the one that fits the selected FPGA, and its accuracy is reduced a 0.83% due to the changes required for FPGA implementation.

4.4.2.3 Validation Results

Once both approaches for the Intelligent Tyre Forces estimator have been implemented on the Xilinx Zynq XC7Z020 SoC, their performance is evaluated by comparing their estimation accuracy with a mathematical model based tyre forces estimator found in the lierature [18] (see Appendix A).

The manoeuvre chosen for the validation of the proposed estimators is the Double Lane Change with a longitudinal acceleration $a_x = 2.83$ m/s^2, as it is challenging enough and covers a wide range of vehicle speed (from 50km/h to 100km/h). Note that the Dynacar's internal high fidelity tyre model [119] is used as the reference to define the accuracy of each approach.

Figure 4.10 and Table 4.9 show the results obtained for the forces estimation in each wheel. They show that the ANFIS estimator provides the best accuracy (approximately 2% of error), while the ANN based estimator offers a good accuracy as well, being both below the 3.5% of error. The benchmark estimator based on [18] provides the lowest accuracy, with an error of approximately 5%, corresponding to the errors obtained in [18].

However, if the computational cost is considered, the ANN Estimator offers the best performance, with a total time to be run by the FPGA of 3.1 microseconds (μs). The total time needed by the analytical model and the ANFIS based estimator to be run in the microcontroller are 750μs and 900 μs. This means that the proposed ANN based tire vertical forces estimator is more than 240 times faster to be executed

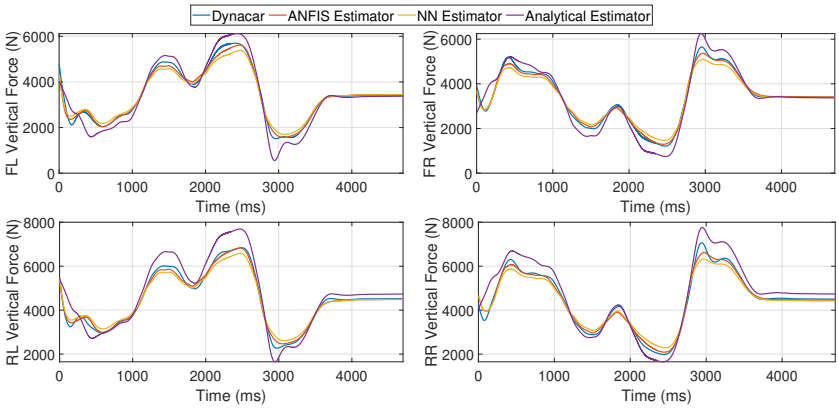

Figure 4.10: Fz Estimation - Double Lane Change

Table 4.9: Double Lane Change Results

		ANFIS	ANN	Model
FL	MAE [N]	109.63	186.74	301.26
	NMAE [%]	1.92	3.28	5.29
FR	MAE [N]	98.33	189.74	281.20
	NMAE [%]	1.73	3.34	4.96
RL	MAE [N]	111.99	191.27	380.30
	NMAE [%]	1.64	2.80	5.56
RR	MAE [N]	144.20	227.57	341.98
	NMAE [%]	2.04	3.22	4.84
	Execution time [μs]	900	3.1	750

thanks to the implementation in a FPGA and the computational optimizations carried out.

In summary, both techniques, ANN and ANFIS, used for the vertical tyre forces estimation have demonstrated to be very suitable approaches to implement tyre forces estimators, as they can compensate both uncertainties in the model and provide abstraction from complexity. In particular, if ANNs are selected for implementation, their computational cost can be greatly reduced by the use of FPGAs, while maintaining a high level of accuracy. Thus, this approach will be implemented in the Intelligent Torque Vectoring validation tests detailed in the next sections.

4.4.3 Validation of the proposed Intelligent TV

In this section, the Intelligent Torque Vectoring proposed in Section 4.3 is validated by using the simulation setup proposed in Section 4.4.1. As previously stated, all the elements that compose the Intelligent TV system (see Figure 2.10) are implemented in the microcontroller, with the exception of the Intelligent Tyre Forces Estimator,

which has been implemented in the FPGA using an ANN-based approach. In order to validate the approach, a comparative analysis will be carried out with two widely used approaches in the literature:

- PID control: PIDs have been widely used for a variety of applications, including TV. The selected PID approach is based on a PID controller with feed-forward contribution [16] (Figure 4.11). Its parameters have been tuned experimentally for both open loop frequency response and the requirements of the closed-loop bandwidth. The obtained values are the following: $K_P = 75200$Nms/rad, $K_I = 0.00365$Nm/rad, $K_D = 0.76$ Nms^2/rad.

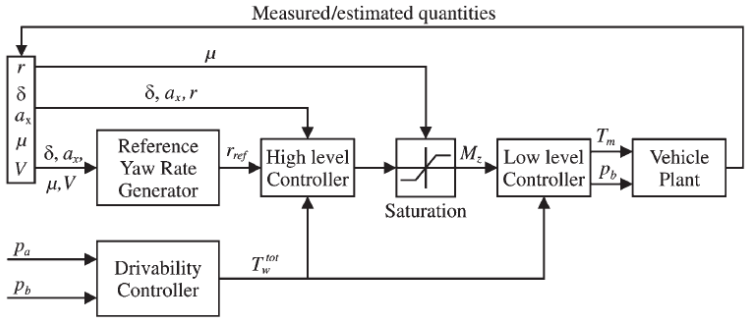

Figure 4.11: PID based TV approach [16]

- Second Order Sliding Mode Controller (SOSMC): Sliding Mode Control methods are able to improve the system performance from both disturbance rejection and convergence points of view. Due to these advantages, they have been used to implement TV approaches. However, First Order Sliding Mode controllers present chattering issues when operating. Hence, in this work a Second Order Sliding Mode Controller [17] (Figure 4.12) has been selected to compare its performance. The control parameters have been tuned as follows: $\beta_1 = 2.5$ and $\beta_2 = 10000$.

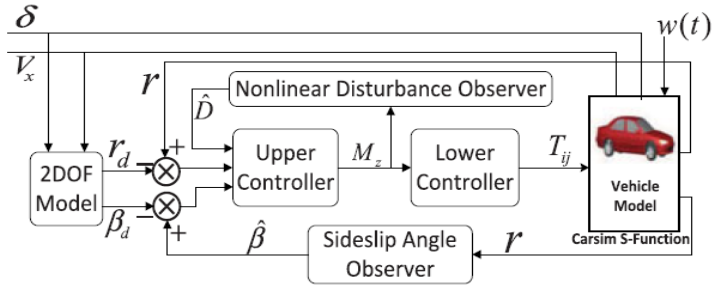

Figure 4.12: SOSMC based TV approach [17]

To determine the performance of the aforementioned approaches, and the proposed one, each approach will be analyzed in the following set of standarized manoeuvres: Ramp Steer, Double Lane Change, and a lap in a Circuit. These manoeuvres allow to evaluate the lateral dynamics performance of the vehicle, and the effect of TV approaches.

4.4.3.1 Ramp Steer Manoeuvre

The first manoeuvre is the called ramp steer. This manoeuvre consists in applying a ramp steer input (15 deg/s) at a constant vehicle speed. This speed has been established at 80 km/h for dry road condition and 50 km/h for wet road condition, as these speeds correspond to the most common situations in urban and medium speed roads. The main objective of this test is to determine the maximum lateral acceleration of a vehicle in steady-state cornering conditions. As stated in Chapter 2, TV algorithms have demonstrated their ability in these conditions to not only modify the understeering characteristics, but also, to extend the linear zone and increase the maximum lateral acceleration.

Figures 4.13-4.14 and Table 4.10 show the results obtained for this manoeuvre for the studied cases: PID TV, SOSMC TV, Intelligent TV, and the passive vehicle. Note that wet (friction condition $\mu = 0.6$) and dry conditions (friction condition $\mu = 0.9$) have been studied.

It can be appreciated in Figures 4.13 and 4.14 that the optimal torque distribution provided by a TV approaches helps to reduce the understeering, extending the linear zone and increasing the maximum lateral acceleration in comparison with the passive vehicle, both in dry and wet conditions.

Table 4.10 summarizes the results. First, it can be appreciated that the PID TV provides the worst performance compared to the other solutions. It only considers the yawrate tracking, while the SOSMC TV and Intelligent TV also consider the sideslip angle. Finally, the maximum improvement is given by the proposed approach (14.99% for dry conditions and 14.12% for wet conditions), demonstrating that having a reliable knowledge of the vertical tyre forces contributes for an optimal torque distribution.

Table 4.10: Ramp Steer Manoeuvre Maximum Lateral Acceleration Comparison

	Dry Conditions		Wet Conditions	
	Max. Lat Acc	% Impr.	Max. Lat Acc	% Impr.
Passive	7.832 m/s^2	-	5.590 m/s^2	-
PID TV	8.858 m/s^2	11.582	6.336 m/s^2	11.780
SOSMC TV	9.161 m/s^2	14.507	6.375 m/s^2	12.321
Intelligent TV	9.214 m/s^2	14.990	6.509 m/s^2	14.124

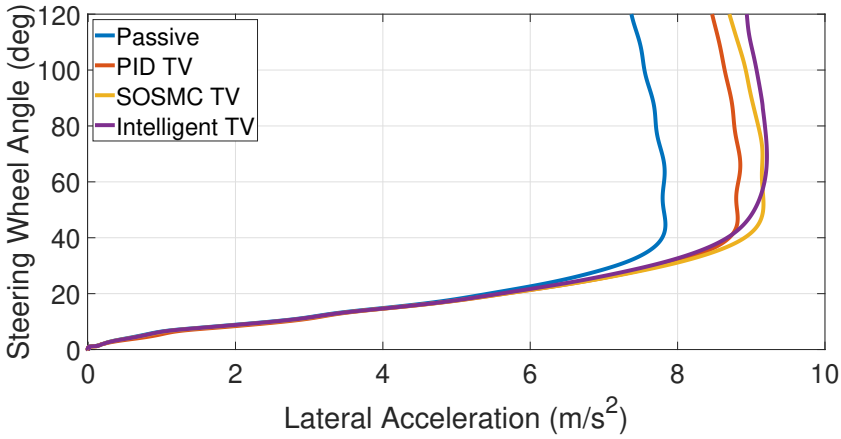

Figure 4.13: Understeering Characteristics (Dry Condition)

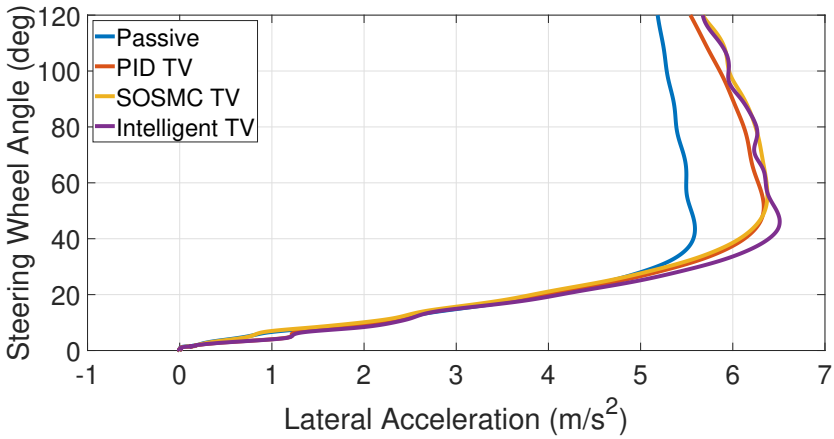

Figure 4.14: Understeering Characteristics (Wet Condition)

4.4.3.2 Double Lane Change Maneouvre

The second manoeuvre that has been performed is the called Double Lane change [160]. This manoeuvre is a typical obstacle avoidance manoeuvre in which the vehicle performs a lane change to avoid the obstacle (or preceding vehicle) and then moves back to its original lane. The lane change is fixed in space and marked with gates made with cones, which the vehicle must go through. Figure 4.15 shows the XY plane projection of this test, with three cone gates marking the limits the vehicle must not surpass.

To perform this test, a initial speed of 50 km/h has been selected for dry and wet road conditions. Accordingly, an appropriate constant torque reference for each case

has been applied (2300 Nm total torque for dry road condition and 1500 total Nm for wet conditions). This provides a longitudinal acceleration of 4.27 m/s^2 (0.43g) and 2.78 m/s^2 (0.284g), allowing to obtain a final speed of almost 100 km/h and 80km/h respectively, covering the most common speed range of passenger vehicles in medium speed roads in both conditions. This manoeuvre is very challenging for the passive vehicle (without TV), but this case has also been considered for reference.

Results for dry conditions are shown in Figures 4.15-4.18. In Figure 4.15 it can be appreciated that the manoeuvre is only performed successfully by the proposed Intelligent TV approach, while the other approaches are not able to follow the required yaw rate reference and surpass the limits imposed by the cones. This phenomenon can be further appreciated in Figures 4.16, 4.17 and 4.18, where the lateral acceleration, the steering wheel angle and the slip angle are analyzed. As it can be seen, the proposed Intelligent Torque Vectoring approach allows to maintain the desired dynamic behaviour thanks to a proper torque distribution algorithm (including regenerative braking, marked in green in Figure 4.16). This enables to achieve higher lateral accelerations while reducing the steering wheel angle and slip angles. Note, in fact, that the steering wheel angle and front wheels slip angle, are considerably higher (44°and 5.5°average, respectively) for the PID TV approach and SOSMC TV approach.

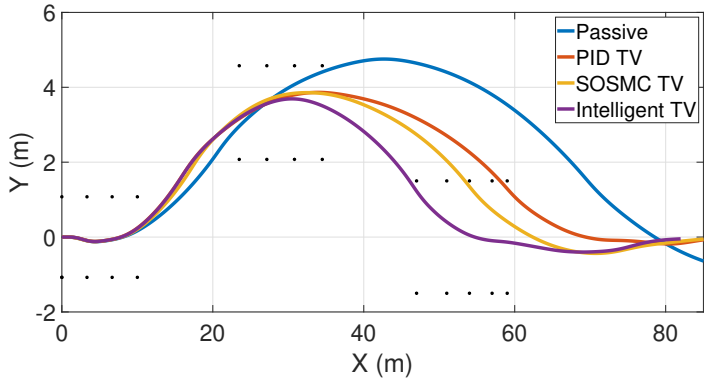

Figure 4.15: Double Lane Change - Trajectory (Dry Conditions)

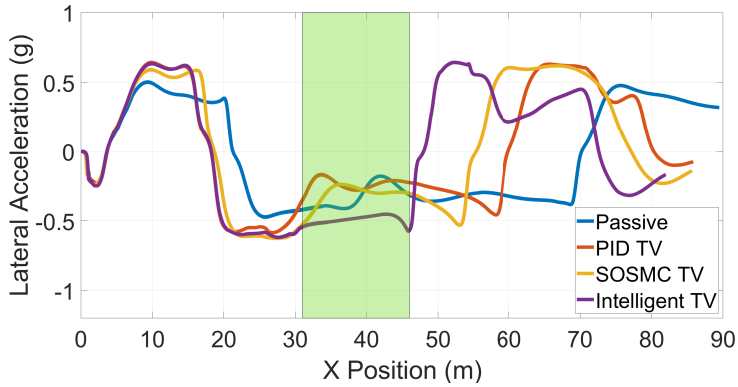

Figure 4.16: Double Lane Change - Lateral Acc. (Dry Conditions)

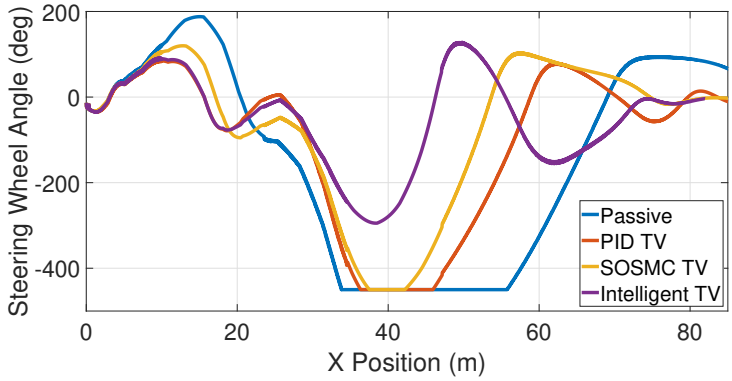

Figure 4.17: Double Lane Change - Steering wheel angle (Dry Conditions)

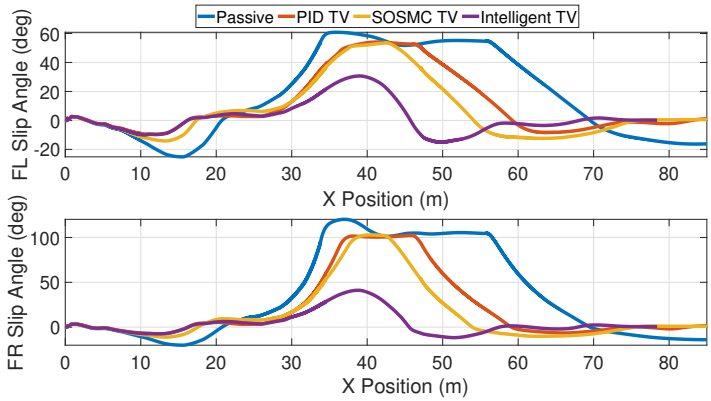

Figure 4.18: Double Lane Change - Slip Angle (Dry Conditions)

In the case of wet conditions (Figures 4.19-4.22) the effect of an optimal torque distribution is much more remarkable. As in the previous case, the proposed Intelligent TV approach is the only one that is able to make the vehicle perform the manoeuvre successfully. However, the difference is higher compared with the dry case. In the case of the steering wheel angle (Figure 4.21) it can be seen that the value is saturated to the maximum physical value (±450°) for all cases. If this aspect is analyzed with the slip angle values (Figure 4.22), it can be seen that all approaches, except the proposed Intelligent Torque Vectoring, present excessive understeering behaviour. Moreover, in this case, the maximum values for the steering wheel and front wheels slip angle are reduced a 35% and a 54% respectively compared to the passive vehicle. Therefore, the results obtained for this manoeuvre, in dry and wet road conditions, demonstrate the effectiveness of the TV approach presented in this work, providing the most optimal torque distribution, thanks to considering the vertical tyre forces and a regenerative braking (marked in green area when this function is activated in Figure 4.16 and 4.20).

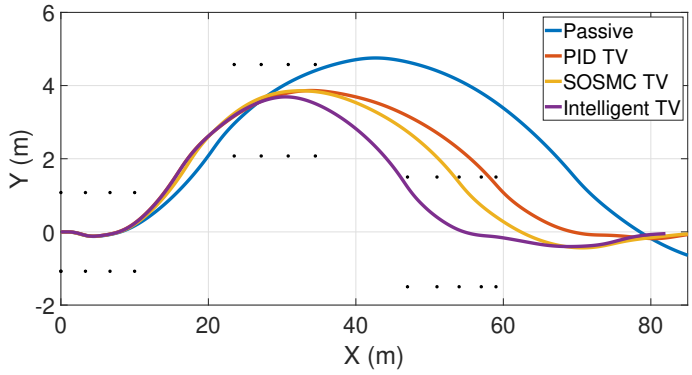

Figure 4.19: Double Lane Change - Trajectory (Wet Conditions)

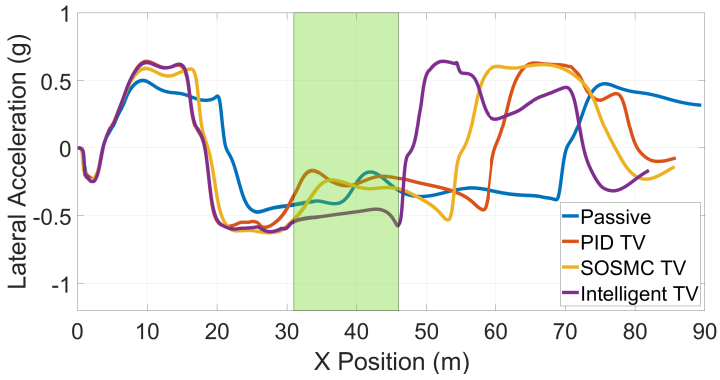

Figure 4.20: Double Lane Change - Lateral Acc. (Wet Conditions)

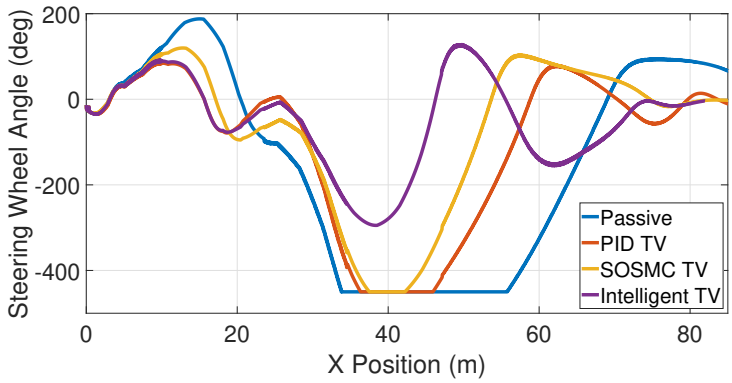

Figure 4.21: Double Lane Change - Steering wheel angle (Wet Conditions)

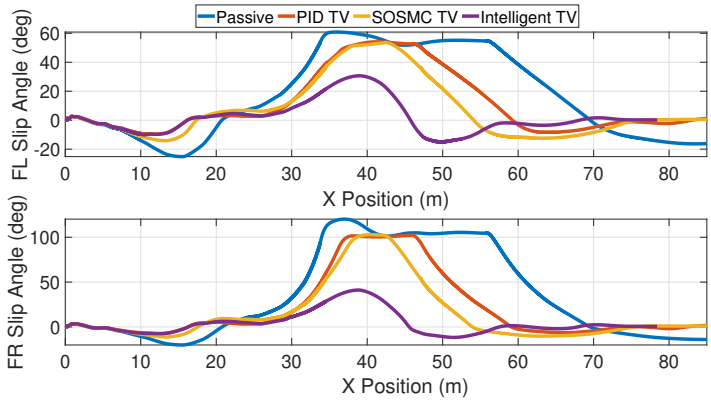

Figure 4.22: Double Lane Change - Slip Angle (Wet Conditions)

4.4.3.3 Circuit test

In the previous tests, the enhancement on the dynamic behaviour of the vehicle has been analysed for the different TV approaches. In this test, an efficiency comparison will be carried out to evaluate the effect of the proposed TV approach on energy consumption.

For that purpose, the study-case vehicle has been simulated on three circuits (Nurburgring, Montmelo and Silverstone), where a whole lap has been simulated by the Virtual Driver of the *Vehicle Dynamics Simulation Framework* (see Figure 4.23). The electrical energy consumed has been computed in each case.

Results are summarized in Table 4.11. As it can be seen the proposed TV approach provides a lower energy consumption (7% average of energy consumption reduction compared to the PID TV and SOSMC TV) thanks to the regenerative braking contribution with its consequent efficiency improvement. It has to be re-

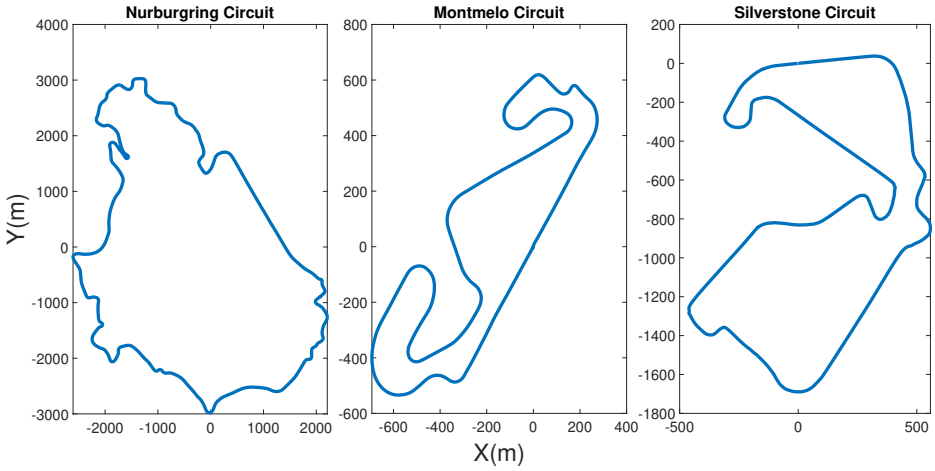

Figure 4.23: Nurburgring, Montmelo and Silverstone circuits

marked that the regenerative braking is not activated in each braking condition, but only when the sideslip angle is greater than 10°, as it has been already explained in Section 4.3.2.

Table 4.11: Electrical Energy Consumption Comparison

	Passive		PID TV	
	Energy	Improvement	Energy	Improvement
Nurburgring	17.01 kWh	N/A	15.71 kWh	7.62%
Montmelo	5.62 kWh	N/A	5.27 kWh	6.61%
Silverstone	8.34 kWh	N/A	7.8 kWh	6.42%
	SOSMC TV		Intelligent TV	
	Energy	Improvement	Energy	Improvement
Nurburgring	15.89 kWh	7.59%	14.65 kWh	13.35%
Montmelo	5.13 kWh	8.88%	4.88 kWh	13.21%
Silverstone	7.82 kWh	6.21%	7.2 kWh	13.67%

4.5 Conclusions

The development of real-time capable, accurate and efficient vehicle dynamics control systems is a key issue for the development of vehicles with independent in-wheel motors. In this chapter a novel Intelligent Torque Vectoring system, that combines a Fuzzy yaw moment controller and an intelligent tyre forces estimator, which allows minimizing model dependency and energy efficiency through reducing the tyre slip.

The developed approach considers both longitudinal and lateral torque distributions. The longitudinal distribution is calculated considering the vertical load of each axle, which is estimated using an intelligent tyre forces estimator. Two implementations for this estimator are proposed and analyzed, considering different hardware targets: An ANFIS-based approach for microcontroller implementation; and a ANN-based approach for FPGA implementation. Both estimators use already available data on current vehicles, and do not require model parameter identification, as they are trained using experimental data. The accuracy of both estimators have been validated by comparing their estimations with a benchmarking analytical estimator found in the literature. Results show that both proposed estimators provide higher accuracy, being the ANFIS based solution the one which provides the highest accuracy (2% average error). However, its execution time is 240 times bigger than the ANN based estimator, which provides the highest balance between accuracy (3% average error) and computational cost.

On the other hand, the lateral torque distribution is achieved using a Fuzzy Yaw Moment Controller. This controller allows to distribute the torque laterally (right and left wheels), to minimize wheel slip and enhance cornering capabilities. Moreover, its rule-based design allows to minimize model dependency.

In order to validate the aforementioned approach a set of challenging maneouvres have been proposed, and the developed Intelligent TV has been compared with other proposed approaches in the literature (PID and SOSMC) by using a HiL setup. Cornering response and power consumption have been evaluated. Regarding the vehicle cornering capabilities and stability, results show that, thanks to the tyre vertical forces knowledge, the vehicle that features the proposed approach achieves the highest vehicle dynamics improvement in high and low friction conditions (3% and 1.15% maximum acceleration improvement with respect to PID TV and SOSMC TV), due to the optimal torque distribution.

Moreover, if power consumption is analysed, energy consumption results show that the proposed approach can effectively reduce (about a 13%) the powertrain and tyre losses thanks to the regenerative braking contribution and the tire vertical forces knowledge.

Hence, in this Chapter the validity of the proposed Intelligent TV approach has been demonstrated, as well as its advantages. However, even having demonstrated that the approach allows reducing the required energy in a EV, it is also true that this is carried out indirectly, by reducing tyre slips and using the regenerative braking. If cornering dynamics and energy efficiency have to be combined, or adaptively consider one term over the other in certain scenarios (i.e., critical situations), the energy efficiency has to be directly considered in the TV formulation. In the next Chapter, this issue will be handled by proposing a novel TV controller.

Energy-efficient NMPC Torque Vectoring

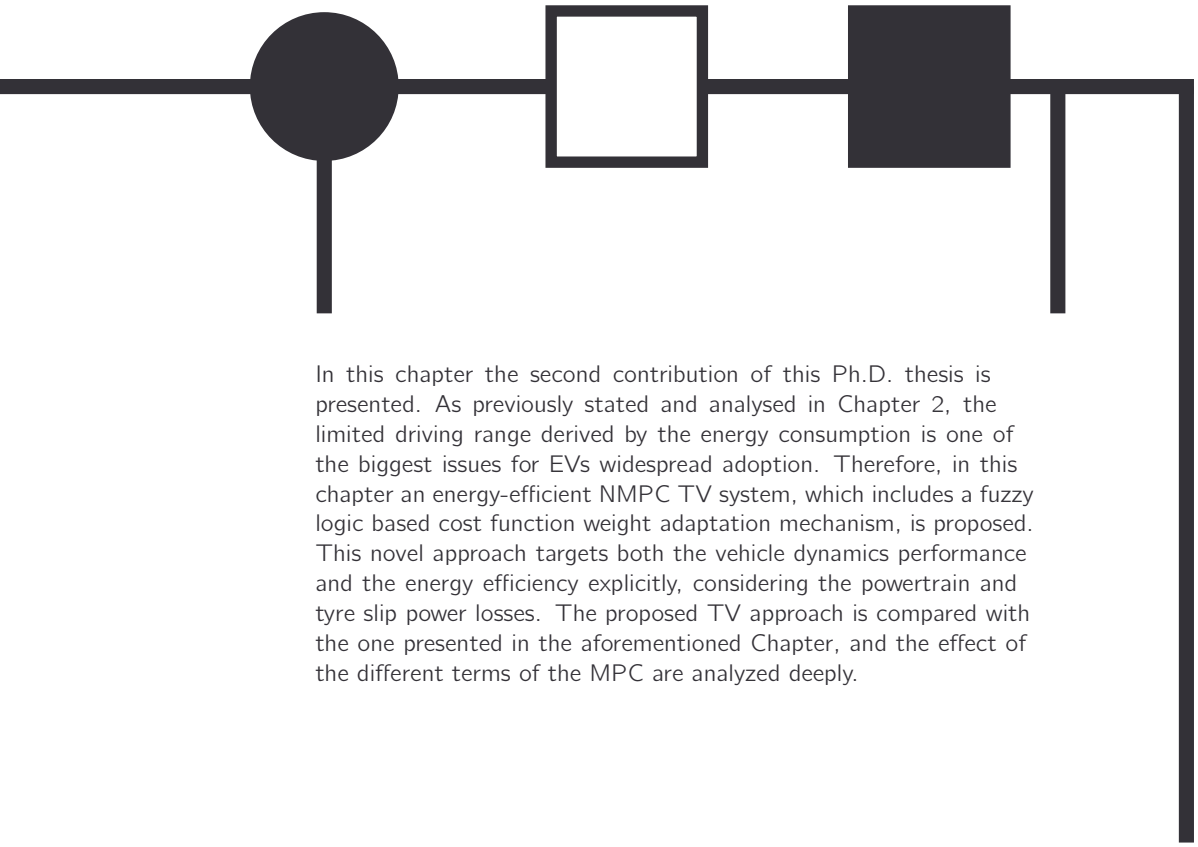

In this chapter the second contribution of this Ph.D. thesis is presented. As previously stated and analysed in Chapter 2, the limited driving range derived by the energy consumption is one of the biggest issues for EVs widespread adoption. Therefore, in this chapter an energy-efficient NMPC TV system, which includes a fuzzy logic based cost function weight adaptation mechanism, is proposed. This novel approach targets both the vehicle dynamics performance and the energy efficiency explicitly, considering the powertrain and tyre slip power losses. The proposed TV approach is compared with the one presented in the aforementioned Chapter, and the effect of the different terms of the MPC are analyzed deeply.

5- Energy-efficient NMPC Torque Vectoring

5.1 Introduction

As stated in Chapter 2, TV systems that not only enhance the vehicle dynamics but also the overall efficiency is one of the most active research topics in the vehicle dynamics control systems area. The limited driving range has been so far one of the main technical constraints to the widespread adoption of EVs. Hence, the development of systems that can help to increase the driving range is crucial for EVs.

The most important power loss sources in EVs are the powertrain (due to the electrical and mechanical power losses) and the tyres (due to the slip). In this sense, TV has a direct impact on both sources, as on the one hand, it generates the electric motor torque commands (determining the operation point), and on the other hand, the generated motor torque commands will affect the vehicle dynamics behaviour (and, therefore the tyre slip power losses).

In Chapter 4 an Intelligent TV system able to enhance both vehicle dynamics behaviour and energy consumption, has been proposed. However, the proposed approach does not consider explicitly the energy consumption in its formulation, and the improvement achieved in this aspect is a consequence of the provided optimal torque distribution, partly thanks to the vertical tyre forces knowledge and the inclusion of the regenerative braking term into the TV, which minimize the aforementioned power losses. Therefore in the proposed approach it is not possible to tune TV behaviour to enhance cornering response or energy efficiency, which also a key issue to be considered in TV approaches for EVs.

Therefore, in order to fully exploit the potential of TV as an energy-saving approach, including explicitly an energy term in the TV formulation is required. However, as seen in Chapter 2, most of the works proposed tend to minimize efficiency in each layer of the controller structure (see Figure 2.10) independently, which may cause problems if overall efficiency is considered.

Hence, in order to address the aforementioned issues, in this Chapter, a novel energy efficient TV approach is proposed, which presents three main contributions over the works proposed in the literature:

- The use of an implicit nonlinear model predictive control approach (NMPC) to combine layers 2 and 3, this is, the direct yaw moment calculation layer with the control allocation layer, which allows to optimize the yaw rate tracking performance and energy-efficient cornering response considering yaw rate, sideslip angle and torque constraints at once.

- The use of a fuzzy-logic based weight adaptation mechanism in the NMPC to mediate between the requirements of vehicle stability and energy efficiency,

thus, allowing to adapt the focus of the TV depending on the scenario.

- The definition of a methodology to define an energy-efficient reference yaw rate (Layer 1), that also considers the torque allocation layer (Layer 3).

In order to describe the proposed approach, first, the fundamentals concepts of model predictive control will be presented. Second, the proposed energy-efficient NMPC TV approach will be deeply explained. Third, the implemented simulation setup and selected study case will be presented. Finally, the obtained results are deeply presented and discussed, and the main conclusions summarized.

5.2 Fundamental Concepts on Nonlinear Model Predictive Control

Model Predictive Control (MPC) [147] was originated in the late seventies and has been developed considerably since then. This type of controllers are based on the following three ideas. First, the explicit use of a model (linear or nonlinear) to predict the process output at future time instants. Second, the calculation of a control sequence minimizing a cost function. And finally, the receding horizon strategy. This is, at each instant, the controller horizon (see Figure 5.1) is displaced towards the future, which involves the application of only the first control signal of the sequence calculated at each step.

These three main characteristics, make the MPC a powerful technique that presents several advantages. For instance, the tuning of the controller is very intuitive, being effective in controlling processes with both simple and complex dynamics. Besides, the multivariable case can be easily addressed, as it can deal with actuator constraints, and it introduces a feedforward control to compensate for measurable disturbances.

Nevertheless, it also presents its drawbacks. One of them is that although the resulting control law is easy to implement, its derivation is more complex than that of the classical PID controllers, increasing its computational cost when constraints are considered. Apart from that, as it is a model-based control technique, its performance relies on model accuracy. Therefore, the greatest drawback is the need for an appropriate model of the process. However, its potential and advantages have increased the interest in this approach lately, and the increase in computational power has extended its use in areas such as Automated Driving or Power Electronics.

5.2.1 MPC Strategy

All MPC controllers are characterized by the following strategy, summarized in Figure 5.1. As MPCs are only implemented in discrete time, at each time step t, the following three steps are carried out:

1. Future outputs $t+k$ for a determined prediction horizon H_p (where $H_p = NT_s$, being N the number of steps and T_s the prediction model's timestep), are predicted at each instant t using the process model. These predicted outputs

$\hat{y}(t+k|t)1$ for $k = 1...N$ depend on the known values up to instant t (past inputs and outputs) and on the future control signals $u(t+k|t)$, $k = 0...N-1$, which are those to be calculated by the MPC.

2. The set of future control signals is calculated by optimizing a determined Cost Function J to keep the process as close as possible to the reference trajectory $w(t+k)$ (which can be the setpoint itself or a close approximation of it) while trying to minimize the required control action $u(t+k|t)$ (or its variation). This Cost Function is usually a quadratic one.

3. Once the optimum control sequence is calculated, only the control signal related to the current time step t, $u(t)$, is sent to the process whilst all the other calculated control signals are rejected. Note that this is carried out in order to ensure proper feedback and keep the system under closed loop control.

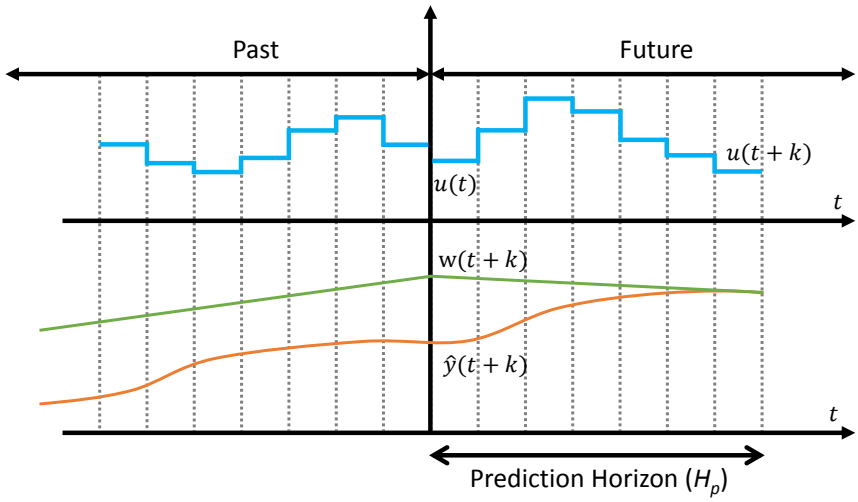

Figure 5.1: MPC Strategy

Once these steps are carried out, the system evolves to time step $t+1$. Note that the obtained $y(t+1)$ may differ from the predicted one $\hat{y}(t+1)$, emphasizing the need to reject all control actions except for the first one. In this new step, the same process is repeated, estimating again the future outputs for the same horizon, from $t+1$ to $t+N+1$, which involves the receding horizon concept.

In order to implement this strategy, the basic structure shown in Figure 5.2 is followed. As previously stated, a model is used to predict the future outputs of the system. This is taken into account by the optimizer, which also considers the form of the Cost Function and the constraints.

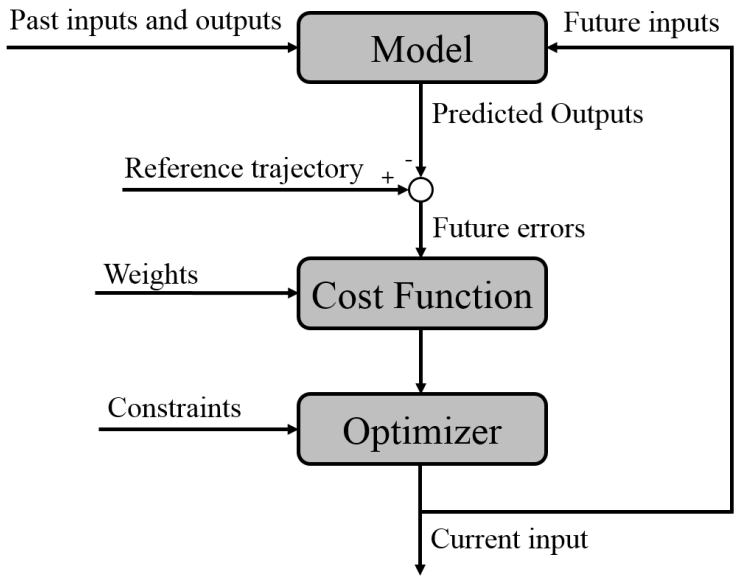

Figure 5.2: Basic structure of MPC

5.2.2 Prediction Model

The process model plays a decisive role in MPC controllers, as the chosen model must be able to capture the process dynamics to precisely predict the future outputs and be simple to be implemented and understandable.

Two main model types can be implemented: linear and nonlinear models. Even if both share the same basic strategy, they have significant differences to be considered when implementing them for real-time applications. MPCs based on linear models have been widely studied in the literature, and currently allow high computational efficiency and reduced complexity due to the use of linear solvers and linear control theory. However, they present drawbacks if the process to be controlled is nonlinear, as significant performance losses may arise.

In these cases, non-linear models are usually the best alternative, although they require the more complex nonlinear MPC formulation, which is not as studied as the linear one and requires higher computational cost. In these cases, a nonlinear state-space form can be used to generically represent a system,

.

$$\dot{\mathbf{x}}(t) = \mathbf{f}(\mathbf{x}(t), \mathbf{u}(t)) \tag{5.1}$$

where $\mathbf{f}$ is a nonlinear function.

Additionally, as MPCs are defined in discrete time, they need also a discretized model. Although this process is quite straightforward for linear models, in the case

of nonlinear models, the process is not trivial, as in general, there is no analytical solution for the discretization procedure,

$$\dot{\mathbf{x}}(t) = \mathbf{f}(\mathbf{x}(t), \mathbf{u}(t)) \rightarrow \mathbf{x}(k+1) = \mathbf{f}_d((\mathbf{x}(k), \mathbf{u}(k)) \tag{5.2}$$

Hence, in the literature, two main approaches have been used. The first is trying to approximate the nonlinear model to a linearized one by using a linearization on a single operation point, a LTV approach or a Piece Wise Affine approximation. Once linearized, the model is discretized and a linear MPC approach can be implemented.

The second approach is based on integrating the model response using numeric computation methods such as Euler or Runge Kutta [161]. This integration is carried out in continuous time, but the inputs are considered constant during the equivalent to a discrete period. Then, the outputs associated with the discretized time steps are considered as the discrete outputs for the system,

$$\mathbf{x}(k+1) = \mathbf{x}(t+T) = \mathbf{x}(t) + \int_0^T \mathbf{f}(\mathbf{x}(t), \mathbf{u}(t))dt \tag{5.3}$$

This latter approach requires higher computation time, as a numeric integrator is required to calculate the discretized outputs at each time step. The use of this approach leads to the use of a nonlinear MPC (NMPC) technique, which will be the focus of this Chapter.

5.2.3 Nonlinear MPC control law

The control law of a nonlinear MPC approach is described as a nonlinear optimization problem which is solved at each time step t,

$$\begin{aligned} &\min_{\mathbf{u}^+} \sum_{k=0}^{N-1} \ell(\mathbf{x}(k), \mathbf{u}(k)) \\ &\text{s.t.} \\ &\qquad \mathbf{x}(0) = \mathbf{x}(t) \\ &\qquad \mathbf{x}(k+1) = \mathbf{f}_{\mathrm{d}}(\mathbf{x}(k), \mathbf{u}(k)) \\ &\qquad \mathbf{x}(k) \in \mathcal{X} \\ &\qquad \mathbf{u}(k) \in \mathcal{U} \\ &\quad k = 0, \ldots, N-1 \end{aligned} \tag{5.4}$$

where $\mathcal{X}$ and $\mathcal{U}$ are the constrained sets for the states and the control actions, and $\ell(\mathbf{x}(k), \mathbf{u}(k))$ is the stage cost function, which is typically quadratic.

Solving the aforementioned nonlinear optimization problem leads to the optimal control sequence $\mathbf{u}^+$ calculated in t for the whole horizon H,

$$\mathbf{u}^+ = [\mathbf{u}(0) \quad \mathbf{u}(1) \quad \ldots \quad \mathbf{u}(N-1)]^T \tag{5.5}$$

Note, however, that only the first control step, $\mathbf{u}(t) = \mathbf{u}(0)$ will be applied, and the process will be repeated in the next time step, as previously detailed.

Once that the fundamentals of the MPC formulation have been introduced, in the following section the proposed energy efficient NMPC TV approach will be detailed.

5.3 Energy Efficient NMPC Torque Vectoring Approach

In this section the proposed TV approach is presented. Figure 5.3 summarizes the overall structure of the proposed TV controller and its fundamental blocks.

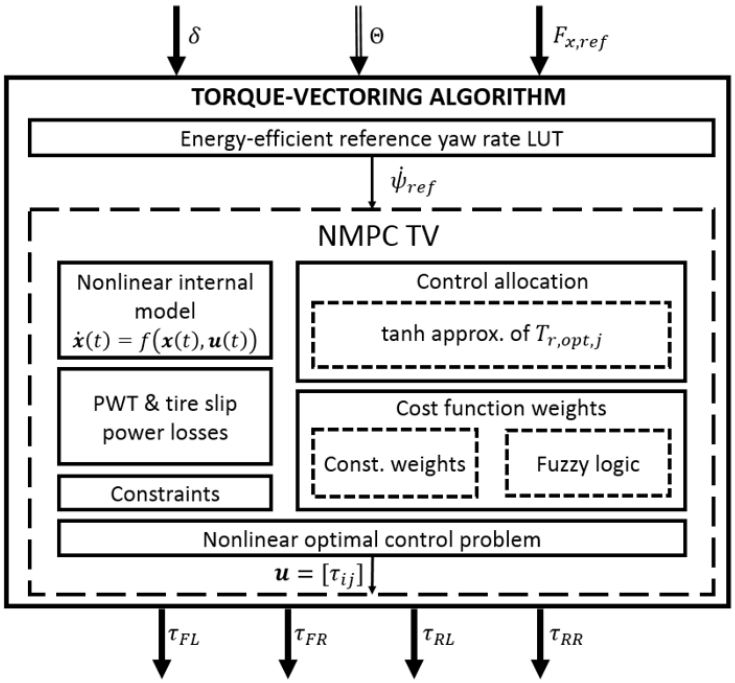

Figure 5.3: NMPC TV Overall structure

The proposed approach requires the total force demand $F_{x,ref}$, the steering angle δ and the vehicle parameters θ to operate, and calculates the individual torques to be applied in each wheel τ_{ij} (with $i = F, R$ (front, rear) and $j = L, R$ (left, right). For that purpose, first the energy efficient yaw rate $\dot{\psi}_{ref}$ (Section 5.3.2) is required, which considers the control allocation, using an optimal front-to-total torque distribution $T_{r,opt,j}$ (Section 5.3.1). Based on this data the designed NMPC approach calculates the final individual torques τ_{ij} (Section 5.3.3). Next, each of these subsystems will be detailed.

5.3.1 Energy-efficient front-to-total wheel torque distribution

As seen in Section 2.4.3, the front-to-total torque distribution can affect the vehicle understeering characteristics, and also the overall vehicle power consumption. Therefore, if an energy efficient yaw rate reference is to be generated, this torque distribution has to be analyzed first.

In this sense, different approaches for energy efficient control allocation [82, 162] have demonstrated that if powertrain losses are considered, the overall power con-

sumption is reduced typically in two scenarios: when a single axle transmits all the torque (100% rear or front) or in the case in which an even distribution (50% rear and 50% front) is applied. Moreover, until certain powertrain operation point, which depends on a particular torque and angular speed, the single axle solution provides the best efficiency. However, when this operation point (switching point) is reached, an even distribution provides the most energy efficient response.

Based on this idea, in this section a procedure to define the energy-efficient front-to-total wheel torque distribution is proposed, which consist on finding the optimal switching point between the aforementioned scenarios (single axle and even distribution). This approach requires to have the efficiency map of each powertrain implemented in the AWD vehicle $\eta(\tau_{ij}, \omega_{ij})$ ($i = F, R$ and $j = L, R$) in terms of its operation point (torque τ_{ij} and angular speed ω_{ij}).

For this purpose, first, the front-to-total wheel torque distribution ratio $T_{r,j}$ is defined. This ratio represents the amount of torque that is assigned to each wheel of a side of a AWD vehicle (left or right) with respect to the total torque assigned to that side,

$$T_{r,j} = \frac{\tau_{Rj}}{\tau_{Fj} + \tau_{Rj}} \tag{5.6}$$

In order to obtain the optimum $T_{r,j}$ distribution, the overall powertrain efficiency $\eta_{tot,j}$ associated to a vehicle side j (Left or Right) needs to be maximized,

$$\max_{T_{r,j}} \eta_{tot,j} \tag{5.7}$$

where $\eta_{tot,j}$ is given by,

$$\begin{aligned} \eta_{tot,j} =& \eta_{tot,j}\left(T_{r,j}, \tau_j, \omega_{Fj}, \omega_{Rj}\right) = \frac{P_{out,j}\left(T_{r,j}, \tau_j, \omega_{Fj}, \omega_{Rj}\right)}{P_{in,j}\left(T_{r,j}, \tau_j, \omega_{Fj}, \omega_{Rj}\right)} \\ =& \frac{T_{r,j}\omega_{Fj} + \left[1 - T_{r,j}\right]\omega_{Rj}}{\frac{T_{r,j}}{\eta(T_{r,j}\tau_j, \omega_{Fj})}\omega_{Fj} + \frac{1-T_{r,j}}{\eta([1-T_{r,j}]\tau_j, \omega_{Rj})}\omega_{Rj}} \end{aligned} \tag{5.8}$$

where $\tau_j = \tau_{Fj} + \tau_{Rj}$ is the total torque assigned to a vehicle side j; ω_{Fj} and ω_{Rj} are the rotational speeds of the front and rear wheels of side j; and $\eta(\tau_{ij}, \omega_{ij})$ is the efficiency map of the powertrain. In order to perform the aforementioned optimization the following will be assumed $\omega_{Fj} = \omega_{Rj} \approx V/R_w$, where V is vehicle speed.

Hence, the resulting energy-efficient front-to-total wheel torque ratio $T_{r,j}$ can be obtained by using a map (which could be implemented as a look-up table, Figure 5.4), that relates,

$$T_{r,j} = T_{r,j}\left(\tau_j, V/R_w\right) \tag{5.9}$$

5.3.2 Energy-efficient yaw rate reference generator

As stated in the literature review (Section 2.4.3), several works [80–82] have demonstrated that layer 1 of a typical TV system structure (Figure 2.10) has at least an

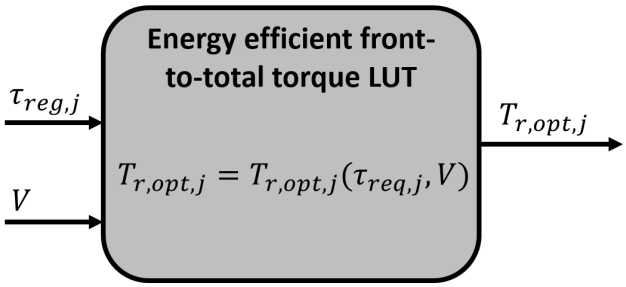

Figure 5.4: Energy Efficient Front-to-total wheel torque distribution LUT

equivalent impact on the energy consumption as the control allocation layer (layer 3). Moreover, these two layers are crucial if energy consumption aims to be reduced by the TV algorithm.

These issues are addressed in this subsection, in which an energy efficient yaw rate reference generation procedure is detailed, which also considers the control allocation layer defined in the previous section (Section 5.3.1). The procedure is based on the use of a set of simulations to determine an energy efficient yaw rate reference map in terms of the vehicle state, the steering angle and the road parameters.

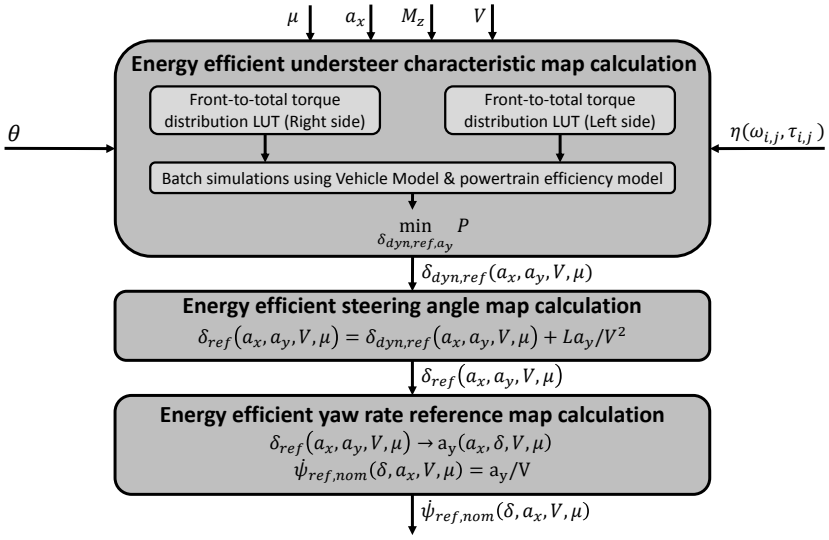

Figure 5.5: Procedure to obtain the energy-efficient yaw rate

Figure 5.5 summarizes the proposed procedure. First, a set of batch simulations are carried out to define the energy-efficient understeer characteristic of the studied vehicle. In these simulations, different yaw moments M_z, vehicle speeds V, longitudinal accelerations a_x and different road conditions μ are considered, and the understeer

characteristic that minimizes the overall power consumption P is calculated. Note that the front-to-total torque distribution defined in Section 5.3.1 is used in these simulations. In a second step, the energy-efficient steering angle reference map is calculated. Finally, the data from the previous stage is manipulated to obtain the energy efficient yaw rate map.

Next, these steps are analyzed.

1. **Energy-efficient reference understeer characteristic:** The goal of this first step is to determine the most energy-efficient understeer characteristic. To this purpose, a set of batch simulations are carried out considering the vehicle and powertrain models (as defined in Chapter 3.2), and the front-to-total torque distribution map defined in Section 5.3.1.

   In order to explore the full range of achievable understeer characteristics, the simulations consider a set of ramp steer maneuvers with slow steering input ramps at different constant speeds V, constant yaw moments M_z and different road conditions μ. Also, to study the cornering response with constant, non-zero longitudinal acceleration, a_x, at a given speed, the tests have been carried with a constant longitudinal force applied at the EV's center of gravity.

   Once the full range of understeer characteristics are evaluated, the power consumption P of each case is calculated and represented for a given lateral acceleration a_y, in order to determine the most energy-efficient understeer characteristic, which considers also the energy-efficient front-to-total distribution ratio $T_{r,j}$ for each vehicle side. This allows to generate a four dimensional map that represents the energy-efficient reference understeer characteristic,

$$\delta_{dyn,ref} = \delta_{dyn,ref}\left(a_y, a_x, V,\ \mu\right) \tag{5.10}$$

2. **Energy efficient steering angle reference calculation:** If the steering angle δ_{ref} is considered, the energy-efficient reference understeer characteristic map can be expressed as,

$$\delta_{ref}\left(a_y, a_x, V,\ \mu\right) = \delta_{dyn,ref}\left(a_y, a_x, V,\ \mu\right) + \frac{L a_y}{V^2} \tag{5.11}$$

   where L is the distance between axles or *wheelbase*.

3. **Energy efficient reference yaw rates:** Through manipulation of $\delta_{ref}\left(a_y, a_x, V,\ \mu\right)$ and considering Eq. 5.12

$$\dot{\psi}_{ref}\left(\delta_{ref}, a_x, V,\ \mu\right) = \frac{a_y\left(\delta_{ref}, a_x, V,\ \mu\right)}{V} \tag{5.12}$$

   the energy-efficient yaw rate maps can be obtained in terms of the steering angle and the vehicle and road parameters. These maps can be implemented using a look-up table as in Figure 5.6.

$$\dot{\psi}_{ref} = \dot{\psi}_{ref}\left(\delta, a_x,\ V,\ \mu\right) \tag{5.13}$$

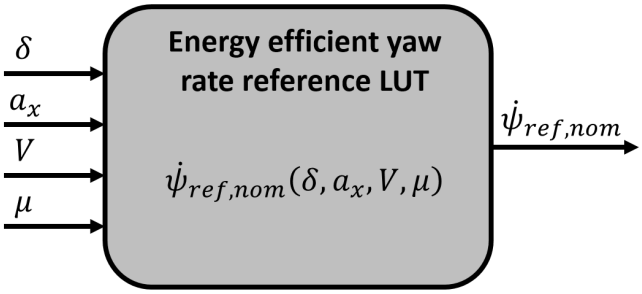

Figure 5.6: Energy-efficient Yaw Rate LUT

5.3.3 Nonlinear MPC

The goal of the Nonlinear MPC (NMPC) is to generate the definitive torque commands of all wheels τ_{ij} considering both the dynamic behaviour of the vehicle and the energy required to provide the expected enhancement.

As detailed in Section 5.2, MPC controllers require the definition of the model of the system to be controlled. Moreover, as the proposed NMPC includes energy terms, the power losses of the vehicle need to be modelled so that they can be optimized. Both the vehicle model and the power losses model will be included in the optimization problem, with the proper cost function weights and constraints, in order to calculate the control law. Next, the definition of each model will be detailed, so that the NMPC-based control law can be derived finally.

5.3.3.1 Internal model formulation

As analyzed in Section 5.2, when a nonlinear MPC is considered, its internal model, which will be used to represent the nonlinear dynamics of the vehicle, can be expressed as follows in continuous time [163],

$$\mathbf{x}(t) = \mathbf{f}(\mathbf{x}(t), \mathbf{u}(t)) \tag{5.14}$$

where the following state vector $\mathbf{x}(t)$ has been defined for the required TV approach,

$$\mathbf{x}(t) = \left[V(t)\, \beta(t)\, \dot{\psi}(t)\, \omega_{FL}(t)\, \omega_{FR}(t)\, \omega_{RL}(t)\, \omega_{RR}(t)\right]^T \tag{5.15}$$

and the control action $\mathbf{u}(t)$ corresponds to the desired wheel torque distribution,

$$\mathbf{u}(t) = [\tau_{FL}(t)\, \tau_{FR}(t)\, \tau_{RL}(t)\, \tau_{RR}(t)]^T \tag{5.16}$$

The choice of the internal model $\mathbf{f}$ depends on the particular choice of balance between accuracy and computational cost. A more complex model will require more parameters to be identified and a higher computational cost, while a simpler one will simplify the implementation, but could have an impact on the TV approach performance. In this work, an analytical 7 degrees of freedom vehicle model has been

selected as a compromise between computational cost and accuracy, following recent NMPC implementations in the field of TV [73]. A simplified schematic of the model used, as well as the angle conventions, can be seen in Figure 5.7.

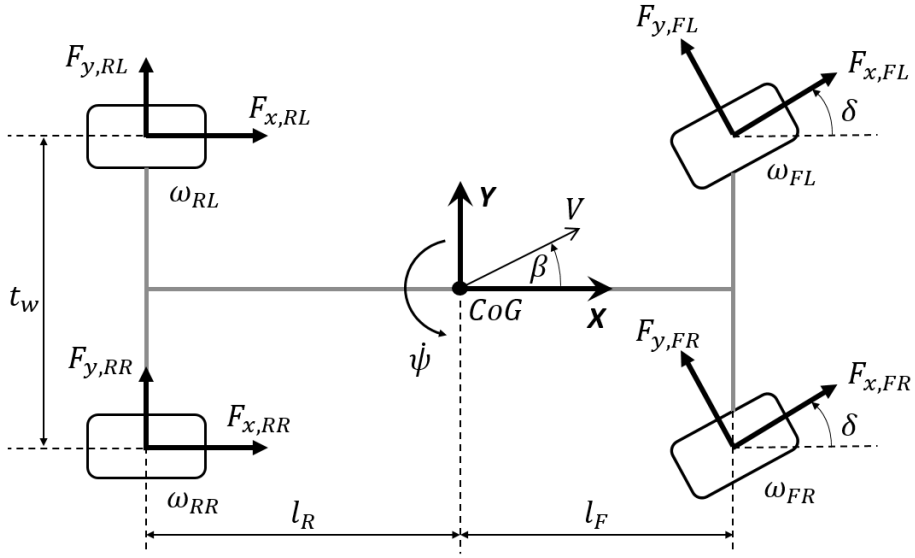

Figure 5.7: Internal Vehicle model Schematic

Hence, the following force and moment balance equations are used. The longitudinal dynamics is represented by,

$$\begin{aligned}\dot{V} = &[F_{x,FL} + F_{x,FR}]\cos(\delta - \beta) - [F_{y,FL} + F_{y,FR}]\sin(\delta - \beta) \\ &+ [F_{x,RL} + F_{x,RR}]\cos\beta + [F_{y,RL} + F_{y,RR}]\sin\beta\end{aligned} \tag{5.17}$$

where V is the vehicle speed, δ is the steering angle, β is the sideslip angle, and $F_{x,ij}$ and $F_{y,ij}$ are the longitudinal and lateral tyre forces, respectively.

If the sideslip angle dynamics is considered,

$$\begin{aligned}\dot{\beta} = &\frac{1}{mV}\{[F_{x,FL} + F_{x,FR}]\sin(\delta - \beta) + [F_{y,FL} + F_{y,FL}]\cos(\delta - \beta) \\ &- [F_{x,RL} + F_{x,RR}]\sin\beta + [F_{y,RL} + F_{y,RR}]\cos\beta\} - \dot{\psi}\end{aligned} \tag{5.18}$$

where m is the mass of the vehicle and $\dot{\psi}$ the yaw rate of the vehicle. Regarding the time evolution of this latter variable, the following expression is followed,

$$\begin{aligned}\ddot{\psi} =& \frac{1}{I_z}[F_{x,FL} + F_{x,FR}]\cos(\delta - \beta) + [F_{y,FL} + F_{y,FR}]\cos\delta\} \, l_F \\ & - [F_{x,RL} + F_{x,RR}] \, l_R + [F_{x,FR}\cos\delta - F_{y,FR}\sin\delta + F_{x,RR}] \, \frac{t_w}{2} \\ & - [F_{x,FL}\cos\delta - F_{y,FL}\sin\delta + F_{x,RL}] \, \frac{t_w}{2}\end{aligned} \tag{5.19}$$

where I_z is the inertia term in z axis, l_F and l_R are the distances of the front and rear axles to the center of gravity of the vehicle, and t_w is the width of the vehicle.

Finally, the dynamics of each wheel is defined as follows,

$$I_\omega \dot{\omega}_{ij} = \tau_{ij} - F_{x,ij} R_\omega \tag{5.20}$$

where I_ω is the rotational inertia of the wheel, ω_{ij} its angular speed, τ_{ij} the applied wheel torque and R_ω the wheel radius. Note that tyre rolling resistance is neglected, as is not affected at the overall EV level by the wheel torque distribution [164].

Eqs. 5.17-5.20 define the internal dynamic model of the vehicle that will be implemented in the NMPC. However, in order to fully define these equations, longitudinal and lateral tyre forces have to be defined. These are calculated in terms of the vertical tyre load $F_{z,ij}$ considering the load friction coefficients $\mu_{x,ij}$ and $\mu_{y,ij}$,

$$\begin{aligned} F_{x,ij} &= \mu_{x,ij} F_{z,ij} \\ F_{y,ij} &= \mu_{y,ij} F_{z,ij} \end{aligned} \tag{5.21}$$

Calculation of $\mu_{x,ij}$ and $\mu_{y,ij}$: In order to determine the resultant tyre force coefficients $\mu_{x,ij}$ and $\mu_{y,ij}$, the total friction coefficient μ_{ij} and the longitudinal and lateral slip coefficients $s_{x,ij}$ and $s_{y,ij}$ are required,

$$\begin{aligned} \mu_{x,ij} &= -\tfrac{s_{x,ij}}{s_{ij}} \mu_{ij} \\ \mu_{y,ij} &= -\tfrac{s_{y,ij}}{s_{ij}} \mu_{ij} \end{aligned} \tag{5.22}$$

where s_{ij} is the total slip, which is calculated from the composition of the longitudinal and lateral slip components,

$$s_{ij} = \sqrt{s_{x,ij}^2 + s_{y,ij}^2} \tag{5.23}$$

On the other hand, the longitudinal and lateral slip components, $s_{x,ij}$ and $s_{y,ij}$ are defined as,

$$\begin{aligned} s_{x,ij} &= \tfrac{V_{slip,x,ij}}{\omega_{ij} R_w} \\ s_{y,ij} &= \tfrac{V_{slip,y,ij}}{\omega_{ij} R_w} \end{aligned} \tag{5.24}$$

where ω_{ij} is the angular speed of each wheel; R_w is the tyre rolling radius; and $V_{slip,x,ij}$ and $V_{slip,y,ij}$ are the tyre longitudinal and lateral slip speeds, defined as,

$$\begin{aligned} V_{slip,x,ij} &= \omega_{ij} \, R_w - V_{x,ij} \\ V_{slip,y,ij} &= -V_{y,ij} \tan\alpha_{ij} \end{aligned} \tag{5.25}$$

with $V_{x,ij}$ and $V_{y,ij}$ being the longitudinal and lateral component of the linear wheel speed in the tyre reference system, and α_{ij} is the tyre slip angle, which are calculated by the use of simplified linearized expressions,

$$\begin{aligned} \alpha_{FL} \approx \alpha_{FR} \approx \delta - \beta - \frac{\dot{\psi} l_F}{V} \\ \alpha_{RL} \approx \alpha_{RR} \approx -\beta - \frac{\dot{\psi} l_R}{V} \end{aligned} \tag{5.26}$$

Finally, μ_{ij} is calculated using a simplified version of the Pacejka magic formula,

$$\mu_{ij}\left(s_{ij}\right) = MF\left(s_{ij}\right) = D \sin\left(C\, atan\left(B s_{ij}\right)\right) \tag{5.27}$$

where MF indicates the magic formula; B, C and D are constant magic formula coefficients [3], calculated to match the actual tyre characteristics.

Calculation of $F_{z,ij}$: The vertical tyre forces $F_{z,ij}$ are calculated as the sum of the static load, $F^0_{z,ij}$, longitudinal load transfer, ΔF^x_z, and lateral load transfer, $\Delta F^y_{z,i}$,

$$\begin{aligned} F_{z,FL} &= F^0_{z,FL} - \Delta F^x_z - \Delta F^y_{z,F} \\ F_{z,FR} &= F^0_{z,FR} - \Delta F^x_z + \Delta F^y_{z,F} \\ F_{z,LR} &= F^0_{z,LR} + \Delta F^x_z - \Delta F^y_{z,R} \\ F_{z,RR} &= F^0_{z,RR} + \Delta F^x_z + \Delta F^y_{z,R} \end{aligned} \tag{5.28}$$

where the static loads $F^0_{z,ij}$ depend on the mass distribution of the vehicle (see Figure 5.7),

$$\begin{aligned} F^0_{z,FL} = F^0_{z,FR} = \tfrac{1}{2} mg \tfrac{l_R}{l_F + l_R} \\ F^0_{z,RL} = F^0_{z,RR} = \tfrac{1}{2} mg \tfrac{l_F}{l_F + l_R} \end{aligned} \tag{5.29}$$

The longitudinal load transfer ΔF^x_z [156] is defined as,

$$\Delta F^x_z = \frac{1}{2} \frac{m\, h\, a_x}{l_F + l_R} \tag{5.30}$$

where h is the height of the center of gravity, and a_x is the longitudinal acceleration in the vehicle CG reference system.

On the other hand, the front $F^y_{z,F}$ and rear $F^y_{z,R}$ lateral load transfers are given by,

$$\begin{cases} \Delta F^y_{z,F} = \frac{m\, a_y}{t_w} \left[\frac{h_{RC}\, l_R}{l_F + l_R} + \gamma h_{Roll} \right] \\ \Delta F^y_{z,R} = \frac{m\, a_y}{t_w} \left\{ \frac{h_{RC}\, l_F}{l_F + l_R} + [1 - \gamma]\, h_{Roll} \right\} \end{cases} \tag{5.31}$$

where h_{RC} is the roll center height; h_{Roll} is the distance between the center of gravity and the roll axis; t_w is the track width; and γ is the front-to-total suspension roll stiffness distribution.

5.3.3.2 Powertrain and tyre slip power losses model

In EVs, the two main sources of power losses come from the powertrain (due to both electrical and mechanical losses) and the tyres (due to the slip phenomenon).

To determine the power losses of the powertrain associated to each wheel $P_{Loss,PWT,ij}$, the powertrain efficiency map (typically given by the motor manufacturer, or obtained experimentally) is required $\eta(\tau_{ji}, \omega_{ij})$, which is a function of the torque and speed.

This way, if τ_{ij} is the torque demand of the ij powertrain ($i = F, R$ to indicate the front or rear axles, and $j = L, R$ to indicate the left or right sides) and ω_{ij} is the angular speed of the associated wheel, the associated power loss can be calculated as,

$$P_{Loss,PWT,ij} = \left\{ \begin{array}{ll} \tau_{ij}\omega_{ij}\left[\frac{1}{\eta(\tau_{ij},\omega_{ij})} - 1\right], & \tau_{ij} > 0 \\ \tau_{ij}\omega_{ij}\left[\eta(\tau_{ij},\omega_{ij}) - 1\right], & \tau_{ij} < 0 \\ P_{Loss,PWT,ij,res}(\omega_{ij}), & \tau_{ij} = 0 \end{array} \right\} \tag{5.32}$$

where $P_{Loss,PWT,res,ij}$ is the power loss of the ij powertrain when this is switched off, caused by the cogging loss and mechanical loss contributions.

At the vehicle level, the total powertrain power loss, $P_{Loss,PWT}$, is given by the contribution of all powertrain losses,

$$P_{Loss,PWT} = \sum_{\substack{i=F,R \\ j=R,L}} P_{Loss,PWT,ij} \tag{5.33}$$

Note that the aforementioned expression depends on the particular efficiency maps $\eta(\tau_{ji}, \omega_{ij})$, which usually are defined as look-up tables or curves, with no analytical expression. As the use of an analytical and preferably continuous model is required for NMPC implementation, an approximation using high order polynomials is proposed to implement these power losses term.

On the other hand, the tyre slip power losses can be divided into the contribution associated to the longitudinal slip $P_{Loss,tyre,Long}$ and the lateral one $P_{Loss,tyre,Lat}$ [65]. In both cases, these power losses are modelled in terms of the tyre forces and the components of the slip speed $V_{slip,ij}$,

$$P_{Loss,tyre,Long} = \sum_{\substack{i=F,R \\ j=R,L}} F_{x,ij} V_{slip,x,ij} \tag{5.34}$$

$$P_{Loss,tyre,Lat} = \sum_{\substack{i=F,R \\ j=R,L}} F_{y,ij} V_{slip,y,ij} \tag{5.35}$$

where $F_{x,ij}$ and $F_{y,ij}$ are the longitudinal and lateral tyre forces, defined in Eq. 5.21; and $V_{slip,x,ij}$ and $V_{slip,y,ij}$ are the longitudinal and lateral slip speeds of each tyre, which have been defined in Eq. 5.25

5.3.3.3 Optimal Control Problem Formulation

Once the internal model of the vehicle and the power losses have been characterized, it is possible to define the NMPC control law for the energy-efficient Torque Vectoring approach.

As stated in Section 5.2, the NMPC approach is defined in discrete time. Hence, if a T_s discretization time is defined, in a time step t, and considering a prediction horizon of N steps (thus, $H_p = N\,T_s$), the NMPC control law has the form,

$$\begin{aligned} \min_{\mathbf{u}^+} & \sum_{k=0}^{N-1} \ell(\mathbf{x}(k), \mathbf{u}(k)) \\ \text{s.t.} & \\ & \mathbf{x}(0) = \mathbf{x}(t) \\ & \mathbf{x}(k+1) = \mathbf{f}_\mathrm{d}(\mathbf{x}(k), \mathbf{u}(k)) \\ & \mathbf{x}(k) \in \mathcal{X} \\ & \mathbf{u}(k) \in \mathcal{U} \\ & k = 0, \ldots, N-1 \end{aligned} \tag{5.36}$$

In the particular TV implementation proposed, the state $\mathbf{x}(k)$ and the control action $\mathbf{x}(k)$ are defined to fit the internal model definition (Section 5.3.3.1),

$$\begin{aligned} \mathbf{x}(k) &= \left[V(k)\,\beta(k)\,\dot{\psi}(k)\,\omega_{FL}(k)\,\omega_{FR}(k)\,\omega_{RL}(k)\,\omega_{RR}(k)\right]^T \\ \mathbf{u}(k) &= \left[\tau_{FL}(k)\,\tau_{FR}(k)\,\tau_{RL}(k)\,\tau_{RR}(k)\right]^T \end{aligned} \tag{5.37}$$

This way, $\mathbf{x}(0)$ represents the initial state value, which corresponds to the current values of the state variables in t, which are measured or estimated. By means of this value and the internal vehicle model $\mathbf{x}(k+1) = \mathbf{f}_\mathrm{d}(\mathbf{x}(k), \mathbf{u}(k))$ future states and its corresponding control actions can be calculated. Note that the model $\mathbf{f}_\mathrm{d}$ is discrete. Hence, as the internal vehicle model defined in Section 5.3.3.1 is continuous, an integration procedure will be required to discretize it, as it will be detailed in the Simulation Setup section (Section 5.4.1) .

The calculation of the optimum control action sequence $\mathbf{u}^+ = [\mathbf{u}(0); \ldots; \mathbf{u}(k+N-1)^T]$ for the proposed TV approach is carried out by minimizing the following cost function ℓ,

$$\begin{aligned} \ell\left(x\left(k\right), u\left(k\right)\right) = & W_{u,F_x}\{F_{x,ref} - [F_{x,FL} + F_{x,FR} + F_{x,RL} + F_{x,RR}]\}^2 \\ & + W_{u,\dot{\psi}}\left[\dot{\psi}_{ref} - \dot{\psi}\right]^2 + W_{u,\alpha_R}\alpha_R^2 + W_{u,PWT}{P_{Loss,PWT}}^2 \\ & + W_{u,tyre}[P_{Loss,tyre,Lg} + P_{Loss,tyre,Lat}]^2 \\ & + W_{u,LD}\left[\frac{\tau_{RL}}{\tau_{FL} + \tau_{RL}} - T_{r,ref,L}\right]^2 \\ & + W_{u,LD}\left[\frac{\tau_{RR}}{\tau_{FR} + \tau_{RR}} - T_{r,ref,R}\right]^2 \end{aligned} \tag{5.38}$$

where $F_{x,ref}$ is the total force demanded by the driver; α_R is the rear axle slip angle; and $P_{Loss,PWT}$, $P_{Loss,tyre,Long}$ and $P_{Loss,tyre,Lat}$ are the powertrain, and longitudinal and lateral tyre slip power losses, as defined in Section 5.3.3.2.

The stage cost function defined in Eq. 5.38 is designed to minimize several terms in the optimization procedure:

- A reference tracking term to ensure that the total force demand is as close as possible to the demanded one by the driver ($F_{x,ref}$).
- A reference tracking term to ensure that the predicted yaw rate is as close as possible to the energy-efficient yaw rate reference $\dot{\psi}_{ref}$ defined in Section 5.3.2.
- A term (α_R) to minimize the rear axle slip angles, and then, improve the stability of the vehicle.
- A term $P_{Loss,PWT}$ to minimize the powertrain power losses calculated using Eq. 5.45.
- Two terms $P_{Loss,tyre,Long}$ and $P_{Loss,tyre,Lat}$ to minimize the longitudinal and lateral tyre slip power losses, calculated using Eq. 5.34 and 5.35, respectively.
- Two terms $T_{r,ref,j}$, one per vehicle side, to track the optimal front to total torque distribution (See Section 5.3.1). Moreover, in order to provide this optimal torque distribution in a continuous form, it is defined as following [162]:

$$T_{r,ref,j} = \xi_1 + 0.5\ (\xi_2 - \xi_3)\{1 + \tanh[\xi_4(\tau_j - \xi_5)]\} \tag{5.39}$$

Each of the terms of the cost function ℓ has an associated weight terms, which can be used to tune the NMPC controller. This way the weigth terms $W_{u,F_x}, W_{u,\dot{\psi}}, W_{u,\alpha_R}$ $W_{u,PWT}, W_{u,tyre}$ and $W_{u,LD}$ are associated respectively to the longitudinal force tracking, reference yaw rate tracking, rear axle slip angle reduction, powertrain power loss reduction, tyre slip power loss reduction, and front-to-total torque distribution tracking within each EV side.

All these weights are calculated by considering a weighting coefficient (i.e. r_{u,F_x}, $r_{u,\dot{\psi}}$, r_{u,α_R}, $r_{u,PWT}$, $r_{u,tyre}$ and $r_{u,LD}$) and a scaling factor coefficient (i.e. U_{sc,F_x}, $U_{sc,\dot{\psi}}$, U_{sc,α_R}, $U_{sc,PWT}$, $U_{sc,tyre}$ and $U_{sc,LD}$). This way, in order to allow equivalent influence of the weights, these are normalized, e.g.

$$W_{u,F_x} = \frac{r_{u,F_x}}{{U_{sc,F_x}}^2} \tag{5.40}$$

Finally, one of the main advantages of the NMPC approaches is the possibility to include constraints in the control law, which ensure proper operation of the controller. These are represented typically by bounded-box (max/min) constraints, represented by the linear constrained sets $\mathcal{X}$ and $\mathcal{U}$. This way, the following constraints have been considered in the proposed controller,

- Individual wheel slip ratio constraints, i.e., $|s_{x,ij}| \leq s_{x,max,ij}$, where $s_{x,max,ij}$ is the maximum allowed value of longitudinal slip. This constraint is crucial to provide traction control system (TCS) functionality and avoid wheels slipping.

- Individual wheel torque constraints, i.e., $|\tau_{ij}| \leq \tau_{max,ij}$, where $\tau_{max,ij}$ is the maximum powertrain torque at V_0. This constraint is necessary to calculate the torque control actions accordingly to the actual powertrain and its operation point.

- Yaw rate constraint fixed for the whole prediction horizon, based on the tyre-road friction coefficient μ, $\dot{\psi} \leq \frac{\mu g}{V_{in}}$. This constraint is used to limit the yaw rate accordingly to the friction conditions. This way, possible stability losses can be avoided.

- Sideslip angle constraint, i.e., $\beta \leq \beta_{max}$. This constraint is used to avoid excessive understeering or oversteering situations.

Considering the aforementioned terms, and solving Eq. 5.36, the optimal control sequence $\mathbf{u}^+$ calculated in t for the whole horizon N,

$$\mathbf{u}^+ = [\mathbf{u}(0) \quad \mathbf{u}(1) \quad ... \quad \mathbf{u}(N-1)]^T \tag{5.41}$$

where only the value related to t, $\mathbf{u}(0)$ is applied to the vehicle.

5.3.3.4 Adaptive Weighting Approach

The tuning of the NMPC cost function weights influences the controller behaviour. As the NMPC formulation includes two main aspects in ℓ, i.e., yaw rate tracking and power loss reduction, a fuzzy logic weight adaptation algorithm was developed to prioritize energy efficiency during normal driving, and yaw rate tracking as well as rear axle sideslip angle limitation in critical conditions. Therefore, adaptation between three configurations are proposed: Energy Oriented, Yaw Rate Tracking, and Balanced energy/tracking.

In this implementation, large values of $\left|e_{\dot{\psi}}\right|$ and $|\beta|$ are considered as indicators of undesirable EV behavior. A distribution of three membership functions was chosen for both inputs, $\left|e_{\dot{\psi}}\right|$ and $|\beta|$, and for the output coefficient. Trapezoidal functions were selected for the boundaries of each variable, while the middle one is triangular. This configuration is computationally efficient while maintaining acceptable response smoothness [158]. The corresponding rules, see Table 5.1, have been implemented based on the authors' experience with the system. The effects of this weight adaptation algorithm will be showed in Section 5.4.3.

5.4 Validation

In this section, the proposed energy-efficient NMPC approach presented is validated through different manoeuvres and compared with other approaches. Section 5.4.1

Table 5.1: Adaptive fuzzy logic system rules

EO= Energy Oriented YR=Yaw Rate Tracking BW=Balanced Weights		$\lvert e_\psi \rvert$		
		Low	Medium	High
$\lvert\beta\rvert$	Low	EO	BW	YR
	Medium	EO	BW	YR
	High	EO	YR	YR

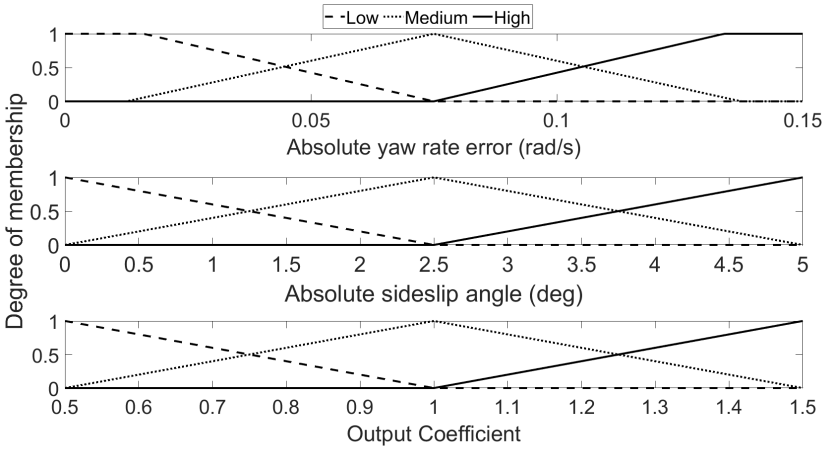

Figure 5.8: Fuzzy logic weight adaptation system membership functions.

presents the used Simulation Setup, detailing the case study EV and the used hardware platform for the HiL setup. Section 5.4.2 details the implementation procedure followed for the proposed approach. Section 5.4.3 studies the effect of the adaptive weighting approach proposed. Finally, Section 5.4.4 presents the obtained results for the different manoeuvres.

5.4.1 Simulation Setup

The overall structure of the implemented setup is detailed in Figure 5.9, where a Hardware-in-the-loop validation approach has been implemented using the *Vehicle Dynamics Simulation Framework* defined in Chapter 3.

In this case, the developed Energy-Efficient NMPC controller has been implemented in a dSPACE MicroAutobox II embedded hardware. This device communicates using CAN with a laptop computer (2.8 Ghz and 16 GB RAM) that runs the simulated study-case EV, a four-wheel-drive variant of a lightweight EV being developed within the European Horizon 2020 STEVE project [22] (Figure 5.10, whose main parameters are summarised in Table 5.2.

The dynamic model of this vehicle has been implemented using the formulation

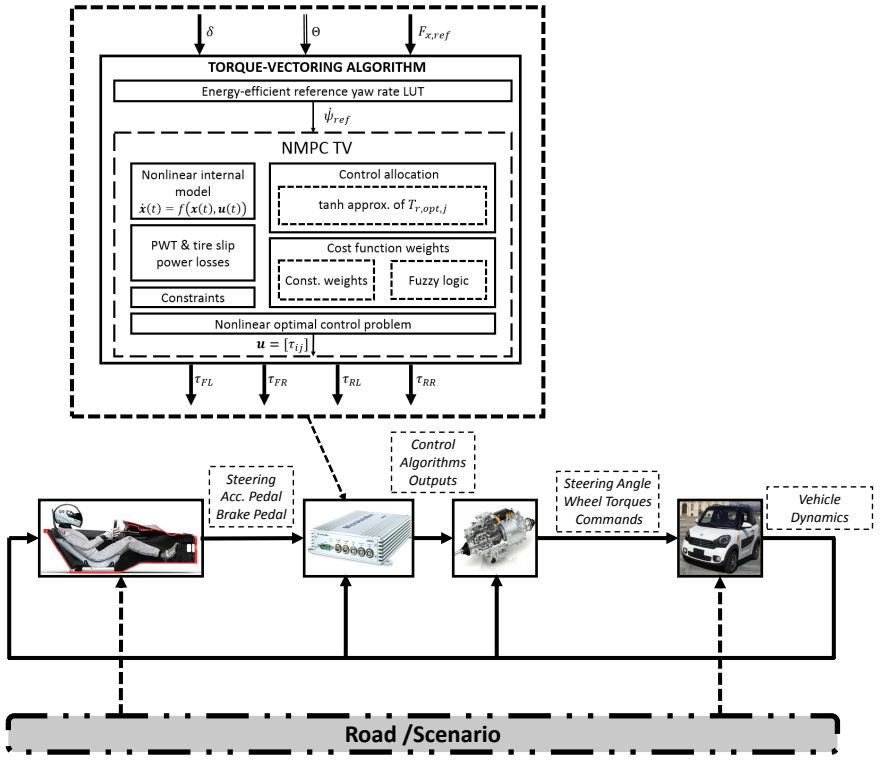

Figure 5.9: Structure of the proposed framework

Table 5.2: Vehicle Main Characteristics

Symbol	Description and unit	Value
M	Vehicle mass (kg)	649
R	Wheel radius (m)	0.2625
h	Center of gravity (CoG) height (m)	0.4
t_w	Track width	1.33
l_F	Distance from front axle to CoG (m)	0.99
l_R	Distance from rear axle to CoG (m)	0.825
L	Wheelbase (m)	1.815
I_x	Roll mass moment of inertia (kg m2)	200
I_y	Pitch moment of inertia (kg m2)	300
I_z	Yaw moment of inertia (kg m2)	400

defined in Chapter 3. A powertrain model has also been implemented, using the parameters provided by the manufacturer (Elaphe Propulsion Technologies Ltd.).

Figure 5.10: Lightweight EV being developed within the European Horizon 2020 STEVE project

The experimentally measured powertrain efficiency map of the vehicle is depicted in Figure 5.11.

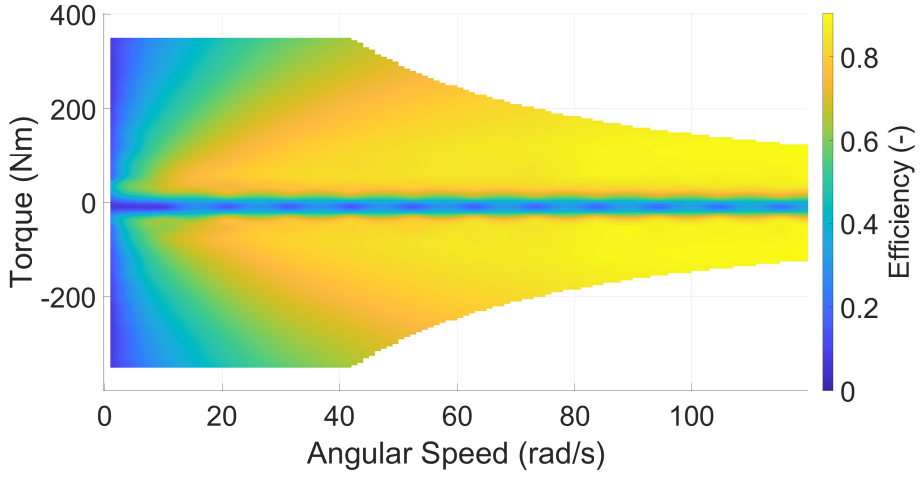

Figure 5.11: Experimentally measured powertrain efficiency map

5.4.2 Energy Efficient NMPC TV Implementation

In this section the implementation of the energy efficient NNMPC TV approach defined in Section 5.3 to the Study Case vehicle defined in the previous section will be detailed. In particular, the procedure required to define the Energy efficient front-to-total torque distribution, the generation of the energy-efficient yaw rate references and the tuning and parametrization of the Nonlinear MPC controller will be detailed.

5.4.2.1 Energy Efficient Front-to-Total Torque Distribution Look-up Table

As seen in Figure 5.3, a front-to-total torque distribution map $T_{r,j} = T_{r,j}(\tau_j, V/R_\omega)$ is required for both the calculation of the energy-efficient yaw rate, and the Cost Function of the NMPC. In this section, the procedure defined in Section 5.3.1 is applied to the study case EV to obtain the energy-efficient front-to-total distribution map.

Considering the full range of speed and torque associated to the vehicle's powertrain (see Figure 5.11), the energy-efficient front-to-total distribution map detailed in Figure 5.12 is obtained. Note that this map is the same for the left side and for the right side of the vehicle, as both sides have the same powertrains

This way, for a given speed, low torque demand values ($< 100 \sim 150Nm$) on a particular (left or right) EV side imply that only the rear powertrain is active , while at medium-to-high side torque demands $T_{r,opt,j}$ is 0.5, indicating an even torque distribution among the powertrains within the same EV side is the most efficient distribution. The transition between the two conditions occurs progressively, at different torque/speed values. Note that the results are consistent with the ones provided in [162].

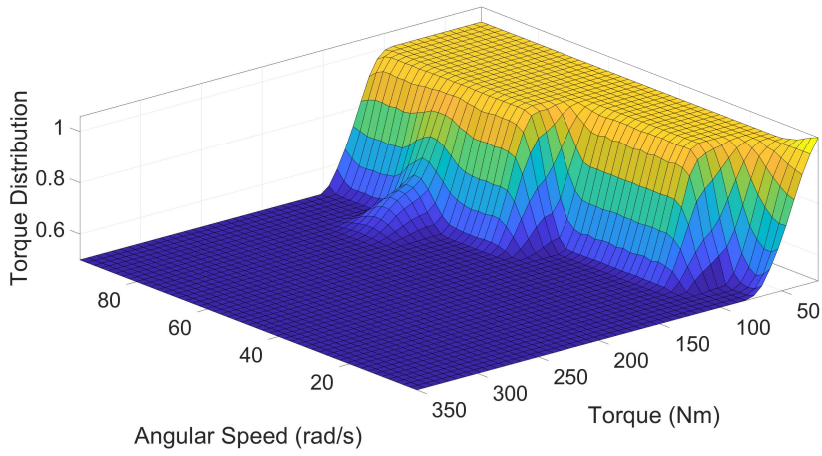

Figure 5.12: Energy-efficient front-to-total wheel torque distribution ratio as a function of vehicle-side torque and speed

The aforementioned map $T_{r,j} = T_{r,j}(\tau_j, V/R_\omega)$ for each side of the vehicle can be implemented as a Look-up Table for an efficient computation. However, as the NMPC TV needs a continuous implementation, Equation 5.39 is used for its implementation in the proposed controller.

5.4.2.2 Energy Efficient Yaw Rate Reference Look-Up Table

The yaw-rate reference has an important impact in the energy consumption of the vehicle. Thus, the procedure defined in Section 5.3.2 is applied to obtain the optimum yaw rate, this is, the one that provides the less energy consumption.

Energy Efficient understeer characteristic maps calculation and analysis: The aforementioned procedure requires to perform a wide set of simulations using the vehicle and powertrain models of the Study-Case EV. The aim of these simulations is to obtain the energy efficient understeer characteristic maps.

In order to explore the full range of achievable understeer characteristics associated to the study case EV, a set of simulated ramp steer maneuvers with slow steering input ramps at constant speed were repeated with different constant direct yaw moment values ranging from -900 Nm to +900 Nm in steps of 100 Nm. In addition, different vehicle speeds, emulated longitudinal accelerations, and tyre-road friction coefficients were evaluated. Table 5.3 summarizes the range of the variables considered in the simulated sets. Finally, note that the front-to-total distribution defined in Figure 5.12 was considered in these simulations.

Table 5.3: Range of the different variables modified in the ramp steer manoeuvre

	Mininum value	Maximum value
Direct yaw moment M_z	-900 Nm	900 Nm
Vehicle speed V	30 km/h	60 km/h
Steering wheel angle δ	0°	120°
Friction coefficient μ	0.6	0.9
Longitudinal acceleration a_x	0 m/s^2	2 m/s^2

Figure 5.13 shows the particular energy map associated to the ramp steer manoeuvre at V= 60 km/h and a tyre-road friction coefficient $\mu = 0.9$. In this figure, two understeer characteristics are shown. The *Passive* one is associated to a constant, even torque distribution among all wheels; while the *Optimal* one is the associated to the energy- efficient front-to-total distribution ratio within each side, and the optimal understeer characteristic which minimizes the power consumption for each a_y. This way, the color scale, obtained by interpolating the ramp steer results, shows the percentage increment of the powertrain power input, $P_{in,incr,\%}$, with respect to the *optimal* condition at the same a_y,

$$P_{in,incr,\%}\left(\delta_{dyn}, a_y\right) = 100\frac{P_{in}\left(\delta_{dyn}, a_y\right) - P_{in,opt}\left(a_y\right)}{P_{in,opt}\left(a_y\right)} \tag{5.42}$$

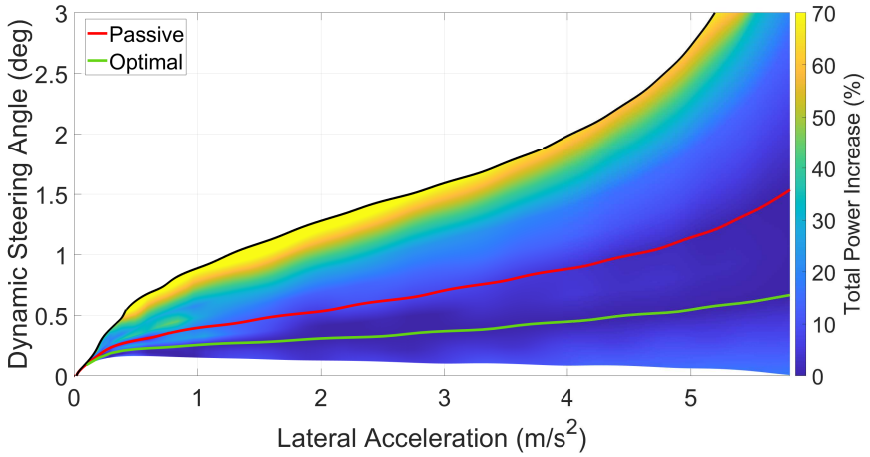

Figure 5.13: Example of % variation of the powertrain power input with the understeer characteristic (V= 60 km/h, μ= 0.9).

where $P_{in}(\delta_{dyn}, a_y)$ is the total input power at the dynamic steering angle δ_{dyn} and lateral acceleration a_y, while $P_{in,opt}$ is the minimum input power at the specific a_y.

If Figure 5.13 is analysed, it can be seen that the influence of the understeer characteristic on the EV energy consumption is very important, with peak values of $P_{in,incr,\%}$ over 50%. In particular, the average difference between the *Passive* and *Optimal* configurations immplies an average energy increment of 6.62% for the considered a_y range. From this, it can be concluded that an energy-efficient TV controller must include an appropriate design of the reference understeer characteristic, and hence the reference yaw rate. Moreover, an energy-efficient TV control system should also be able to determine the most appropriate reference yaw rate in transient conditions, based on quasi-static cornering conditions.

More conclusions can be drawn if the powertrain power lossess are evaluated over the total power losses $P_{Loss,\%}$ (which are defined in Section 5.3.3.2, and use the efficiency map in Figure 5.11),

$$P_{Loss,\%}(\delta_{dyn}, a_y) = 100\frac{P_{Loss,PWT}}{P_{Loss,PWT} + P_{Loss,tyre,Lg} + P_{Loss,tyre,Lat}} \tag{5.43}$$

Figure 5.14 shows the values of $P_{Loss,\%}$ for the particular case analyzed berfore (V= 60 km/h and a tyre-road friction coefficient $\mu = 0.9$). As it can be seen, at low a_y, the contribution of the electric powertrains is the most important one, accounting for up to 75% of the total relevant power. When a_y increases the relative motor power loss contribution progressively reduces, and becomes less than 50% of the TV-affected total power loss above 5 m/s^2. This observation, implies that an energy-efficient TV controller should consider all power loss sources, as each one could become predominant depending on the operating condition.

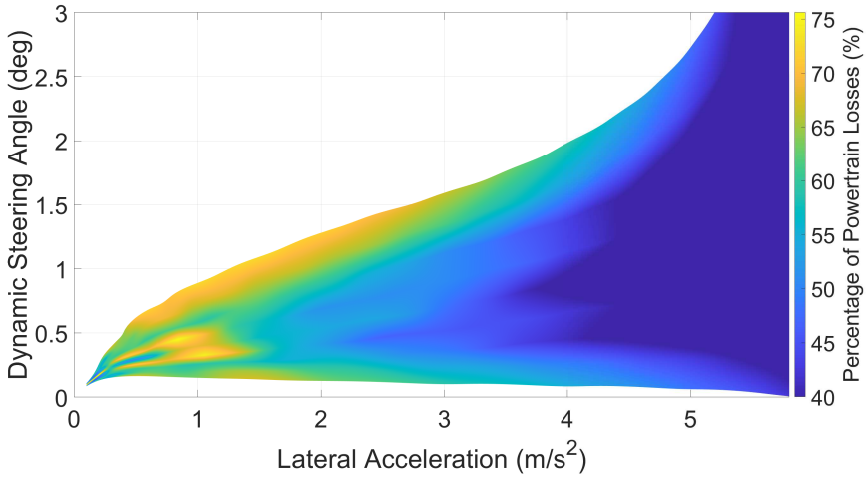

Figure 5.14: Example of % significance of the powertrain power loss with respect to the total power loss (powertrain and tyre slip power losses (V= 60 km/h, μ= 0.9).

As previously detailed, the aforementioned analysis was repeated for different vehicle speeds, emulated longitudinal accelerations, and tyre-road friction coefficients (see Table 5.3) . The results allowed creating a set of energy-efficient reference understeer characteristics expressed as a four-dimensional map, $\delta_{dyn,ref}\,(a_y, a_x,\ V,\ \mu)$.

Energy efficient reference yaw rate angles map: Once the energy-efficient reference understeer characteristics map $\delta_{dyn,ref}\,(a_y, a_x,\ V,\ \mu)$ is obtained, the energy-efficient steering angle reference can be calculated adding the kinematic steering angle (see Eq. 5.44).

$$\delta_{ref}\,(a_y, a_x,\ V,\ \mu) = \delta_{dyn,ref}\,(a_y, a_x,\ V,\ \mu) + \frac{L\,a_y}{V^2} \tag{5.44}$$

Through manipulation of $\delta_{ref}\,(a_y, a_x,\ V,\ \mu)$, and considering the relationship between a_y and $\dot{\psi}$ (see Eq. 5.12), the nominal reference yaw rate maps are obtained, in terms of $\dot{\psi}_{ref,nom}\,(\delta, a_x,\ V,\ \mu)$.

Some examples of energy-efficient reference yaw rate profiles as functions of steering wheel angle, for different values of vehicle speed (V), longitudinal acceleration (a_x), and tyre-road friction coefficient (μ) are shown in Figs. 5.15 to 5.17. While the dependency on V and μ is evident, the effect of a_x is rather limited for the studied longitudinal acceleration values corresponding to normal driving conditions. With appropriate first-order filtering to achieve the desired reference dynamics, the nominal reference yaw rate characteristics can be used to calculate the reference yaw rate, $\dot{\psi}_{ref}$.

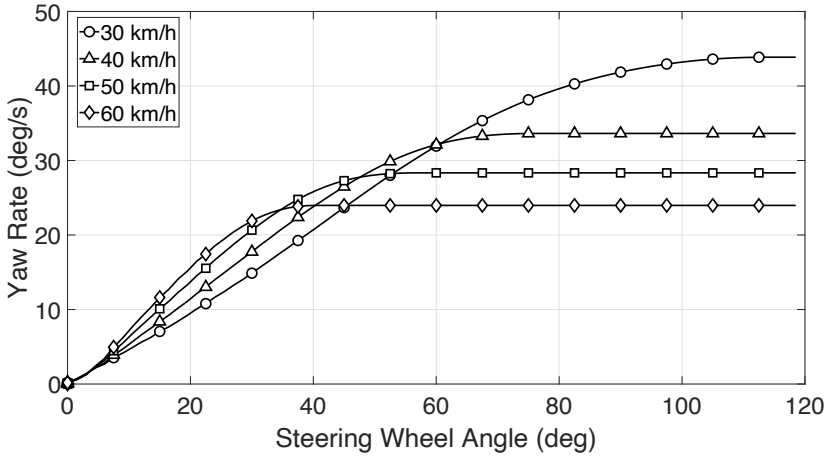

Figure 5.15: Examples of nominal energy-efficient reference yaw rate profiles as function of steering wheel angle, for different values of vehicle speed.

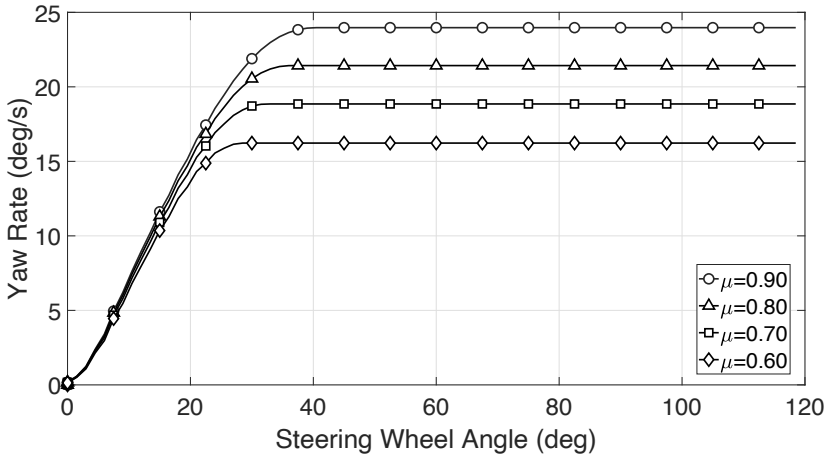

Figure 5.16: Examples of nominal energy-efficient reference yaw rate profiles as functions of steering wheel angle, for different values of tyre-road friction coefficient.

5.4.2.3 Nonlinear MPC implementation

The developed NMPC TV has been set up through the ACADO toolkit [161], which allows to easily introduce the internal model, the cost function and the constraint sets.

The internal model is defined using the set of equations defined in Section 5.3.3.1, particularized for the study case EV parameters. Similarly, the procedure detailed in Section 5.3.3.2 is used to define the power losses. Note that the powertrain losses de-

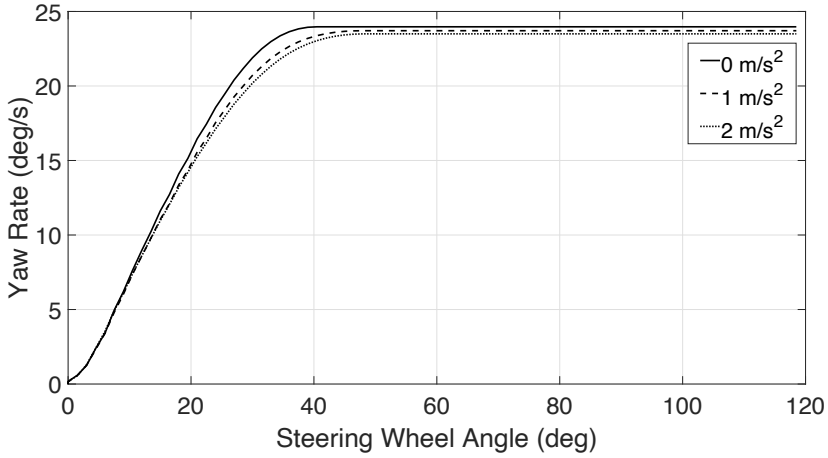

Figure 5.17: Examples of nominal energy-efficient reference yaw rate profiles as function of steering wheel angle, for different longitudinal accelerations

pend on the powertrain efficiency map (Figure 5.11) and the particular torque/speed combination (Eq. 5.32). In order to implement these losses in the NMPC formulation Cost Function (Eq. 5.38), a polinomial approximation is used,

$$\begin{aligned} P_{loss,PWT} = \sum_{\substack{i=F,R \\ j=R,L}} & p00 + p10\tau_{ij} + p01\omega_{ij} + p20\tau_{ij}^2 + p11\tau_{ij}\omega_{ij} \\ & + p02\omega_{ij} + p30\tau_{ij}^3 + p21\tau_{ij}^2\omega_{ij} + p12\tau_{ij}\omega_{ij}^2 \\ & + p03\omega_{ij}^3 + p40\tau_{ij}^4 + p31\tau_{ij}^3\omega_{ij} + p22\tau_{ij}^2\omega_{ij}^2 \\ & + p13\tau_{ij}\omega_{ij}^3 + p04\omega_{ij}^4 + p50\tau_{ij}^5 + p41\tau_{ij}^4\omega_{ij} \\ & + p32\tau_{ij}^3\omega_{ij}^2 + p23\tau_{ij}^2\omega_{ij}^3 + p14\tau_{ij}\omega_{ij}^4 + p05\omega_{ij}^5 \end{aligned} \tag{5.45}$$

where the p_{ij} parameters are summarized in Table 5.4.

Table 5.4: Powertrain losses polynomial approximation parameters

Name	Value	Name	Value	Name	Value
p00	-70.9	p21	0.001553	p04	-3.53e-09
p10	36.23	p12	0.0009236	p50	3.62e-07
p01	2.172	p03	6.30e-05	p41	7.16e-09
p20	-1.388	p40	-0.000156	p32	3.66e-08
p11	-0.1039	p31	-7.75e-06	p23	1.93e-09
p02	0.0303	p22	-1.03e-05	p14	3.65e-10
p30	0.02298	p13	-5.75e-07	p05	-4.59e-11

Figure 5.18 show the results for the powertrain power losses polynomial approx-

imation for the study case EV, which in this particular case provide a RMS error of 75W compared with the results provided by Eq. 5.32.

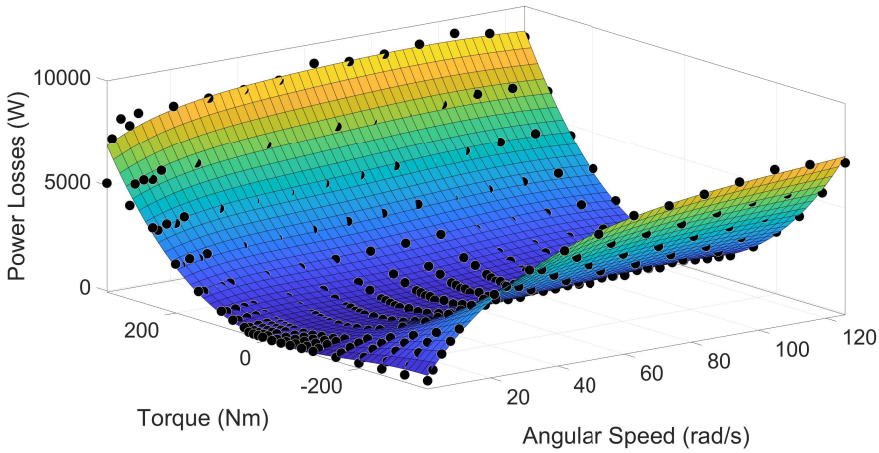

Figure 5.18: Experimental power loss characteristic of the case study individual in-wheel powertrain as a function of torque and speed (the dots indicate the measurement points), and its approximation adopted within the NMPC formulation.

In addition, the following constraints were considered,

- Individual wheel slip ratio constraints, i.e., $|s_{x,ij}| \leq s_{x,max,ij}$, where $s_{x,max,ij}$ is the maximum allowed value of longitudinal slip, set to 0.15 for the simulations of this study.
- Individual wheel torque constraints, i.e., $|\tau_{ij}| \leq \tau_{max,ij}$, where $\tau_{max,ij}$ is the maximum powertrain torque at the current time step. For that, considering the current vehicle speed V_0, zero slip conditions ($\omega_{ij} R_w = V_0$), and the maximum power of each powertrain $P_{max,ij}$ (15kW), the maximum torque is calculated as $\tau_{max,ij} = P_{max,ij}/\omega_{ij}$.
- Yaw rate constraint fixed for the whole prediction horizon, based on the tyre-road friction coefficient μ, $\dot{\psi} \leq \frac{\mu g}{V_0}$.
- Sideslip angle constraint, i.e., $\beta \leq \beta_{max}$, set to 5 deg.

The control law in Eq. 5.36 was implemented in ACADO by using the multiple shooting discretization method and fourth order Runge Kutta integrator. The resulting C code was implemented in real time on a dSPACE MicroAutoBox II unit, as previously defined.

A sensitivity analysis was carried out to investigate the effect of the NMPC prediction horizon, H_P, and internal model discretization time, T_S, and identify the best compromise between controller performance and computational effort. H_P ranged from 250 ms to 750 ms, while T_S ranged from 10 ms to 30 ms. The implementation

step of the controller, ΔT, i.e., the time step at which the controller updates its outputs, was set to be larger, with appropriate and consistent margin, than the maximum execution time on the available control hardware, and therefore was different for each set of H_P and T_S.

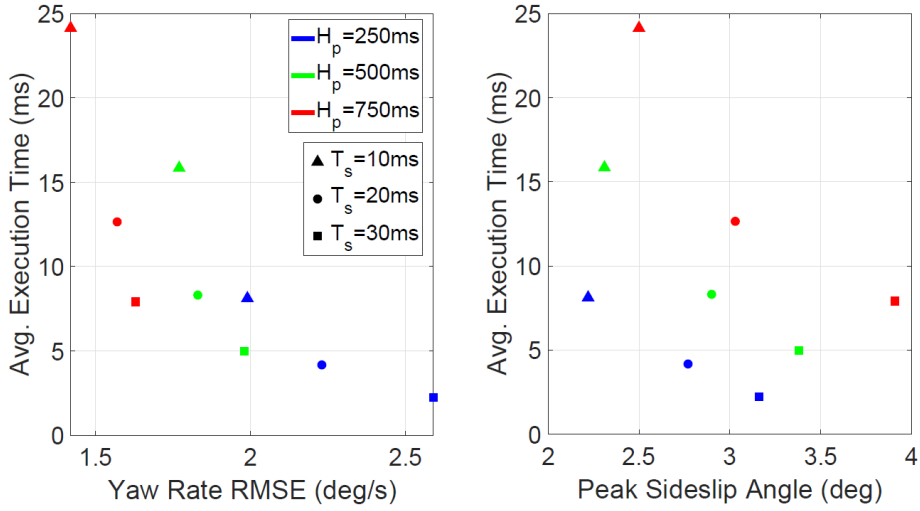

Figure 5.19: Effect of H_P and T_S on the average execution time on a dSPACE MicroAutoBox II device, RMS of the yaw rate error, and peak value of sideslip angle, during an obstacle avoidance from an initial speed of 56 km/h.

Figure 5.19 reports the average NMPC execution time as a function of the RMS value of the yaw rate error, $e_{\dot{\psi}}$, and the peak value of β, for a double lane change from an initial speed of 56 km/h and with $\mu = 0.9$. In all configurations, β is below the critical threshold of 5 deg, set as a constraint for high tyre-road friction conditions, and therefore the controller performance should be evaluated in terms of yaw rate tracking. As $H_P = 500$ ms and $T_S = 20$ ms represent a good compromise between performance and computational effort, with a maximum recorded execution time of 10.81 ms, this controller set up, indicated by the dashed circles in Figure 5.19, was selected for this simulation setup, with $\Delta T = 20$ ms.

5.4.3 Analysis of Cost Function Weight Adaptation Approach

Prior to analyzing the performance of the developed Energy Efficient TV approach, a brief analysis of the effect of the proposed Adaptive Weighting approach is carried out.

For this purpose, a Double Lane Change manoeuvre with an initial speed challenging enough (56km/h in this particular case) to show the difference between the following four different cost function weight configurations will be simulated,

1. yaw rate tracking oriented weights, which prioritize vehicle dynamics performance and safety.
2. energy efficiency oriented weights, which prioritize energy saving
3. balanced weights between energy efficiency and vehicle dynamics
4. the proposed Adaptive Weighting Approach (Section 5.3.3.4), which combines all the aforementioned ones.

Table 5.5 summarizes the weights for the first three approaches.

Table 5.5: Cost function weights for the different configurations

	Energy Oriented	Yaw Rate Tracking	Balanced Weights
r_{u,F_x}	2.5	2.5	2.5
$r_{u,\dot{\psi}}$	1	5	3
$r_{u,\alpha}$	1.5	1.5	1.5
$r_{u,PWT}$	5	1	2.5
$r_{u,tyre}$	5	1	2.5
$r_{u,LD}$	2.5	2.5	2.5

Figure 5.20 shows the resulting EV trajectories for dry road ($\mu = 0.9$). The adaptation mechanism provides an EV response that is very similar to the first weight configuration, focused on vehicle dynamics. Moreover, Table 5.6 reports the maximum speed - the critical speed, V_{cr} - at which each configuration successfully completes the test, i.e., without hitting a cone. In this case, the NMPC with the adaptation mechanism provides the same performance as the vehicle dynamics oriented weight configurations, corresponding to 5 km/h and 3 km/h higher initial speeds than for the energy-efficiency and balanced weight configurations.

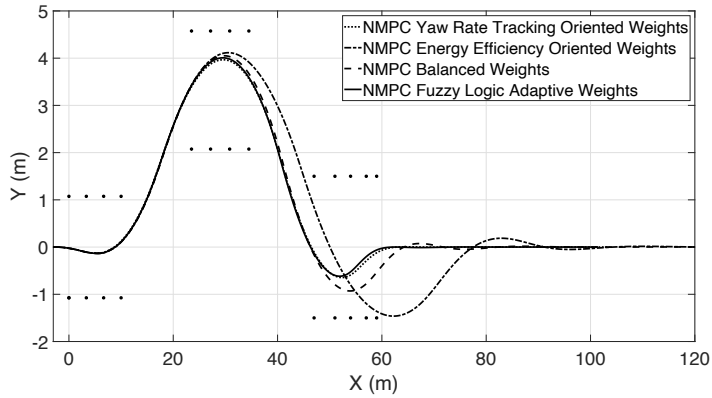

Figure 5.20: Double lane change trajectories (initial speed of 56 km/h) associated with different tunings of the NMPC cost function weights ($\mu = 0.9$).

Table 5.6: Effect of cost function weights on critical speed for double lane change

	NMPC Yaw Rate Oriented Weights	NMPC Energy Efficiency Oriented Weights	NMPC Balanced Weights	NMPC Fuzzy Logic Adaptive weights
Critical speed	61 km/h	56 km/h	58 km/h	61 km/h

5.4.4 Validation of the proposed Energy Efficient TV approach

In this section the proposed TV approach is evaluated using a set of benchmarking TV controllers in order to determine the dynamics performance and efficiency of each approach. The benchmarking controllers include a passive approach, the Fuzzy Yaw Moment Controller developed in Chapter 4 and a set of NMPC controllers based on the formulation proposed in this chapter. In the latter case, the aim is to analyze the effect of each term in the cost function to the overall performance of the TV controller. The complete list of appoaches is detailed next, m

- Passive, evenly distributing the torque among the wheels.
- Passive + LUT, providing the same total wheel torque on the two EV sides, i.e., zero direct yaw moment, while the front-to-total torque distribution within each side is carried out according to Figure 5.12.
- Fuzzy + LUT, providing a direct yaw moment generated by the benchmarking controller in Chapter 4, while the front-to-total torque distribution within each side is carried out according to Figure 5.12.
- NMPC Yaw Rate, i.e., the proposed NMPC TV approach only considering the yaw rate tracking and rear sideslip terms in the cost function, while $W_{u,PWT} = W_{u,tyre} = W_{u,LD} = 0$.
- NMPC PWT Losses, which, on top of the NMPC Yaw Rate features, considers the powertrain power loss term in the cost function, while $W_{u,tyre} = W_{u,LD} = 0$.
- NMPC tyre Losses, i.e., the proposed NMPC TV approach that considers the yaw rate tracking, rear sideslip and tyre slip power loss terms in the cost function, while $W_{u,PWT} = W_{u,LD} = 0$.
- NMPC Complete, i.e., the proposed NMPC TV approach that considers yaw rate tracking, rear sideslip, powertrain losses and tyre slip power losses, without using the cost function terms related to the front-to-total wheel torque distribution within each side, i.e., $W_{u,LD} = 0$.
- NMPC Complete WCA, i.e., the proposed NMPC TV approach using all cost function terms, with constant values of the weights.

- NMPC Complete WCA Adaptive, i.e., the proposed NMPC TV approach using all cost function terms, and also including the fuzzy adaptation mechanism of the cost function weights.

It has to be noted that the *Balanced Weights* values (see Section 5.4.3) has been taken as reference for the aforementioned NMPC configurations, with except for the *NMPC Complete WCA Adaptive* approach, which is the proposed approach in this Chapter.

These controllers will be compared in a set of manoeuvres and standarized tests: Skid-Pad; Double Lane Change; WLTP, NEDC and ARTEMIS road cycles; and circuit laps. Results are detailed next.

5.4.4.1 SkidPad test

50 m radius skid pad simulations for $\mu = 0.9$ and 0.7 (wet and dry conditions) were run to assess the relative importance of: a) the reference yaw rate characteristic; and b) the wheel torque control allocation, in the energy efficiency. Additionally, some tests with incorrect friction conditions information in the yaw rate reference have been carried out in order to evaluate the ability of the proposed NMPC TV to compensate this issue.

The tests were carried out for different constant speeds, each corresponding to a lateral acceleration a_y. The power consumption related to the performance of five of the aforementioned controllers was calculated: Passive, Passive + LUT, NMPC Yaw Rate, Fuzzy + LUT and NMMPC Complete WCA Adaptive.

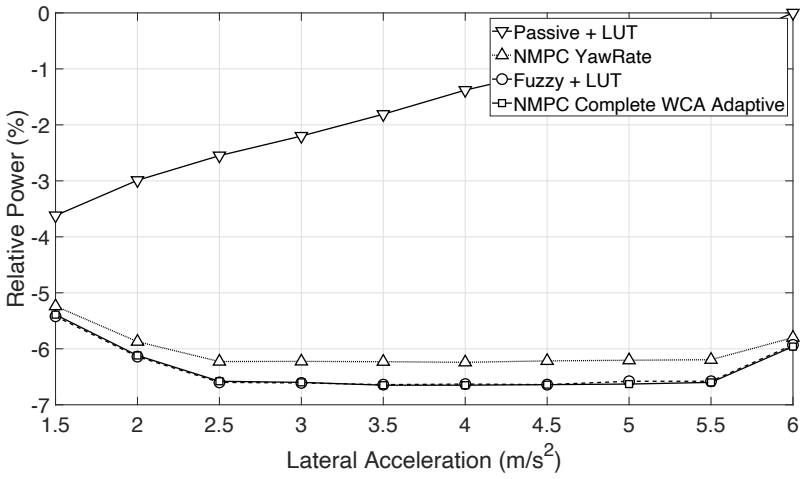

Figure 5.21: Percentage power input variation for a selection of configurations, with respect to the Passive configuration, for $\mu = 0.9$.

The relative power input reduction with respect (w.r.t) to the Passive TV approach is shown in Figures 5.21 and 5.22 for both selected μ. As it can be seen, all controllers

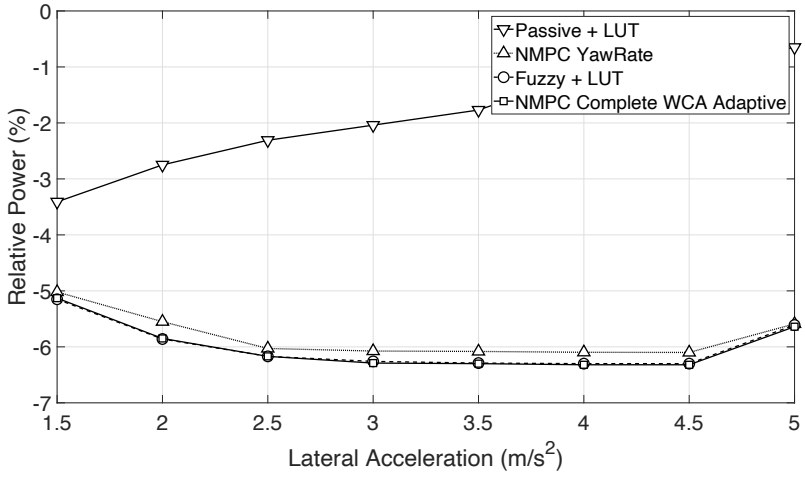

Figure 5.22: Percentage power input variation for a selection of configurations, with respect to the Passive configuration, for $\mu = 0.7$.

using the energy-efficient reference yaw rate maps show similar benefits, with power input reductions ranging from 5.0% to 6.8% with respect to the Passive configuration. The control allocation layer of the Passive + LUT configuration can reduce the energy consumption only up to 3.6%, with an average saving of 1.8%, and its effect is more significant at low a_y values, corresponding to low speeds. In these conditions the electric powertrains operate in their least efficient region, therefore, the LUT based control allocation algorithm deactivates one of the axles according to the map in Figure 5.12, and the torque demand is only provided by the rear axle, which thus operates in a more efficient region. The considerable consumption difference between the Passive + LUT and all the other controlled configurations can be associated to the effect of the energy-efficient yaw rate reference.

In sum, the results show that during steady-state cornering i) the control allocation aspects of the TV controller, which are the focus of the majority of the existing literature, are less important than the reference yaw rate characteristics; and ii) a TV controller capable of tracking the appropriate energy-efficient reference yaw rate provides rather similar energy consumption results.

However, a sophisticated TV algorithm can still provide energy efficiency benefits in specific quasi-steady-state cornering conditions. In fact, as discussed in Section 5.3.2, the optimal yaw rate reference depends on μ, and thus the friction coefficient estimation is crucial to the correct operation of the algorithm. However, in practice, accurate μ estimation when the EV operates below its friction limits is rather difficult to accomplish. Therefore, a second set of skidpad tests at $\mu = 0.7$ was simulated at a constant a_x of 1 m/s^2, with incorrect ($\mu = 0.9$) and correct ($\mu = 0.7$) friction information provided to the TV controller, to evaluate its ability to compensate for incorrect $\dot{\psi}_{ref}$ profiles.

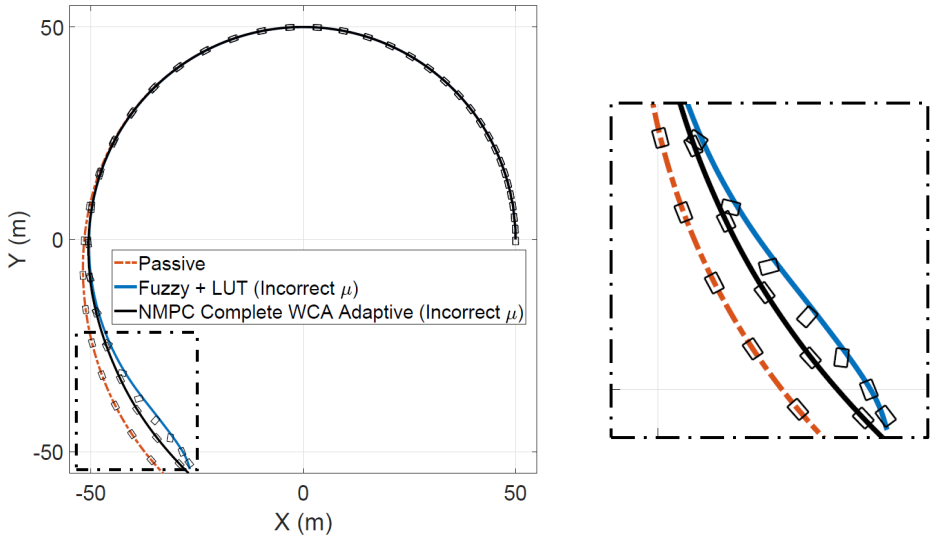

Figure 5.23: Skidpad trajectories for a selection of controllers, with $a_x = 1$ m/s^2 and $\mu = 0.7$. The solid boxes indicate the motion of the cars. Left: full maneuver; right: zoom of trajectories towards end of maneuver.

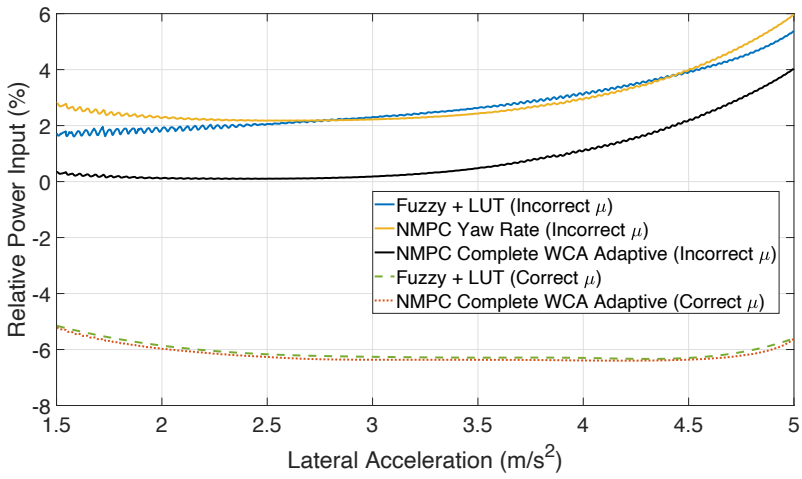

Figure 5.24: Percentage power input variation for a selection of controller configurations with respect to the Passive configuration, during skidpad test with $a_x = 1$ m/s^2 and $\mu = 0.7$.

Results are shown in Figures 5.23 and 5.24, where the dynamic performance and relative power increase is detailed. As it can be seen, the Fuzzy + LUT configuration is unstable, while the Passive one is affected by significant understeer, with respect

to the NMPC TV. Regarding the power consumption, for the cases with the incorrect yaw rate reference, the power consumption always greater than for the Passive vehicle, with up to 6% at around 5 m/s^2 for the NMPC Yaw Rate. In contrast, the configurations with the correct yaw rate reference achieve a power saving of about 6% compared to the Passive case almost across the entire investigated lateral acceleration range. Although the NMPC Complete WCA Adaptive configuration receives the same incorrect $\dot{\psi}_{ref}$, its power consumption is lower, on average by 2%, than for the other cases with the incorrect $\dot{\psi}_{ref}$. In fact, the complex NMPC cost function defined in Eq.5.38 accounts and partially compensates for the increased tyre slip power losses caused by the inappropriate reference understeer characteristic.

These results, effectively demonstrate that the inclusion of the different relevant power loss contributions in the cost function allows to compensate for inaccuracies, e.g., related to the estimation of the tyre-road friction coefficient, in the online generation of the energy-efficient reference yaw rate, thus providing robustness not only to the energy efficiency enhancement, but also to the dynamic behaviour.

5.4.4.2 Double Lane Change

The Double Lane Change maneouvre, or obstacle avoidance maneouvre, is frequently used by car makers and suppliers to assess vehicle dynamics control systems. In this particular case, the aforementioned two road scenarios were considered (dry and wet), with $\mu = 0.9$ and 0.7. According to the ISO 3888 specification [160], the vehicle enters the course at a set speed, and the accelerator pedal is released; then the driver, i.e., the driver model defined in the framework defined in Section 3.2, attempts to track the reference path without hitting a cone.

In order to evaluate the dynamic handling performance of the analyzed TV controllers, the Double Lane Change test speed is progressively increased up to its critical value, V_{cr}, at which the course can no longer be successfully negotiated. Results are summarized in Table 5.7, where the V_{cr} values for the Passive vehicle and the controlled configurations are shown. The best performance is provided by the NMPC Yaw Rate and the NMPC Complete WCA Adaptive, achieving 61 km/h and 45 km/h with the two friction conditions, respectively, against 54 km/h and 37 km/h of the Passive vehicle, and 58 km/h and 43 km/h of the NMPC Complete. The V_{cr} results confirm the functionality of the fuzzy adaptation mechanism.

Table 5.7: Critical speed achieved during double lane change

	Passive	Passive + LUT	Fuzzy + LUT	NMPC Yaw Rate	NMPC PWT Losses	NMPC tyre Losses	NMPC Complete	NMPC Complete WCA	NMPC Complete WCA Adaptive
$\mu = 0.9$	54 km/h	54 km/h	56 km/h	61 km/h	58 km/h	59 km/h	58 km/h	58 km/h	61 km/h
$\mu = 0.7$	37 km/h	37 km/h	40 km/h	45 km/h	42 km/h	45 km/h	43 km/h	43 km/h	45 km/h

Figures 5.25 and 5.26 show the vehicle sideslip angle, powertrain power losses, tyre slip power losses and total power losses for four configurations, at $\mu = 0.9$ and 0.7. The inclusion of the tyre slip power loss term in the NMPC cost function reduces

the sideslip angle, as β is directly related to the tyre slip angles (see Eq.5.26), and the lateral tyre slip power losses (see Eq. 5.35). As expected, the combination of all cost function terms in the NMPC Complete configuration brings the most balanced, and therefore, most efficient result.

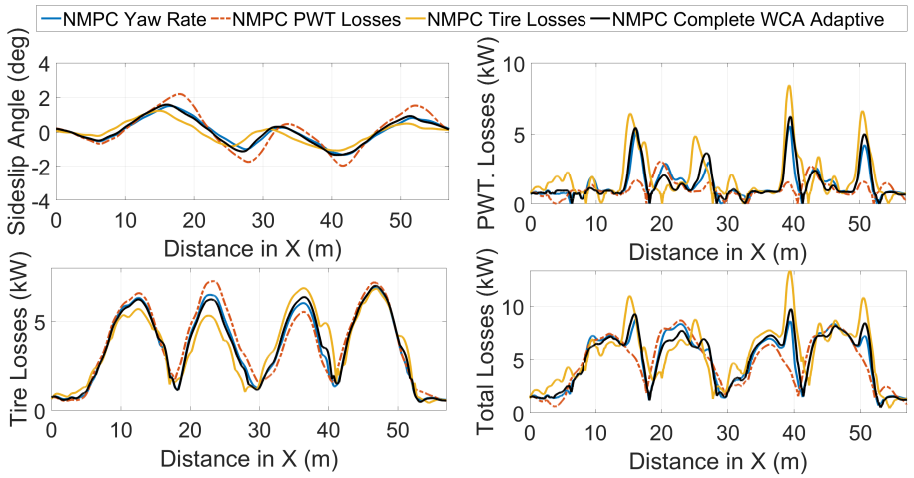

Figure 5.25: Power loss profiles during a double lane change test, for $\mu = 0.9$ and an initial speed of 56 km/h.

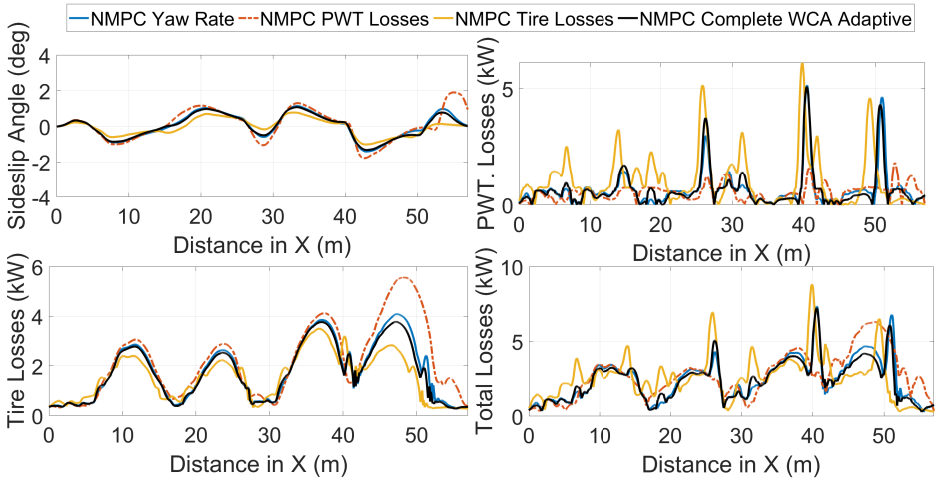

Figure 5.26: Power loss profiles during a double lane change test, for $\mu = 0.7$ and an initial speed of 40 km/h.

In addition, to objectively assess the performance of the different configurations during the obstacle avoidance test, the following set of indicators are selected and compared,

Table 5.8: Double lane change results for $\mu = 0.9$ and 56km/h

	Fuzzy + LUT	NMPC Yaw Rate	NMPC PWT Losses	NMPC Tyre Losses	NMPC Complete	NMPC Complete WCA	NMPC Complete WCA Adaptive
V_{fin} (km/h)	42.39	44.04	44.17	44.75	44.46	44.29	45.40
$RMS(e_{\psi})$(deg/s)	2.32	1.52	2.57	1.88	1.88	1.96	1.60
$\lvert\alpha_{R,max}\rvert$(deg)	3.08	4.80	5.02	4.33	4.82	4.57	4.16
$IA_{\delta_{SW}}$(deg)	45.87	48.09	52.73	54.60	51.43	53.38	44.91
$IA_{M_z,ref}$(Nm)	410.31	402.69	380.25	391.06	391.89	399.98	368.96

- The final vehicle speed, V_{fin}, i.e., the speed at the exit of the course, which is an indicator of vehicle agility and the level of tyre slip power loss.
- The root mean square value of the yaw rate error, $\mathrm{RMS}\big(e_{\dot{\psi}}\big)$, which evaluates the yaw rate tracking performance and vehicle agility.
- The peak absolute value of the rear axle slip angle, $|\alpha_{R,max}|$, which assesses vehicle stability as well as tyre slip power losses.
- The normalized integral of the absolute value of the steering angle δ_{SW}:

$$IA_{\delta_{SW}} = \frac{1}{t_{fin} - t_{in}} \int_{t_{in}}^{t_{fin}} |\delta_{SW}|\, dt \tag{5.46}$$

  where t_{in} and t_{fin} are the initial and final times of the relevant part of the test, calculated when the EV enters and leaves the obstacle avoidance course. $IA_{\delta_{SW}}$ assesses the required steering effort to follow the reference path.

- The normalized integral of the absolute value of the reference direct yaw moment, $M_{z,ref}$, calculated from the individual reference wheel torque demands:

$$IA_{M_{z,ref}} = \frac{1}{t_{fin} - t_{in}} \int_{t_{in}}^{t_{fin}} |M_{z,ref}|\, dt \tag{5.47}$$

Two speeds based on the lowest critical speed achieved by the Fuzzy+LUT setup for the dry and wet road scenarios were considered: a speed of 56 km/h with $\mu = 0.9$ and 40 km/h with $\mu = 0.7$. Results are summarized in Tables 5.8 and 5.9.

The results confirm the superior performance of the NMPC Complete WCA Adaptive, which has the highest V_{fin} in both tests (ultimate proof of reduced tyre slip power losses), and consistently good performance in all other indicators. The results also highlight that energy-efficient TV control should account for both powertrain and tyre slip power losses to achieve energy saving in a wide range of vehicle operation. For $\mu = 0.9$, V_{fin} is comparable for the NMPC PWT Losses and NMPC Tyre Losses configurations, while for $\mu = 0.7$ the latter configuration is significantly more efficient.

Table 5.9: Double lane change results for $\mu = 0.7$ and 40km/h

	Fuzzy + LUT	NMPC Yaw Rate	NMPC PWT Losses	NMPC Tyre Losses	NMPC Complete	NMPC Complete WCA	NMPC Complete WCA Adaptive
V_{fin} (km/h)	30.58	32.80	31.76	34.06	33.86	33.10	34.17
$RMS(e_{\psi})$(deg/s)	3.48	1.32	2.91	1.29	1.60	1.67	1.34
$\lvert\alpha_{R,max}\rvert$(deg)	4.14	3.36	3.60	2.93	3.54	3.49	3.04
$IA_{\delta_{SW}}$(deg)	68.97	42.23	56.25	32.95	45.11	47.85	42.27
$IA_{M_z,ref}$(Nm)	255.41	179.54	168.11	275.68	179.95	191.27	181.00

5.4.4.3 Driving Cycles

In order to evaluate the effect on power consumption of the front-to-rear wheel torque distribution during straight-line operation, a set of standarized driving cycles were simulated:

- World harmonized Light vehicles Test Procedure (WLTP) [146], excluding the extra high speed section
- New European Driving Cycle (NEDC)
- ARTEMIS road
- ARTEMIS urban

The results are reported in Table 5.10 only for the most advanced NMPC configuration as the energy consumption is very similar with all controlled configurations. This result is expected considering the nature of the mission profiles (a straight-line) and the low torque and, thus, low longitudinal tyre slip values. Hence, the energy consumption during the driving cycle is dominated by the powertrain power loss characteristics. For all the tests, the NMPC Complete WCA Adaptive leads to reduced energy consumption with respect to the single axle configuration, using only the rear powertrains (while the front powertrains are switched off), and the even distribution strategy, i.e., the Passive configuration defined in Section V.A. Depending on the driving cycle, the saving of the NMPC TV implementation ranges between 0.21% and 2.46%, with an average saving of 1.06%, with respect to the single axle case, and between 0.47% and 3.18%, with an average saving of 2.04%, compared to the even distribution configuration. The driving cycle results are aligned with those in other recent energy-efficient front-to-total wheel torque distribution studies [162].

Table 5.10: Energy consumption results along a selection of driving cycles

	Energy consumption (kWh)			Improvement (%) of NMPC with respect to	
Driving Cycle	Single Axle	Even distribution	NMPC Complete WCA Adaptive	Single Axle	Even Distribution (Passive)
WLTP	1.433	1.477	1.43	0.21	3.18
NEDC	0.593	0.604	0.589	0.77	2.58
ARTEMIS road	1.985	2.008	1.969	0.8	1.94
ARTEMIS urban	0.495	0.485	0.483	2.46	0.47

5.4.4.4 Circuit Lap Test

The final test assesses the controllers in a complex scenario, i.e., the circuit of the 2015 Formula Student Germany competition. Figure 5.27 shows the vehicle path along the track, and the fixed speed profile followed by all controller configurations, which corresponds to a rather "aggressive" driving style within the limit of handling, with peak values of lateral acceleration of 6 m/s^2.

Table 5.11 reports the main performance indicators. The fast driving style does not allow the LUT based control allocation to bring substantial benefits, which is confirmed by the energy saving of only 0.59% of the Passive + LUT with respect to the Passive. Thanks to the adoption of an energy-efficient reference yaw rate characteristic, the Fuzzy + LUT achieves a 3.93% energy consumption reduction with respect to Passive configuration. Importantly, all NMPC implementations, including the NMPC Yaw Rate, consume less than the benchmarking Fuzzy + LUT configuration. In fact, although the NMPC Yaw Rate formulation does not consider the power loss contributions or the energy-efficient front-to-total wheel torque distribution within its cost function, it demonstrates significantly better yaw rate tracking performance than the Fuzzy + LUT, which is beneficial to active safety and consumption. The energy saving is very similar for the NMPC PWT Losses and the NMPC Tyre Losses, i.e., 6-7%, while all NMPC configurations that consider both power loss terms in the Cost Function reduce the consumption by more than 9%. In general, these results confirm the importance of the reference understeer characteristic on the EV energy consumption.

Moreover, it can be seen that the implementation of energy-efficient TV configurations does not compromise the vehicle cornering response with respect to the Passive vehicle; on the contrary, despite achieving higher stability, i.e., larger values of V_{cr} in the double lane change tests, the energy-efficient TV controlled configurations alleviate the steering effort, with $IA_{\delta_{SW}}$ reductions ranging from 6% to nearly 13%.

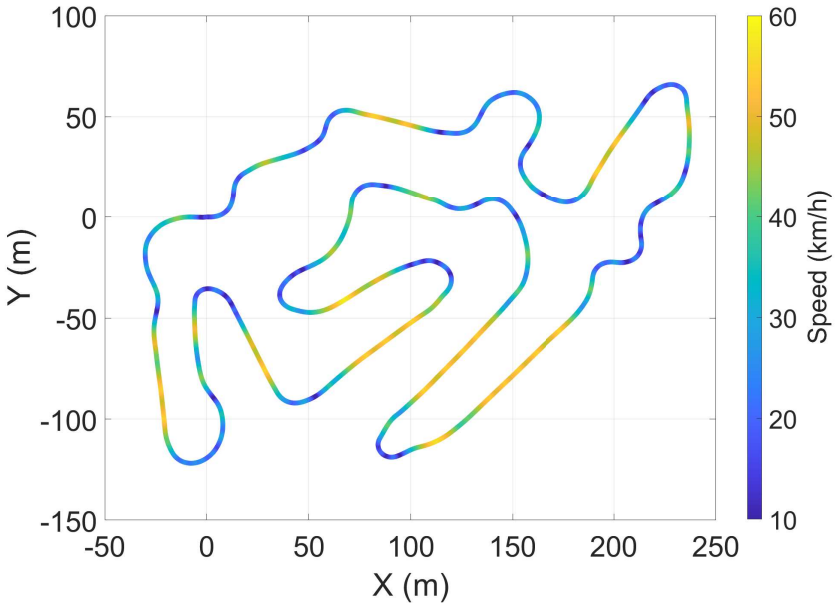

Figure 5.27: Top view of the vehicle with indication of the sign conventions for the main variables.

Table 5.11: Performance indicators of the EV configuration along the selected circuit

	Passive	Passive + LUT	Fuzzy + LUT	NMPC Yaw Rate	NMPC PWT Losses	NMPC tyre Losses	NMPC Comp.	NMPC Comp. WCA	NMPC Comp. WCA Adapt.
En. consumption (kWh)	1.178	1.171	1.132	1.118	1.095	1.103	1.072	1.070	1.067
En. cons. w.r.t Pass. (%)	-	-0.59	-3.93	-5.13	-7.06	-6.38	-9.01	-9.16	-9.43
$RMS(e_{\dot{\psi}})$(deg/s)	4.75	4.76	2.69	1.90	2.33	2.04	2.10	2.12	1.93
$IA_{\delta_{SW}}$(deg)	41.27	41.35	37.88	36.16	38.76	36.46	37.55	37.71	36.00
$IA_{\delta_{SW}}$ w.r.t. Pass. (%)	-	+0.20	-8.21	-12.37	-6.06	-11.65	-9.01	-8.62	-12.75

5.4.5 Summary and discussion

The results of the extensive simulation analysis on the case-study lightweight electric vehicle with in-wheel motors can be summarized as follows:

- In quasi-steady-state cornering conditions, the reference understeer characteristic has more influence on the energy consumption than the control allocation algorithm. This effect is progressively more evident with increasing lateral acceleration (see Section 5.4.4.1).
- Although the inclusion of the power loss terms in the TV controller formulation only marginally improves the power consumption during steady-state cornering, it significantly enhances system robustness by compensating for the power

consumption increase caused by state estimation errors, e.g., on the tire-road friction coefficient (see Section 5.4.4.1).

- The adaptation mechanism of the cost function weights of the nonlinear model predictive controller formulation provides significant operational flexibility depending on the actual driving situation, i.e., by prioritizing energy efficiency during normal driving and vehicle safety and stability in extreme manoeuvres during sub-limit driving. With such mechanism, the NMPC TV system is characterized by the same critical speed in obstacle avoidance maneuvers as its version tuned only for vehicle dynamics performance, i.e., 61 km/h at $\mu = 0.9$ and 45 km/h at μ= 0.7, against 54 km/h and 37 km/h of the Passive configuration (see Section 5.4.4.2).

- With respect to the Passive configuration, the most advanced control configuration proposed in this study, the NMPC Complete WCA Adaptive, reduces energy consumption by 2% on average during the selected driving cycles in straight-line conditions (see Section 5.4.4.3), and 9% along the considered circuit (see Section 5.4.4.4).

5.5 Conclusions

The development of systems that reduce EVs energy consumption and contribute to their widespread adoption is a key issue in the Automotive Industry. In this sense, TV systems have demonstrated their ability not only in the vehicle dynamics behaviour enhancement, but also in reducing the overall energy consumption. This last effect is due to the fact that the output torque commands calculated by the corresponding TV system will affect both the powertrain's operation point (and therefore their efficiency) and also the vehicle cornering response (and therefore tyre slip power losses).

With the aim of addressing the aforementioned two aspects directly, this is, vehicle dynamics and energy efficiency, in this chapter a novel energy-efficient NMPC based TV system for electric vehicles with multiple powertrains is proposed. This new approach targets the energy efficiency enhancement through the appropriate control of the cornering response and wheel torque allocation, with formulations considering powertrain power losses and tyre slip power losses directly, while providing the expected level of vehicle dynamics performance.

Different to other approaches in the literature, the proposed approach does not use the typical 3-layer TV structure, combining several layers to optimize efficiency in all of them. Moreover, an efficient yaw rate generator has also been developed, which includes the control allocation layer considerations. In addition, the direct consideration of the energy efficient term, allows to implement an adaptive weighting approach that allows to change the focus of the TV approach on enhancing vehicle dynamics, efficiency or both (balanced), depending on the current scenario. This strategy allows to increase efficiency, while maintaining the best cornering response, with the same critical speed in a challenging obstacle avoidance than the TV approach that only considers the yaw rate tracking in the cost function (NMPC Yaw Rate).

A comprehensive set of simulation experiments have been carried to demonstrate the validity of the approach, comparing its performance with the controller proposed in Chapter 4, and analyzing the effect of each term of the NMPC in the overall performance of the approach. On the one hand, results in different driving cycles, where powertrain losses account for most of the total losses, demonstrate that the proposed approach is able to reduce the energy consumption between a 0.47% and a 3.18% with respect to the passive approach, depending on the specific driving cycle to be performed. On the other hand, results in the selected circuit show an even higher energy consumption reduction, as in this case the tyre slip power losses have more impact. This way, the proposed NMPC TV is able to reduce the energy consumption a 9.43% with respect to the passive approach and a 5.5% with respect to the controller proposed in Chapter 4.

Moreover, results for the Skid-Pad test have demonstrated that being a model-based approach, the inclusion of the different relevant power loss contributions in the cost function of the developed NMPC formulations allows to compensate for inaccuracies, e.g., related to the estimation of the tyre-road friction coefficient, in the online generation of the energy-efficient reference yaw rate. This way, the robustness to not only the energy efficiency enhancement (2% average energy consumption reduction with respect to the other cases with the incorrect $\dot{\psi}_{ref}$), but also to the dynamic behaviour robustness (being the proposed approach the only one which does not suffer understeering or oversteering during the test) is improved.

Finally, it is to be considered that the proposed NMPC provides real-time performance thanks to the use of current high efficiency NMPC toolkits, which ensure a controller cycle of 20ms.

In summary, it has been demonstrated that use of energy related explicit terms in the proposed NMPC and the consideration of efficient yaw rate generation approaches can provide important power losses reduction to EVs, while maximizing the cornering response of the vehicle and thus, ensuring safety in stability loss scenarios.

Conclusions and future work

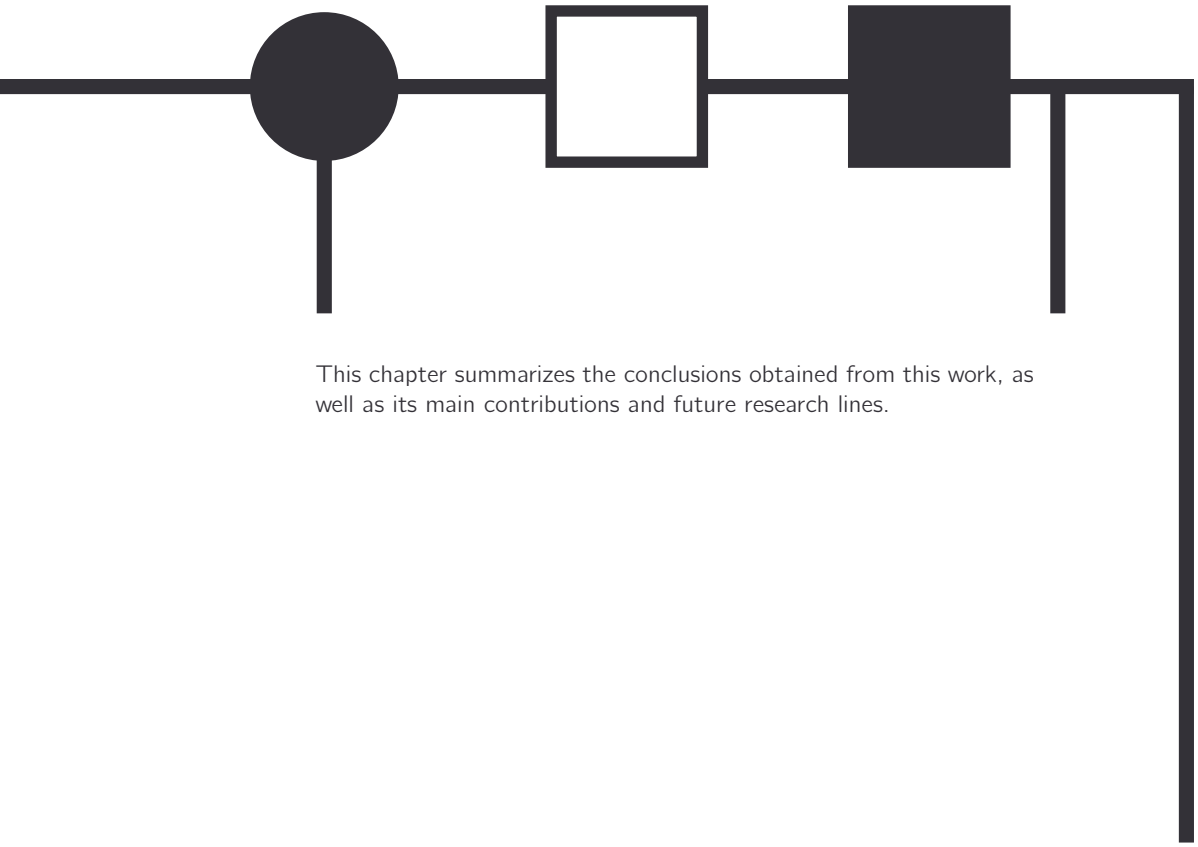

This chapter summarizes the conclusions obtained from this work, as well as its main contributions and future research lines.

6- Conclusions and future work

6.1 Conclusions and relevant contributions

6.1.1 Open Issues in Torque Vectoring for EVs

The need for reducing global warming, air pollution and oil dependency has motivated not only the use of renewable energies, but also some paradigm changes in other areas, such as transportation systems, where the development of electric vehicles (EV) has become a key strategy. The interest of vehicles with electrified powertrains has increased in the last years, becoming one of the main research areas in the automotive industry.

The integration of electric motors in propulsion systems not only provides better energy efficiency and lower pollution, but also increased controllability, as electric motors offer better accuracy and response time. These features are fuelling a notable interest in the development of vehicle dynamics control systems, which also address the efficiency and energy consumption.

Torque vectoring systems have positioned themselves as one of the most successful solutions for achieving these two objectives due to the following reasons. On the one hand, they are based on the same theory as the widely known ESP, and therefore, their ability to improve the vehicle dynamics performance in terms of cornering response and stability is based on the same principles. Their control actions are the motor torque commands, and therefore they can affect both main EVs power loss sources (the powertrain and the tyres). First, they can modify the powertrain operation point, affecting its efficiency, and second, they can modify the vehicle cornering response, affecting to tyres slip.

However, in the development of TV approaches for EVs, the analysis carried out in Chapter 2 concluded that there are several open points regarding torque vectoring systems. These open points can be summarized as follows:

1. It is important to choose properly the specific control technique to be used. The most promising ones are the model-based control systems, although they still present high model dependency and excessive computational cost, and the intelligent control techniques, as they do not present model dependency and provide a good balance between performance and computational cost.

2. Considering tyre forces in TV systems helps not only to generate a more optimal torque distribution, but also to reduce the tyre slip.

3. In the typical TV structure, the three layers work separately. This can lead to conflicts between them, especially when energy efficiency is considered. There-

fore, combining these layers can help to avoid these conflicts, improving the performance of the TV system.

4. In EVs, the main power losses sources are the powertrain (due to its efficiency) and the tyres (due to the slip). As TV systems affect both sources, modifying the powertrain operation point and vehicle's cornering response, both power losses must be considered.

5. In certain critical situations, such as emergency manoeuvres, considering the efficiency aspect can limit the ability of TV systems to improve the stability, which in this kind of situations can be critical. Therefore, the development of TV systems that provide significant operational flexibility depending on the actual driving situation, i.e., prioritize energy efficiency during normal driving, and stability in extreme manoeuvres, can be determined.

6. The implementability is crucial in this application. Too complex TV systems can be able to provide optimal performance, but not real-time capabilities, making impossible to be used in real vehicles. Hence, a balance between performance and computational cost is mandatory in the development of TV systems.

6.1.2 The need for simulation-based testing frameworks.

In order to validate vehicle dynamics control systems (such as TV) before track tests, simulation frameworks are mandatory. Nowadays, this kind of framework is commonly used in the automotive industry, as they not only allow to reduce the costs and time associated to track-based tests, but also to test extreme manoeuvres, such as those required for validating TV systems, in a safe manner.

Therefore, in Chapter 3, a *Vehicle Dynamics Simulation Framework* has been presented. The aforementioned framework permits HiL based tests and is composed by four main blocks: a virtual driver, a specific block for the implementation of the control system to be tested, a block for the implementation of the powertrain model, and finally, a multibody vehicle dynamics model. At the same time, the proposed framework is characterized by:

1. A novel multibody vehicle dynamics model that provides optimal accuracy and low computational cost (<1ms) thanks to the use of *macro-joints* and an efficient formulation.

2. A C code based implementation, with the objective of avoiding compatibility issues with different hardware platforms and permit flexibility to perform HiL tests.

3. A MPC based virtual driver, which permits to ensure repeatability and different driving styles (calm, aggressive...).

4. A specific block for the powertrain, which helps to easily test same vehicles with different powertrains.

The proposed framework has been validated in two different ways. On the one hand, comparing the obtained results with those obtained in four standardized tests performed with the real vehicle in IDIADA. On the other hand, analysing its real-time and flexible capabilities through its implementation on a Hardware in the Loop setup. Results show the proper performance of the proposed framework in both aspects, accuracy and real-time capabilities, demonstrating its effectiveness and ability to be used for the validation of vehicle dynamics control systems. Hence, the TV systems proposed in this Ph.D. Thesis have been validated using this framework.

6.1.3 Intelligent TV system

In Chapter 4 a novel Intelligent TV system, based on intelligent control techniques, including a fuzzy logic-based yaw moment controller and an ANN/ANFIS based vertical tyre forces estimator, is proposed. The use of intelligent control techniques permits a higher model abstraction as well as a good balance between performance and computational cost. Besides, this intelligent TV systems consider the energy efficiency indirectly through a torque distribution that uses the vertical tyre forces and through the utilization of the regenerative braking, reducing the overall energy consumption.

The proposed approach is characterized by:

1. A typical three layer-structure: Layer 1 is responsible for generating the yaw rate reference to be tracked using a bicycle model. Layer 2 includes a fuzzy yaw moment controller and a regenerative braking contribution, which helps to reduce energy consumption. Finally, layer 3 calculates the exact wheel torque commands, where the estimation of tyre forces is crucial.

2. An intelligent vertical tyre forces estimator, which is one of the main contributions of this approach. It allows to know which axle has more load, and therefore more grip. Thanks to that, it is possible to not only distribute the torque more optimally, sending higher torque commands to those wheels that can transmit more force to the road, but also to reduce the slip, reducing the tyre slip power losses. Unlike other estimators found in the literature, the proposed approach only uses easily to measure variables and does not require a complex model, as it is based on intelligent control techniques (ANN or ANFIS, depending on the hardware to be implemented) that use experimentally obtained data to tune their internal model.

3. A flexible hardware implementation, in which the proposed TV subsystems can be implemented in hetereogeneous hardware (uC+FPGA) to maximize computational efficiency.

The validation of the approach has been carried in two steps. First, the Vertical Tyre Forces estimator has been validated. For that purpose, both ANFIS and ANN approaches have been implemented and compared with a benchmarking estimator found in the state of the art. Results demonstrate that not only the proposed

approach is able to provide better results, but also allows flexibility in hardware implementation. The ANN implementation can be implemented in FPGA and provide a high accuracy at a minimum computational cost.

After validating both vertical tyre forces estimators, the validation of the whole Intelligent TV system has been presented for a C-class vehicle. For that, the performance of the proposed approach has been tested and evaluated through several manoeuvres and compared against two benchmarking TV systems found in the literature. Results show that the proposed Intelligent TV system can enhance the vehicle dynamics behaviour in both high-friction and low-friction conditions and the EV overall efficiency. This energy consumption reduction demonstrates the ability of TV systems to improve the overall efficiency although this aspect is not explicitly considered by the proposed approach.

Although the Intelligent TV system provides good performance in both vehicle dynamic behaviour aspect and energy efficiency, it still presents the following limitations: 1) the energy efficiency is not explicitly considered; 2) it is not possible to prioritize the energy efficiency aspect or the vehicle dynamic behaviour depending on the situation. Thus, in Chapter 5 an energy-efficient NMPC TV system addresses these two issues considering the energy efficiency in an explicit manner.

6.1.4 Energy-efficient NMPC TV system

The proposed energy-efficient NMPC TV system presents several points of novelty respect to those analysed in the state of the art, considering some of the issues arisen from the carried out state of the art analysis:

1. The proposed NMPC TV integrates different layers to avoid conflicts between them.

2. A methodology for the generation of an energy-efficient reference yaw rate, which considers the control allocation, is defined.

3. As the energy efficiency is explicitly considered and the proposed controller belongs to the optimal control category, it allows to modify the importance of each aspect, vehicle dynamics behaviour and energy efficiency, depending on the specific driving situation. This weight adaptation is carried out using a fuzzy logic system. This way, it is possible to take advantage of both model-based controllers and intelligent control techniques.

The formulation of the proposed NMPC TV is more complex than the Intelligent TV approach. However, some simplifications have been established in the internal model to reduce the execution time. Besides, the proposed controller has been implemented using a computationally high efficient toolbox (ACADO toolbox), which contributes to its implementation in real time. To evaluate the computational cost of the proposed approach, an analysis of the effect of different prediction horizons and timesteps in a HiL setup using the proposed *Vehicle Dynamics Simulation Framework*, has been carried out. This analysis permits to choose the configuration for the

better balance between performance and execution time, demonstrating the real time capabilities of the proposed energy efficient NMPC TV.

Once, the real time capabilities have been demonstrated, the proposed system has been validated within the scope of the STEVE European Project (selecting a lightweight EV as study case) and comparing the results against several configurations, which include the fuzzy yaw moment controller developed for the Intelligent TV previously proposed. Results showed the positive impact of the generated energy-efficient reference yaw rate map on energy consumption in steady-state cornering conditions. Such improvement was evident also for the Intelligent TV controller, coupled with an energy-efficient control allocation layer, showing both approaches the same relative power reduction (6% average of improvement). Nevertheless, the inclusion of the different relevant power loss contributions in the cost function terms of the developed NMPC TV system allows to compensate for inaccuracies, e.g., related to the estimation of the tyre-road friction coefficient in the online generation of the energy-efficient reference yaw rate, and for the effect of cornering transients, thus providing robustness to the energy efficiency enhancement.

Although this model-based controller, i.e. NMPC, can provide good performance, it was unable to concurrently provide the best energy consumption performance in normal driving conditions, and the safest cornering response during emergency maneuvers, e.g., obstacle avoidance tests. Therefore, as previously stated, to address this issue a fuzzy logic based adaptation mechanism of the NMPC weights has been developed. The proposed mechanism allows operational flexibility in prioritizing the energy efficiency or vehicle dynamics aspects and has demonstrated that effectively contributes to provide significant improvements in all considered scenarios. More specifically, results have shown that thanks to the proposed weight adaptation algorithm, the critical speed for the obstacle avoidance manoeuvre remains the same as the one achieved by the NMPC TV configuration that only consider the yaw rate tracking in its cost function. And, at the same time, results in this critical manoeuvre have also shown that the weight adaptation mechanism does not limit the performance in the energy efficiency aspect, being the approach that includes this mechanism the one that achieves the higher final speed in both high and low friction conditions, demonstrating its ability to reduce the power losses.

Finally, several tests have been carried out for different driving cycles in a selected circuit. On the one hand, as the powertrain losses account for most of the total losses, being the control allocation layer critical, the performance of the proposed NMPC TV system has been compared against an even distribution configuration (passive vehicle) and against a single axle configuration (only the rear axle powertrain activated). Results show that the proposed approach can reduce the energy consumption depending on the specific driving cycle to be performed. On the other hand, results in the selected circuit show an even higher energy consumption reduction, as in this case the tyre slip power losses have more impact. This way, the proposed NMPC TV can reduce even more the energy consumption.

6.1.5 Summary

The final conclusiones of this Ph.D. Thesis are:

1. TV systems are fundamental for EVs, as they permit to enhance the vehicle dynamic performance and, at the same time, reduce the energy consumption, increasing their driving range.

2. Due to the complexity of these systems and current EVs, the use of advanced control techniques is necessary.

3. Considering explicitly the energy efficiency in the developed TV systems effectively contributes to the enhancement of this key aspect without limiting the performance in other aspects, such as the vehicle stability, if mechanisms that allow to prioritize each aspect depending on the specific situation are implemented.

In this sense, the proposed TV systems, the Intelligent TV and the energy-efficient NMPC TV, have addressed these issues, demonstrating their ability to handle them properly and providing optimal performance, and helped to progress in these research lines. However, there are still certain areas where research needs to be done.

6.2 Future work

Considering the research work developed in this thesis, the author proposes the following research lines for future investigation:

- **Experimental validation:** in this Ph.D. thesis the validation of both contributions has been carried out based on simulation. Although, both proposed systems have been implemented in real hardware and their real-time capabilities have been demonstrated, the results have been obtained through an accurate vehicle dynamics model. In this sense, Tecnalia has developed and built their EV with multiple motor powertrain topology to validate new control systems, such as the TV systems proposed in this Ph.D. Tesis. Therefore, one of the future works will include the validation of both approaches in a this vehicle.

- **Extension to vehicle plants with additional chassis control actuators:** in this Ph.D. thesis the control actions of both proposed TV systems are the electric motor torques. However, if vehicles with more chassis actuators are considered, such as those required for an active suspension, new control actions can be added, and the effectiveness of the whole system can be further improved.

- **Include pre-emptive functionalities:** due to the recent advances in communication infrastructures, the *connected vehicles* concept is one of the most interesting topics for the Automotive Industry. In this sense, having information of the environment provided by other vehicles or systems, could help to extend the functionality of TV systems to a whole stability control system,

which, could limit the maximum speed considering the future trajectory and friction conditions.

- **Combination with automated driving algorithms:** undoubtedly Automated Vehicles is one of the main research areas not only for the Automotive Industry, but also for the whole scientific community. Traditionally, when TV systems have been implemented in Automated Vehicles, both systems, the TV algorithm and the automated driving algorithm, are usually differentiated and implemented using a cascade control architecture. Therefore, one of the future works will include the combination of these two systems.

Appendix

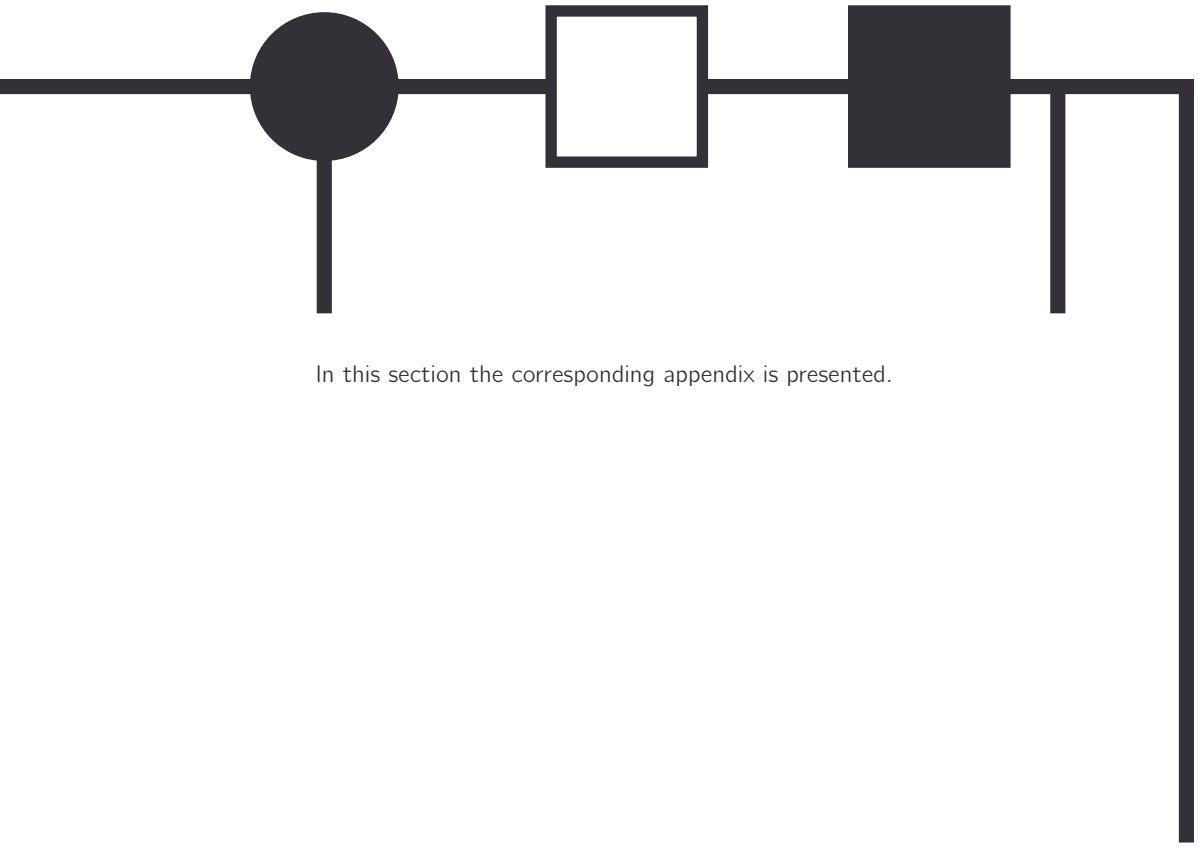

In this section the corresponding appendix is presented.

A- Benchmarking vertical tyre forces estimator

A.0.0.1 Benchmarking estimator

The benchmarking estimator has been proposed and validated in [18], providing good results, but requiring the estimation of many variables (such as longitudinal speed, vehicle mass and pitch and roll angles) for the vertical tyre forces estimation. This increases the dependency on a good model parametrisation and therefore, compromises the performance when model uncertainties arise.

The operation of this estimator can be derived in two main steps. First, the vertical forces actuating in both axles are estimated using Equation A.1 and Equation A.2, making use of the pitch and roll models showed in Figures A.1 and A.2.

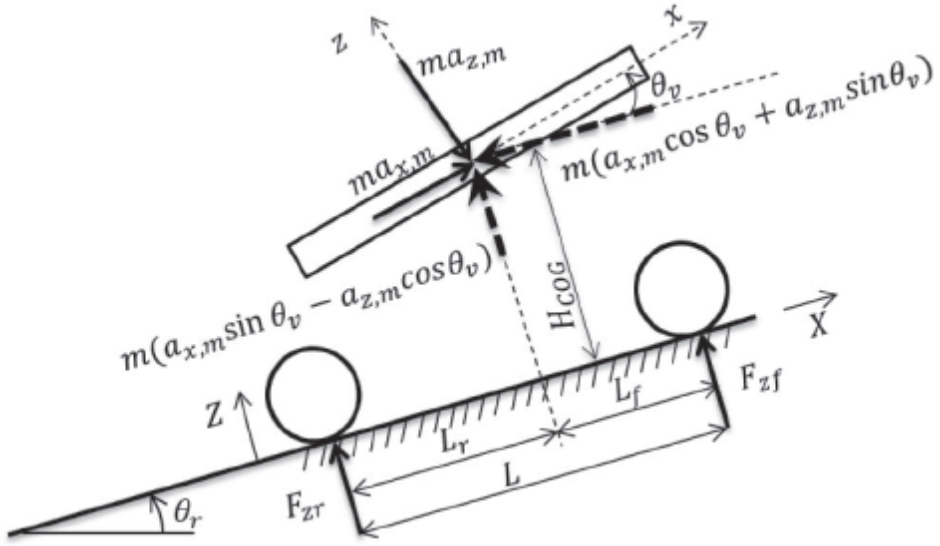

Figure A.1: Pitch Model [18]

$$F_{zf} = -m\frac{H_{CoG}}{L}(a_{x,m}\cos(\theta_v) + a_{z,m}\sin(\theta_v)) \\ -m\frac{L_r}{L}(a_{x,m}\sin(\theta_v) - a_{z,m}\cos(\theta_v)) \tag{A.1}$$

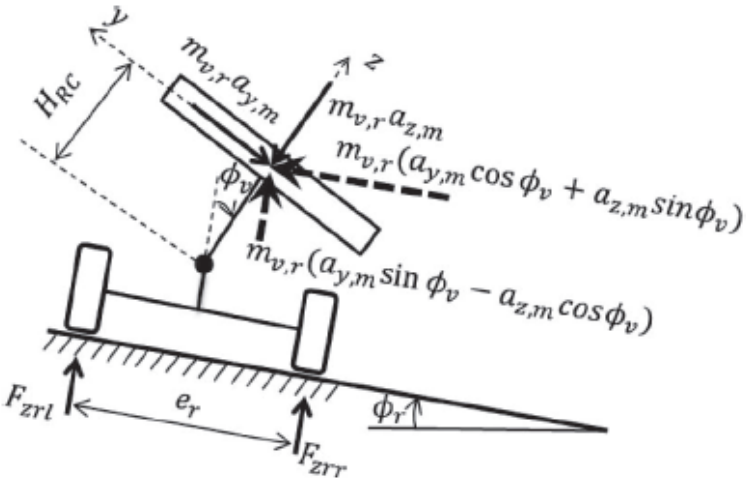

Figure A.2: Roll Model [18]

$$\begin{aligned} F_{zr} = m\frac{H_{CoG}}{L}(a_{x,m}\cos(\theta_v) + a_{z,m}\sin(\theta_v)) \\ -m\frac{L_f}{L}(a_{x,m}\sin(\theta_v) - a_{z,m}\cos(\theta_v)) \end{aligned} \tag{A.2}$$

where m is the mass of the vehicle $a_{z,m}$ and $a_{x,m}$ are the measured vertical and longitudinal accelerations of the Center of Gravity (CoG), L_f is the longitudinal distance between the CoG and the front axle, L_r is the longitudinal distance between the COG and the rear axle and H_{COG} is the height of the CoG. θ_v is body pitch angle and L is the wheelbase. F_{zf} and F_{zr} are vertical forces for front and rear axles, respectively.

For instance, the vertical force acting on the rear right tyre can be calculated by taking moment around the contact point of the rear left tyre and using Equation A.1 and Equation A.2 as follows:

$$\sum M_{rl} = 0 \tag{A.3}$$

$$\begin{aligned} F_{zrr} = -\frac{m_{v,r}H_{CoG}}{e_r}(a_{y,m}\cos(\phi_v) - a_{z,m}\sin(\phi_v)) \\ -\frac{m_{v,r}}{e_r}(a_{y,m}\sin(\phi_v) + a_{z,m}\cos(\phi_v)) \\ \times(\frac{e_r}{2} - H_{RC}\sin(\phi_v)) \end{aligned} \tag{A.4}$$

F_{zrl}, F_{zfr}, F_{zfl} are calculated in the same way as:

$$F_{zrl} = \frac{m_{v,r} H_{CoG}}{e_r}(a_{y,m}\cos(\phi_v) - a_{z,m}\sin(\phi_v)) - \frac{m_{v,r}}{e_r}(a_{y,m}\sin(\phi_v) + a_{z,m}\cos(\phi_v)) \times (\frac{e_r}{2} + H_{RC}\sin(\phi_v)) \tag{A.5}$$

$$F_{zfr} = -\frac{m_{v,f} H_{CoG}}{e_r}(a_{y,m}\cos(\phi_v) - a_{z,m}\sin(\phi_v)) - \frac{m_{v,f}}{e_r}(a_{y,m}\sin(\phi_v) + a_{z,m}\cos(\phi_v)) \times (\frac{e_f}{2} - H_{RC}\sin(\phi_v)) \tag{A.6}$$

$$F_{zfl} = \frac{m_{v,f} H_{CoG}}{e_r}(a_{y,m}\cos(\phi_v) - a_{z,m}\sin(\phi_v)) - \frac{m_{v,f}}{e_r}(a_{y,m}\sin(\phi_v) + a_{z,m}\cos(\phi_v)) \times (\frac{e_f}{2} + H_{RC}\sin(\phi_v)) \tag{A.7}$$

where $m_{v,f}$ and $m_{v,r}$ are the effective masses on the front and rear axles and e_f and e_r are the front and rear track widths, respectively, H_{RC} is the height of the roll center, and it is assumed that the height of the front and rear roll centers are the same. F_{zfl}, F_{zfr}, F_{zrl} and F_{zrr}, are the vertical tyre forces for the tyres.

Bibliography

[1] S. Beiker, *Deployment Scenarios for Vehicles with Higher-Order Automation*, 05 2016, pp. 193–211. v, 6

[2] M. Kissai, B. Monsuez, X. Mouton, D. Martinez, and A. Tapus, "Adaptive robust vehicle motion control for future over-actuated vehicles," *Machines*, vol. 7, p. 26, 04 2019. v, 14

[3] H. B. Pacejka, *Tyre and Vehicle Dynamics*. Butterworth-Heinemann, 2006. v, 15, 17, 28, 42, 111

[4] "Understeering & oversteering." [Online]. Available: https://en.wikipedia.org/ v, 16

[5] L. De Novellis, A. Sorniotti, P. Gruber, L. Shead, V. Ivanov, and V. Hoepping, "Torque vectoring for electric vehicles with individually controlled motors: State-of-the-art and future developments," *World Electric Vehicle Journal*, 2012. v, 17, 18, 19

[6] Y. Ushiroda, K. Sawase, N. Takahashi, K. Suzuki, and K. Manabe, "Development of super ayc," *Mitsubishi Motors Technical Review*, 2003. v, 19, 20, 21, 22

[7] V. Ivanov, D. Savitski, and B. Shyrokau, "A survey of traction control and antilock braking systems of full electric vehicles with individually controlled electric motors," *IEEE Transactions on Vehicular Technology*, vol. 64, no. 9, pp. 3878–3896, 2015. v, 24

[8] M. Acosta Reche, S. Kanarachos, and M. Blundell, "Virtual tyre force sensors: An overview of tyre model-based and tyre model-less state estimation techniques," *Proceedings of the Institution of Mechanical Engineers Part D Journal of Automobile Engineering*, vol. In press., 09 2017. v, 30

[9] P. V and C. SK, "Tire force estimation with strain gauge measurement." in *ASME 2014 International Mechanical Engineering Congress and Exposition, IMECE*, 2014. v, 30

[10] J. Cuadrado, D. Dopico, M. Gonzalez, and M. Naya, "A combined penalty and recursive real-time formulation for multibody dynamics," *Journal of Mechanical Design*, vol. vol. 126, no. 4, pp. 602-608, 2004.126, no. 4, pp. 602–608, 2004. v, 39, 40, 41

[11] A. Schmeitz, "A semi-empirical three-dimensional model of the pneumatic tyre rolling over arbitrarily uneven road surfaces," Ph.D. dissertation, TU Delft, 2004. v, 43

[12] S.Mata, "Control predictivo basado en modelo para control lateral de vehículos," Ph.D. dissertation, University of Basque Country, 2018. v, 46, 47

[13] R. Isanta, "Study of a neural network-based system for stability augmentation of an airplane," Ph.D. dissertation, Universitat Polytecnica de Catalunya, 2013. vi, 70

[14] V. Pandiyan, W. Caesarendra, T. Tjahjowidodo, and P. Gunasekaran, "Predictive modelling and analysis of process parameters on material removal characteristics in abrasive belt grinding process," *Applied Sciences*, vol. 7, p. 363, 04 2017. vi, 71

[15] "Axi4 interface." [Online]. Available: www.xilinx.com/ vi, 80, 82

[16] L. De Novellis, A. Sorniotti, P. Gruber, and A. Pennycot, "Comparison of feedback control techniques for torque- vectoring control of fully electric vehicles," *IEEE Transactions on Vehicular Technology*, 2014. vi, 25, 74, 87

[17] S. Ding, L. Liu, and W. X. Zheng, "Sliding mode direct yaw-moment control design for in-wheel electric vehicles," *IEEE Transactions on Industrial Electronics*, vol. 64, no. 8, pp. 6752–6762, Aug 2017. vi, 87

[18] A. Rezaeian, R. Zarringhalam, S. Fallah, W. Melek, A. Khajepour, S. . Chen, N. Moshchuck, and B. Litkouhi, "Novel tire force estimation strategy for real-time implementation on vehicle applications," *IEEE Transactions on Vehicular Technology*, vol. 64, no. 6, pp. 2231–2241, June 2015. viii, 29, 85, 153, 154

[19] "3ccar eu project." [Online]. Available: https://3ccar.eu/ 4

[20] "ADVICE." [Online]. Available: http://www.iesta.at/advice/ 4

[21] "ACHILES." [Online]. Available: https://www.h2020-achiles.eu/ 4

[22] "STEVE." [Online]. Available: http://www.steve-project.eu/index.php/en/ 4, 116

[23] Y. Furukawa and M. Abe, "Advanced chassis control systems for vehicle handling and active safety," *Vehicle System Dynamics*, vol. 28, no. 2-3, pp. 59–86, 1997. [Online]. Available: https://doi.org/10.1080/00423119708969350 5

[24] W. Manning and D. Crolla, "A review of yaw rate and sideslip controllers for passenger vehicles," *Transactions of the Institute of Measurement and Control*, vol. 29, no. 2, pp. 117–135, 2007. [Online]. Available: https://doi.org/10.1177/0142331207072989 5, 21

[25] R. Kim, H. Harada, and H. Minabe, "Electronic control of car chassis present status and future perspective," in *International Congress on Transportation Electronics,*, Oct 1988, pp. 173–188. 5, 18

[26] A. van Zanten, R. Erhardt, G. Pfaff, F. Kost, U. Hartmann, and T. Ehret, "Control aspects of the bosch-vdc," in *AVEC*, 1996. 5, 20

[27] Y. Shibahata, "Progress and future direction of chassis control technology," *Annual Reviews in Control*, vol. 29, pp. 151–156, 2005. 5

[28] J. C. Wheals, H. Baker, K. Ramsey, and W. Turner, "Torque vectoring awd driveline: Design, simulation, capabilities and control," in *SAE 2004 World Congress & Exhibition*. SAE International, mar 2004. [Online]. Available: https://doi.org/10.4271/2004-01-0863 5, 22

[29] S. Manzetti and F. Mariasiu, "Electric vehicle battery technologies: From present state to future systems," *Renewable and Sustainable Energy Reviews*, vol. 51, no. C, pp. 1004–1012, 2015. 5

[30] "Ionity." [Online]. Available: https://www.ionity.eu/ 5

[31] W. Dib, A. Chasse, P. Moulin, A. Sciarretta, and G. Corde, "Optimal energy management for an electric vehicle in eco-driving applications," *Control Engineering Practice*, vol. 29, 08 2014. 5

[32] I. Takahashi and T. Noguchi, "A new quick-response and high-efficiency control strategy of an induction motor," *IEEE Transactions on Industry Applications*, vol. IA-22, no. 5, pp. 820–827, 1986. 5

[33] L. Huber and D. Borojevic, "Space vector modulated three-phase to three-phase matrix converter with input power factor correction," *IEEE Transactions on Industry Applications*, vol. 31, no. 6, pp. 1234–1246, 1995. 5

[34] A. Roychoudhury, *Embedded Systems and Software Validation*. San Francisco, CA, USA: Morgan Kaufmann Publishers Inc., 2009. 6, 35

[35] R. B. S. Consultants, "Consolidation in vehicle electronic architectures," 2015. 6

[36] "Iso 8855:2011: Road vehicles - vehicle dynamics and road-holding ability." 13, 40

[37] G. Heeß and A. V. Zanten, "System approach to vehicle dynamic control," in *SAE Technical Paper*. SAE International, 09 1988. [Online]. Available: https://doi.org/10.4271/885107 18, 19

[38] Y. Shibahata, K. Shimada, and T. Tomari, "Improvement of vehicle maneuverability by direct yaw moment control," *Vehicle System Dynamics*, 1993. 18, 20

[39] E. Liebemann, K. Meder, J. Schuh, and G. Nenninger, "Safety and performance enhancement: the bosch electronic stability control(esp)," *SAE Technical Paper*, 01 2004. 20

[40] A. T. van Zanten, R. Erhardt, and G. Pfaff, "Vdc, the vehicle dynamics control system of bosch," in *International Congress & Exposition*. SAE International, feb 1995. [Online]. Available: https://doi.org/10.4271/950759 20

[41] W. Klier, G. Reimann, and W. Reinelt, "Concept and functionality of the active front steering system," 01 2004. 20

[42] S. C. Baslamisli, I. Polat, and I. E. Kose, "Gain scheduled active steering control based on a parametric bicycle model," *2007 IEEE Intelligent Vehicles Symposium*, pp. 1168–1173, 2007. 20

[43] R. Tchamna and I. Youn, "Yaw rate and side-slip control considering vehicle longitudinal dynamics," *International Journal of Automotive Technology*, vol. 14, 02 2013. 20

[44] D. Piyabongkarn, J. Lew, R. Rajamani, and J. Grogg, "Active driveline torque-management systems: Individual wheel-torque control for automotive safety applications," *IEEE Control Systems*, vol. 30, no. 4, pp. 86–102, 1 2010. 21, 22

[45] K. Sawase, Y. Ushiroda, and T. Miura, "Left-right torque vectoring technology as the core of super all wheel control (s-awc)," *Mitsubishi Motors Technical Review*, 2006. 21

[46] Y. Shibahata, N. Kuriki, K. Kitamura, K. Honda, K. Wada, H. Kajiwara, A. Nori, K. Kuwahara, and S. Okuma, "Development of left-right torque distribution system," *HONDA R&D Technical Review*, 1997. 21

[47] K. Sawase and K. Inoue, "Classification and analysis of lateral torque-vectoring differentials using velocity diagrams," *Proceedings of the Institution of Mechanical Engineers, Part D: Journal of Automobile Engineering*, vol. 222, no. 9, pp. 1527–1541, 2008. [Online]. Available: https://doi.org/10.1243/09544070JAUTO824 21

[48] K. Sawase and Y. Sano, "Application of active yaw control to vehicle dynamics by utilizing driving/breaking force," in *JSAE Review*, 1999. 21

[49] D. Piyabongkarn, J. Lew, R. Rajamani, J. Grogg, and Q. Yuan, "On the use of torque-biasing systems for electronic stability control: Limitations and possibilities," *IEEE Transactions on Control Systems Technology*, vol. 15, no. 3, pp. 581–589, 5 2007. 22

[50] S. Motoyama, H. U. K. Isoda, and H. Yuasa, "Effect of traction force distribution control on vehicle dynamics," *Vehicle System Dynamics*, vol. 22, no. 5-6, pp. 455–464, 1993. [Online]. Available: https://doi.org/10.1080/00423119308969043 22

[51] J. C. Wheals, "Torque vectoring driveline: Suv-based demonstrator and practical actuation technologies," *SAE Transactions*, vol. 114, pp. 631–648, 2005. [Online]. Available: http://www.jstor.org/stable/44725096 22

[52] J. Wheals, M. Deane, S. Drury, G. Griffith, P. Harman, R. Parkinson, S. Shepherd, and A. Turner, "Design and simulation of a torque vectoring™ rear axle," in *SAE 2006 World Congress & Exhibition*. SAE International, apr 2006. [Online]. Available: https://doi.org/10.4271/2006-01-0818 22

[53] United States Environmental Protection Agency, "Inventory of U.S. greenhouse gas emissions and sinks: 1990-2015," *Tech. report, US Government*, 2017. 22

[54] J. Riba, C. López-Torres, L. Romeral, and A. Garcia, "Rare-earth-free propulsion motors for electric vehicles: A technology review," *Renewable and Sustainable Energy Reviews*, no. 57, pp. 367–379, 2016. 22

[55] European Environment Agency, "Greenhouse gas emissions from transport," *Tech. report*, 2017. 22

[56] European Commission, "Reducing emissions from transport, a Europe strategy for low-emission mobility," *Tech. report*, 2014. 22

[57] European. Commission, "Roadmap to a single Europe transport area - toward a competitive and resource-efficient transport system," *Tech. report*, 2014. 22

[58] European Road Transport Research Advisory Council, "The electrification approach to urban mobility and transport," *Tech. report*, 2009. 22

[59] A. Zubaryeva and C. Thiel, "Paving the way to electrified road transport," *Tech. report, European Commission*, 2013. 22

[60] A. Rojas Rojas, H. Niederkofler, and W. Hirschberg, "Mechanical design of in-wheel motor driven vehicles with torque-vectoring," in *SAE-Brasil Congresso 2011*. SAE, 2011, pp. 1–15. 23

[61] D. Crolla and D. Cao, "The impact of hybrid and electric powertrains on vehicle dynamics, control systems and energy regeneration," *Vehicle System Dynamics*, vol. 50, pp. 95–109, 01 2012. 23

[62] M. Griffin, *Handbook of Human Vibration*. Academic Press, 1996. 23

[63] Y. Hori, Y. Toyoda, and Y. Tsuruoka, "Traction control of electric vehicle based on the estimation of road surface condition-basic experimental results using the test ev "uot electric march"," in *Proceedings of Power Conversion Conference - PCC '97*, vol. 1, Aug 1997, pp. 1–8 vol.1. 23

[64] B. Jacobsen, "Potential of electric wheel motors as new chassis actuators for vehicle manoeuvring," *Proceedings of the Institution of Mechanical Engineers, Part D: Journal of Automobile Engineering*, vol. 216, no. 8, pp. 631–640, 2002. [Online]. Available: https://doi.org/10.1177/095440700221600801 23

[65] G. D. Filippis, B. Lenzo, A. Sorniotti, P. Gruber, and W. D. Nijs, "Energy-efficient torque-vectoring control of electric vehicles with multiple drivetrains," *IEEE Transactions on Vehicular Technology*, vol. 67, no. 6, pp. 4702–4715, 2018. 23, 26, 112

[66] L. D. Novellis, A. Sorniotti, and P. Gruber, "Driving modes for designing the cornering response of fully electric vehicles with multiple motors," *IEEE Transactions on Vehicular Technology*, vol. 64-65, pp. 1–15, 2015. 25

[67] H. Guo, D. Cao, H. Chen, C. Lv, H. Wang, and S. Yang, "Vehicle dynamic state estimation: state of the art schemes and perspectives," *IEEE/CAA Journal of Automatica Sinica*, vol. 5, no. 2, pp. 418–431, Mar 2018. 25, 37, 48, 72

[68] Q. Lu, P. Gentile, A. Tota, A. Sorniotti, P. Gruber, F. Costamagna, and J. D. Smet, "Enhancing vehicle cornering limit through sideslip and yaw rate control," *Mechanical Systems and Signal Processing,*, vol. 75, pp. 455–472, 2016. 25

[69] M. Viehweger, C. Vaseur, S. van Aalst, M. Acosta, E. Regolin, A. Alatorre, W. Desmet, F. Naets, V. Ivanov, A. Ferrara, and A. Victorino, "Vehicle state and tyre force estimation: demonstrations and guidelines," *Vehicle System Dynamics*, pp. 1–28, 01 2020. 25

[70] G. Kaiser, Q. Liu, C. Hoffmann, M. Korte, and H. Werner, "Lpv torque vectoring for an electric vehicle with experimental validation," in *IFAC Proceedings*, 2014. 25

[71] T. Goggia, A. Sorniotti, L. D. Novellis, A. Ferrara, P. Gruber, J. Theunissen, D. Steenbeke, B. Knauder, and J. Zehetner, "Integral sliding mode for the torque-vectoring control of fully electric vehicles: Theoretical design and experimental assessment„" *IEEE Transactions on Vehicular Technology*, 2015. 25

[72] A. Tota, B. Lenzo, Q. Lu, A. Sorniotti, P. Gruber, S. Fallah, M. Velardocchia, E. Galvagno, and J. D. Smet, "On the experimental analysis of integral sliding modes for yaw rate and sideslip controlof an electric vehicle with multiple motors," *International Journal of Automotive Technology,*, vol. 19, no. 5, pp. 811–823, 2018. 25

[73] E. Siampis, E. Velenis, S. Gariuolo, and S. Longo, "A real-time nonlinear model predictive control strategy for stabilization of an electric vehicle at the limits if handling„" *IEEE Transactions on Control Systems Technology*, vol. 26, no. 6, pp. 1982–1994, 2019. 25, 109

[74] A. Haddoun, D. D. Benbouzid, R. Abdessemed, J. Ghouili, and K. Srairi, "Modeling, analysis, and neural network control of an ev electrical dierential," *IEEE Transactions on Industrial Electronics*, 2008. 26

[75] H. Kahveci, H. Ibrahi, and M. Ekici, "An electronic dierential system using fuzzy logic speed controlled in-wheel brushless dc motors," *Power Engineering Energy and Electrical Drives*, 2013. 26

[76] D. W. Y. Bai, *Fundamentals of Fuzzy Logic Control - Fuzzy Sets, Fuzzy Rules and Defuzzifications, Advanced Fuzzy Logic Technologies in Industrial Applications*. Springer, 2006. 26

[77] J. Kang, Y. Kyongsu, and H. Heo, "Control allocation based optimal torque vectoring for 4wd electric vehicle," 2012. 26

[78] W. Cho, J. Yoon, S. Yim, B. Koo, and K. Yi, "Estimation of tire forces for application to vehicle stability control," *Vehicular Technology, IEEE Transactions on*, vol. 59, pp. 638 – 649, 03 2010. 26, 28, 29

[79] W. Cho, J. Choi, C. Kim, S. Choi, and K. Yi, "Unified chassis control for the improvement of agility, maneuverability, and lateral stability," *IEEE Transactions on Vehicular Technology*, vol. 61, no. 3, pp. 1008–1020, March 2012. 26, 28

[80] T. Kobayashi, E. Katsuyama, H. Sugiura, E. Ono, and M. Yamamoto, "Direct yaw moment control and power consumption of in-wheel motor vehicle in steady-state turning," *Vehicle System Dynamics*, vol. 55, pp. 104–120, 2017. 26, 28, 105

[81] T. Kobayashi, E. Katsuyama, H. Sugiura, E. Ono, M. Yamamoto, and Masaki, "Efficient direct yaw moment control: tyre slip power loss minimisation for four-independent wheel drive vehicle," *Vehicle System Dynamics*, vol. 56, pp. 1–15, 2017. 26, 28, 105

[82] G. D. Filippis, B. Lenzo, A. Sorniotti, P. Gruber, K. Sannen, and J. D. Smet, "On the energy efficiency of electric vehicles with multiple motors," in *IEEE Vehicle Power and Propulsion Conference (VPPC)*, 2016. 26, 104, 105

[83] C. Chatzikomis, M. Zanchetta, P. Gruber, A. Sorniotti, B. Modic, T. Motaln, L. Blagotinsek, and G. Gotovac, "An energy-efficient torque-vectoring algorithm for electric vehicles with multiple motors," *Mechanical Systems and Signal Processing*, vol. 128, pp. 655–673, 2019. 27, 28

[84] C. Lin, S. Liang, J. Chen, and X. Gao, "A multi-objective optimal torque distribution strategy for four in-wheel-motor drive electric vehicles," *IEEE Access*, vol. 7, pp. 64 627–64 640, 2019. 27

[85] X. Hu, P. Wang, Y. Hu, and H. Chen, "A stability-guaranteed and energy-conserving torque distribution strategy for electric vehicles under extreme conditions," *Applied Energy*, vol. 259, p. 114162, 2020. [Online]. Available: http://www.sciencedirect.com/science/article/pii/S0306261919318495 27

[86] K. Oh, E. Joa, J. Lee, J. Yun, and K. Yi, "Yaw stability control of 4wd vehicles based on model predictive torque vectoring with physical constraints," *International Journal of Automotive Technology*, vol. 20, no. 5, pp. 923–932, Oct. 2019. [Online]. Available: https://doi.org/10.1007/s12239-019-0086-8 27

[87] B. Zhao, N. Xu, H. Chen, K. Guo, and Y. Huang, "Stability control of electric vehicles with in-wheel motors by considering tire slip energy," *Mechanical Systems and Signal Processing*, vol. 118, pp. 340–359, 2019. 27

[88] Z. Li, R. Hou, T. Sun, and S. Kavuma, "Continuous steering stability control based on an energy-saving torque distribution algorithm for a four in-wheel-motor independent-drive electric vehicle," *Energies*, 2018. 27

[89] M. Blundell and D. Harty, "The multibody systems approach to vehicle dynamics," *The Multibody Systems Approach to Vehicle Dynamics*, pp. 1–741, 01 2014. 28, 37, 39, 41

[90] M. Doumiati, A. Charara, A. Victorino, and D. Lechner, "Vehicle dynamics estimation using kalman filtering: Experimental validation," *Vehicle Dynamics Estimation using Kalman Filtering: Experimental Validation*, 12 2012. 28, 29, 30

[91] J.-I. Park, J.-Y. Yoon, D.-S. Kim, and K.-S. Yi, "Roll state estimator for rollover mitigation control," *Proceedings of The Institution of Mechanical Engineers Part D-journal of Automobile Engineering - PROC INST MECH ENG D-J AUTO*, vol. 222, pp. 1289–1312, 08 2008. 28, 29, 30

[92] A. Tuononen, "Vehicle lateral state estimation based on measured tyre forces," *Sensors*, vol. 9, 11 2009. 28

[93] G. Erdogan, S. Hong, F. Borrelli, and K. Hedrick, "Tire sensors for the measurement of slip angle and friction coefficient and their use in stability control systems," *SAE Int. J. Passeng. Cars – Mech. Syst.*, vol. 4, pp. 44–58, 04 2011. [Online]. Available: https://doi.org/10.4271/2011-01-0095 28

[94] L. Zhang, H. Liu, H. Zhang, and Y. Xu, "Component load predication from wheel force transducer measurements," in *SAE Technical Paper*. SAE International, 04 2011. [Online]. Available: https://doi.org/10.4271/2011-01-0737 28

[95] K. Nam, S. Oh, H. Fujimoto, and Y. Hori, "Estimation of sideslip and roll angles of electric vehicles using lateral tire force sensors through rls and kalman filter approaches," *Industrial Electronics, IEEE Transactions on*, vol. 60, pp. 988–1000, 03 2013. 28

[96] A. Viehweider and Y. Hori, "Electric vehicle lateral dynamics control based on instantaneous cornering stiffness estimation and an efficient allocation scheme," in *IFAC Proceeding Volumes*, 02 2012. 28

[97] F. Cheli, E. Leo, S. Melzi, and E. Sabbioni, "On the impact of 'smart tyres' on existing abs/ebd control systems," *Vehicle System Dynamics*, vol. 48, pp. 255–270, 12 2010. 28

[98] M. Doumiati, A. Victorino, A. Charara, and D. Lechner, "Estimation of vehicle lateral tire-road forces: A comparison between extended and unscented kalman filtering," *2009 European Control Conference, ECC 2009*, 08 2009. 28, 29

[99] L. L, R. X, and L. L., "Hybrid vehicle road loads simulation and correlation," in *Sae Technical Paper*, 2007. 28

[100] S. Antonov, A. Fehn, and A. Kugi, "Unscented kalman filter for vehicle state estimation," in *Vehicle System Dynamics*, 2015. 28, 29

[101] C. Song, F. Xiao, S. Song, L. Shaokun, and J. Li, "Design of a novel nonlinear observer to estimate sideslip angle and tire forces for distributed electric vehicle," *Mathematical Problems in Engineering*, vol. 2015, pp. 1–11, 11 2015. 28

[102] L. R. Ray, "Nonlinear state and tire force estimation for advanced vehicle control," *IEEE Trans. Contr. Sys. Techn.*, vol. 3, pp. 117–124, 1995. 28

[103] M. Wilkin, W. Manning, D. Crolla, and M. Levesley, "Use of an extended kalman filter as a robust tyre force estimator," *Vehicle System Dynamics - VEH SYST DYN*, vol. 44, pp. 50–59, 01 2006. 28

[104] A. Albinsson, F. Bruzelius, M. Jonasson, and B. Jacobson, "Tire force estimation utilizing wheel torque measurements and validation in simulations and experiments," in *Proceedings of the 12th International Symposium on Advanced Vehicle Control*, 09 2014. 28, 29

[105] R. Rajamani, D. Piyabongkarn, J. Y. Lew, and J. A. Grogg, "Algorithms for real-time estimation of individual wheel tire-road friction coefficients," *IEEE/ASME Transactions on Mechatronics*, vol. 17, pp. 1183–1195, 2006. 28

[106] W. R. Pasterkamp and H. B. Pacejka, "Application of neural networks in the estimation of tire/road friction using the tire as sensor," in *SAE Technical Paper*. SAE International, 02 1997. [Online]. Available: https://doi.org/10.4271/971122 28

[107] P. Luque, D. A Mantaras, E. Fidalgo, J. Álvarez, P. Riva, P. Girón, D. Compadre, and J. Ferran, "Tyre-road grip coefficient assessment - part ii: Online estimation using instrumented vehicle, extended kalman filter, and neural network," *Vehicle System Dynamics*, vol. 51, 12 2013. 28

[108] M. Acosta and S. Kanarachos, "Tire lateral force estimation and grip potential identification using neural networks, extended kalman filter, and recursive least squares," *Neural Computing and Applications*, 2018. 28, 31

[109] R. Jayachandran, S. D. Ashok, and S. Narayanan, "Fuzzy logic based modelling and simulation approach for the estimation of tire forces," *Procedia Engineering*, vol. 64, pp. 1109 – 1118, 2013, international Conference on Design and Manufacturing (IConDM2013). [Online]. Available: http://www.sciencedirect.com/science/article/pii/S1877705813017037 28, 31

[110] N. L. Kiencke Uwe, *Automotive Control Systems for Engine, Driveline, and Vehicle*, Springer, Ed. Springer, 2005. 29

[111] J. Ryu and J. Gerdes, "Estimation of vehicle roll and road bank angle," in *American Control Conference, Boston*, 01 2004, pp. 2110 – 2115 vol.3. 29

[112] H. E. Tseng, L. Xu, and D. Hrovat, "Estimation of land vehicle roll and pitch angles," *Vehicle System Dynamics*, vol. 45, no. 5, pp. 433–443, 2007. [Online]. Available: https://doi.org/10.1080/00423110601169713 29

[113] K. Jiang, A. C. Victorino, and A. Charara, "Adaptive estimation of vehicle dynamics through rls and kalman filter approaches," *2015 IEEE 18th International Conference on Intelligent Transportation Systems*, pp. 1741–1746, 2015. 30

[114] M. Dendaluce Jahnke, F. Cosco, R. Novickis, J. Pérez Rastelli, and V. Gomez-Garay, "Efficient neural network implementations on parallel embedded platforms applied to real-time torque-vectoring optimization using predictions for multi-motor electric vehicles," *Electronics*, vol. 8, no. 2, 2019. [Online]. Available: https://www.mdpi.com/2079-9292/8/2/250 31, 84

[115] R. Berger, "Consolidation in vehicle electronic architectures." 2015. 35

[116] D. E. Conseil, "Extract from the report world electronic industries 2012–2017." *General outlook: Towards more professional electronics, a chance for North America and Europe.*, 2014. 35

[117] D. Coulon, "Future of the automotive industry, electronics is the key," *Tti Mark.*, 2014. 35

[118] R. Lattarulo, J. Pérez, and M. Dendaluce, "A complete framework for developing and testing automated driving controllers," *IFAC-PapersOnLine*, vol. 50, pp. 258–263, 07 2017. 35

[119] Tecnalia, "Dynacar." [Online]. Available: http://www.dynacar.es/en/home.php 35, 85

[120] "Tecnalia research & innovation." [Online]. Available: www.tecnalia.com 35

[121] "Mathworks." [Online]. Available: https://es.mathworks.com/products/matlab.html 35, 84

[122] "National instruments." [Online]. Available: www.ni.com/ 35

[123] H.-Y. Guo, H. Chen, H.-T. Ding, and Y.-F. Hu, "Vehicle side-slip angle estimation based on uni-tire model," vol. 27, pp. 1131–1139, 09 2010. 37

[124] H. Guo, H. Chen, D. Cao, and W. Jin, "Design of a reduced-order non-linear observer for vehicle velocities estimation," *IET Control Theory Applications*, vol. 7, no. 17, pp. 2056–2068, 2013. 37

[125] H. Du, N. Zhang, and G. Dong, "Stabilizing vehicle lateral dynamics with considerations of parameter uncertainties and control saturation through robust yaw control," *IEEE Transactions on Vehicular Technology*, vol. 59, no. 5, pp. 2593–2597, 2010. 37

[126] C. V. Pablo Luque, Daniel Álvarez, *Ingeniería del Automóvil. Sistemas y Comportamiento Dinámico*. Thomson, 2005. 37

[127] E. B. Javier Garcia de Jalon, *Kinematic and Dynamic Simulation of Multibody Systems*. Springer-Verlag New York, 1994. 37, 38

[128] J. Cuadrado, D. Vilela, I. Iglesias, A. Martín, and A. Peña, "A multibody model to assess the effect of automotive motor in-wheel conguration on vehicle stability and comfort," in *ECCOMAS Multibody Dynamics*, 2013. 38, 39

[129] A. Schmeitz, "A semi-empirical three-dimensional model of the pneumatic tyre rolling over arbitrarily uneven road surfaces," Ph.D. dissertation, TU Delft, 2004. 42

[130] J. Pérez, F. Nashashibi, B. Lefaudeux, P. Resende, and E. Pollard, "Autonomous docking based on infrared system for electric vehicle charging in urban areas," *Sensors (Basel, Switzerland)*, vol. 13, pp. 2645–63, 02 2013. 44

[131] J. Pérez, V. Milanés, and E. Onieva, "Cascade architecture for lateral control in autonomous vehicles," *IEEE Transactions on Intelligent Transportation Systems*, vol. 12, no. 1, pp. 73–82, 2011. 44

[132] R. Lattarulo, J. Ibañez-Guzmán, and A. Peña, "Lateral controllers using neuro-fuzzy systems for automated vehicles : A comparative study," 2017. 44

[133] P. Falcone, F. Borrelli, J. Asgari, H. E. Tseng, and D. Hrovat, "Predictive active steering control for autonomous vehicle systems," *IEEE Transactions on Control Systems Technology*, vol. 15, no. 3, pp. 566–580, May 2007. 44

[134] R. Lattarulo, E. Marti, M. Marcano, J. Matute-Peaspan, and J. Pérez, "A speed planner approach based on bezier curves using vehicle dynamic constrains and passengers comfort," 05 2018, pp. 1–5. 44

[135] J. Matute-Peaspan, M. Marcano, A. Zubizarreta, and J. Pérez, "Longitudinal model predictive control with comfortable speed planner," in *2018 IEEE International Conference on Autonomous Robot Systems and Competitions (ICARSC)*, 04 2018, pp. 60–64. 44

[136] S. Cheng, L. Li, H. Guo, Z. Chen, and P. Song, "Longitudinal collision avoidance and lateral stability adaptive control system based on mpc of autonomous vehicles," *IEEE Transactions on Intelligent Transportation Systems*, pp. 1–10, 2019. 44

[137] J. A. Matute, R. Lattarulo, A. Zubizarreta, and J. Perez, "A comparison between coupled and decoupled vehicle motion controllers based on prediction models," in *2019 IEEE Intelligent Vehicles Symposium (IV)*, 2019, pp. 1843–1848. 44

[138] A. Ungoren and H. Peng, "An adaptive lateral preview driver model," *Vehicle System Dynamics - VEH SYST DYN*, vol. 43, pp. 245–259, 04 2005. 44

[139] T. Keviczky, P. Falcone, F. Borrelli, J. Asgari, and D. Hrovat, "Predictive control approach to autonomous vehicle steering," in *2006 American Control Conference*, June 2006, pp. 6 pp.–. 44

[140] F. Borrelli, P. Falcone, T. Keviczky, J. Asgari, and D. Hrovat, "Mpc–based approach to active steering for autonomous vehicle systems," *International Journal of Vehicle Autonomous Systems*, vol. 3, pp. 265–291, 01 2005. 44

[141] P. Falcone, E. Tseng, F. Borrelli, J. Asgari, and D. Hrovat, "Mpc-based yaw and lateral stabilisation via active front steering and braking," *Vehicle System Dynamics*, vol. 46, pp. 611–628, 09 2008. 44

[142] S. Keen and D. Cole, "Application of time-variant predictive control to modelling driver steering skill," *Vehicle System Dynamics*, vol. 49, pp. 527–559, 04 2011. 44

[143] V. Milanes, J. Villagra, J. Pérez, and C. Gonzalez, "Low-speed longitudinal controllers for mass-produced cars: A comparative study," *Industrial Electronics, IEEE Transactions on*, vol. 59, pp. 620 – 628, 02 2012. 44

[144] A. Katriniok, J. Maschuw, F. Christen, L. Eckstein, and D. Abel, "Optimal vehicle dynamics control for combined longitudinal and lateral autonomous vehicle guidance," in *European Control Conference (ECC)*, 07 2013, pp. 974–979. 44

[145] B. Gutjahr, L. Gröll, and M. Werling, "Lateral vehicle trajectory optimization using constrained linear time-varying mpc," *IEEE Transactions on Intelligent Transportation Systems*, vol. 18, pp. 1586–1595, 2017. 44

[146] "Worlwide harmonized light vehicles test procedure https://wiki.unece.org/pages/viewpage.action?pageid=2523179." 48, 135

[147] C. B. A. Eduardo F. Camacho, *Model Predictive Control*. Springer-Verlag London, 2007. 50, 51, 100

[148] "Idiada." [Online]. Available: https://www.applusidiada.com/global/es/ 53

[149] "Iso 7401:2011: Road vehicles - lateral transient response test methods - open-loop test methods." 54

[150] "Iso 4138:1996: Passenger cars - steady-state circular driving behaviour - open-loop test procedure." 56

[151] A. Joshi, "Hardware-in-the-loop (hil) implementation and validation of sae level 2 autonomous vehicle with subsystem fault tolerant fallback performance for takeover scenarios," in *Intelligent and Connected Vehicles Symposium*, 2017. 58

[152] "dspace." [Online]. Available: https://www.dspace.com/ 59

[153] L. Zadeh, *Fuzzy Sets*. Information and Control, 1965. 68, 69

[154] F. Dernoncourt, *Introduction to fuzzy logic*. Massachusetts Institute of Technology., 2013. 69

[155] T. M. Mitchell, *Machine Learning*, 1st ed. USA: McGraw-Hill, Inc., 1997. 69, 70, 79

[156] W. F. Milliken and D. L. Milliken, "Race car vehicle dynamics," in *SAE Internationa*, 1995. 75, 111

[157] M. Blej and M. Azizi, "Comparison of mamdani-type and sugeno-type fuzzy inference systems for fuzzy real time scheduling," *International Journal of Applied Engineering Research*, vol. 11, pp. 11 071–11 075, 01 2016. 75

[158] Y. Bai and D. Wang, *Fundamentals of Fuzzy Logic Control — Fuzzy Sets, Fuzzy Rules and Defuzzifications*, Springer, Ed. Springer, 01 2007. 75, 80, 115

[159] S. Y. Kevin M. Passino, *Fuzzy Control*, L. Cheu, Ed. Addison-Wesley, 1998. 80

[160] "Iso 3888-2:2011 passenger cars – test track for a severe lane-change manoeuvre - part 2: Obstacle avoidance." 89, 132

[161] M. D. B. Houska, H. J. Ferreau, "An auto-generated real-time iteration algorithm for nonlinear mpc in the microsecond range," *Automatica*, vol. 47, no. 10, p. 2279–2285, 2011. 103, 123

[162] A. Pennycott, L. D. Novellis, A. Sabbatini, P. Gruber, and A. Sorniotti, "Reducing the motor power losses of a four-wheel drive, fully electric vehicle via wheel torque allocation," *Proceedings of the Institution of Mechanical Engineers, Part D: Journal of Automobile Engineering*, vol. 228, no. 7, pp. 830–839, 2014. 104, 114, 119, 135

[163] L. Grüne and J. Pannek, *Nonlinear Model Predictive Control*. Springer, 2011. 108

[164] A. Dizqah, B. Lenzo, A. Sorniotti, P. Gruber, S. Fallah, and J. D. Smet, "A fast and parametric torque distribution strategy for four-wheel-drive energy-efficient electric vehicles," *IEEE Transactions on Industrial Electronics*, vol. 63, p. 4367 – 4376, 2016. 110